University of Washington
Department of Civil Engineering
Environmental Engineering and Science

Numerical Modeling of Tides and Currents in Central Puget Sound and Elliott Bay

Jiing-Yih Liou

and

Wen-Sen Chu

Numerical Modeling of Tides and Currents in
Central Puget Sound and Elliott Bay

by

Jiing-Yih Liou

and

Wen-Sen Chu

Department of Civil Engineering
University of Washington
Seattle WA 98195

June 1991

ABSTRACT

A linked set of numerical models, which are primarily based on a three-dimensional hydrodynamics model and a three-dimensional particle tracking model, were used to better understand the complex dynamics of currents in central Puget Sound and Elliott Bay. A coarse-grid two-layer model of the central Puget Sound, which obtained tidal transports as boundary conditions from an existing one-dimensional model, provides the current boundary conditions for the fine-grid four-layer model of the Elliott Bay region. The particle tracking model is applied to trace the possible trajectories of neutrally-buoyant water borne pollutants from known sources in central Puget Sound and Elliott Bay. According to the model simulation results, central Puget Sound and Elliott Bay flows are both tide driven systems. Detailed tidal currents and residual currents in central Puget Sound and Elliott Bay are presented. The influence of bathymetry on residual currents in the study is also demonstrated. The simulated currents replicate the two large tidal eddies observed in Elliott Bay. In addition to tidal forcing, effects of river inflow, wind, and density were also investigated in the models. Results show that the wind forcing has important effects on the currents in Elliott Bay. The developed models are useful tools for the better understanding of the complex tidal flow system in Puget Sound and its urban bays.

ACKNOWLEDGEMENTS

This report is dedicated to

Our families,
whose love and support have enabled us to
build this model;

and

Puget Sound,
the beautiful water body that has stimulated
so much of our thoughts

TABLE OF CONTENTS

iv

LIST OF FIGURES

LIST OF TABLES

LIST OF NOTATION

A : horizontal momentum exchange coefficient

C : Chezy coefficient ($m^{1/2}s^{-1}$)

C* : wind drag coefficient

D_x, D_y : horizontal diffusion coefficient

E : vertical momentum exchange coefficient

f : Coriolis parameter

g : acceleration of gravity

h : layer thickness

K_v : a constant

ΔL : horizontal dimension of the control volume

N_k : shape function defined at node k

p : pressure

P : representing a particle P

Q(t) : tidal transport

q_j : tidal transport amplitude

Ri : gradient Richardson number

rm : a constant

S : layer-averaged salinity

s : salinity

T : tidal period

t : time

$\overline{U_e}$: Eulerian velocity of the marked fluid particle

$\overline{U_l}$: Lagrangian velocity of the marked fluid particle

U, V : respective x, y components of horizontal layer-averaged velocities

u, v, w : respective components of velocity

V : horizontal velocity vector

V_p : velocity of marked particle P

W : 10-meter wind speed

W(t) : wind function (wind speed or wind direction)

$\overline{X_o}$: location of marked fluid particle at time t_o (a position vector)

$\overline{X_t}$: location of marked fluid particle at time t (a position vector)

$\Delta \overline{X}$: distance between $\overline{X_o}$ and $\overline{X_t}$

$\hat{x}, \hat{y}, \hat{z}$: special coordinates for particle tracking model, positive eastward, northward, and downward, respectively

x, y, z : Cartesian coordinates positive eastward, northward, and upward, respectively

Z_d : one-fifth of the total water depth

$\Delta\phi$: phase lag

γ : a dimensional constant (kg/m^3)

φ_j : tidal transport phase

κ : vertical diffusion coefficient

θ : angle between wind direction and model y-axis

ρ : water density

ρ_a : atmospheric density

ρ_0 : density of pure water

$\tau^{xx}, \tau^{xy}, \tau^{xz}, \tau^{yx}, \tau^{yy},$ and τ^{yz} : components of stress tensor

ω : z-component vorticity

ω_j : tidal transport frequency

ξ : water surface elevation

CHAPTER ONE

INTRODUCTION

Puget Sound (Fig.1.1) is a fjord-type estuary consisting of several deep basins separated by shallow sills (Burns, 1985). During the last 50 years, urban, industrial and national defense developments, as well as marine transportation, commercial fishing, and recreational activities have expanded rapidly around the shores of Puget Sound. With the increasing reports of contamination in the Sound, public concern for the pollution problem has grown in recent years. Pollutants enter the Sound from many different sources; some of the known potential pollution sources are uncontrolled non-point surface runoff, combined sewer overflows, municipal and industrial waste discharges, and maintenance dredging disposal. According to Puget Sound Water Quality Authority (PSWQA, 1989), pollutant concentrations in the sediments of the urban bays are up to 100 times the levels of those found in the cleanest rural bays. The potential threat from projected industrial and population growth in the region is serious.

One of the critical elements in managing Puget Sound water quality problem is the better understanding of the flow and transport dynamics in the Sound. When wastes are discharged into the receiving water, it is important to know how they are transported. Do they all leave the disposal sites ? Or, how long (and how far) do they remain in the particular waters ? Some important future management and planning decisions depend heavily on the answers to these and other related questions.

Puget Sound is an estuary where fresh river inflow volume is very small compared to the tidal prism. Because it was scoured by retreating glaciers, the bathymetry of the Sound is composed of several deep basins (average depth exceeding 150 meters) separated by several shallow sills (40 to 60 meters at Tacoma Narrows and
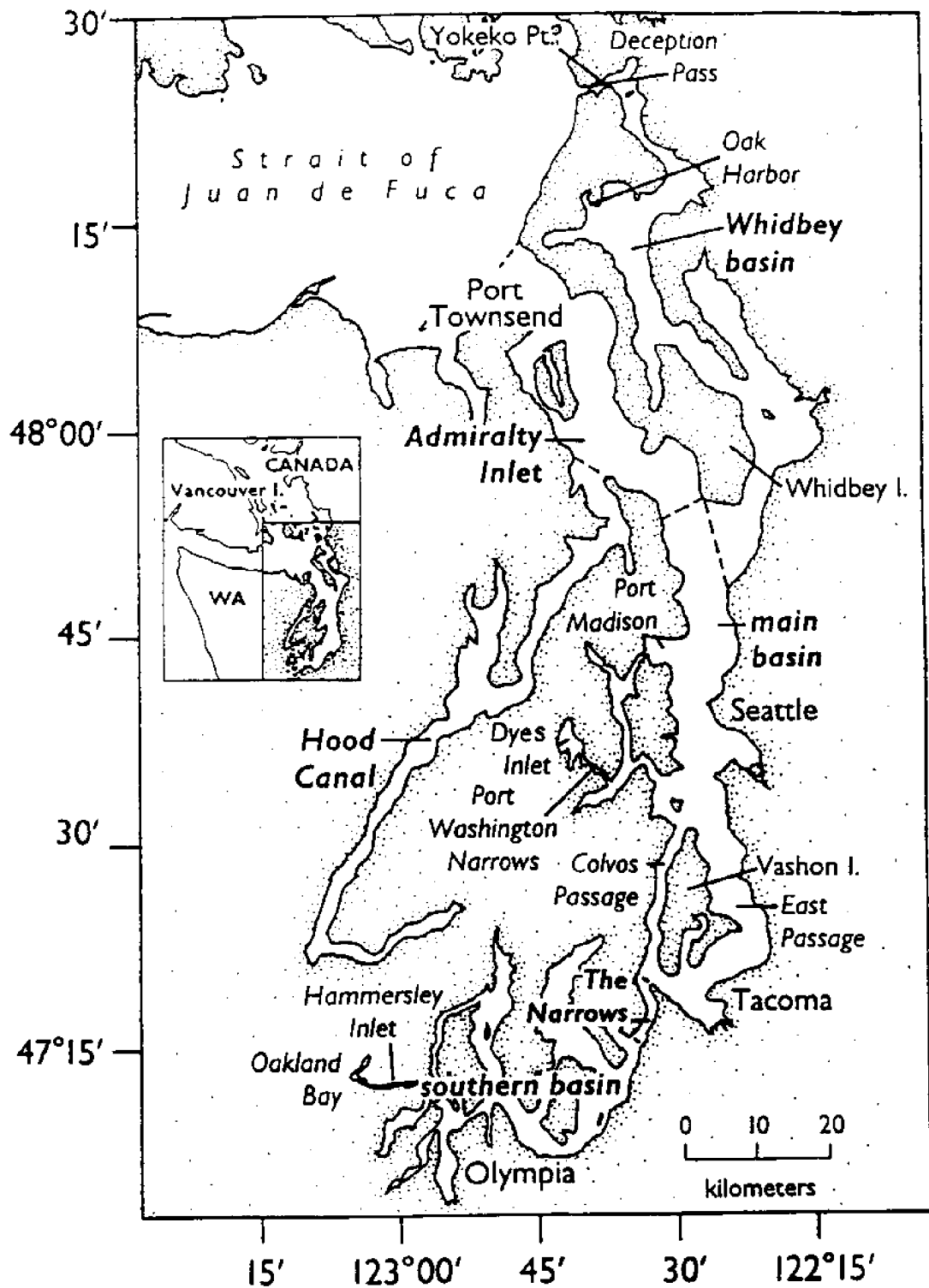
Fig.1.1 Map of Puget Sound. The shoreline is based on the MLLW water datum from NOAA charts. Dashed lines separate the principal basins, which are identified in bold type (from Lavelle et al., 1988)

Admiralty Inlet for examples) (Burns, 1985). Water movement in the Sound is forced by tide, wind, river inflow, and density gradients and is confined by irregular geometric and bathymetric features. All these factors render the tidal hydrodynamics and transport processes in the Sound very complex. Flow and transport in such complex estuaries have been studied by engineers and scientists using field surveys, analytical models, physical hydraulic models, and numerical models.

Field study is the most direct way to understand the characteristics of a physical system. Analyses of field data can often provide the most basic understanding of the dynamic processes in estuaries. Field studies for the derivation of detail spatial and temporal understandings of the hydrodynamics can however be prohibitively expensive.

Analytical models are mathematical models in which closed form solutions to the problem can be obtained. Analytical models have been applied to study basic dynamics in estuaries for decades. The formulations of analytical models are usually based on assumption of simple topography, and only include the most dominating physical terms. Analytical models are simple to use, but they lack the resolution power for small scale (in time and in space) movements in complex water bodies.

Physical hydraulic models have been widely used to simulate tidal hydraulics and pollutants transport in coastal waters. An hydraulic model which encompasses the entire area of Puget Sound was constructed by the Department of Oceanography of the University of Washington (Rogers, 1955; Winter, 1977). The model was constructed to a horizontal scale of 1:40000 and a vertical scale of 1:1152 (with a distortion ratio of 1:35). The construction of an hydraulic model with smaller distortion ratio will require significant land space and calibration effort (Nece, 1987). Wind forces cannot be simulated in the present hydraulic model.

Following the continuing development of computing power in the past two decades, numerical models have become the more popular tools for studying the behavior of flows and pollutant transport in coastal waters. Owing to different application purposes and simplifying assumptions, the structures of these numerical models can be very different. It is the modelers who have to choose, based on the purpose of the study, the available data and computing resources, and the physical features of the water body (bathymetry, geometry, etc.), the appropriate model for each study.

In this study, a comprehensive numerical model system has been developed for the understanding of small scale (250 m horizontally and 15 m vertically) circulation and transport characteristics in Puget Sound and its urban bays at tidal time scale (hours to days). This model was designed to effectively incorporate the relevant physical effects of tide, wind, density, river inflow, and Coriolis force for the most efficient computation of tides and currents in Puget Sound basins and urban bays (see Fig.1.2). The results of the model are to be presented in forms that can be used by scientific communities as well as the general public.

The developed hydrodynamics model was first validated by sets of laboratory data and field observations, before it was applied to characterize and quantify tidal circulation and transport features in Central Puget Sound (at 762 m horizontal scale and two vertical layers) and Elliott Bay (at 254 m horizontal scale with four vertical layers). The massive results from the models are summarized and presented using various support graphics softwares.

In the remainder of this report, a review of past and present estuarine numerical modeling technologies is first given in Chapter 2. The numerical hydrodynamics and particle tracking models are introduced in Chapter 3. The model validation work is presented in Chapter 4. In Chapter 5, the model application for the study of tidal circulation and transport in Central Puget Sound and Elliott Bay is

Puget Sound Model System

Tide channel model
(Lavelle,et al., 1988)
domain of model :
entire Puget Sound

↓

Provide tidal transport
at particular cross sections
as boundary conditions
for coarse grid model

↓

wind model →

Coarse grid model
domain of model:
major Puget Sound basin
(762 m and 2 layers)

Linear interpolation scheme →

Provide open boundary conditions for fine grid model

Large scale circulation and transport characteristics →

Data management and graphic display

wind model →

Reduced density model →

Fine grid model
domain of model :
urban bay and part
of the main basin
(254 m and 4 layers)

END USER

Fine scale circulation and transport characteristics →

Data management and graphic display

Fig.1.2 Puget Sound Model System

described. Lastly, the conclusions and recommendations for future work are given in Chapter 6.

CHAPTER TWO

LITERATURE REVIEW

For the concerns over our coastal environments, various forms of numerical models have been proposed and applied to characterize water movement and mixing processes in the estuaries and coastal waters. This chapter will provide a brief classification of coastal and estuarine numerical models and their solution methods. The ideas of particle tracking and nested grid systems and existing numerical models for Puget Sound studies are also presented.

In a typical estuary, water motions are induced by tide, river inflow, wind and density effects. Such flow phenomena can be very complex and are usually three-dimensional. To describe such hydrodynamic systems, several physical variables, such as velocity, density, salinity, pressure, and temperature, and their relationship to each other must be represented by a system of equations based on appropriate physical laws. These equations includes equations of motion and continuity for water, equations for the conservation of salt and heat, and the equation of state. For a complete representation of the physics, the above system of equations should be solved without any simplification. To accomplish this, the synoptic boundary conditions for all the variables must be known and the parameters and variables relating the exchange of mass, momentum and heat must also all be known. With our present computer and budgetary constraints and understanding of the physics, this is simply impossible.

Therefore, most of the models are derived with some simplifying assumptions and approximations (time and spatial averaging, parameterization, etc.) to the governing equations. Even with such simplifications, only approximate solutions to the equations can be obtained at discrete points (or nodes) within the domain. The averaging, parameterization, and discretization will

create models that can only capture the flow phenomena at the time and spatial scales for which they are developed.

2.1 Existing Estuarine Numerical Models

Depending on the purpose of the study, the availability of data, the computing resources, and the skill or sometimes the preference of the modelers, different simplifications and approximations are introduced in the development of numerical models. One most commonly encountered simplification is the averaging of the governing equations over one or more spatial dimensions. Based on the number of spatial dimensions in the velocity variables, these models may be classified as: zero-dimensional (mass conservation only); one-dimensional; two-dimensional laterally-averaged; two-dimensional depth-averaged; and three-dimensional models.

An example of a zero-dimensional model is the one developed by Cokelet and Stewart (1985). They created a mass conservation based (therefore zero-dimension) box model to study the long-term flushing characteristics of the entire Puget Sound. In an estuary which is formed by long and narrow channels, one-dimensional models can often provide good estimations of tidal variation and cross-sectional velocities (Kamphuis, 1970; Lavelle et al., 1988). For the flow and transport phenomena in deep but narrow estuaries, a two-dimensional laterally-averaged model can be used (Perrels and Karelse, 1981; Lavelle, 1987; Bloss et al., 1988). For many free-surface flow problems, in which the flow movements can be assumed to be mainly in the horizontal direction (Abbott et al., 1985), then many modelers have used two-dimensional depth-averaged models (see e.g., Leendertse, 1970; Blumberg, 1977; and Spaulding and Beauchamp, 1983). Three-dimensional estuarine models were introduced in the early 1970's (Liu and Leendertse, 1978). Some of the earlier three-dimensional models include the ones developed by Leendertse and his colleagues (Leendertse et al., 1973; 1977), Heaps (1973), Sundermann (1974), Simons (1974, 1975), Laevastu (1975), Hess (1976), Backhaus (1979), and Tee (1979). Some more recent

three-dimensional models includes those developed by Owen (1980), Nihoul (1982), Sheng (1983), Blumberg and Mellor (1983), Oey and Mellor (1985), Raithby et al. (1988), Sarraf et al. (1988), Chu et al. (1989), and Leendertse (1989).

Different from these spatial-averaged models, some models are developed by averaging the governing equations over different time intervals. Tidal models, which are the most common estuarine models, can be used to simulate flow and transport variations over a short time intervals (hours to days). Some examples of tidal time scale model are the ones by Leendertse (1970), Blumberg (1977), and Spaulding and Beauchamp (1983). Residual models are derived from integrating the governing equations of the tidal model over one or more tidal cycles (Tee, 1981; Falconer, 1985; Smith and Cheng, 1987). These models are applied to study the long term variations of particular estuarine properties (salt, current, etc.).

Some estuarine models include the effect of density stratification; some assume the estuaries or coastal waters are homogeneous. To include baroclinic effects in the model, the heat and salt transport equations must be solved along with the hydrodynamic equations. The solution of salt and heat transport always demands a very long "spin-up time" during which the model is run for an extended period to remove the unwanted influence of the input initial conditions (Chu and Yeh, 1980; Oey and Mellor, 1985).

Numerical estuarine models can be further classified to include those with different spatial reference frames. Earlier but more thorough reviews of numerical estuarine models have been given by Hinwood and Wallis (1975) and Liu and Leendertse (1978).

2.2 Solution Techniques for Estuarine Numerical Models

In the last section, numerical estuarine models with different simplifying approaches were briefly described. Depending on the

resources and skill and preference of the model developer, the equations in these models are solved by different numerical techniques. Generally, finite difference and finite element methods are two of the most popular solution techniques used to solve the hydrodynamic equations and the solute transport equations. More recently, some new approaches such as the Eulerian-Lagrangian method have been introduced for solving the transport equations. These methods are introduced briefly below.

2.2.1 Solution Techniques for the Hydrodynamic Equations

Since Leendertse (1970) first applied an implicit finite difference scheme to solve his two-dimensional estuarine model in 1970, this solution technique has received tremendous popularity in estuarine modeling. Use of the alternating direction implicit (ADI) idea and a space-staggered grid system makes this scheme very efficient. To date, this scheme has been applied to two-dimensional models only. Some examples of such applications are the work by Liu and Leendertse (1978), Leendertse et al. (1981), Awaji (1980), Spaulding and Beauchamp (1983), Smith and Cheng (1987), and Chu et al. (1988).

Several other finite difference schemes have been developed and applied earlier to two-dimensional estuarine modeling (Hansen, 1962; Dronkers, 1964). Other examples include the work by Reid and Bodine (1968), Brandes and Masch (1971), and Blumberg (1977). The two-dimensional scheme by Hansen (1962) was also extended by Sundermann (1974) and Laevastu (1975) to study three-dimensional multilevel and multilayer flow systems.

In their first three-dimensional model, Leendertse and Liu (1973) used an explicit leap-frog scheme to solve the model equations. The scheme was later modified to a depth-direction implicit scheme to improve numerical stability in long term simulation (Leendertse and Liu, 1977). Some other three-dimensional finite difference models include the ones by Hess

(1976), Blumberg and Mellor (1983), Sheng (1983), Oey and Mellor (1985), Chu et al. (1989), and Leendertse (1989).

Some modelers prefer to use finite element methods to solve the model governing equations (Cheng and Tung, 1970; Wang et al., 1972; Wang and Connor, 1975; Taylor and Davis, 1975; Smith and Cheng, 1976; Jamart, 1983, etc.). Since this method allows the use of flexible elements and nodes, the complex boundaries of estuaries can be more accurately represented than by the finite difference method. In comparison with the finite difference method, the finite element method requires more computer resource (Pinder and Gray, 1977).

2.2.2 Solution Techniques for the Solute Transport Equation

The finite difference method is one of the earliest numerical techniques used in solving the transport equation. Some examples of finite difference transport models are those reported in Leendertse (1970), Leendertse et al. (1981), Boulot (1981), and Oey and Mellor (1985). One of the main drawbacks of the finite difference method is the presence of numerical dispersion error in its solution.

The finite element method had been applied in studying estuarine water quality problems in the 1970's (Leumkuhler, 1975; Cheng, 1978). The main advantage of of this method is the ability to handle complex geometry and bathymetry of the estuaries. But, besides being more difficult to code, numerical dispersion errors can also plague its solutions.

As an alternative to the above two methods, several Eulerian-Lagrangian methods have recently been proposed for the solution of the transport equations. In these methods, the advection terms are discretized along a streamwise coordinate (therefore the name Lagrangian), while the diffusion term is resolved with respect to fixed Eulerian grid. Using this approach, Cheng and Casulli (1982) and Cheng et al. (1984) successfully developed a model to study two-dimensional salt transport in upper San Francisco Bay. The method

was shown (Cheng and Casulli, 1982) to be superior to the finite difference or finite element method for solving the transport equation.

2.3 The Particle Tracking Idea

Tidal flow and transport characteristics in an estuary can also be simulated by a particle tracking model. In such model, the movement of the water is marked by particles which are allowed to move passively with the current. In some models, even the diffusive effect can be simulated by a "random walk" scheme. Particle tracking is an effective tool to illustrate flow features in a more dynamic sense and can be used as an aid to the better understanding of transport characteristics of the water body. In the literature, a particle tracking model was developed by Awaji (1980, 1982) to study tidal exchange through a strait. A similar "tracer" model was reported by Maier-Reimer and Sundermann (1982). A simpler particle tracking model was built by Chu and Gardner (1986) to simulate sewage release effects in Humboldt Bay. More recently, a particle tracking model was developed by Jozsa (1989) for the study of pollutant and oil slick transport in a river.

2.4 The Nested Model Concept

All numerical models are built to seek solutions to flow problems at some pre-determined discrete nodes or in some control volumes. Generally speaking, the smaller the grid resolution, the more accurate (or realistic) simulated results are expected. But smaller grid spacing requires more computing resources, more initial and boundary conditions, and more validation data. For some estuarine problems, people are concerned with only larger flow processes and therefore would choose larger grid resolution to characterize the flow system. But for some other problems, small scale phenomena become more important and therefore should be characterized by a more refined grid. A commonly used modeling approach is called nested grid approach. According to Verboom et al.

(1984), a model is called nested if it covers just a part of the problem area and if it gets its boundary conditions from a model that covers a larger area. This approach has been used in many coastal water modeling projects. Some examples are the works by Leendertse et al. (1981), Boulot (1981), Falconer and Mardapitta-Hadjipandeli (1986), Choi (1986), and Liu and Leendertse (1987).

2.5 Previous Hydrodynamics and Transport Models for Puget Sound

Research of physical oceanography in Puget Sound area has been done for many years (e.g. Rogers, 1955; Collias et al., 1974; Winter, 1977; Mofjeld et al., 1987; Curl et al., 1988). Most of the research up to 1985 can be classified as analytical approaches based on field observation data (see for example, Sillcox et al., 1981; Geyer and Canon, 1982; Mofjeld and Larsen, 1984; and Bretschneider et al., 1985). Numerical modeling studies of Puget Sound hydrodynamics and pollutant transport began only recently.

One of the earliest reported numerical modeling research studies of Puget Sound was that conducted by Water Resources Engineers (WRE), Inc. (1975). This work used a one-dimensional link (channel) and node model to characterize the tidal hydrodynamics and water quality in Puget Sound. However, this one-dimensional approximation of the tidal hydrodynamics, especially with respect to momentum transport, is now considered too rough for many planning and engineering applications. In 1978, Jamart and Winter built a model using a harmonic method and finite element technique to calculate tidal flow in a part of Hood Canal, a major basin in Puget Sound outside the proposed study area. Later in 1983, Jamart extended the same model to East Passage in Puget Sound for a sewage treatment plant outfall siting study. More recently, Downing et al. (1985) developed a two-dimensional vertically averaged transport model to investigate far field dilution for another sewage outfall siting study in Central Puget Sound. Furthermore, as part of the Puget Sound Dredge Disposal Analysis program, Schmalz (1986)

applied a two-dimensional model to Puget Sound to provide tidal current information for selecting dredge disposal sites. Because of the nature of the studies (objective, budget, and time limitations), these previous researches all used only two-dimensional models. For the concerns related to outfall and dredge disposal site selections, more refined tidal current information might need to be considered. Such information can be provided by a three-dimensional model with refined resolution.

Other more recently developed models include a conservation of mass based box model for studying long term basin wide flushing characteristics of Puget Sound (Cokelet et al., 1984), an one-dimensional channel tide model of the entire Puget Sound by Lavelle et al. (1988), a laterally-averaged model for studying sediment transport and salinity intrusion by Lavelle (1987) and a two-dimensional depth-averaged model for studying the transport characteristics in central Puget Sound (Chu et al., 1989). Nakata (1987) in Japan applied his three-dimensional model to the entire Puget Sound by assuming uniform depth throughout the Sound. The application was an "operational test" for the model; no scientific conclusions were drawn from the application. None of the currently available numerical models has been shown to be capable of characterizing three-dimensional tidal flow phenomena at 750 m (or less) spatial scale.

CHAPTER THREE

THE PROPOSED NUMERICAL MODELS

3.1 Three-Dimensional Hydrodynamics Model

3.1.1 The Basic Three-Dimensional Equations

In estuaries and coastal seas, flow is predominantly horizontal, i.e., vertical velocities are several orders of magnitude smaller than the horizontal velocities, and vertical acceleration is negligible compared with gravitational acceleration. If the vertical acceleration is ignored, then the vertical momentum equation can be reduced to the hydrostatic equation. If it is further assumed that density variation is small except when multiplied by gravity (Boussinesq assumption), then the equations of motion can be written as (Leendertse et al., 1973) :

$$\frac{\partial u}{\partial t} + \frac{\partial (uu)}{\partial x} + \frac{\partial (uv)}{\partial y} + \frac{\partial (uw)}{\partial z} - fv + \frac{1}{\rho}\frac{\partial p}{\partial x} - \frac{1}{\rho}\left(\frac{\partial \tau^{xx}}{\partial x} + \frac{\partial \tau^{xy}}{\partial y} + \frac{\partial \tau^{xz}}{\partial z}\right) = 0 \quad (3.1)$$

$$\frac{\partial v}{\partial t} + \frac{\partial (uv)}{\partial x} + \frac{\partial (vv)}{\partial y} + \frac{\partial (vw)}{\partial z} + fu + \frac{1}{\rho}\frac{\partial p}{\partial y} - \frac{1}{\rho}\left(\frac{\partial \tau^{yx}}{\partial x} + \frac{\partial \tau^{yy}}{\partial y} + \frac{\partial \tau^{yz}}{\partial z}\right) = 0 \quad (3.2)$$

$$\frac{\partial p}{\partial z} + \rho g = 0 \quad (3.3)$$

$$\frac{\partial u}{\partial x} + \frac{\partial v}{\partial y} + \frac{\partial w}{\partial z} = 0 \quad (3.4)$$

$$\frac{\partial s}{\partial t} + \frac{\partial (us)}{\partial x} + \frac{\partial (vs)}{\partial y} + \frac{\partial (ws)}{\partial z} - \frac{\partial}{\partial x}\left(Dx\frac{\partial s}{\partial x}\right) - \frac{\partial}{\partial y}\left(Dy\frac{\partial s}{\partial y}\right) - \frac{\partial}{\partial z}\left(\kappa\frac{\partial s}{\partial z}\right) = 0 \quad (3.5)$$

$$\rho = \rho (s,p) \quad (3.6)$$

where u, v, and w are velocities in Cartesian x-, y-, and z- directions, p is the pressure, $\tau^{xx}, \tau^{xy}, \tau^{xz}, \tau^{yx}, \tau^{yy}$, and τ^{yz} are components of turbulent shear stresses, f is the Coriolis parameter, g is the gravitational acceleration, ρ is the water density, and s is the salinity.

Dx, Dy, and κ are the dispersive coefficients of salinity in x-, y-, and z- directions. Eqs. (3.1) and (3.2) are x- and y-components of the momentum equation, eq. (3.3) is the hydrostatic equation, eq. (3.4) is the fluid continuity equation, eq. (3.5) is the salt transport equation, and eq. (3.6) is the equation of state. It is assumed that ρ is a function of salinity only here.

3.1.2 The Layered Three-Dimensional Model

If an estuary can be schematized into a finite number of control volumes as shown in Fig.3.1, and if all the turbulent shear stress terms can be parameterized by flow variables and momentum exchange coefficients, then the equations of motion can be vertically integrated over each layer, and expressed with respect to any control volume in a middle (K^{th}) layer (see Fig.3.1) as (Leendertse, et al., 1973) :

$$\frac{\partial(hU)}{\partial t} + \frac{\partial(hUU)}{\partial x} + \frac{\partial(hUV)}{\partial y} + (wU)_{k-1/2} - (wU)_{k+1/2} - fhV + \frac{h}{\rho}\frac{\partial p}{\partial x}$$

$$- \left(\frac{1}{\rho}\tau^{xz}\right)_{k-1/2} + \left(\frac{1}{\rho}\tau^{xz}\right)_{k+1/2} - \frac{1}{\rho}\frac{\partial}{\partial x}\left(hA\frac{\partial U}{\partial x}\right) - \frac{1}{\rho}\frac{\partial}{\partial y}\left(hA\frac{\partial U}{\partial y}\right) = 0 \quad (3.7)$$

$$\frac{\partial(hV)}{\partial t} + \frac{\partial(hUV)}{\partial x} + \frac{\partial(hVV)}{\partial y} + (wV)_{k-1/2} - (wV)_{k+1/2} + fhU + \frac{h}{\rho}\frac{\partial p}{\partial y}$$

$$- \left(\frac{1}{\rho}\tau^{yz}\right)_{k-1/2} + \left(\frac{1}{\rho}\tau^{yz}\right)_{k+1/2} - \frac{1}{\rho}\frac{\partial}{\partial x}\left(hA\frac{\partial V}{\partial x}\right) - \frac{1}{\rho}\frac{\partial}{\partial y}\left(hA\frac{\partial V}{\partial y}\right) = 0 \quad (3.8)$$

$$w_{k-1/2} - w_{k+1/2} = -\frac{\partial(hU)}{\partial x} - \frac{\partial(hV)}{\partial y} \quad (3.9)$$

$$\frac{\partial(hS)}{\partial t} + \frac{\partial(hUS)}{\partial x} + \frac{\partial(hVS)}{\partial y} + (wS)_{k-1/2} - (wS)_{k+1/2} - \frac{\partial}{\partial x}\left(hDx\frac{\partial S}{\partial x}\right)$$

$$- \frac{\partial}{\partial y}\left(hDy\frac{\partial S}{\partial y}\right) - \left(\kappa\frac{\partial S}{\partial z}\right)_{k-1/2} + \left(\kappa\frac{\partial S}{\partial z}\right)_{k+1/2} = 0 \quad (3.10)$$
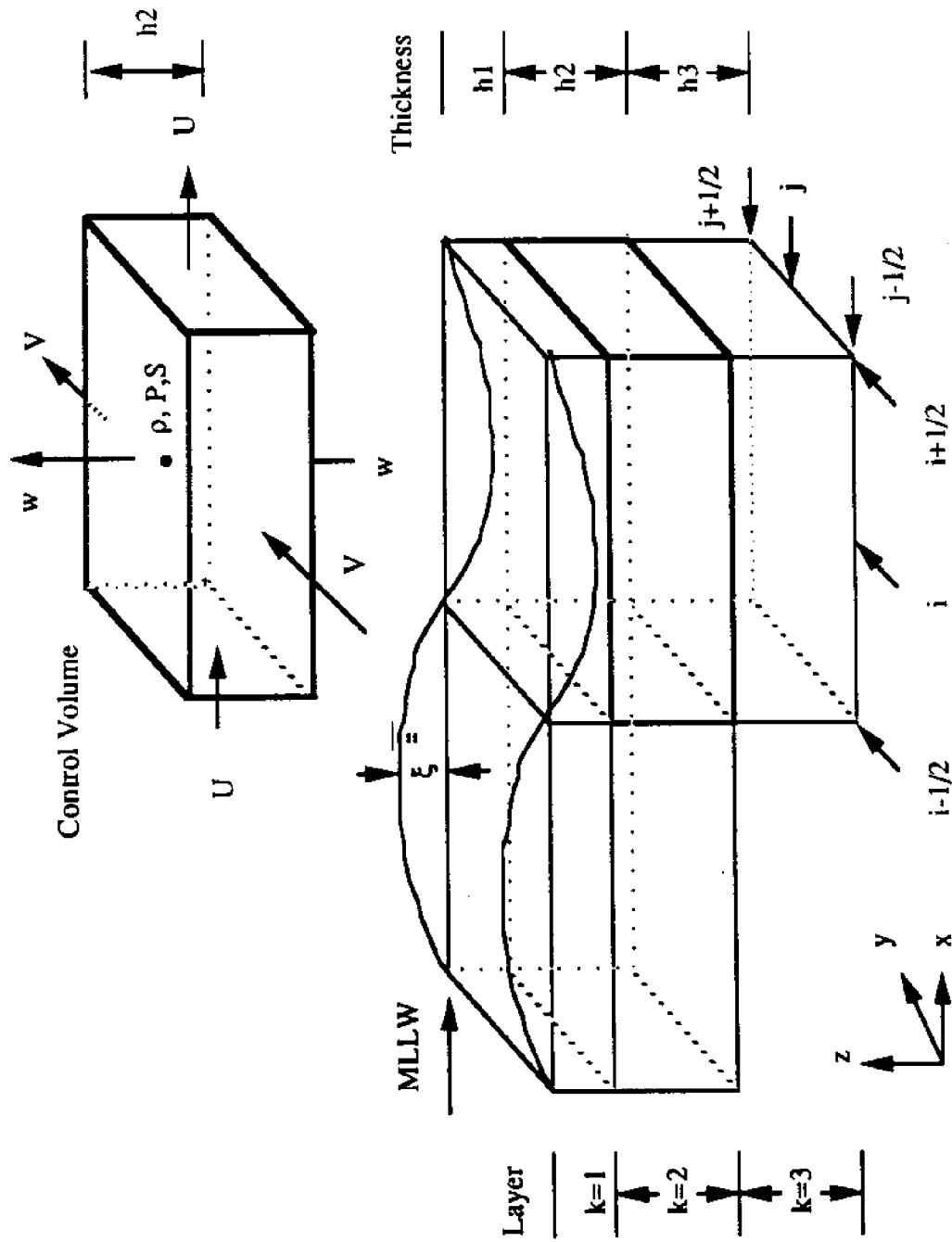
Fig. 3.1 Control volume for hydrodynamics model

where U and V are the layer-averaged horizontal velocities in x- and y- directions, w is the vertical velocity, h is the layer thickness (see Fig.3.1), S is the layer-averaged salinity, p is the hydrostatic pressure, ρ is the water density, and τ^{xz} and τ^{yz} are the x- and y-component turbulent shear stresses between two layers. The last two terms in eqs. (3.7) and (3.8) are turbulent shear stresses on the vertical surface between two adjacent control volumes in the horizontal directions, f is the Coriolis parameter, and A is a horizontal momentum exchange coefficient.

In this model, the horizontal momentum exchange coefficient is defined by a relationship suggested by Leendertse and Liu (1977):

$$A = \gamma \left| \frac{\partial \omega}{\partial x} + \frac{\partial \omega}{\partial y} \right| (\Delta L)^3 \tag{3.11}$$

where γ is a constant, ω is the z-component vorticity ($\omega = \frac{\partial V}{\partial x} - \frac{\partial U}{\partial y}$), and ΔL is the horizontal dimension of the control volume, which is also the minimum size of eddies resolvable by the model.

The vertical momentum exchange in eqs. (3.7) and (3.8) for the Kth layer is represented in the model by:

$$- \left(\frac{1}{\rho} \tau^{xz} \right)_{K-1/2} + \left(\frac{1}{\rho} \tau^{xz} \right)_{K+1/2} = - \left(E \frac{\partial U}{\partial z} \right)_{K-1/2} + \left(E \frac{\partial U}{\partial z} \right)_{K+1/2} \tag{3.12}$$

$$- \left(\frac{1}{\rho} \tau^{yz} \right)_{K-1/2} + \left(\frac{1}{\rho} \tau^{yz} \right)_{K+1/2} = - \left(E \frac{\partial V}{\partial z} \right)_{K-1/2} + \left(E \frac{\partial V}{\partial z} \right)_{K+1/2} \tag{3.13}$$

where E is a vertical momentum exchange coefficient which can be expressed as:

$$E = \upsilon \left| \frac{\partial V}{\partial z} \right| \tag{3.14}$$

in which $V = Ui + Vj$, $\upsilon = L^2$, and L is defined by a simple linear relationship suggested by Sundermann (1974):

$$L = \left\langle \begin{array}{ll} Kv\,Z & \text{if } Z \leq Z_d \\ \\ Kv\,Z_d & \text{if } Z > Z_d \end{array} \right. \tag{3.15}$$

where Z is the local depth measured from the bottom, Z_d is taken as one-fifth of the total depth, Kv is a constant. The values of Kv and γ (in eq. (3.11)) are to be determined for particular estuaries.

In a stratified environment, the vertical momentum exchange coefficient becomes a function of the gradient Richardson number Ri as:

$$E = \upsilon \left| \frac{\partial V}{\partial z} \right| \exp(-rm\ Ri) \tag{3.16a}$$

where Ri is defined as:

$$Ri = -\frac{g}{\rho} \frac{\partial\rho/\partial z}{(\partial V/\partial z)^2} \tag{3.16b}$$

and rm is another parameter (Leendertse and Liu, 1975).

The momentum and continuity equations for the top and bottom layers differ slightly from eqs. (3.7), (3.8), and (3.9). For the top layer, the continuity equation becomes:

$$\frac{\partial \xi}{\partial t} + \sum_{K=1}^{b} \left\{ \frac{\partial(hU)}{\partial x} + \frac{\partial(hV)}{\partial y} \right\}_K = 0 \tag{3.17}$$

where ξ is the free surface elevation with respect to a coastal datum plane (Fig.3.1), and b is the total number of layers in any column of water.

In the top layer, the shear stress terms $(\frac{1}{\rho}\tau^{xz})_{K-1/2}$ and $(\frac{1}{\rho}\tau^{yz})_{K-1/2}$ in eqs. (3.7) and (3.8) are replaced by wind shear stresses as:

$$\left(\frac{1}{\rho} \tau^{xz} \right)_{K-1/2} = \frac{\rho_a}{\rho} C* W^2 \sin \theta \qquad (3.18)$$

and

$$\left(\frac{1}{\rho} \tau^{yz} \right)_{K-1/2} = \frac{\rho_a}{\rho} C* W^2 \cos \theta \qquad (3.19)$$

where ρ_a is the atmospheric density, W is the 10-meter wind speed, θ is the angle between wind direction and model y-axis, and $C*$ is the wind drag coefficient.

For the bottom layer, the shear stresses terms $(\frac{1}{\rho} \tau^{xz})_{K+1/2}$ and $(\frac{1}{\rho} \tau^{yz})_{K+1/2}$ in eqs. (3.7) and (3.8) will be replaced by:

$$\left(\frac{1}{\rho} \tau^{xz} \right)_{K+1/2} = g \frac{U(U^2+V^2)^{1/2}}{C^2} \qquad (3.20)$$

and

$$\left(\frac{1}{\rho} \tau^{yz} \right)_{K+1/2} = g \frac{V(U^2+V^2)^{1/2}}{C^2} \qquad (3.21)$$

where C is a bottom roughness parameter that also needs to be selected for particular applications.

Pressure gradient terms $\frac{\partial p}{\partial x}$ and $\frac{\partial p}{\partial y}$ in eqs. (3.7) and (3.8) are calculated by :

$$\frac{\partial p}{\partial x} = g \frac{\partial \rho}{\partial x} \frac{h}{2} + \rho g \frac{\partial \xi}{\partial x}$$

$$\frac{\partial p}{\partial y} = g \frac{\partial \rho}{\partial y} \frac{h}{2} + \rho g \frac{\partial \xi}{\partial y} \qquad (3.22)$$

where ξ is the water surface elevation with respect to a coastal datum and is determined by eq. (3.17). The terms $g \frac{\partial \rho}{\partial x} \frac{h}{2}$ and $g \frac{\partial \rho}{\partial y} \frac{h}{2}$ represent the baroclinic effects.

Several explicit equations of state have been used by coastal engineers and oceanographers. The one used for this study is suggested by Cokelet and Stewart (1985) :

$$\rho = \rho_0 (1 + 0.790703 \times 10^{-3} S) \qquad (3.23)$$

where ρ_0 is the density of pure water, and S is the layer-averaged salinity in parts of per thousand. This empirical equation is suited for seawater at 10 °C and atmospheric pressure.

In this study, the density in Central Puget Sound is assumed to be constant. In that case, eqs. (3.23) and (3.24) were not solved and the Richardson number in eq. (3.16) is dropped. In the modeling of Elliott Bay, the density effect is modeled by a simpler approach in which the salinity is assumed to be only horizontally transported in each layer. In that case, the salt transport equation (eq. 3.10) is reduced to :

$$\frac{\partial (hS)}{\partial t} + \frac{\partial (hUS)}{\partial x} + \frac{\partial (hVS)}{\partial y} - \frac{\partial}{\partial x}\left(hD_x \frac{\partial S}{\partial x}\right) - \frac{\partial}{\partial y}\left(hD_y \frac{\partial S}{\partial y}\right) = 0 \qquad (3.24)$$

The justification of such modeling of density effects in both Central Puget Sound and Elliott Bay is presented in section 5.1.2.4.

Assuming that all initial and boundary conditions and all the parameter values are given, the unknowns in this model are the velocity components U, V, w, pressure p, salinity S (if density effect

is considered), and density ρ. These unknowns may be obtained only by numerical solution schemes. The particular solution approach adopted in the model is introduced in the next section. The treatment of initial and boundary conditions and the determination of model parameters are given in Chapters 4 and 5.

3.1.3 Three-Dimensional Model Solution Method

The momentum and continuity equations in the above section are solved by Lilly's explicit (leapfrog) mass and momentum conservative finite difference scheme. The lengthy finite difference equations and the integration procedure are given in detail in Leendertse et al. (1973), and will not be repeated here.

Because of its minimal numerical damping property, Lilly's leapfrog scheme is one of the most desirable finite difference methods in computational fluid dynamics (Roache, 1976; Messinger and Arakawa, 1976). However, the leapfrog type scheme is only marginally stable, especially when applied to partial differential equations containing second order derivative terms. The marginal stability makes the leapfrog scheme rather unattractive when long-term simulation is required (Kurihara, 1965; Messinger and Arakawa, 1976).

One of the remedies to the stability problem is the DuFort-Frankel leapfrog scheme. But it has been shown that the DuFort-Frankel leapfrog scheme may not be significantly more stable than the regular leapfrog scheme in multi-dimensional cases (Roache, 1976). The DuFort-Frankel leapfrog scheme also requires a few more computations per time step which could significantly increase the solution time in long-term simulation. The other remedial strategy that had been suggested involves the intermittent use of other dissipative finite difference schemes during the long-term integration of a leapfrog scheme (Kurihara, 1965). Although the incorporation of any of the strategies suggested by Kurihara (1965) in the model would not be difficult, they may again require a

significant increase in computing requirements in long-term simulation.

Leendertse and Liu (1977) in their second three-dimensional model, reformulated the finite difference equations so that the variables are solved implicitly in the z- (vertical) direction to ensure long-term stability. Although the z-direction implicit scheme resulted in only tri-diagonal linear systems of equations, it still does not necessarily allow the use of significantly larger time steps in applications to complex water bodies. The development of a z-direction implicit code is rather difficult.

One simpler method to ensure long-term stability is the use of smoothing (filtering) operators (Richtmeyer and Morton, 1967). The smoothing schemes can be used every N (N is a user input parameter) integration steps to smooth out the undesirable higher modes of the solutions before they are amplified. Recently, a number of efficient and stable smoothing schemes have been proposed by Killworth (1984). One of the convenient smoothing schemes was adopted for the three-dimensional model and is described here.

Let us assume the computation has advanced to time level n+1, and let Q_{n-1}, Q_n, and Q_{n+1} be vectors containing all the model solutions (velocity components, water surface elevation, pressure gradient, etc.) at time levels n-1, n, and n+1, respectively.

The smoothing operation begins by first obtaining intermediate solutions $Q_{n-1/2}$ and $Q_{n+1/2}$ which are defined as:

$$Q_{n-1/2} = (Q_n + Q_{n-1}) /2$$

$$Q_{n+1/2} = (Q_n + Q_{n+1}) /2$$

(3.25)

From these intermediate values solutions, a new $Q_{n+3/2}$ is then recalculated from the model, before the solution procedure advances to the next time level.

For a one-dimensional equation, it has been shown that the above smoothing operator is stable and preserves the accuracy of the leapfrog scheme (Killworth,1984). The smoothing procedure however creates a minor nuisance in that the solutions are no longer available at the regular time intervals once the smoothing operator is used. This problem was eliminated in this study by smoothing the solutions twice (double smoothing) each time the operator is used.

The three-dimensional model can accommodate either tide or velocities (current) as open boundary conditions along any domain boundaries. If tide is used as the boundary condition at an open boundary, then it is assumed that the horizontal velocity gradient in the direction perpendicular to the open boundary is zero. If however, velocity is used as the open boundary condition, then it is assumed that the water surface elevation gradient in the direction perpendicular to the open boundary is zero. Using the staggered grid system, the calculation at any closed boundary (assumed as a vertical wall) is handled by setting the appropriate velocity component (perpendicular to the wall) to zero. The model in the present form does not have the capability to calculate moving boundary conditions as would be observed in the drying and wetting of tide flats.

The above solution scheme was programmed in FORTRAN 77. The code was written in generic form. The code can be used as a multi-layer three-dimensional model or a single-layer two-dimensional depth-averaged model.

This code has been checked against laboratory and field observation data (to be shown in next chapter). Because of its explicit solution scheme, numerical integration requires the use of a very small time step to satisfy the stability criterion. Therefore for large scale application, the three-dimensional version of this model can only be run on supercomputers.

The layer-averaged salt transport equation (eq. (3.24)) is solved by an Eulerian-Lagrangian scheme (Chu et al., 1988) in which

the advection and the diffusion terms of the transport equation are respectively solved with a streamwise coordinate system and a fixed Eulerian coordinate system. The solution approach has been described in Chu et al. (1988).

3.2 Three-Dimensional Particle Tracking Model

One of the main uses of the above hydrodynamics model is the simulation of water movement in Puget Sound. Since the velocity information generated from the hydrodynamics model is massive, and velocities are located on thousands of discrete finite difference grid points, it is difficult to derive transport characteristics from the velocity information alone. One way to help resolving this problem is to use a particle tracking model which can calculate the movement of specific particles in the water from velocity information generated by the hydrodynamics model.

3.2.1 Mathematical Formulation

If a weightless particle is allowed to move from an initial location $\overline{X_0}$ in the water body at time t_0 to a new location $\overline{X_t}$ at time t, this new location $\overline{X_t}$ can be determined by integrating the Lagrangian velocity along the particle pathline, i.e.

$$\overline{X_t} = \overline{X_0} + \int_{t_0}^{t} \overline{U_l} \; (\overline{X}(\overline{X_0},t),t) \; dt \qquad (3.26)$$

where :

$\overline{X_t}$ = location of water particle at time t (a position vector)

$\overline{X_0}$ = location of water particle at time t_0 (a position vector)

$\overline{U_l}$ = Lagrangian velocity of the marked fluid particle

The velocity vectors obtained from numerical hydrodynamics models are usually given on fixed finite difference or finite element nodes (Eulerian velocity). In oscillating tidal flow, the Lagrangian

velocity can be related to Eulerian velocity by Taylor series expansion (Longuet-Higgins, 1969) and expressed as:

$$\overline{U}_l(\ \overline{X}(\ \overline{X}_o,t)\ ,t\ )\ =\overline{U}e(\overline{X},t)=\overline{U}e(\overline{X}_o,t)+\Delta\overline{X}\cdot\nabla\overline{U}e(\overline{X}_o,t) \qquad (3.27)$$

where $\overline{U}e\ (\overline{X}_o,t)$ is Eulerian velocity at $\overline{X}_o$ and at time t, and $\Delta\overline{X}$ is the distance between $\overline{X}_o$ and $\overline{X}_t$. This equation is correct only on the order of $\Delta\overline{X}$, therefore the value of $\Delta\overline{X}$ has to be made very small relative to the length scale of velocity for the equation to apply.

Eqs. (3.26) and (3.27) were used by Awaji (1980,1982) to study tidal exchange through a narrow strait. Since the velocity shear and phase lag were significant near the narrow strait, the tidal exchange caused by the $\Delta\overline{X}\cdot\nabla\overline{U}e(\overline{X}_o,t)$ term was claimed to be important in the case studied. In another study, Chu and Gardner (1986) used Eulerian velocities from a two-dimensional hydrodynamics model to calculate particle movement patterns. The term $\Delta\overline{X}\cdot\nabla\overline{U}e(\overline{X}_o,t)$ in eq. (3.27) was neglected in their study. The equation used in Chu and Gardner (1986) is equivalent to

$$\overline{X}_t=\overline{X}_o+\int_{t_o}^t\overline{U}_e\ (\overline{X}_o,t)\ dt \qquad (3.28)$$

Different from previous particle tracking models which are all two-dimensional, a three-dimensional particle tracking model will be developed in this study. Because of small time steps used in this study (2 to 6 seconds) and weak spatial variations of the amplitude and the phase of the tidal current in the study area, the displacement of a fluid particle caused by the $\Delta\overline{X}\cdot\nabla\overline{U}e(\overline{X}_o,t)$ term is insignificant. In Elliott Bay for example, the velocity $\overline{U}e$ is of the order of 0.3 m/s, which is much larger than the $\Delta\overline{X}\cdot\nabla\overline{U}e(\overline{X}_o,t)$ term, which is 0.003 m/s. Therefore, the $\Delta\overline{X}\cdot\nabla\overline{U}e(\overline{X}_o,t)$ term can be ignored, and the trajectories of fluid particles will be calculated based on eq. (3.28).

Because the Eulerian velocities generated by the hydrodynamics model are known only at the discrete grid points located on the surfaces of the control volumes, the velocity values at any given location between grid points must be estimated by spatial interpolation scheme. The velocity interpolation scheme is described below.

3.2.2 Velocity Interpolation Scheme

A hexahedron formed by connecting three-dimensional finite difference velocity nodes (this velocity could be either U, V, or w from the hydrodynamics model) is shown in Fig.3.2. Since the velocity at its eight corners are known, the velocity at any point P in the hexahedron at any time can be determined by an interpolated function as (Pinder and Gray, 1977) :

$$V_p(\hat{x},\hat{y},\hat{z}) = \sum_{k=1}^{8} N_k \cdot V_k \qquad (3.29)$$

where V_p = velocity at location P (represents a particle P)

V_k = known velocity at the kth corner of the hexahedron

N_k = shape (or basis) function defined at node k. N can be linear, quadratic, cubic or higher order.

$\hat{x}$, $\hat{y}$, and $\hat{z}$ are a special coordinates used to determine the location of the particle inside the hexahedron, and a, b, and c are the length, width, and height of the hexahedron. The linear shape function used in this model is explained in Fig.3.2.

Using this interpolation scheme, the velocity of any particle within any control volume (Fig.3.1) can be interpolated from the velocities (calculated from the hydrodynamics model) at all the neighboring nodes. Unfortunately, owing to the staggered finite difference grid used by the hydrodynamics model, the velocity components u, v, and w are not all located at the same positions in the control volume (Fig.3.1). Therefore, the velocity components, U,
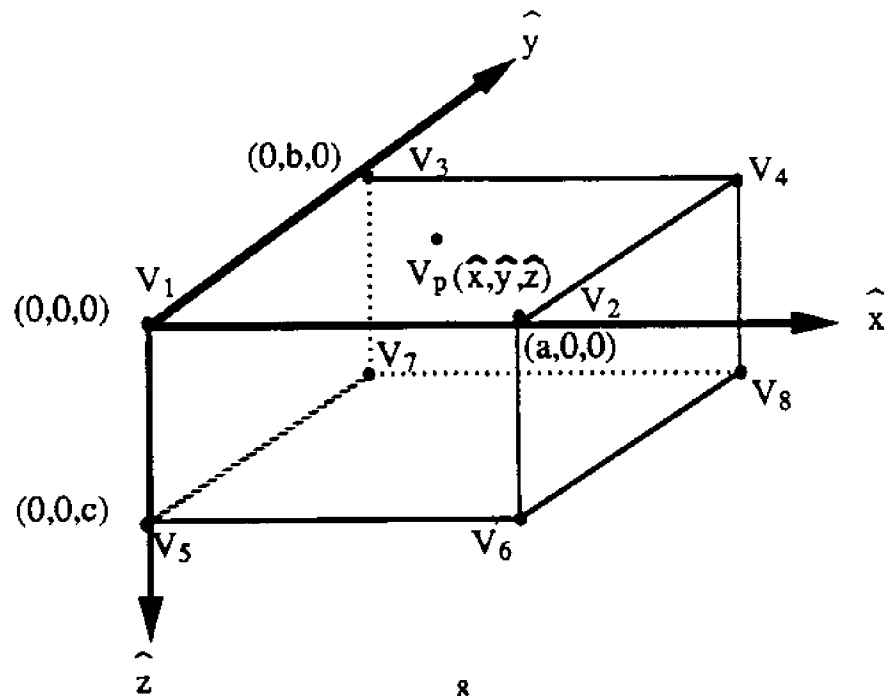
$$V_p(\widehat{x},\widehat{y},\widehat{z}) = \sum_{k=1}^{8} N_k \cdot V_k$$

$$N_1 = (1 - \frac{\widehat{x}}{a})(1 - \frac{\widehat{y}}{b})(1 - \frac{\widehat{z}}{c})$$

$$N_2 = \frac{\widehat{x}}{a}(1 - \frac{\widehat{y}}{b})(1 - \frac{\widehat{z}}{c})$$

$$N_3 = (1 - \frac{\widehat{x}}{a}) \frac{\widehat{y}}{b}(1 - \frac{\widehat{z}}{c})$$

$$N_4 = \frac{\widehat{x}}{a}\frac{\widehat{y}}{b}(1 - \frac{\widehat{z}}{c})$$

$$N_5 = (1 - \frac{\widehat{x}}{a})(1 - \frac{\widehat{y}}{b}) \frac{\widehat{z}}{c}$$

$$N_6 = \frac{\widehat{x}}{a}(1 - \frac{\widehat{y}}{b}) \frac{\widehat{z}}{c}$$

$$N_7 = (1 - \frac{\widehat{x}}{a}) \frac{\widehat{y}}{b} \frac{\widehat{z}}{c}$$

$$N_8 = \frac{\widehat{x}}{a}\frac{\widehat{y}}{b} \frac{\widehat{z}}{c}$$

Fig.3.2 Linear interpolation scheme in hexahedron

V, and w of the particle P will be interpolated separately from known velocity components, U, V, and w which are located at the corners of their respective hexahedron (because of staggered grid system, there is a hexahedron for each velocity component).

The selection of the appropriate hexahedrons (to surround the water particle) will depend on the location of the particle. To determine the location, each control volume is partitioned into eight equal divisions by three orthogonal cuts from each side (Fig.3.3). The model will first identify within which division the particle is located. Then, the velocity components on the corners of hexahedrons surrounding the particle are identified and used to interpolate the velocity at the particle location.

For instance, if a marked particle P is located at the second division of control volume (i, j, k) as shown in Fig.3.4a, then, its velocity can be obtained by interpolating the known velocity components, U, V, and w which are represented in Figs.3.4b, 3.4c, and 3.4d. Since these known velocity components are located on the corners of three different hexahedrons (see Fig.3.5), the velocity of the particle P can be calculated by eq. (3.29). However, due to the relative positions of the control volume to these hexahedrons, the position of the marked particle P at these hexahedrons are all different.

The above approach is appropriate only when the particle is located inside the internal control volumes which do not interact with any boundary. For the control volumes at the air-sea interface (top layer), the ocean bottom (bottom layer) or side boundaries, the above approach would require further modifications. Since the shape and form of land boundaries and bathymetry of any estuary are always very complex, the types of these boundary control volumes, which have at least one no-flow boundary on their surfaces, are rather complex. The design of a method for the proper handling of

3rd cut

2nd cut

1st cut

upper part

lower part

z

y

x
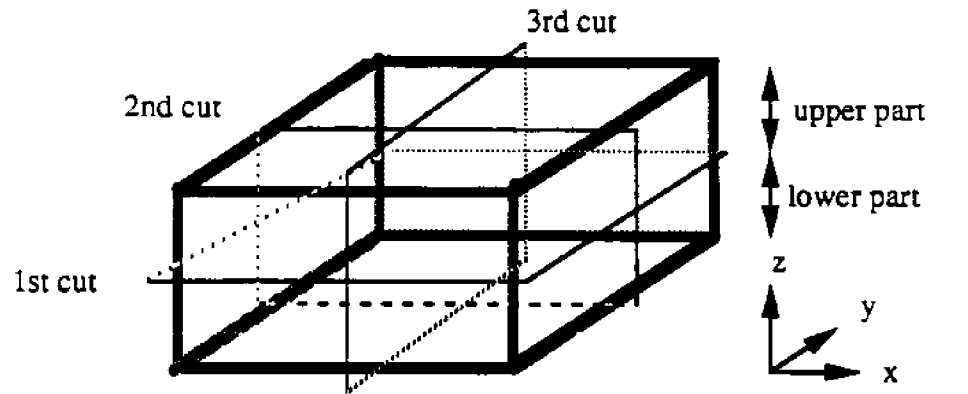
Divide control volume (i,j,k) into 8 divisions

i-1   i   i+1

k-1 layer

w   w   w

U   U   U   U

w   w

k layer

k+1 layer

upper layer

lower layer

z

x

Control volume (i,j,k) from plane view (j section)

i-1   i   i+1

j+1

j | 3 | 4 |
     | 1 | 2 |

j-1   V   U

y

x

upper layer

i-1   i   i+1

j+1

j | 7 | 8 |
     | 5 | 6 |

j-1

lower layer
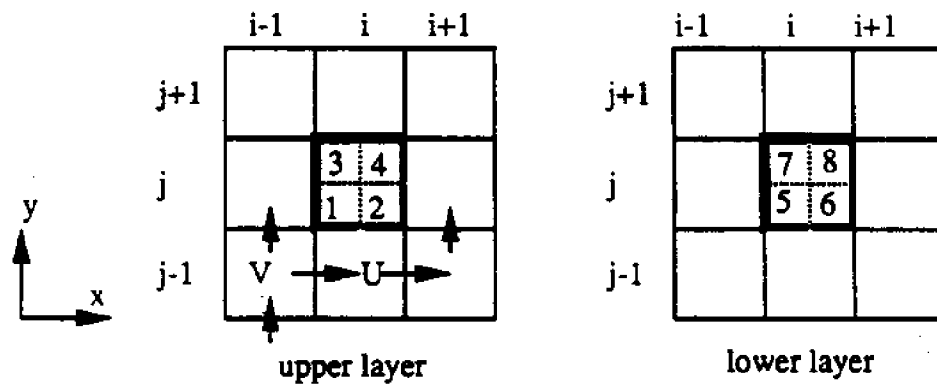
Control volume (i,j,k) form top view (k layer)
The numbers shown are "division numbers"

Fig.3.3 Control volume for particle tracking model

Control volume(i,j,k)
from plane view
(j section)

Control volume(i,j,k)
from plane view
(i section)

Control volume(i,j,k)
from top view
(k layer)
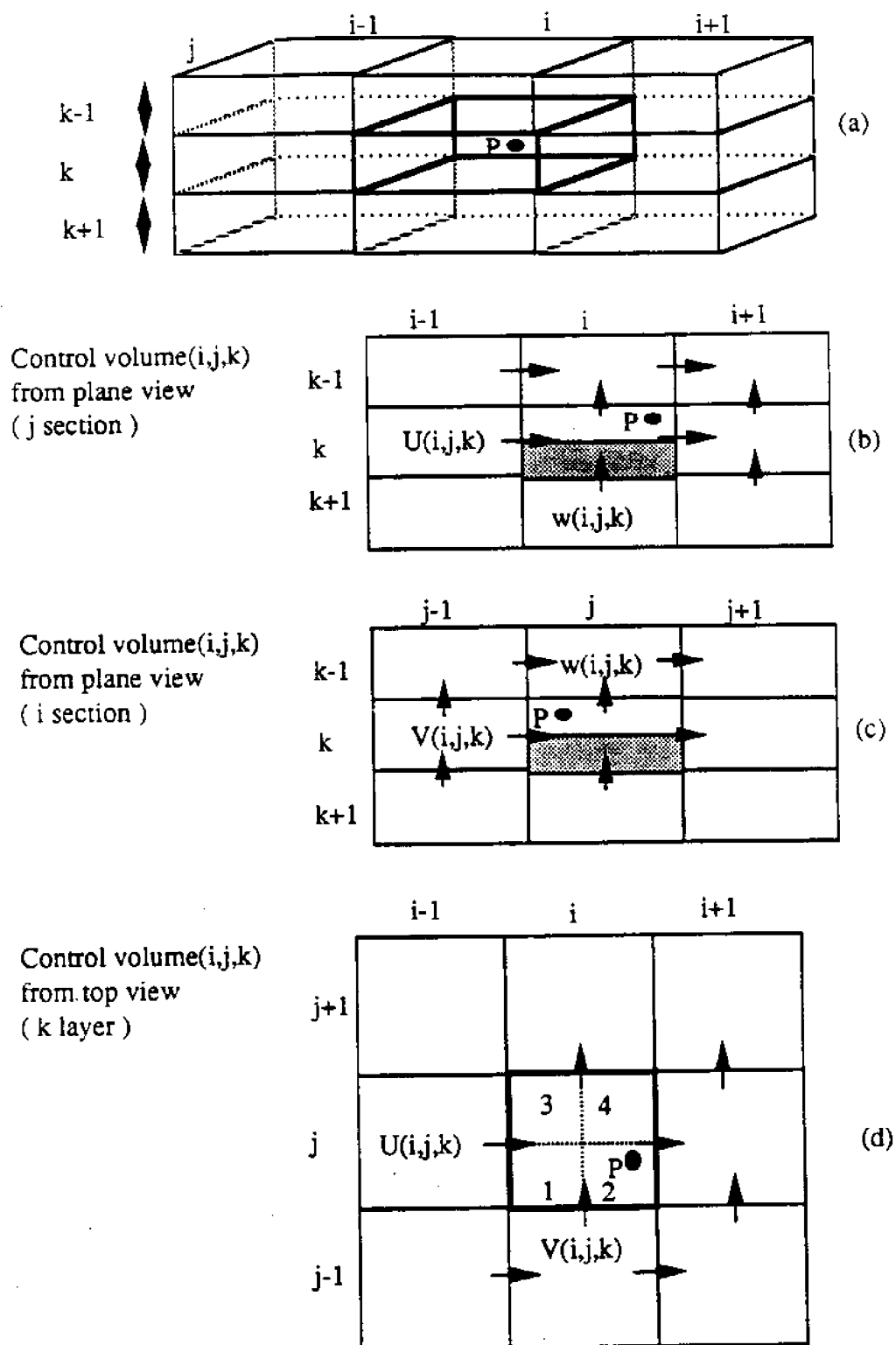
Fig.3.4 Position of marked particle P
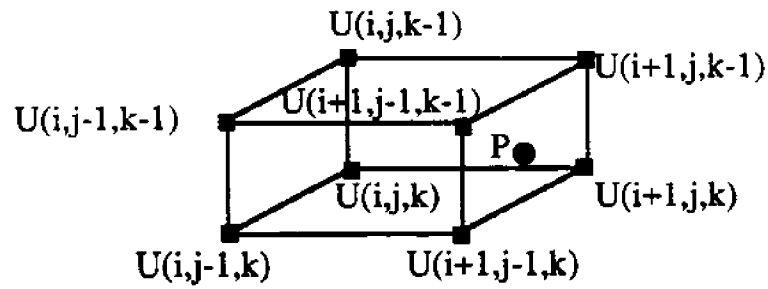
Hexahedron used to calculate U component of particle P
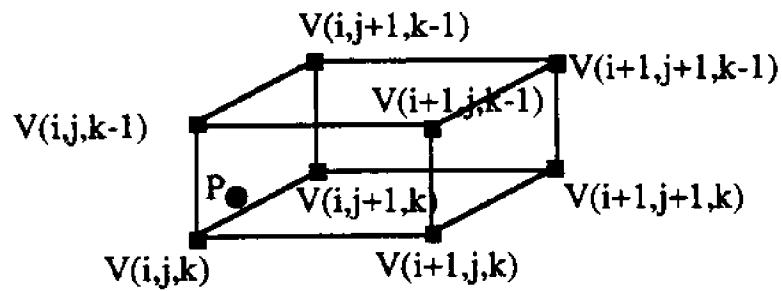
Hexahedron used to calculate V component of particle P
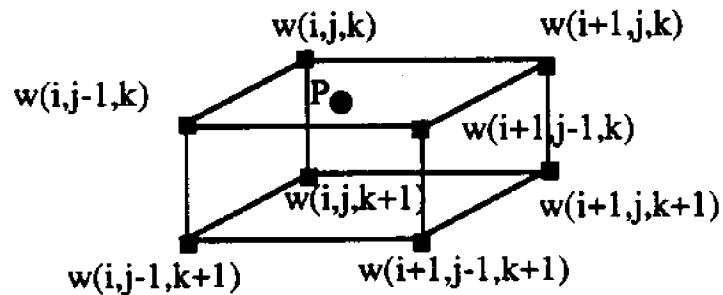
Hexahedron used to calculate w component of particle P

Fig. 3.5 Hexahedrons for velocity components U,V, and w

water particles inside these boundary control volumes is the most difficult task in the development of this model.

3.2.3 Boundary Conditions

The movement of the particles inside the flow domain is governed by mass conservation and momentum principles. However, when these particles in the water reach the boundaries of the calculation domain, such as a no-flow boundary or an open boundary, the calculated movement of these particles is governed by different rules.

Generally speaking, the particle should not be allowed to cross a no-flow boundary (which can be a land boundary or the sea bottom) or the free surface. But because of the discrete solution method used, the particle in the water may advance outside of the domain during any given discrete time increment. When this occurs in the model, this particle will simply be projected back into the domain as shown in Fig.3.6. Once the particle is relocated, it will then be allowed to be carried by the flow in the next time step.

The main difficulty in handling the open boundary conditions for the transport of particles is the lack of flow information outside of the flow domain. When a particle travels across the open boundary to the outside of the domain, its fate is hard to predict. It may be carried back into the domain on the next flood tide or it may leave the domain permanently. Therefore, an appropriate assumption at the open boundary is needed to handle this problem. The assumption for the open boundary depends very much on the flow characteristics near the open boundary, and it differs from one application to another. The open boundary conditions used for Central Puget Sound and Elliott Bay will be determined later.

No flow boundaries include : land boundary
sea bottom
free surface

No-flow boundaries

● t=n+3

□ t=n+3

t= n+1

t=n+2

t= n

t= n
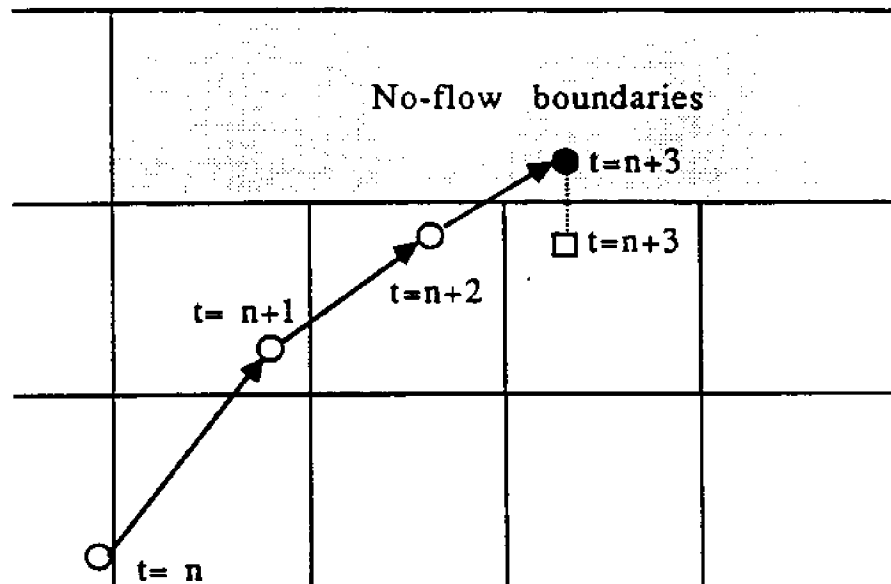
t = Time

O The location of marked particle at different times

→ Flow line

● particle over the no-flow boundary

□ projected location of the particle over the
no-flow boundary

Fig.3.6 No-flow boundary condition

3.2.4 Additional Notes

The developed three-dimensional particle tracking model allows a large number of particles to be released continuously (in every time step) or instantaneously (released once as a pulse) from any location within the domain at any time. This feature could allow the model to simulate the movement of contaminants (labeled by the particles) from various point and nonpoint sources within the flow domain. However, because dispersion is neglected, this model is appropriate only for the cases where the transport is dominated by advection alone.

The hydrodynamics model only provides velocity information at discrete nodal points. Based on this information, the interpolation scheme computes the velocity values at any location within the domain. The accuracy of this interpolated velocity information is only as good as that of the calculated velocities at the grid points. If the velocity structure between two grid points is smooth, then the interpolation idea will work quite well. If the flow pattern is complex, especially when eddies (of grid size or larger) are present, then the interpolated velocity may not be accurate enough. To ensure proper accuracy of the particle tracking model, smaller time and spatial steps in the hydrodynamics model and higher order interpolation schemes must be used.

So far, the particles have been assumed weightless so that they can only be passively carried by the flowing water. For the simulation of the transport of certain pollutants, such as dredge spoil, the model can be modified to include a settling velocity for the particles considered. Such settling velocity depends on the density, shape, volume, and chemical properties of the pollutants and the flow conditions around them. Some theoretical and empirical values from previous research can be used in such cases.

This developed particle tracking model can be attached to the hydrodynamics model. The time increment used in the integration of eq. (3.28) can therefore be as small as the time step used in integrating the hydrodynamics model. A smaller time step however requires more computer time. The application of this model is introduced in Chapter Five.

CHAPTER FOUR

MODEL VALIDATION

The Fortran 77 code of the developed three-dimensional model consists of several thousands statements and many complicated arrays. All computer codes of this scale should be validated before they are applied for any engineering or scientific purposes. Validation is a process through which the results of the codes are compared with analytical solutions, experimental data, field observations, or even numerical results from other models so that coding errors, numerical properties, and capabilities (and limitations) of the model can be determined. Validation does not necessarily mean calibration and verification (Chu and Yeh, 1985).

To validate the hydrodynamics model, results from the model were compared with data obtained from a laboratory experiment and field observations. The laboratory data were provided to us by Nece (1989) and field data of Puget Sound collected and analyzed by scientists from PMEL / NOAA (Mofjeld and Larsen, 1984; Lavelle et al., 1988).

4.1. Comparison with Laboratory Data

In unrelated research on the distortion effect of a physical hydraulic model and its relationship with numerical models, Nece and Falconer (1989) collected a set of "depth-averaged" current data from a laboratory tide tank (Fig.4.1) at University of Bradford. The data set was made available for comparison purposes in this study by Prof. Nece. The laboratory experimental procedure and the comparison between one particular data set from Nece and Falconer (1989) and the hydrodynamics model results are presented here.

The laboratory tank has a spatial dimension of length 5.3 m, width 3.8 m, and depth 0.60 m. A model marina covers a square area, 1.08 m by 1.08 m (432 m by 432 m in prototype) and has a

1860mm ▯ The numerical domain for present study

1860mm

Water Supply Manifold

Platform Width = 3000 mm

400 mm

Fixed Wall

Fixed Wall

Tide
Weir

Marina

1080 mm

120 mm

3800
mm

Honeycamb
Baffle

Sloping
Beach

Movable Walls

1080 mm

Tide Gage

Fixed Wall

5300 mm

5900 mm

Tide Tank-Plan

Overflow

320 mm

Weir Manifold

280 mm

620
mm

Section through Harbour
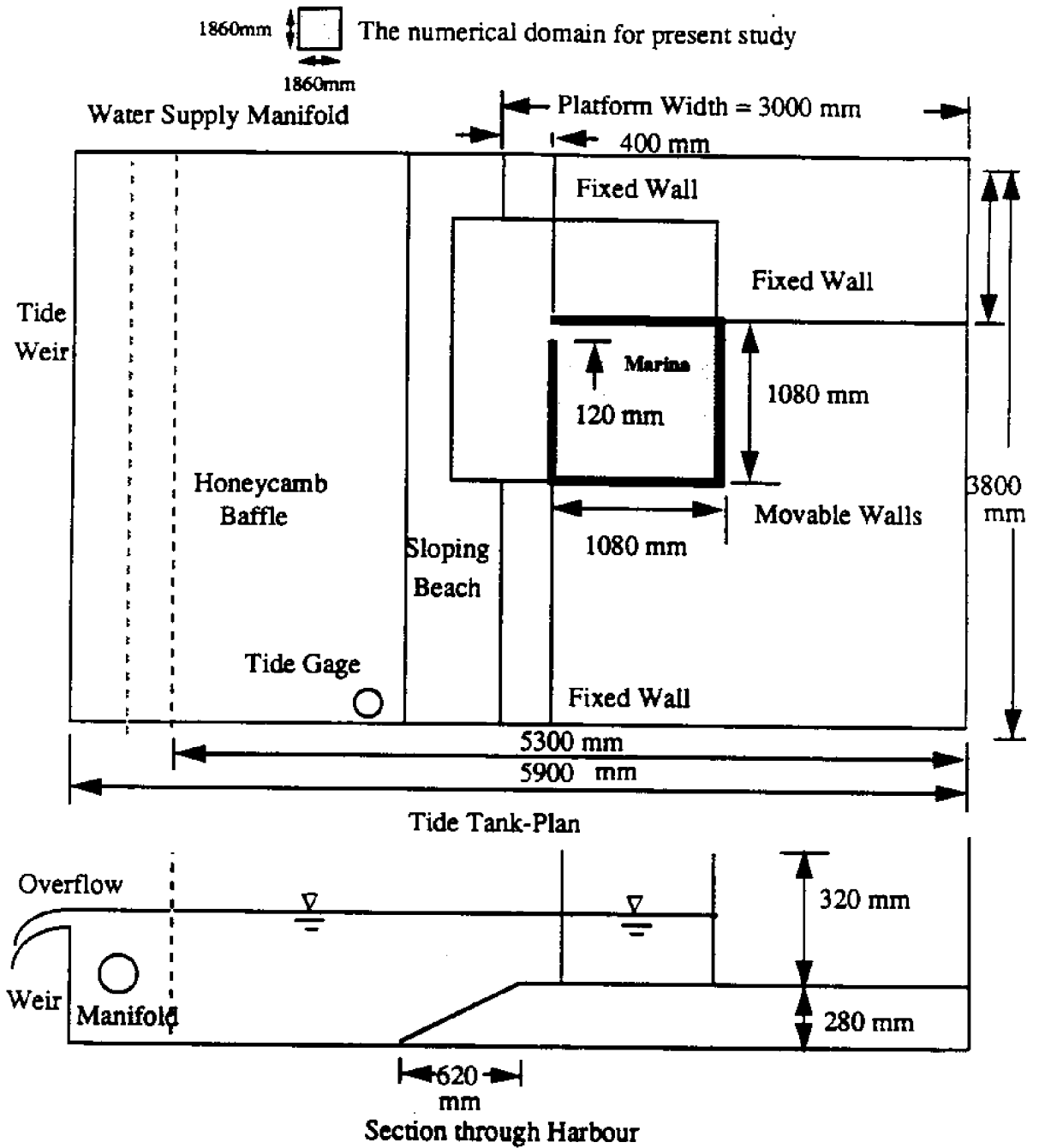
Fig.4.1 Laboratory tide tank at University of Bradford
(from Nece and Falconer, 1989)

mean water depth 0.15 m (6 m in prototype) as shown in Fig.4.1. The vertically distorted model thus had a horizontal length scale ratio of 1 : 400 and vertical length scale ratio of 1 : 40. The tidal boundary condition is represented by a simple sinusoidal tide function with a period of 708 seconds (12.42 hours in prototype) and range of 0.1 m (4 m in prototype) (Fig.4.2).

The depth-averaged velocity data in the study marina were determined from plotted pathlines of 5 mm diameter plastic fishing bobbers which were released into the water. In order to maintain the floats in a vertical orientation that penetrates most of the water column (and therefore obtaining the depth-averaged current), these floats of selected length were weighted with lead shot. The floats were tracked visually. The positions of floats were marked by hand at two-second increments on a perspex overlay sheet. Then, these plotted pathlines of floats were used to calculate the velocity components U and V based on $U = dx/dt$ and $V = dy/dt$.

According to Nece (1989), all hydraulic model runs began with the weir at its lowest level and with no residual currents in the tank; time were measured from the start of weir operation, at $t = 0$ second. The data collected were depth-averaged velocity profiles along the axes AOC and BOD shown in Fig.4.3, on flood and ebb tides at t=177 seconds and 531 seconds respectively (Fig.4.2). Three velocity data sets were collected for different distortion ratios tested.

These velocity data also have been compared with the results calculated from a two-dimensional depth-averaged model (Nece and Falconer, 1989). In the numerical model application, the calculation domain covered an area with 29 x 29 60 mm square grids (Fig.4.4). The open boundary condition prescribed was the tidal elevation on the boundary parallel to the marina entrance. The boundaries perpendicular to the marina entrance were regarded as free streamlines with normal velocity component and lateral velocity gradient equal to zero. Using the same grid resolution, and boundary
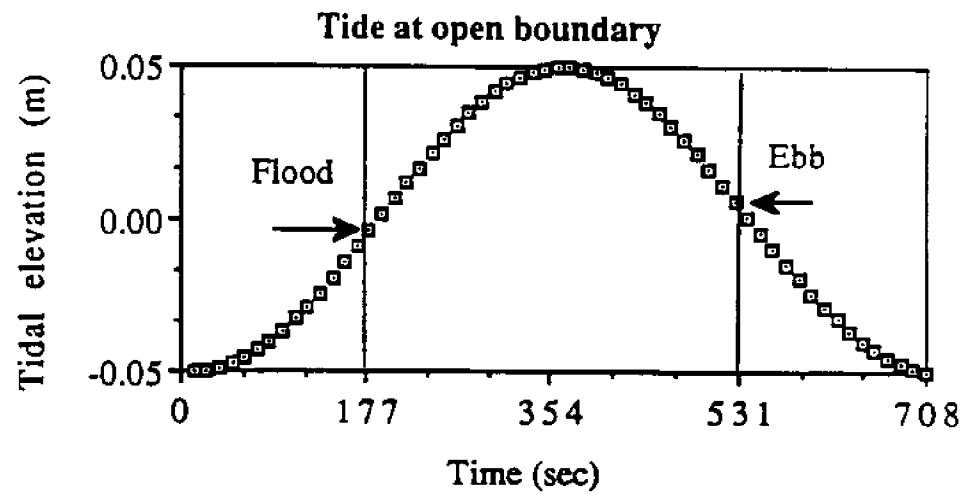
Fig. 4.2 The tidal elevation at open boundary
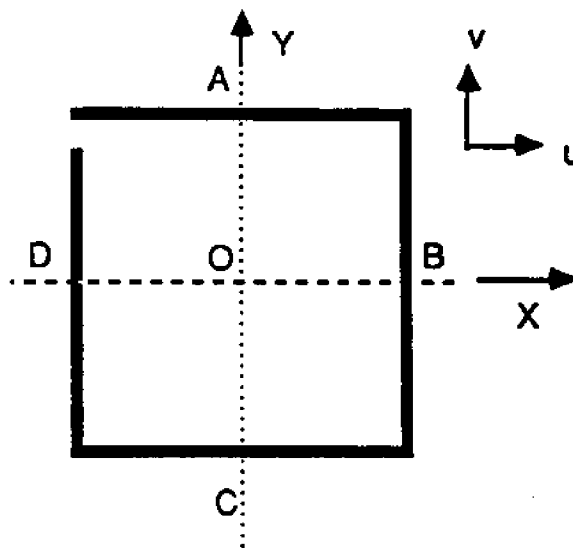
Fig.4.3 The coordinate system of the marina

dy = 60 mm

☒ open boundary

☐ land

☐ water

dx= 60 mm
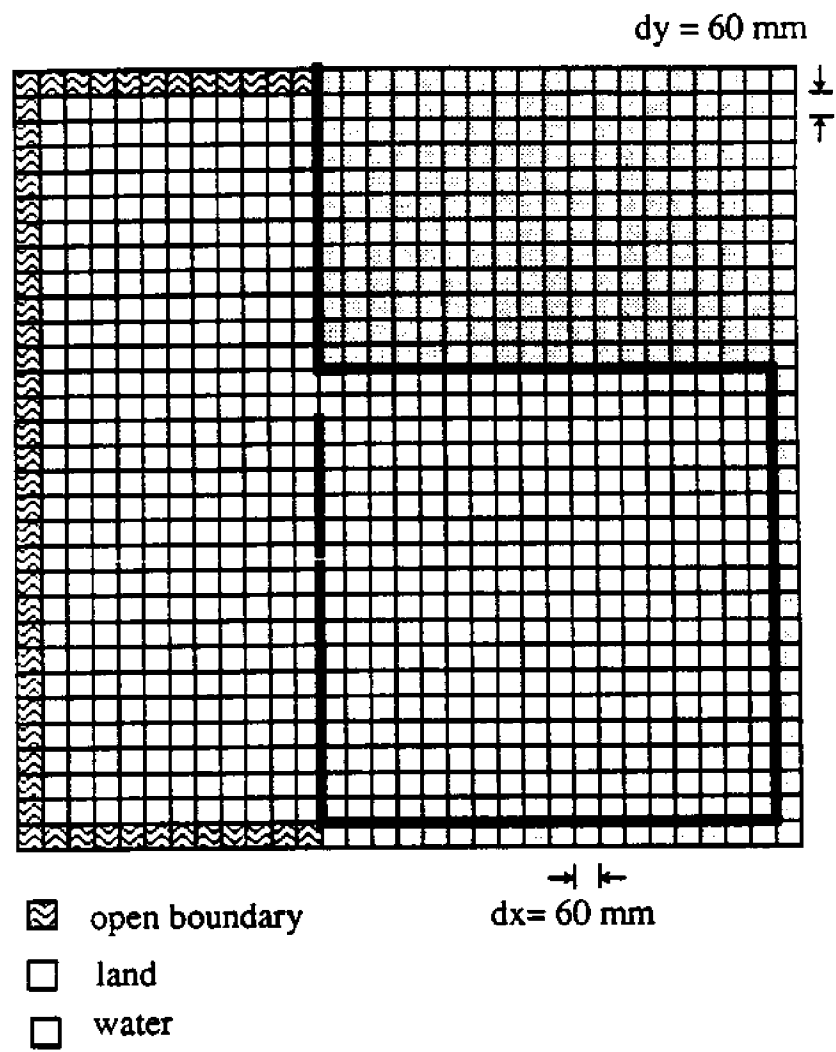
Fig.4.4 The mesh and domain of the numerical model

conditions, the developed three-dimensional hydrodynamics model was compared with one of the laboratory data sets (for distortion ratio of 1:10 as described above) from Nece (1989).

Because the laboratory data were designed to provide data for verifying two-dimensional depth-averaged hydrodynamics models, the developed three-dimensional hydrodynamics model can only be run as a one layer model. In the comparison study, the data will be taken not as those from a physical model for a prototype but as actual data in the tide tank. To model the laboratory-scale marina, the domain used has a square area, 1860 mm by 1860 mm, which covers the entire model marina and the region just beyond the marina entrance as shown in Fig.4.1. This model domain is selected so that we can avoid using the narrow marina entrance as open boundary. When the 60-mm grid spacing is used, the model domain will consists of a mesh of 31 x 31 grid squares (Fig.4.4) in this test.

Similar to Nece and Falconer (1989), the open boundary conditions in this study are specified as shown in Fig.4.5. A sinusoidal tide, $\xi=0.05COS(t / T- \pi - \Delta\phi)$, was specified at the open boundary parallel to the plane of marina entrance (section a in Fig.4.5), where ξ is the tidal elevation (meter); t is the time (second); T is the 708-second period and $\Delta\phi$ is the phase lag (6 degrees) between weir elevation curve and tide curve. For the other two open boundaries perpendicular to the marina entrance plane (sections b and c in Fig.4.5), the boundary conditions were assumed to be free streamlines with velocity component V equated to zero and a free slip boundary condition giving rise to a zero lateral velocity gradient along the boundary. In the no-flow boundaries, the no-slip boundary condition was prescribed.

Since two tidal periods spin-up time was required in this study, the numerical model was started from a state of rest at low tide and run for three tidal periods with a time step of 0.012 second. These runs took 30 minutes of CPU time on a Cray X/MP 48. The numerical
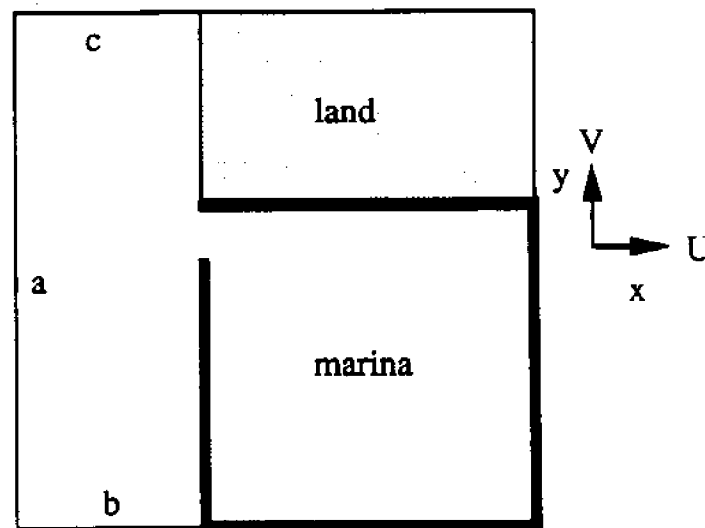
open boundary conditions at sections

a : tidal elevation $\xi = 0.05 \cos(\text{time}/708(\text{sec.})-3.2463)$

b and c : velocity $V = 0$ and $\dfrac{\partial U}{\partial y} = \dfrac{\partial V}{\partial y} = 0$

Fig.4.5 Open boundary conditions of numerical model

model was calibrated by adjusting the values of horizontal momentum exchange parameter γ (in eq. (3.11)) and bottom roughness coefficient C (in eqs. (3.20) and (3.21)). With a C value of 20 $m^{1/2}s^{-1}$ and γ of 20 kg/m^3, the model produced the best matches to the observations.

The calculated flow patterns at ebb tide (at t=177 seconds) and flood tide (at t=531 seconds) at the third period are shown in Figs.4.6 and 4.7. On the flood tide, the current enters the marina from the entrance and is forced to form a marina-scale clockwise circulation gyre. This circulation has strong and narrow current on the right and top boundaries of the marina as plotted in the figure rather than on the left and bottom boundaries. On the ebb tide, the clockwise circulation still exists but it has become much weaker. At this time, the flow goes out the marina from the left and not the top side boundary of the marina because of the effect of clockwise residual circulation. Although there are not enough data to verify these calculated flow patterns, they appear reasonable. On the ebb tide, the locations of the stagnation point on the "top" boundary agrees with observed flows in the laboratory tank.

The velocity profiles along axes AOC and BOD on ebb and flood tides (Fig.4.3) were compared with laboratory data (Nece,1989) and shown in Figs.4.8, 4.9, 4.10, and 4.11. These comparisons reveal that the results of numerical model and laboratory model match pretty well in most parts except the maximum values of velocity components U in AOC axis (Fig.4.8) and V in BOD axis (Fig.4.9) on the flood tide. These discrepancies are analyzed below.

On the flood tide, the strong flow enters the marina from the narrow entrance like a jet. Although this jet is slowed down by the upper (top) boundary wall and the water around it, it still moves ahead along the marina walls. This explains why the maximum velocity components U and V are near the top and right side boundary walls respectively. Due to the same reason, the velocity
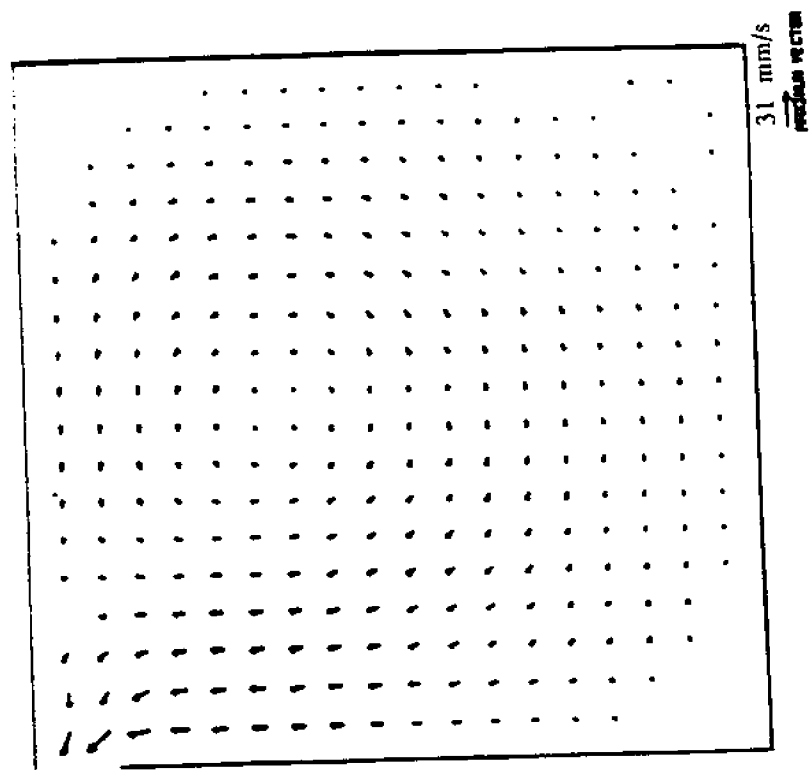
at t= 531 seconds

Fig.4.7 Flow pattern on ebb tide
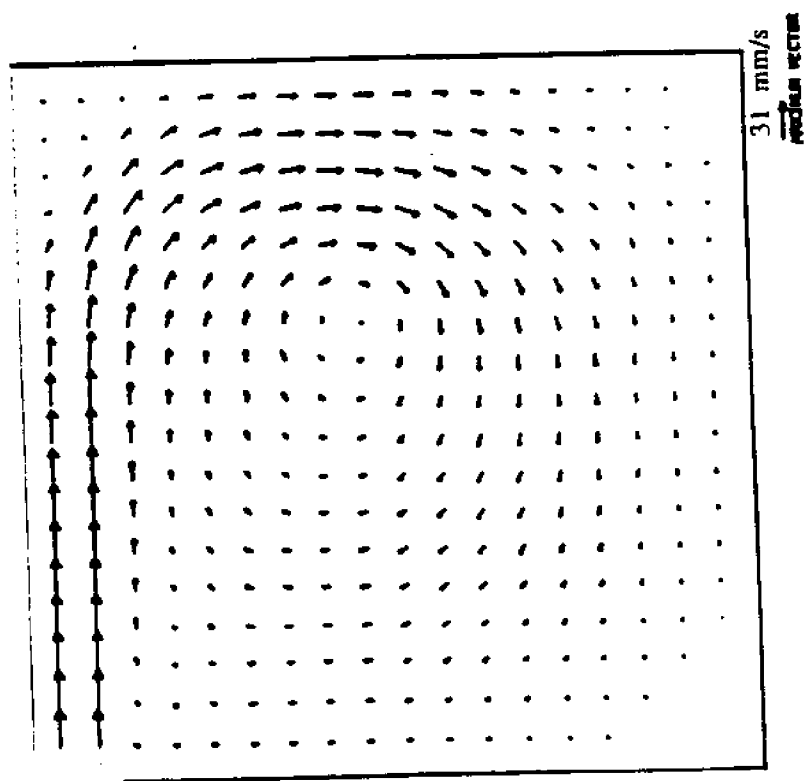
at t= 177 seconds

Fig.4.6 Flow pattern on flood tide

Velocity U at AOC axis
- flood tide

Velocity V at AOC axis
- flood tide
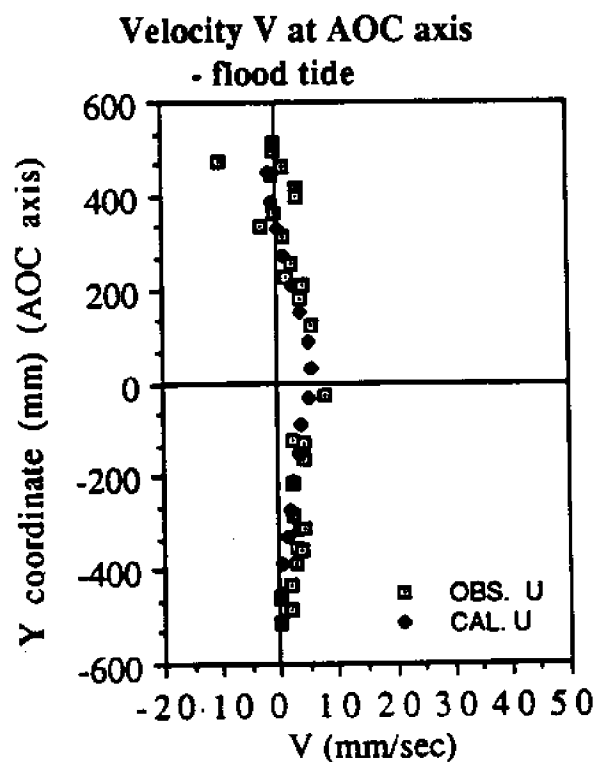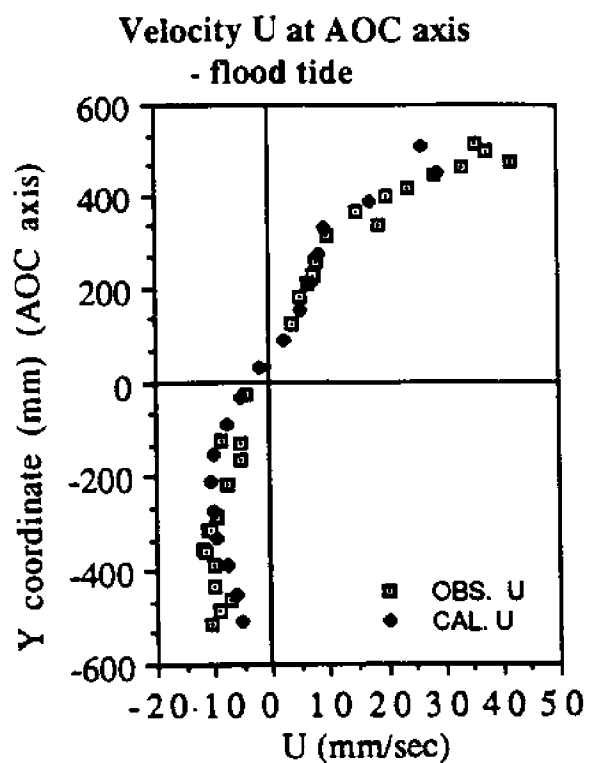
Fig. 4.8   Velocity at AOC axis on flood tide

Velocity U at BOD axis - flood tide

Velocity V at BOD axis - flood tide
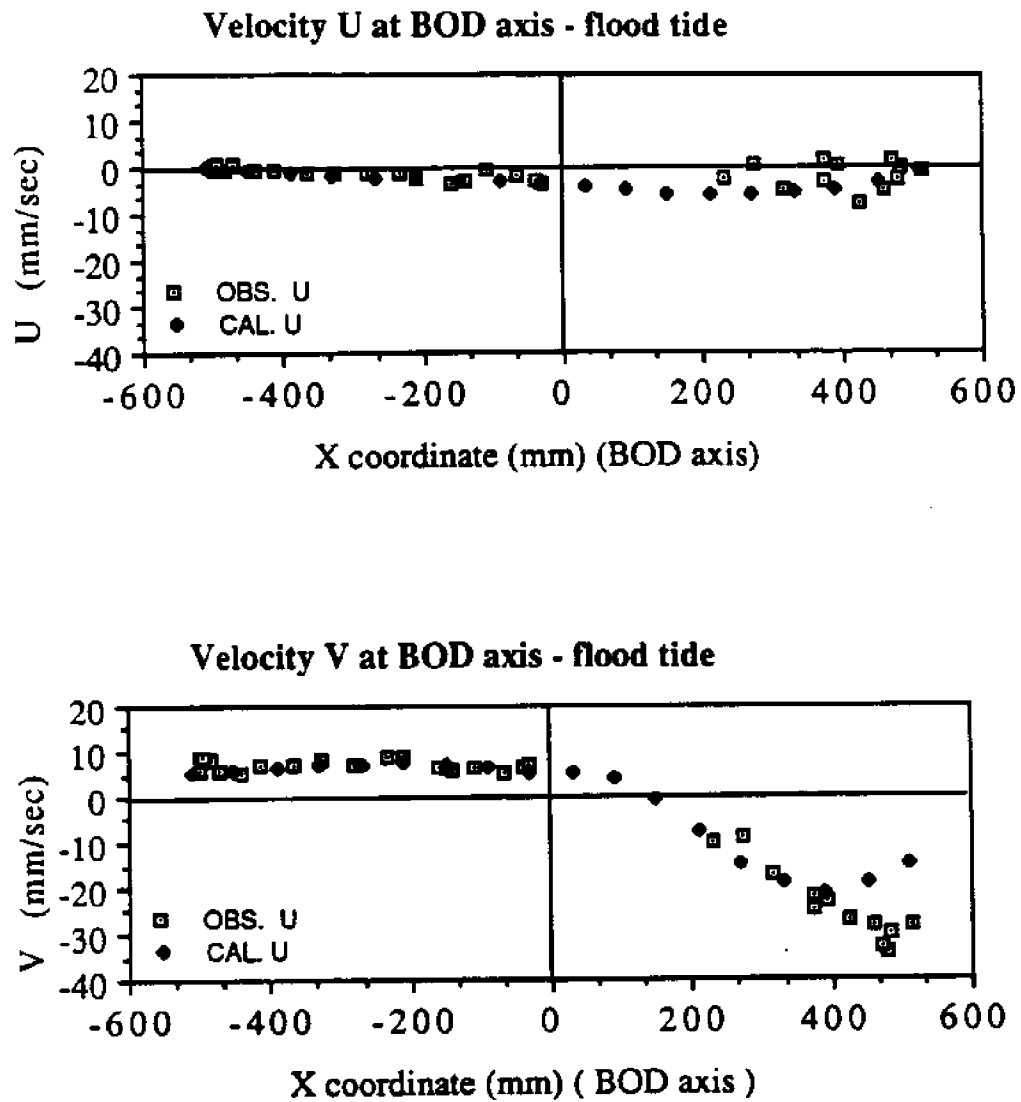
Fig. 4.9 Velocity at BOD axis on flood tide

Velocity U at AOC axis
- ebb tide

Velocity V at AOC axis
- ebb tide
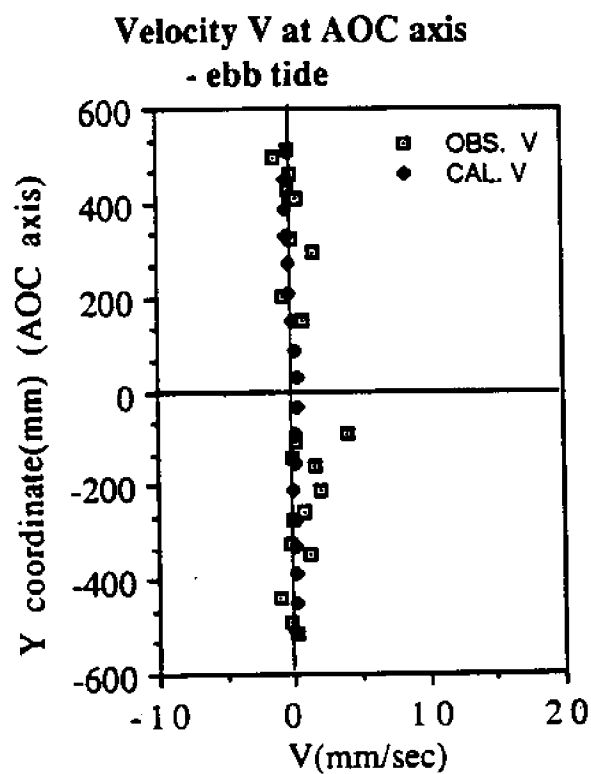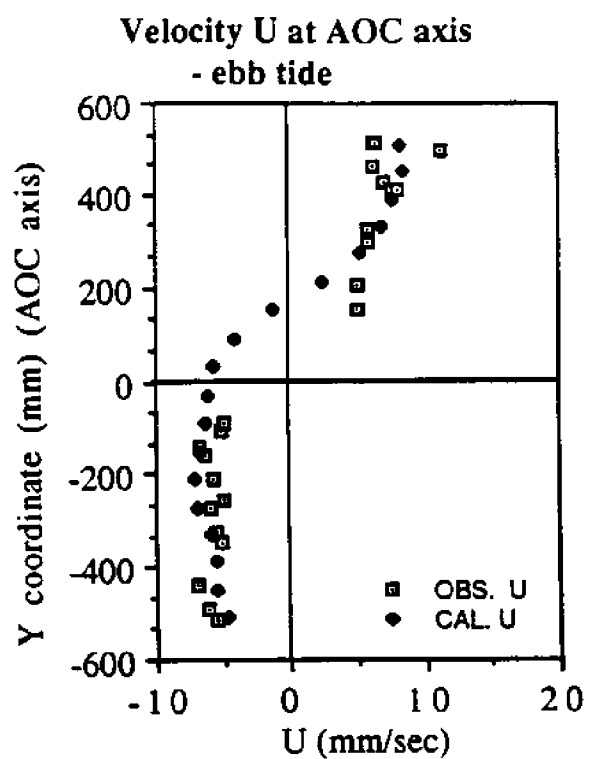
Fig. 4.10 Velocity at AOC axis on ebb tide

Velocity U at BOD axis - ebb tide

Velocity V at BOD axis - ebb tide
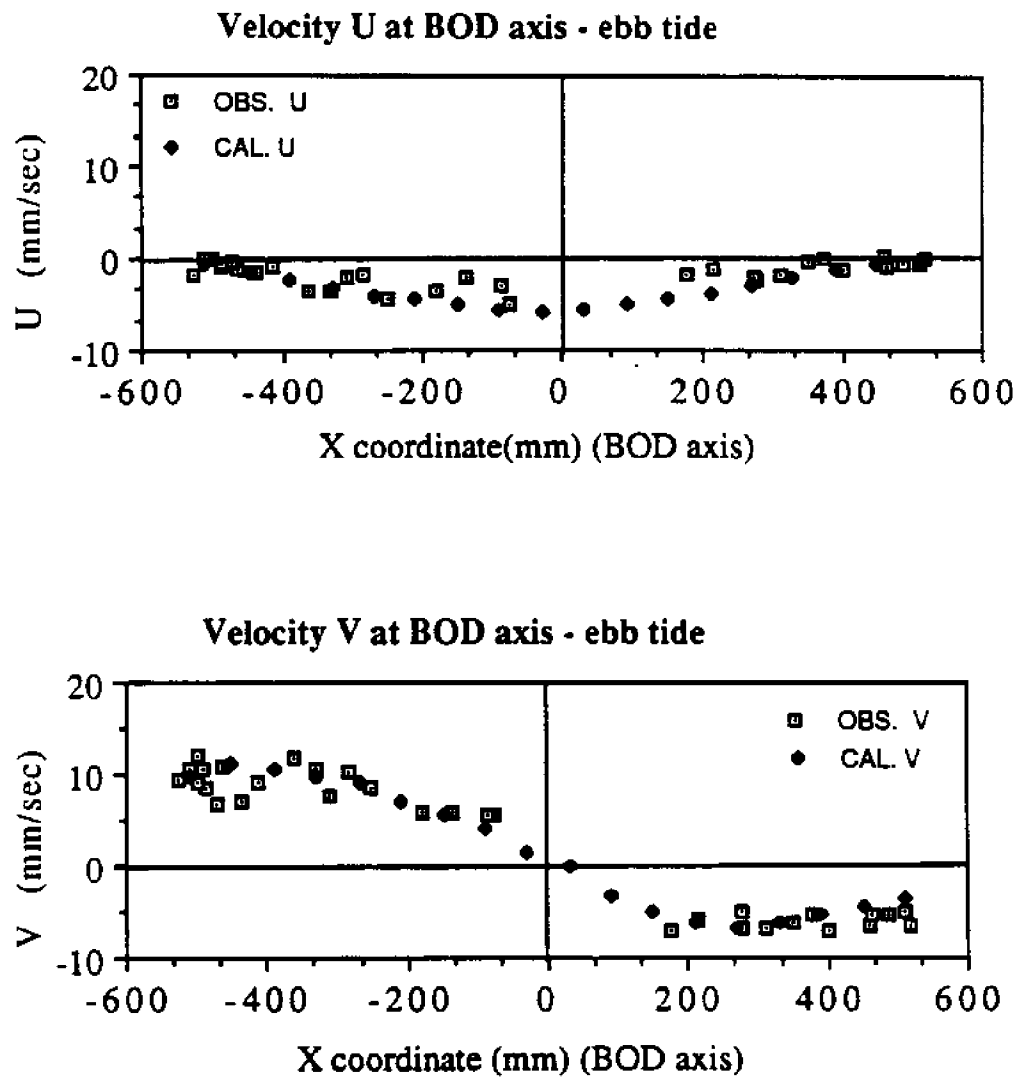
Fig. 4.11 Velocity at BOD axis on ebb tide

gradients near these walls are also very high. In this study, these high velocity gradients near the marina entrance were resolved by only two grid spaces. The grid resolution is probably still not fine enough. However, on the ebb tide, the velocity comparisons between model results and laboratory data are much better in the same areas with the same grid resolution (see Figs. 4.10 and 4.11). This may be ascribed to weak velocity gradients on the ebb tide. Based on the above argument, it is concluded that the discrepancies in Figs.4.8 and 4.9 are caused mainly by inadequate resolution of high velocity gradients in the immediate vicinity of marina entrance where the grid spacing did not take account of the contracting streamlines around the tip of the "breakwater" as the flow entered the marina. The zero order turbulence closure scheme and numerical errors in the model could be the other reasons for these discrepancies.

4.2 Comparison with Field Observations (Central Puget Sound)

The region in Puget Sound chosen for the comparison study is that part of the main basin from Point Wells to The Narrows at Tacoma, referred to in the study as Central Puget Sound (Fig.4.12). This particular area was selected for three main reasons. First, the region covers the major population centers and some of the most polluted urban embayments in Puget Sound. Second, a relatively large amount of existing data were available at several oceanographic observational stations. Third, and most important from a modeling standpoint, the northern and southern boundaries (Point Wells and The Narrows) of the study area coincide with two cross-sections used in a channel tide model by Lavelle et al. (1988), at which the calculated tidal transports from the channel model can be used as boundary conditions for the study numerical model.

Using a 762 m by 762 m square finite difference grid, the Central Puget Sound area was schematized and represented by the model as shown in Fig.4.13. To minimize the number of dry nodes

Point Wells

LIBERTY
BAY

Port Madison

6

BAINBRIDGE
ISLAND

West Pt.

DYES
INLET

Elliott Bay

SEATTLE

Alki
Pt.

Duwamish
River

YUKON
HBR

Blake
Island

BREMERTON

East

Three Tree Pt.

N

VASHON
ISLAND

Passage

Colvos Passage

Maury
Island

Dalco Passage

5 km   The Narrows

3

5

Commencement Bay

2

TACOMA
Puyallup River
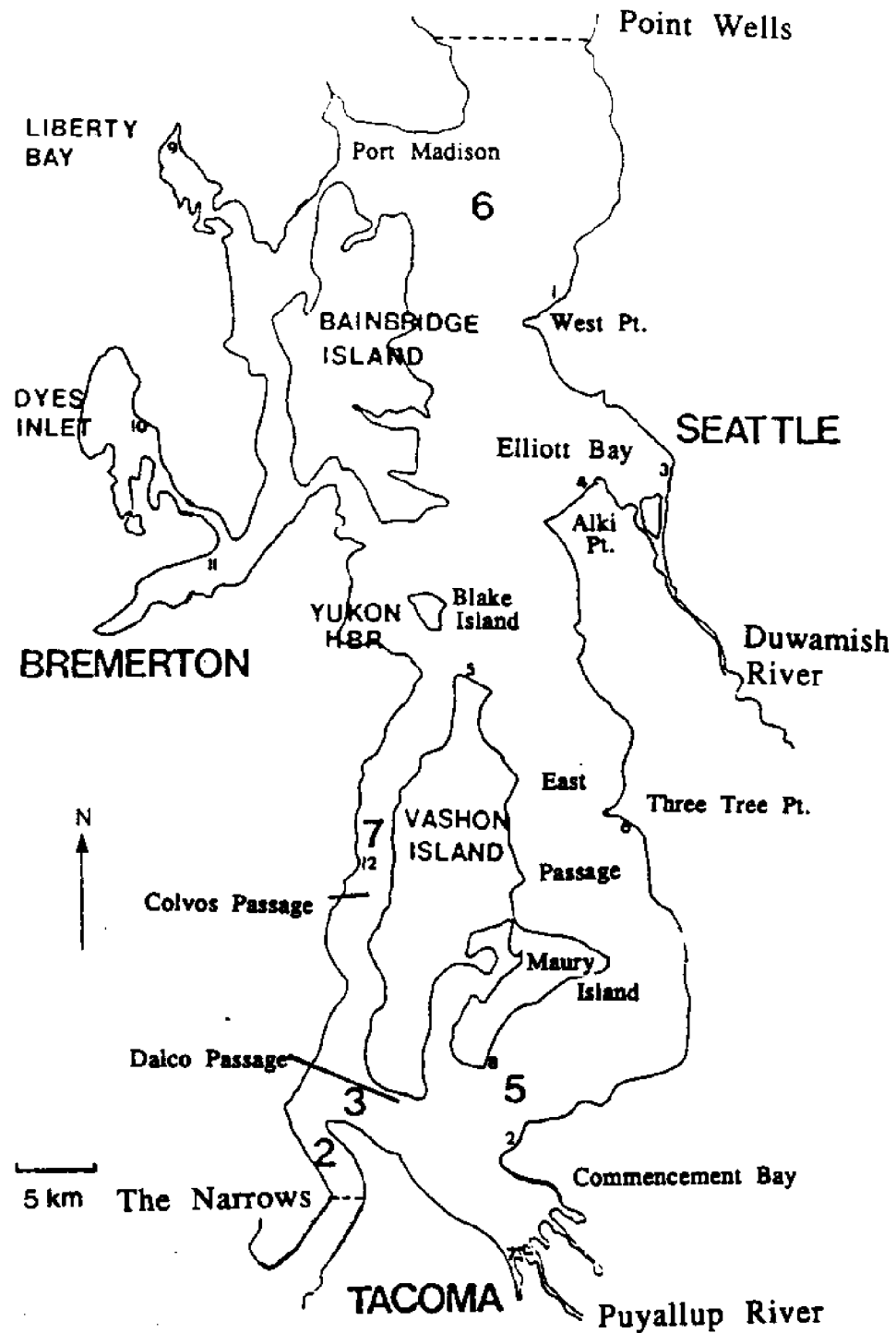
Fig.4.12 Central Puget Sound - study area. The large bold numbers
represent NOAA MESA current station, the small numbers
represent tide stations, and the dashed lines represent the open
boundaries of the model
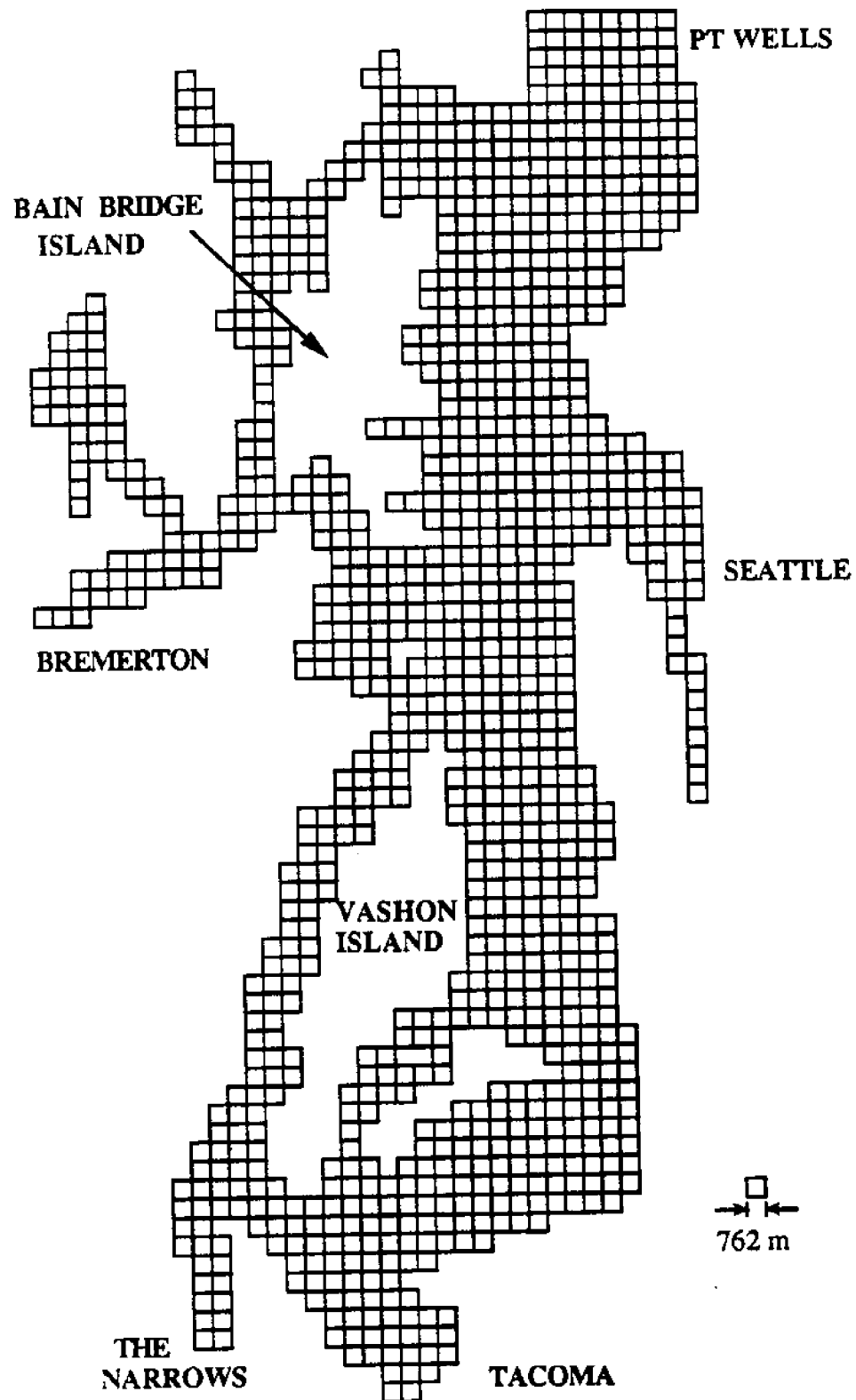
Fig.4.13 Horizontal resolution of Central Puget Sound

(nodes that cover dry land or islands) and provide the best resolution of the essential geometric features with this orthogonal grid system, the model area grid was rotated 10 degrees counterclockwise from the magnetic north on National Ocean Survey Chart No. 18440. Except for some narrow channels and river channels, the chosen resolution captures most of the essential geometric features of Central Puget Sound.

Bathymetry information at all grid nodes for the models was interpolated from data points on National Ocean Survey Chart No. 18440. The contours of Central Puget Sound bathymetry are shown in Fig.4.14. The study model resolved the bathymetry in two variable thickness layers. The first layer has a variable thickness of 60 meters or less. The second layer resolved the deeper portion of Central Puget Sound with a variable thickness that follows the Sound's bottom bathymetry.

Because most of the presently available field data were not collected for the purpose of numerical modeling, clearly defined boundary conditions for modeling Central Puget Sound simply do not exist. For this study, the boundary conditions were obtained from a channel tide model. The channel model divides the entire Puget Sound into a series of 79 connected one-dimensional channels (Fig.4.15). Forced by tides at the entrance (Admiralty Inlet), the water level changes within each channel and transport through the cross-sections connecting the channels is calculated from one-dimensional continuity and momentum equations. The model results have been shown to have matched the observed tidal characteristics of most major tidal constituents through the Sound (Lavelle et al.,1988).

The calculated semidiurnal (M_2) and diurnal (K_1) components (two of the most significant tidal components) transport at Point Wells and The Narrows were used as boundary conditions for the model in the present study. To do that, the cross-sectionally

Contour interval
10 fathoms
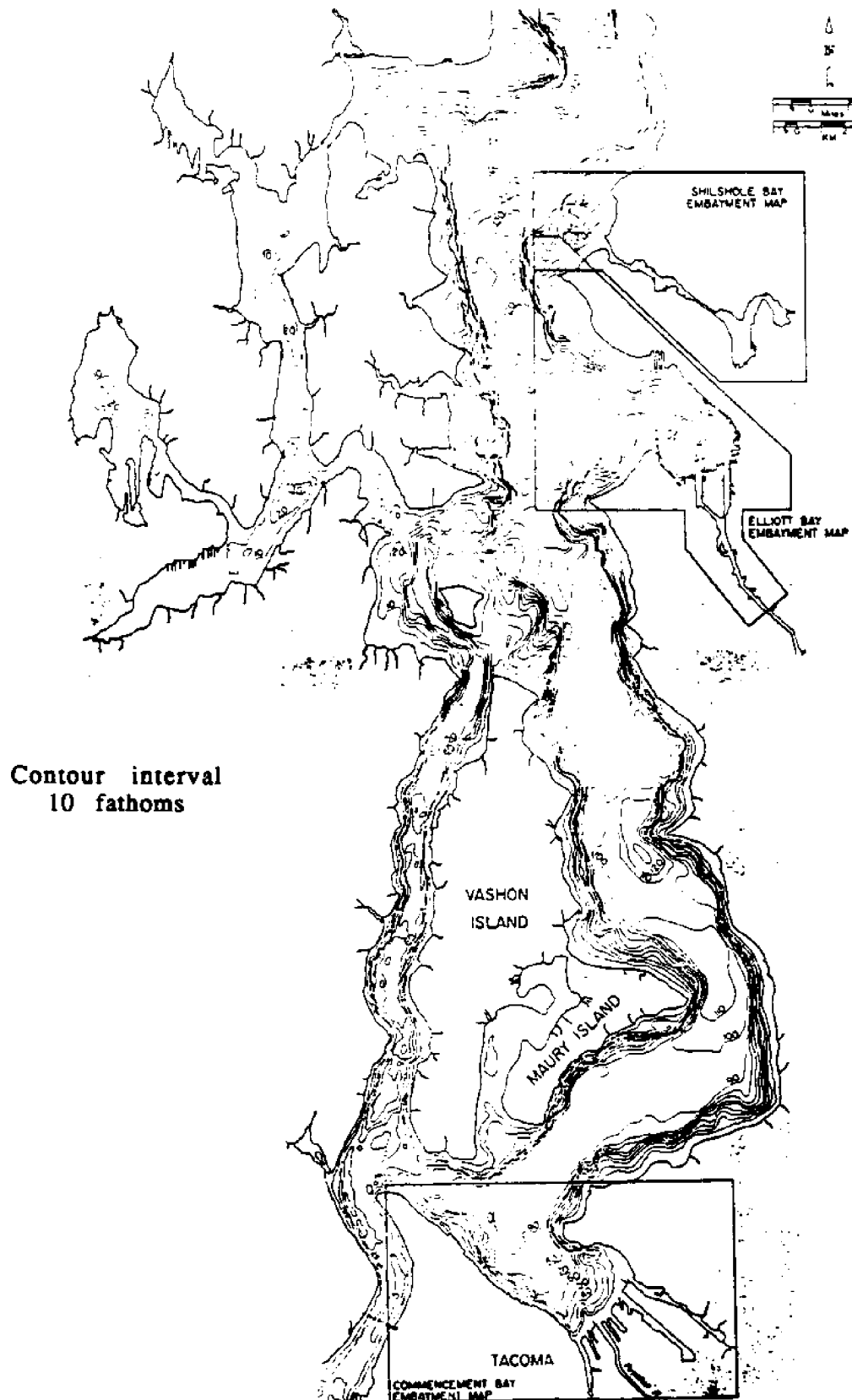
Fig.4.14 The bathymetry of Central Puget Sound (modified from Puget Sound Environmental Atlas, compiled by Evans-Hamiton, Inc., 1986).
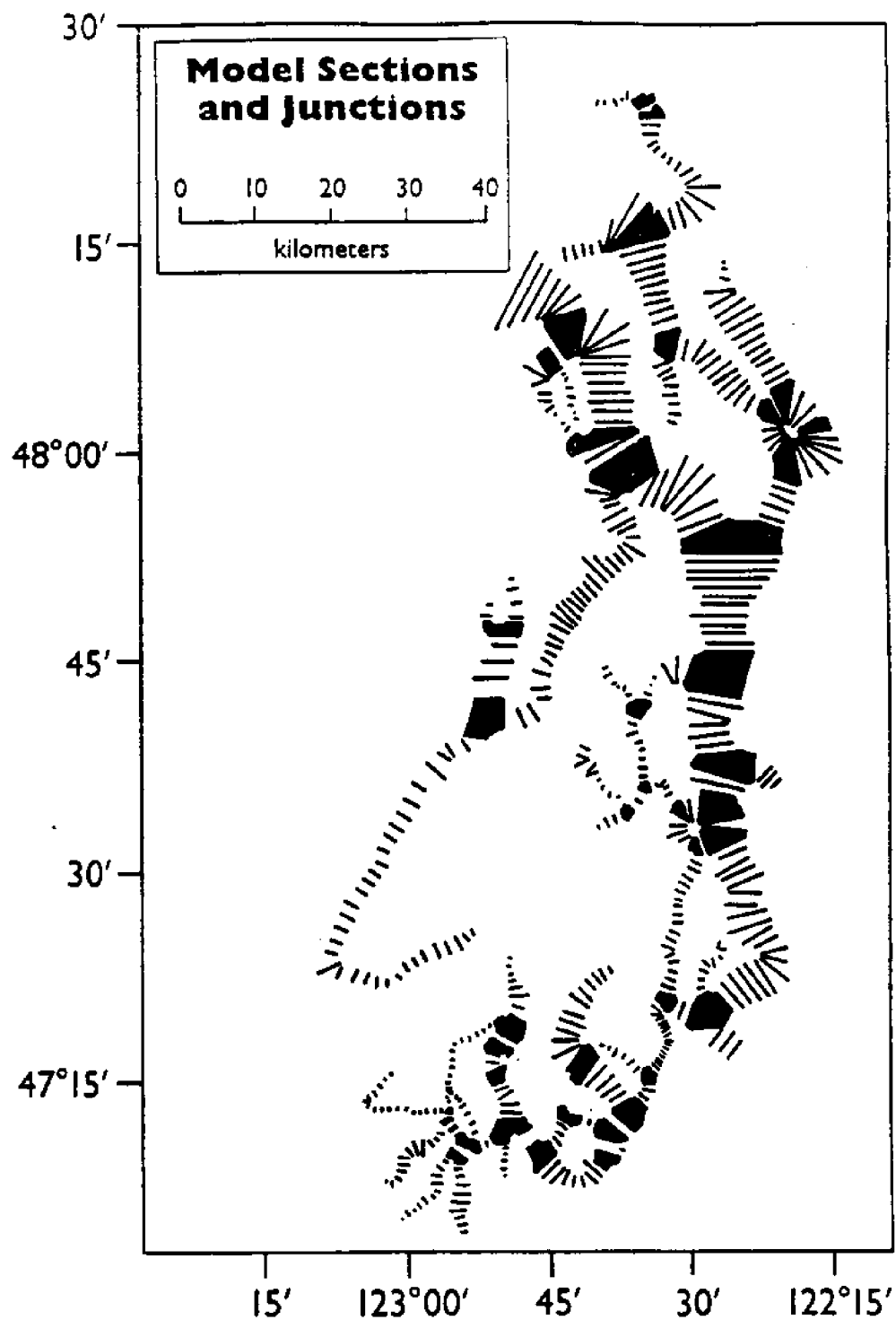
Fig.4.15 Transects and junctions (solid areas) used in Tide Channel Model (Copied from Lavelle et al., 1988)

averaged currents were obtained by dividing the transport by the model cross-sections areas and entered at every boundary node. The model was run with M_2 and the K_1 boundary conditions separately. Since neither the open boundary conditions from the channel tide model nor the observed data contain the effects of wind and density variation (or they maybe filtered out), the density variation, wind stress, and river inflows (from the Duwamish and the Puyallup) are all ignored in the model.

As initial conditions, the water level in the study area at the beginning of each simulation was assumed to be zero (at chart datum, mean lower low water) everywhere in the domain. Starting from such conditions, the model is run with the same boundary conditions for seven repeated cycles for M_2 tide (12.42 hours) and three repeated cycles for K_1 tide (23.92 hours) respectively to eliminate the "residuum" of the initial conditions in the solution. This simulation period is often referred to as "spin-up time". The seven M_2 tidal cycles spin-up time for this study was required mainly for tidal currents. The calculated tide settled down to the prescribed boundary conditions within three tidal cycles.

From all the validation runs (results are discussed below), the best values for the bottom roughness coefficient (C in eqs. (3.20) and (3.21)), the horizontal momentum exchange parameter (γ in eq. (3.11)) and the vertical momentum exchange parameter (Kv in eq. (3.15)) were found to be 60 $m^{1/2}s^{-1}$, 50 kg/m^3, and 0.4 respectively. With the given γ and Kv values, the maximum values for the horizontal momentum exchange coefficient (A/ρ) and the vertical momentum exchange coefficient (E) had the order of magnitude 10^2 m^2s^{-1} and 10^{-1} m^2s^{-1} respectively which are within the range of reported values by other investigators (Sundermann, 1974; Backhaus, 1979; Tee, 1981; Perrels and Karelse, 1981; Blumberg and Mellor, 1983; Smith and Cheng, 1987). The C values reported for other estuaries ranged from 10 $m^{1/2}s^{-1}$ to 140 $m^{1/2}s^{-1}$ (Blumberg, 1977; Spaulding and Beauchamp, 1983; Smith and Cheng, 1987; Chu

et al., 1988). The model responses were clearly dominated by the prescribed boundary conditions, the pressure gradient (water surface elevation changes), and the input bathymetry data.

The observed tidal amplitude and phase of the M_2 and K_1 constituents at twelve stations (Lavelle et al.,1988) were used for comparison with the calculated values from the study model. These comparisons of M_2 tide are shown in Figs.4.16 and 4.17. In general, the amplitudes and phases (Greenwich phase lags) calculated form the numerical model were smaller than observed data at most stations. The largest differences between the observed data and calculated results near Dyes Inlet were due mainly to the poor resolution of geometry of the Port Washington Narrows leading into Dyes Inlet. Amplitude differences at other stations are all within 4 centimeters, and the phase differences at all stations are all within 3 degrees except the station near Bremerton (4.6 degrees).

The comparisons of K_1 amplitude and phase are plotted on Figs. 4.18 and 4.19. The difference between the calculated and the observed K_1 characteristics are all within 5 centimeters for the amplitude and 3 degrees for the phase. However, unlike the M_2 case, the discrepancies for this component did not appear to be affected by grid resolution at all since the differences between the computed and observed values match very well at all stations.

Tidal current ellipses derived from near surface current observations at five stations within the study area were presented by Mofjeld and Larsen (1984). To compare model results with the observations, the computed first (top) layer tidal current ellipses from the three-dimensional model were plotted against the observations. Both the M_2 and the K_1 constituents are shown in Figs.4.20, 4.21, 4.22, 4.23, and 4.24.

At Station 2 (in The Narrows at Tacoma), the model produced currents that were significantly stronger than observed currents (Fig.4.20). There are two explanations for this. The current

M₂
AMPLITUDE
(m)

1.114 OBS
1.085 CAL

1.043 OBS
1.015 CAL

1.190 OBS
1.082 CAL

1.086 OBS
1.045 CAL

1.070 OBS
1.044 CAL

1.102 OBS
1.081 CAL

1.090 OBS
1.067 CAL

1.090 OBS
1.095 CAL

1.081 OBS
1.076 CAL

1.114 OBS
1.098 CAL

1.102 OBS
1.098 CAL

1.133 OBS
1.103 CAL
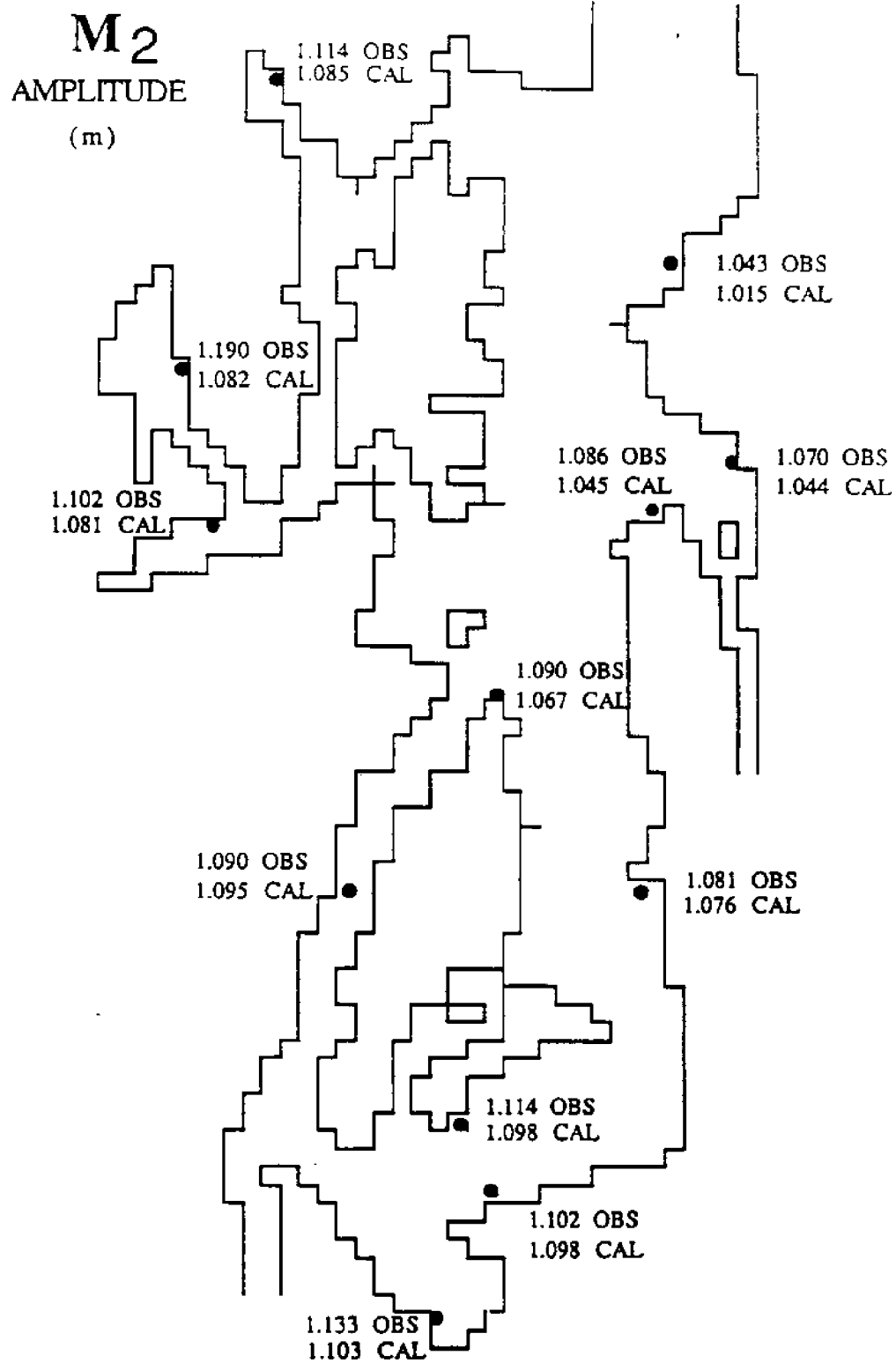
Fig.4.16 Comparison of calculated and observed M2 tidal amplitude (in meters).

M2

PHASE

$(^{\circ}G)$

15.7 OBS
13.4 CAL

11.9 OBS
10.0 CAL

29.0 OBS
31.5 CAL

13.2 OBS
10.3 CAL

11.5 OBS
10.3 CAL

18.1 OBS
13.5 CAL

10.9 OBS
10.5 CAL

10.5 OBS
11.3 CAL

11.5 OBS
10.9 CAL

11.2 OBS
11.0 CAL

11.6 OBS
10.3 CAL

13.0 OBS
11.4 CAL
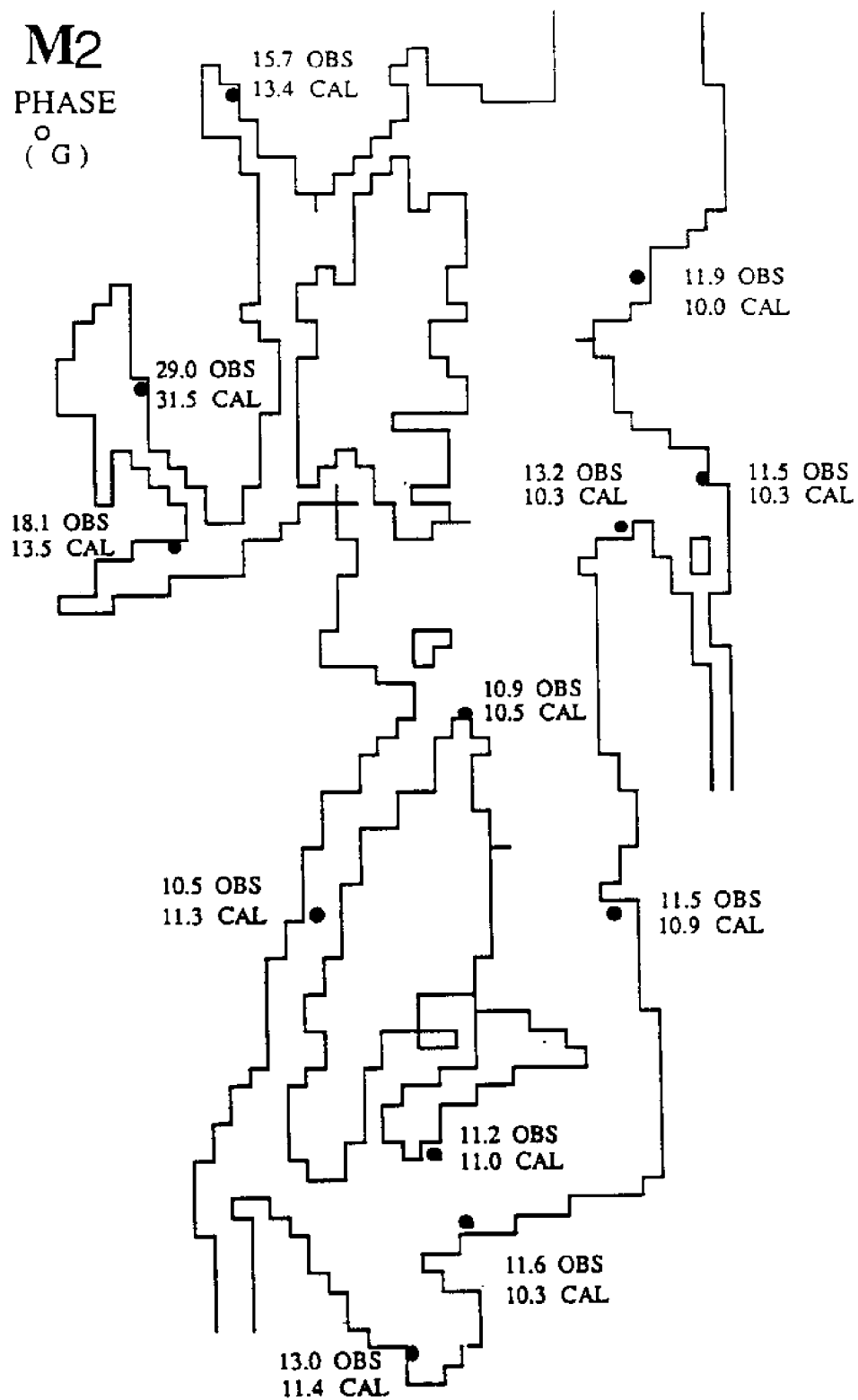
Fig.4.17 Comparison of calculated and observed M2 tidal phases (in degrees). Phases are Greenwich phase lags.

K₁
AMPLITUDE
(m)

0.817 OBS
0.801 CAL

0.829 OBS
0.788 CAL

0.841 OBS
0.793 CAL

0.831 OBS
0.793 CAL

0.825 OBS
0.801 CAL

0.823 OBS
0.797 CAL

0.815 OBS
0.803 CAL

0.820 OBS
0.799 CAL

0.825 OBS
0.801 CAL

0.824 OBS
0.803 CAL

0.828 OBS
0.803 CAL

0.834 OBS
0.804 CAL
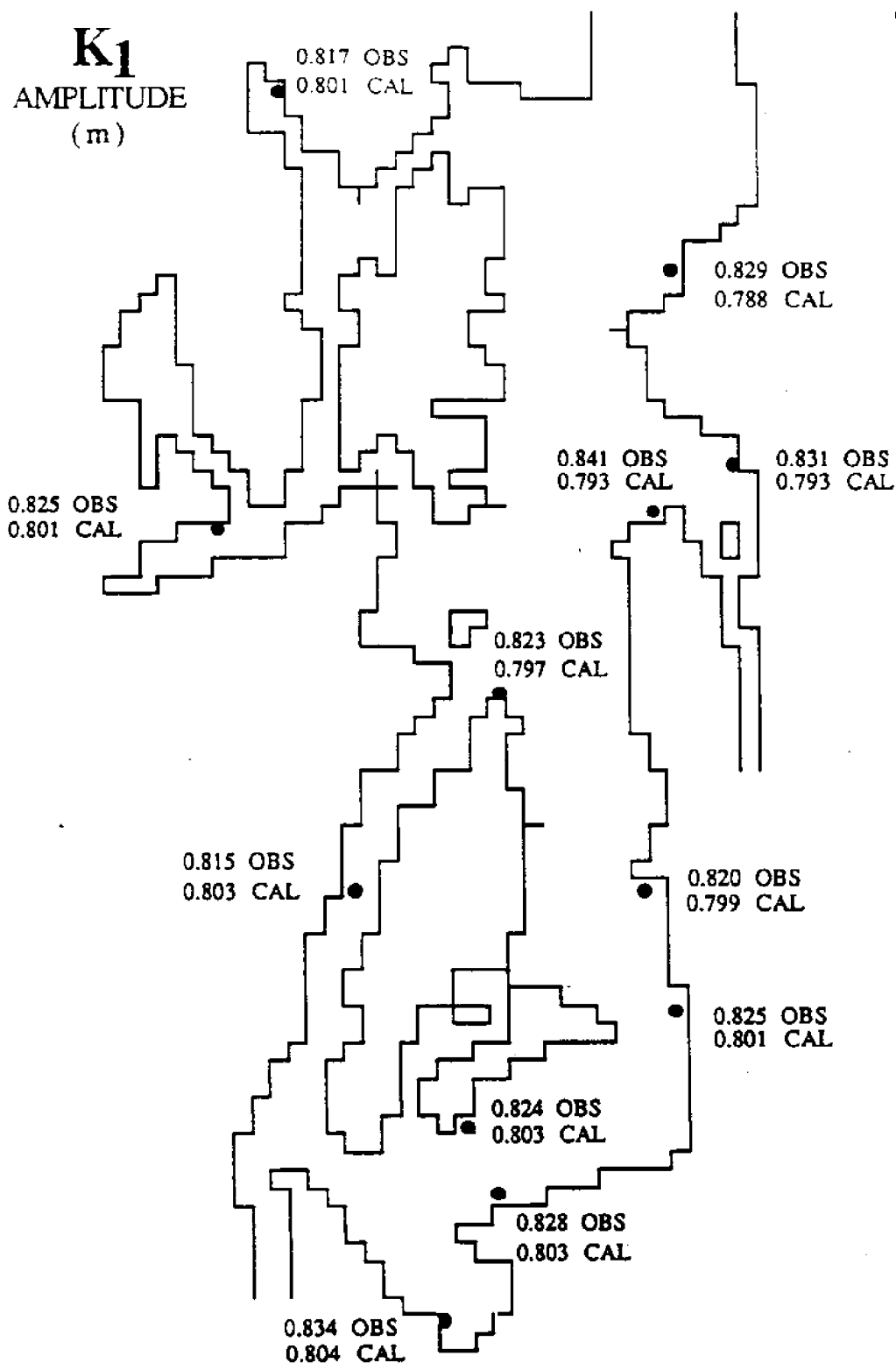
Fig.4.18 Comparison of calculated and observed K1 tidal amplitude (in meters).

K₁

PHASE
(°G)

281.2 OBS
279.0 CAL

277.8 OBS
278.6 CAL

276.5 OBS
278.3 CAL

277.3 OBS
278.3 CAL

281.8 OBS
279.0 CAL

277.9 OBS
278.2 CAL

277.6 OBS
278.5 CAL

278.3 OBS
278.4 CAL

276.8 OBS
278.6 CAL

278.2 OBS
278.6 CAL

277.6 OBS
278.7 CAL

278.0 OBS
278.7 CAL
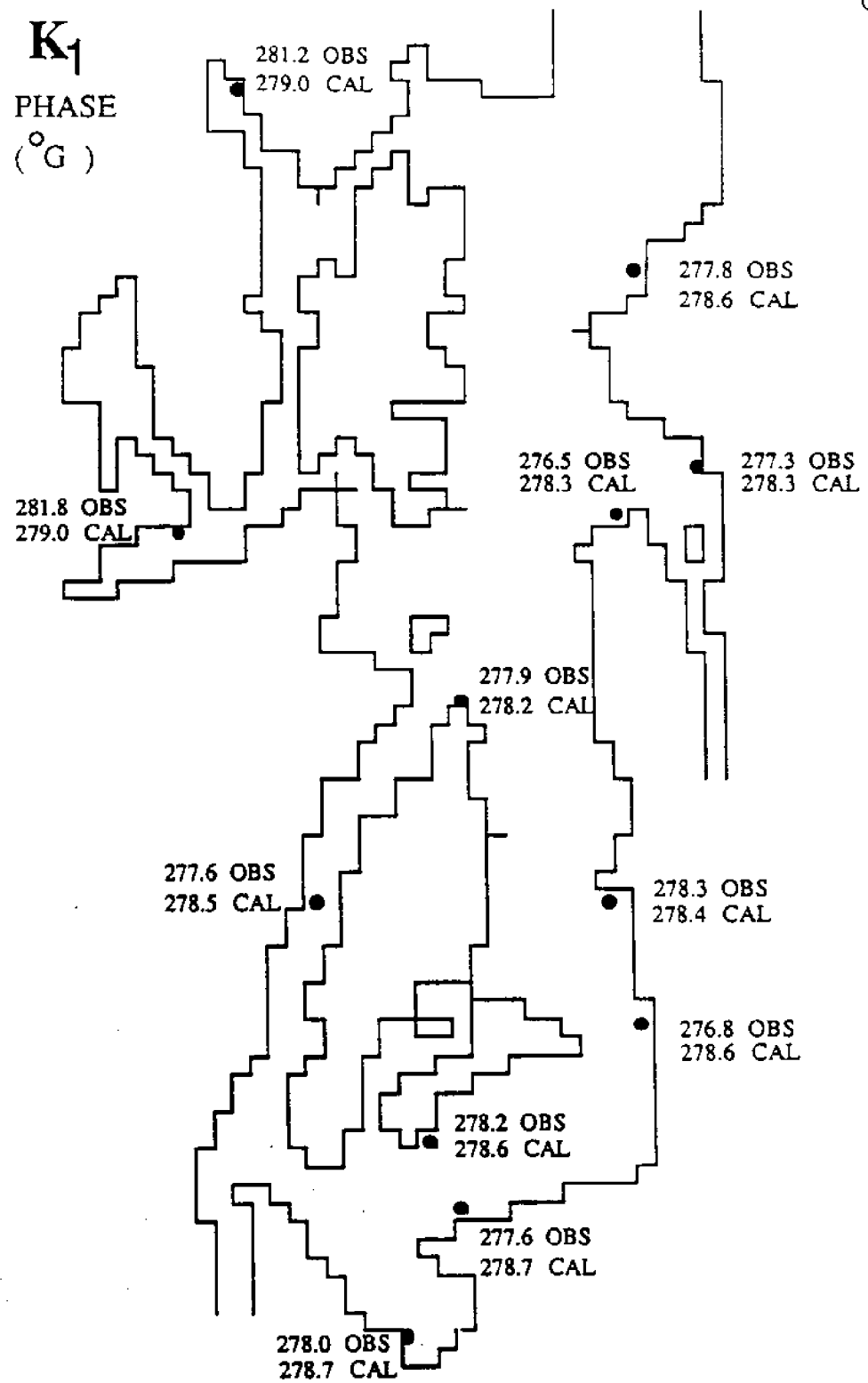
Fig.4.19 Comparison of calculated and observed K1 tidal phases
(in degrees). Phases are Greenwich phase lags.
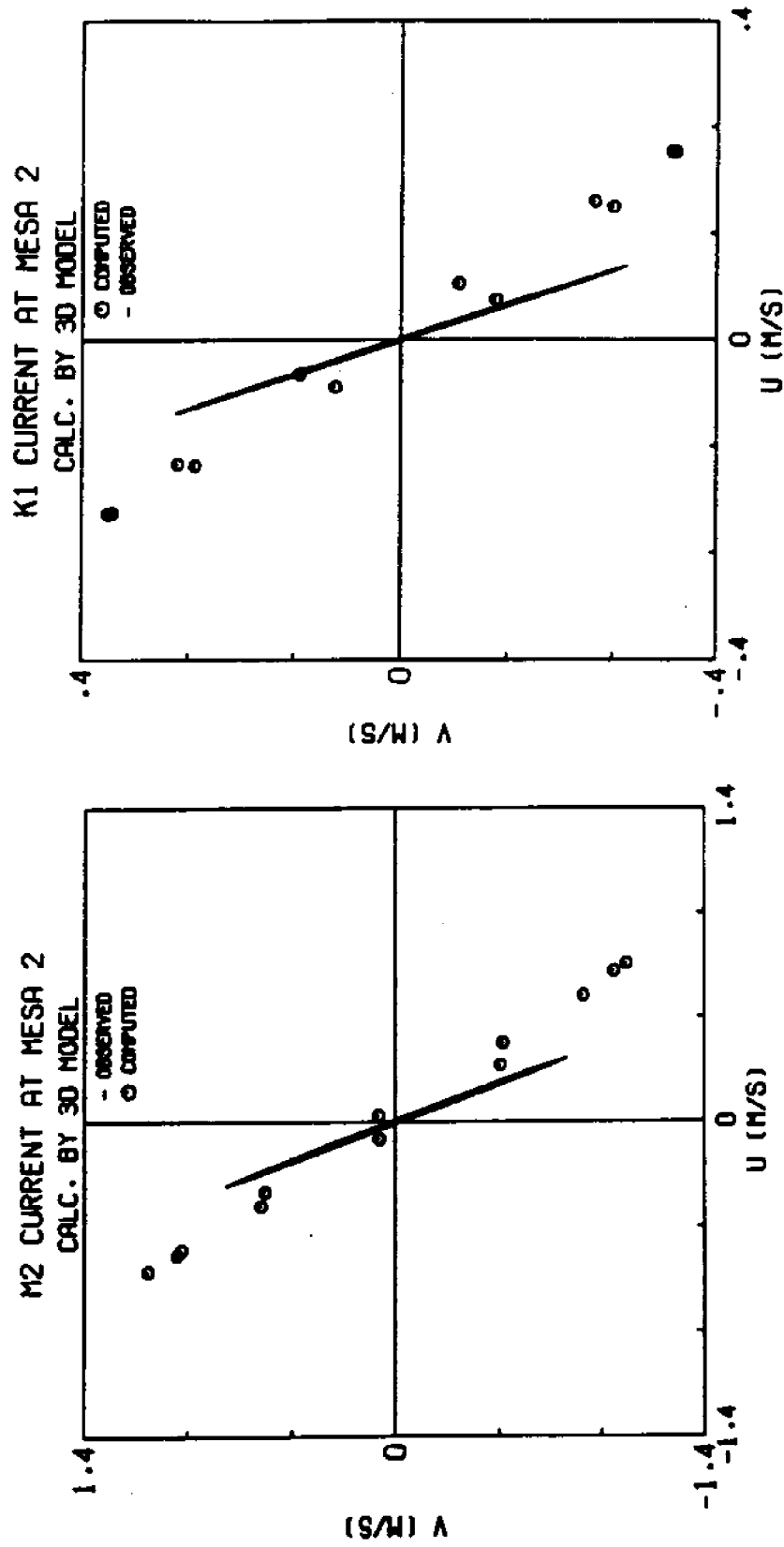
Fig.4.20 Comparison of calculated and observed M2 and K1 current
ellipses at MESA station No. 2
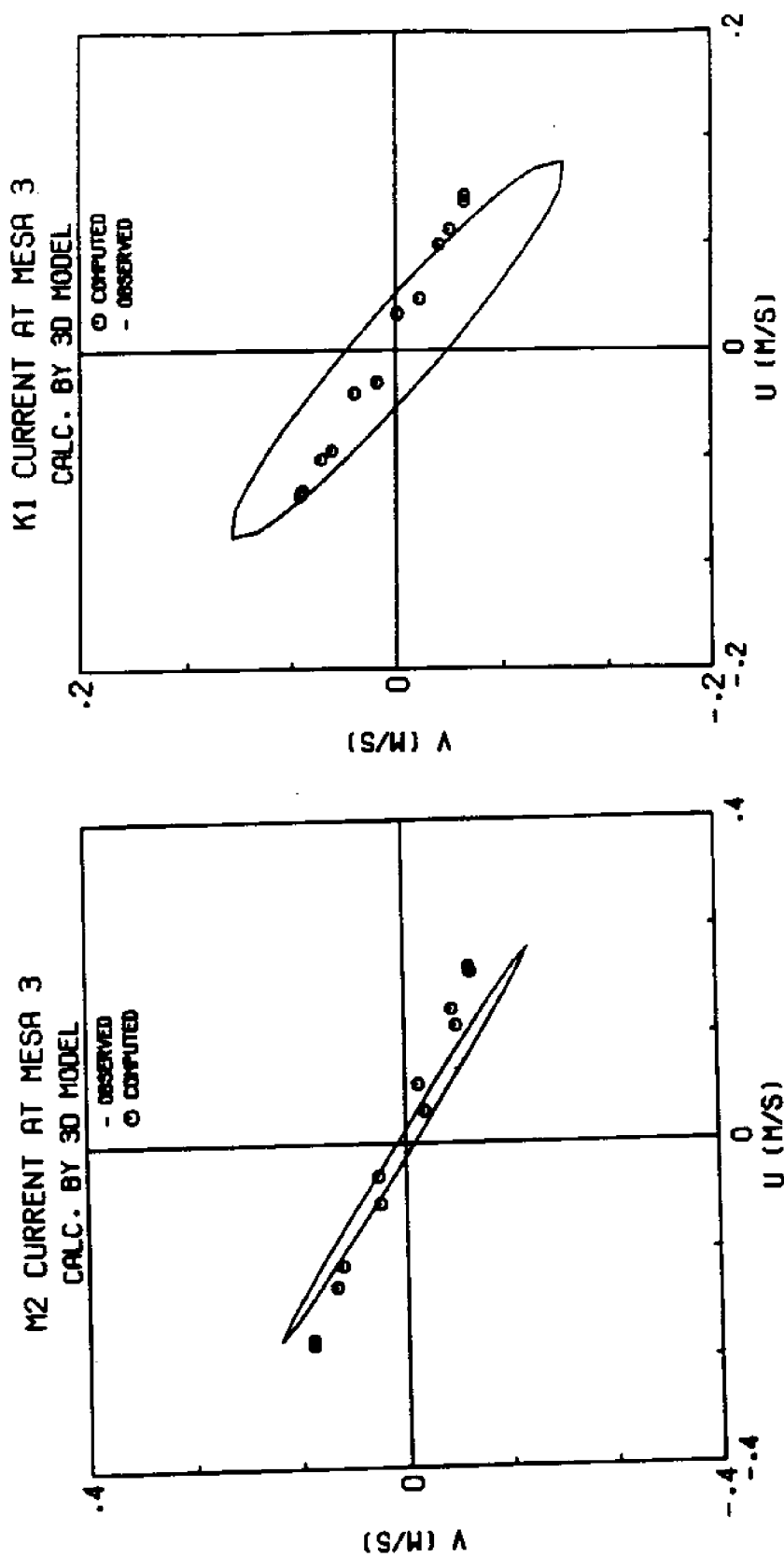
Fig.4.21 Comparison of calculated and observed M2 and K1 current ellipses at MESA station No. 3
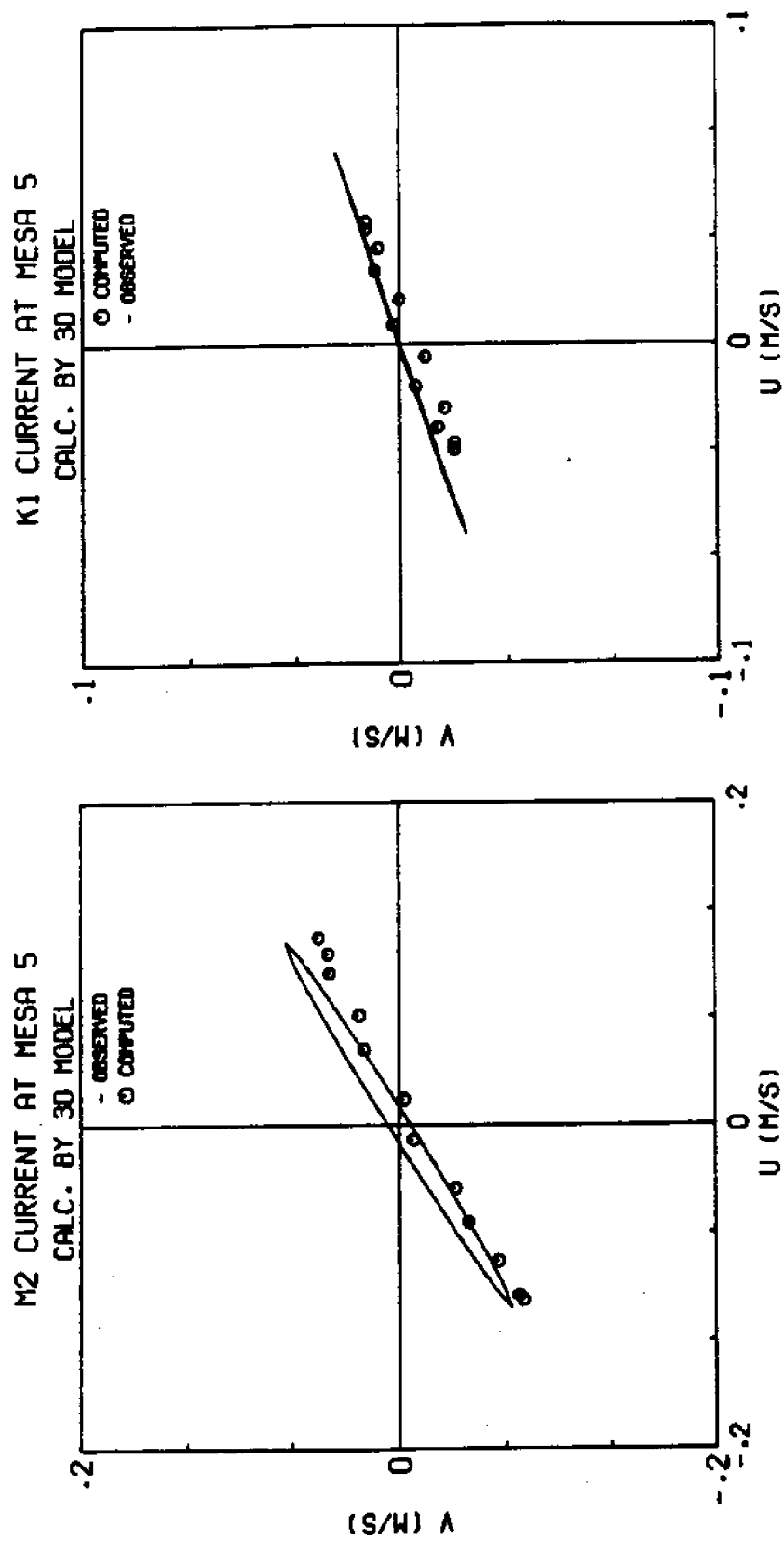
Fig.4.22 Comparison of calculated and observed M2 and K1 current
ellipses at MESA station No. 5
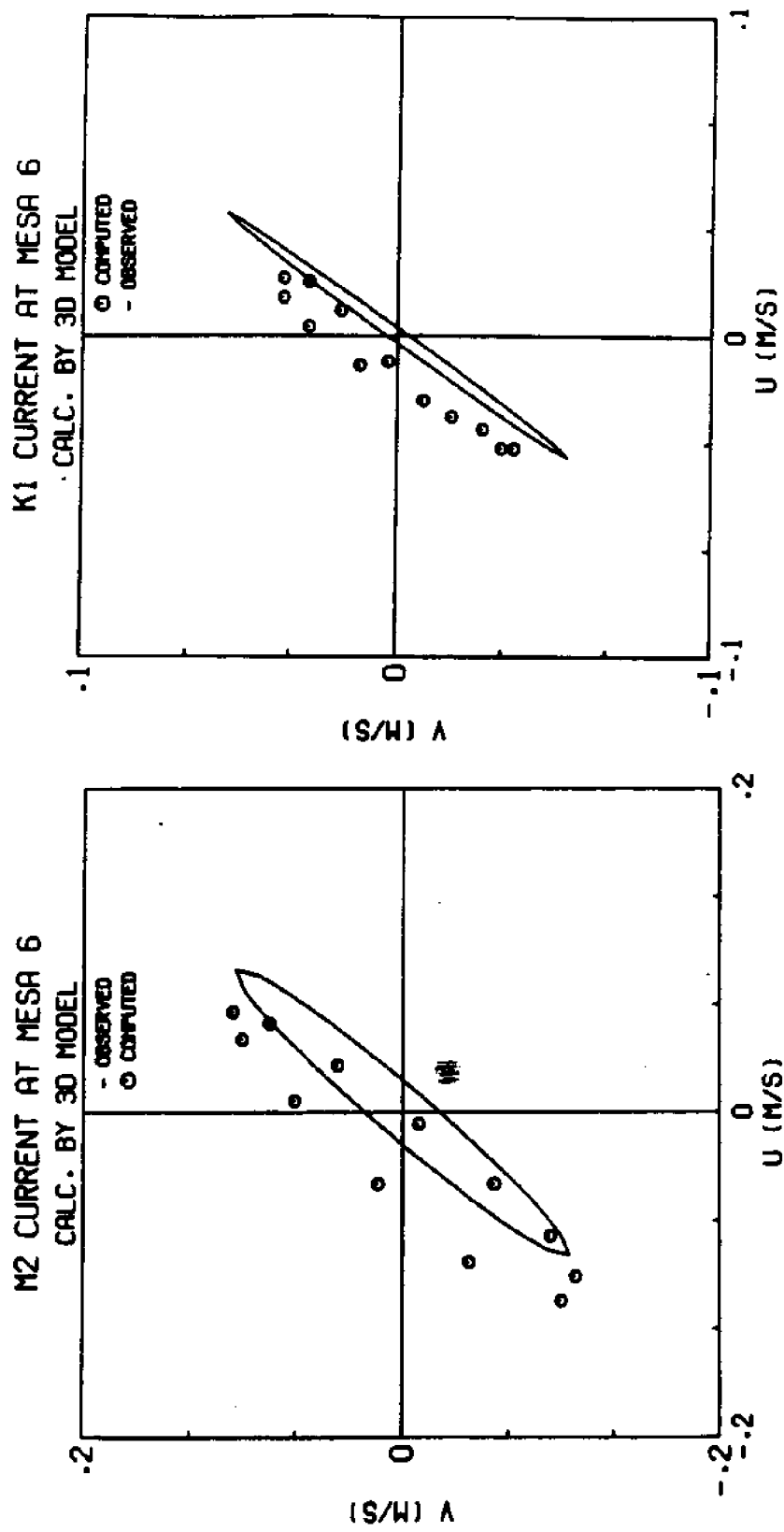
Fig.4.23 Comparison of calculated and observed M2 and K1 current ellipses at MESA station No. 6
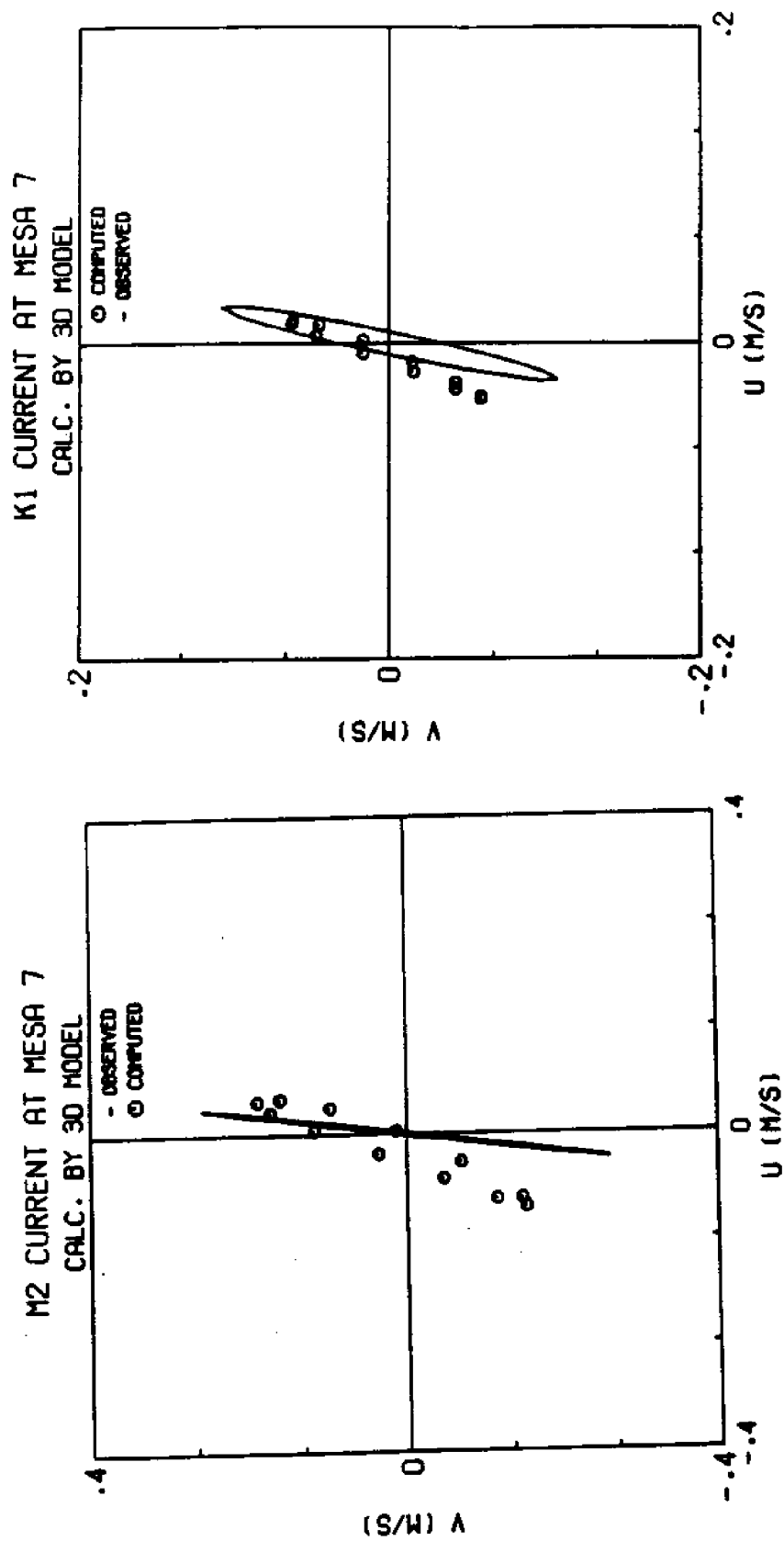
Fig.4.24 Comparison of calculated and observed M2 and K1 current ellipses at MESA station No. 7

measurement at this station was actually taken near the bottom of the channel (Mofjeld and Larsen, 1984) while the calculated currents are depth averaged (since the depth in The Narrows is between 40 and 60 meters there is only one layer over The Narrows for the three-dimensional model). Secondly, the chosen finite difference grid resolution near the station in the study model straightened the actual natural curvature of the channel at The Narrows and therefore caused the increase in the calculated velocities as well as change of direction.

As to Stations 3, 5, 6, and 7, the calculated and observed current ellipses (Figs.21, 22, 23, and 24) show a much better match than that of Station 2 for both M_2 and K_1 tidal constituents. These better matches can be ascribed to the better resolution of the bathymetry by the model around these stations. In general, the matches between the calculated and observed M_2 current ellipses in these stations are better than those for K_1 component.

Although the current comparisons are not as good as those for the tides, it should be noted that the comparisons were actually made at different depths and only at approximate locations. The current comparisons shown above are actually better than most of the similar comparisons in the literature. It is clear from the results shown in this Chapter that the model is fully capable of characterizing the tide and tidal current features of Puget Sound.

Full scale application of the model, which uses composite tidal transport (summation of transports from six major tidal constituents), recorded wind sequences and river discharges, and observed synthetic (from observed data) density profiles to drive the model, is given in the next Chapter.

CHAPTER FIVE

APPLICATION TO CENTRAL PUGET SOUND AND

ELLIOTT BAY

To fulfill the primary objective of the research, the hydrodynamic and transport models introduced in Chapters 3 and 4 were used to characterize the tidal hydrodynamics and transport in Central Puget Sound and Elliott Bay. To obtain actual tidal response, composite tides (rather than individual tidal constituents), representative river inflow and wind, and density variation were introduced in the model.

5.1 Model Setup

5.1.1 Geometric and Bathymetric Resolution

The grid size used in an estuarine numerical model study is normally determined by two conflicting factors. A smaller grid size is desired to better resolve key geometric and bathymetric features, but at the same time the grid size cannot be so small that it consumes too much computer storage and computing time. One solution to this problem is the application of a nested grid system.

Adopting the nested grid idea in this study, a coarse grid resolution was first used to cover Central Puget Sound from Point Wells to The Narrows at Tacoma exactly as shown in the previous chapter, and a fine grid resolution was used to cover Elliott Bay and its surroundings. The study domains and the relationship between the two grid systems are shown in Fig.5.1. Since all the input parameters used in the coarse grid model have already been introduced in Chapter 4, only those regarding the fine grid model are discussed here.

The fine grid model domain covers the entire Elliott Bay and part of the main basin between the bay entrance and Bainbridge
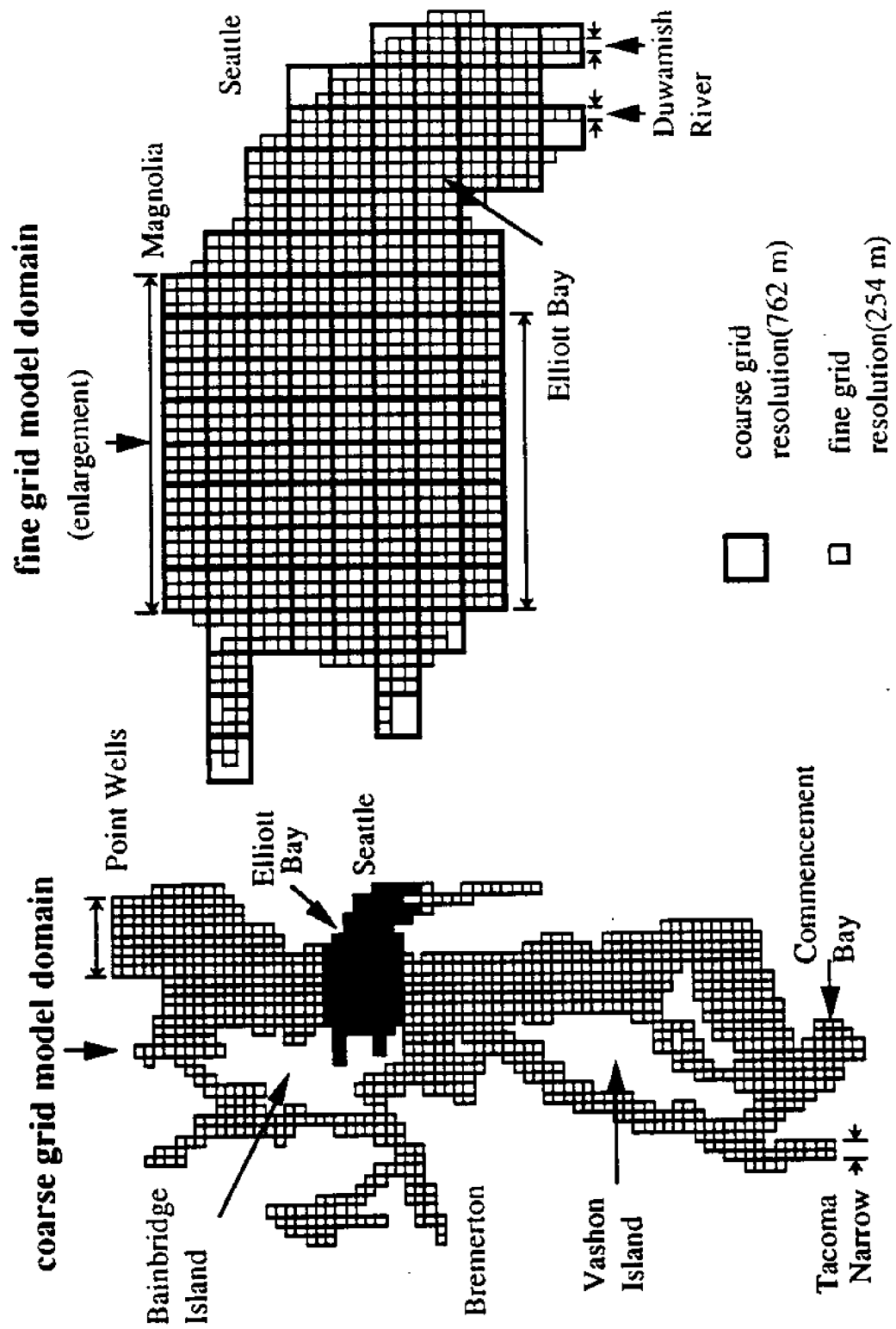
Fig.5.1 Grid spacings of fine grid model and coarse grid model

Island (Fig.5.1). The bathymetry of the domain is schematized by four variable thickness layers with depths of 15 m (top), 45 m, 80 m, and 80 m (bottom) respectively. Because of the smaller spatial grid cell, the integration time step used in the fine grid model is 2 seconds.

Bathymetry data for the fine grid model can be obtained by two methods. The first method is to simply interpolate the data from the input file of the coarse grid model. Although it is simpler, this method is less accurate because the resolution of the bathymetry near the shoreline where depth changes rapidly could be distorted by the coarse grid resolution. The second method is to read bathymetric data directly from more refined National Ocean Survey charts. The second approach was adopted here. The different bathymetric input data for the coarse grid and the fine grid domain, especially near the open boundaries, may significantly affect the input open boundary flow rates. To alleviate this problem, the depths near the open boundaries have to be adjusted so that the flow rates in the coarse grid model and the fine grid model are as close to each other as possible.

The open boundary conditions for the fine grid model include the velocities at the north and the south ends of the domain, and the velocities at the mouths (East and West Waterways) of the Duwamish River. These boundary condition data were all calculated from the coarse grid model. Because the grid spacing and time step used in coarse grid model are larger than those in the fine grid model, the calculated open boundary conditions had to be interpolated in time and in space before they were used by the fine grid model. A simple linear interpolation was used for this study.

The same bottom roughness coefficient and horizontal and vertical momentum exchange coefficients described in Chapter 4 were used for both model resolutions.

5.1.2 Model Inputs

The water movement in study area is influenced by tidal transport, river discharge, wind, and density variation (in Elliott Bay simulation only). The description and preparation of these input data are given here.

5.1.2.1 Tidal Transport

The tide in Puget Sound can be characterized as a mixed tide. Two high and two low tides occur during a lunar day with considerable inequality in the ranges of the highs and the lows. To calculate actual tide driven flow features in the Sound, composite tidal current data were used as boundary conditions for the model. Although the model is programmed to read an input tidal current function with as many as 62 tidal constituents, only six major constituents (O_1, K_1, P_1, M_2, N_2, and S_2) were used for this study. The observed O_1, K_1, P_1, M_2, N_2, and S_2 tidal amplitudes at Seattle are 0.46, 0.83, 0.25, 1.07, 0.21, and 0.26 m respectively; the amplitudes of the other tidal constituents at Seattle are all less than 0.07 m (Lavelle et al., 1988).

Tidal transport of each constituent which represents the flux of water through a cross-channel transect can be expressed by a cosine function with transport amplitude q_j in m^3s^{-1}, and a phase lag φ_j in degrees (Lavelle et al., 1988). The composite tidal transport $Q(t)$ can then be represented as :

$$Q(t) = \sum_{j=1}^{6} q_j \cos (\omega_j t + \varphi_j) \tag{5.1}$$

where $Q(t)$ is a function of time t; ω_j is the frequency of each tidal constituent. For the Central Puget Sound model, the values of q_j and φ_j were provided in Lavelle et al. (1988). The tidal current boundary conditions were obtained by dividing the tidal transport $Q(t)$ by the cross section areas of the model boundaries. The longest simulation

period considered in this study is 10 days, selected so as to include one neap tide and one spring tide. The composite tidal currents at The Narrows and Point Wells during the 10-day simulation period are shown in Fig.5.2. The tides in Seattle during the same period are also shown in the figure for comparison.

Based on the tide at Seattle, the 10-day duration is divided into three periods and 9 tidal cycles (Fig.5.2). The first and the third periods are identified as "spring tide" and "neap tide" respectively, each lasting 3.5 days. The 3-day period in between will be referred to as "medium tide". The model will be run separately with the "spring tide", the "medium tide", and the "neap tide" tidal currents as its boundary conditions to determine the influence of tide range on the hydrodynamics of Central Puget Sound and Elliott Bay.

5.1.2.2   River   discharge

To investigate tidal circulation and transport in the Sound, especially inside Elliott Bay, the effect of fresh river inflow should be studied. The two large rivers within Central Puget Sound are the Puyallup which discharges into Commencement Bay and the Duwamish which discharges into Elliott Bay (Fig.4.12). Annual distributions of the discharges from the two rivers are shown in Fig.5.3 (Ebbesmeyer et al, 1982). For both rivers, the higher flows occur in December and January and the lower flows occur in August and September. The smaller peaks in April for the Duwamish and in June for the Puyallup are due to snowmelt (Ebbesmeyer et al., 1982).

Since the duration of this model simulation is only for a few days, constant flow rate is assumed for both rivers. Two constant flow rates representing high (winter) and low (summer) flows for each river were selected from the data. The high and low flow rates for the Duwamish and the Puyallup are 60 m^3s^{-1}, 10 m^3s^{-1} and 120 m^3s^{-1}, 10 m^3s^{-1} respectively.

Currents on open boundaries

The Narrows
Point Wells

Current speed (m/s)

Tide at Seattle station

Tidal cycles

Water elevation (m)

spring tide   medium tide   neap tide

Time (hours)
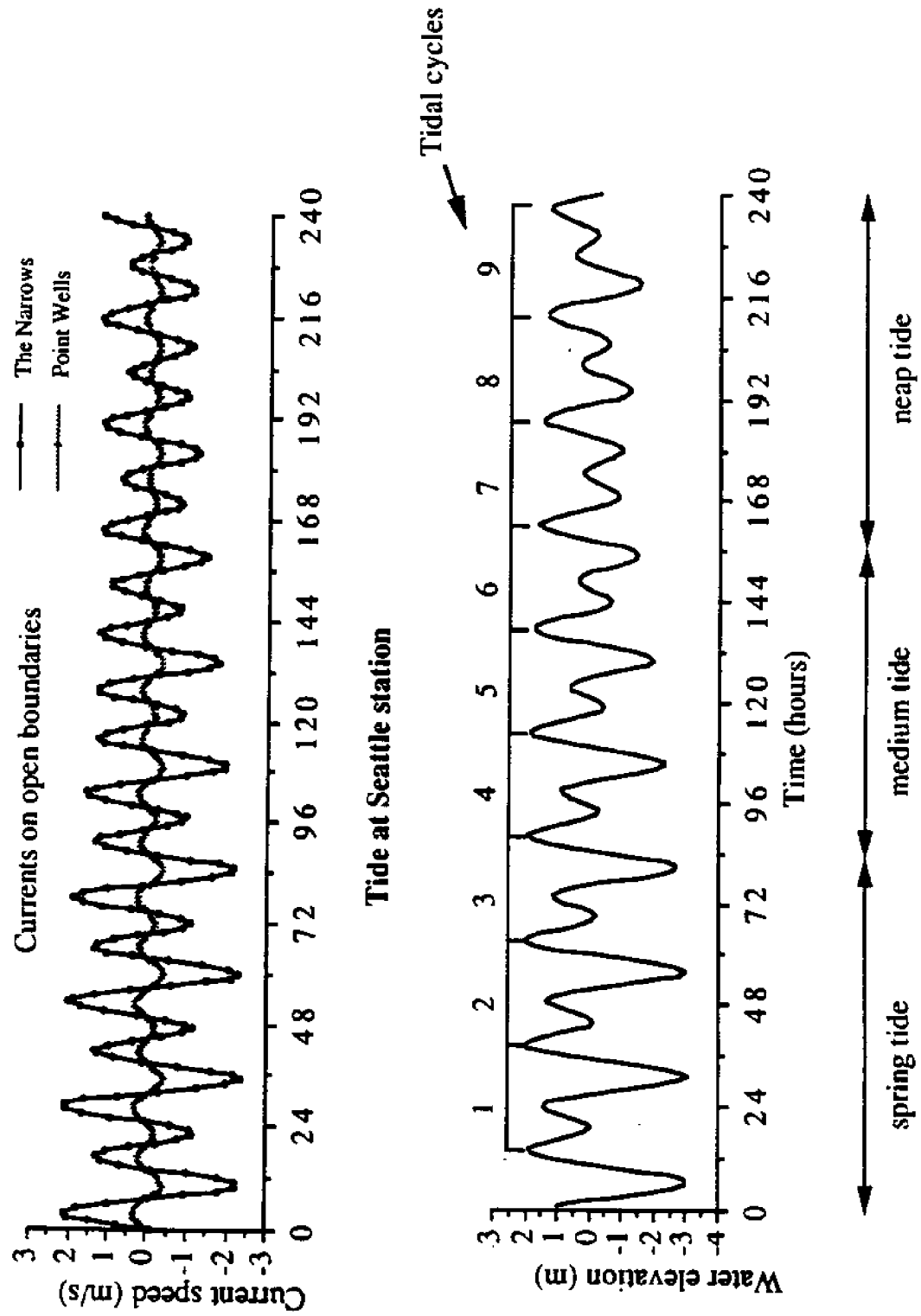
Fig.5.2 Currents at open boundaries and tide at Seattle
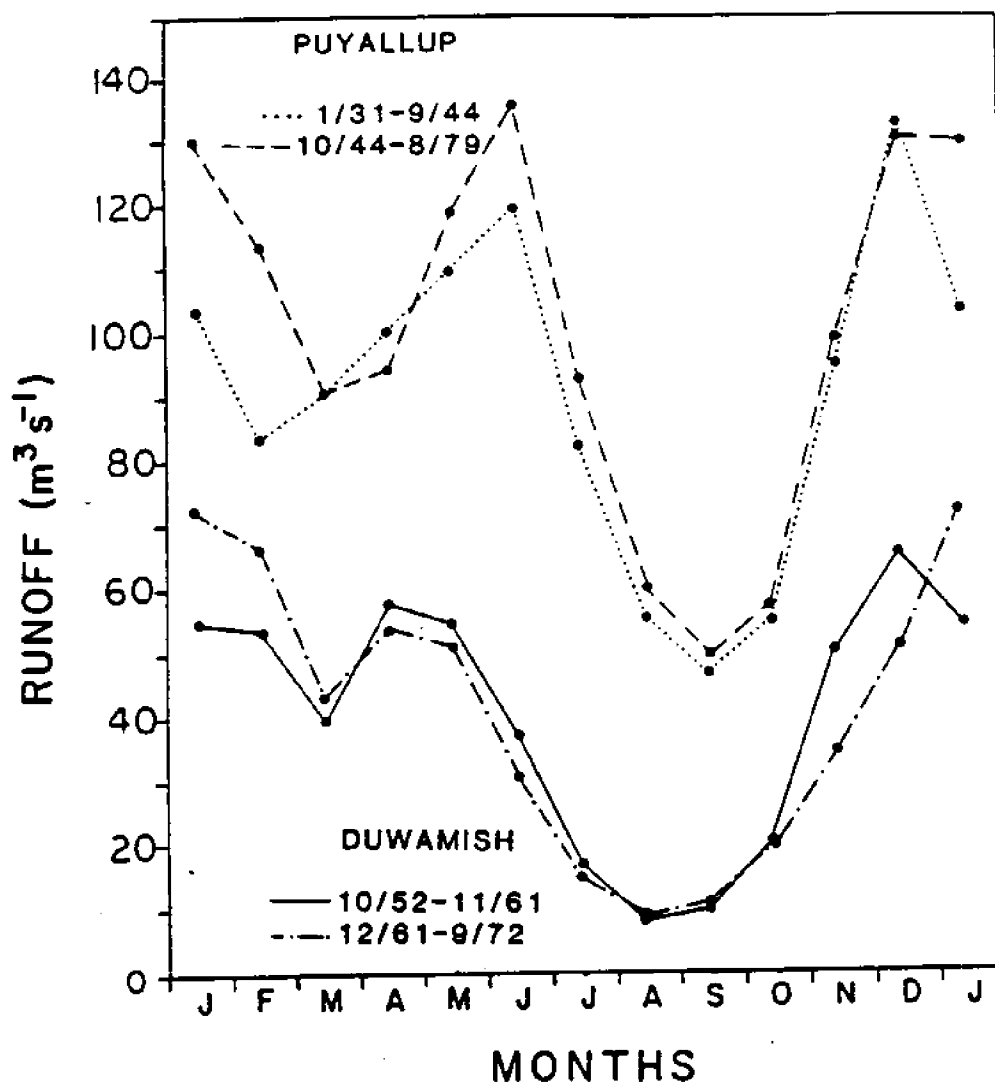
Fig.5.3 Average seasonal cycles of runoff for the Duwamish River (based on 1952-1972) and the Puyallup River (based on 1931-1979). Two runoff cycles are presented for each river corresponding to years prior to and following dates when flood water storage began. (From Ebbesmeyer et al., 1982)

5.1.2.3 Wind Field

Wind is important in the study of surface layer transport in the Sound and its embayments. Study of the effect of winds on the current and transport in Puget Sound has been limited to date.

Ideal wind data for estuarine simulation should be obtained from long term records observed at weather stations widely distributed in the study area. Unfortunately, this is never the case. To date, most wind data for coastal water modeling have to be obtained by using (1) constant wind speeds and directions, (2) spatially and temporally varying wind functions, (3) probabilistic wind functions, or (4) the results from numerical atmospheric circulation models. The choice of the methods depends mainly on the availability of wind data and the purpose of the study.

In Puget Sound, the number of existing weather stations are not enough to provide a representative spatially varying wind field within our study area (Horton, 1989). Therefore, the wind field used for this study is assumed to be homogeneous in space but time dependent. Based on the results of a statistical analysis of long term wind record, the wind direction in Central Puget Sound was determined to be primarily along-channel (Ebbesmeyer et al., 1982). Therefore, two recorded wind sequences representing a southerly wind in the winter and a northerly wind in the summer were chosen to simulate wind generated circulation and transport (Fig.5.4). The two wind sequences were chosen because they have relatively strong speeds and consistent directions in the simulation period. Since the time intervals of the wind data are 15 minutes to an hour, which are much larger than the time step used in the hydrodynamics model, the chosen wind data had to be interpolated by a scheme which is described below.

A wind function W(t) can be defined to represent the given discrete wind data (either wind speed or wind direction) on the time
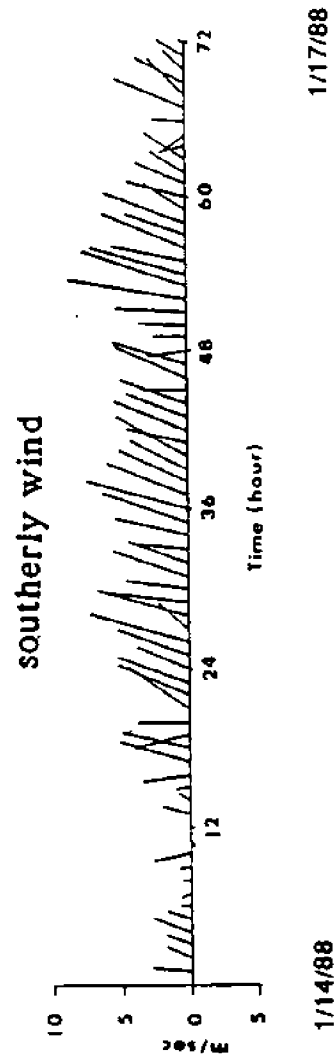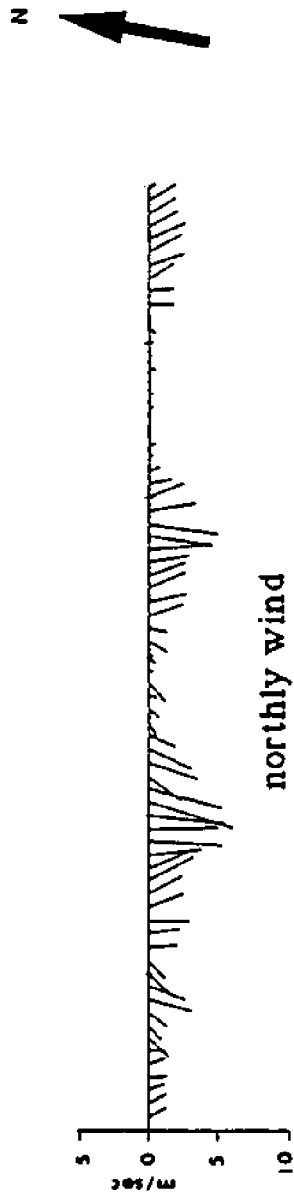
Fig.5.4 Observed wind at Duwamish Weather Station

series $\{t_0, t_1, t_2, t_3 \dots, t_n\}$ by a discrete Fourier Series (or trigonometric polynomial) (Dahlquist et al., 1974) as :

$$W(t) = \frac{1}{2} a_0 + \sum_{j=1}^{k} (a_j \cos jt + b_j \sin jt) + \frac{1}{2} a_{k+1} \cos((k+1)t) \tag{5.2}$$

$$a_j = 2 (n+1)^{-1} \sum_{\alpha=0}^{n} W(t_\alpha) \cos jt_\alpha, \quad b_j = 2 (n+1)^{-1} \sum_{\alpha=0}^{n} W(t_\alpha) \sin jt_\alpha \tag{5.3}$$

where $t_\alpha = 2\pi\alpha / (n+1)$, α is from 0 to n, j is from 0 to k+1, and n is the number of interval. $k = (n-1)/2$ and n is an odd integer.

Once the discrete Fourier coefficients a_j and b_j (there is one for wind speed and one for wind direction) are determined from the data (by eq. (5.3)), the wind functions $W(t)$'s (there is one for wind speed and one for wind direction) can then be used to provide input wind data at desired intervals to the hydrodynamic model.

Measurements of wind drag coefficient (see eq. (3.19)) has been reported by many investigators, but its values derived from these various experiments and field studies are always different. The wind drag coefficient used in this research was suggested by Wu (1980) :

$$C* = (0.8 + 0.065\ W)/1000 \tag{5.4}$$

where C* is the wind drag coefficient and W is the 10-meter wind speed. This formula was proposed to represent the wind drag coefficient over the sea surface under "light" winds (wind speed less than 15 m/s) (Wu, 1980). The two wind sequences used in this study are both "light" winds.

5.1.2.4 Modeling the Density Effect

Among all the possible forcing functions, the density effect is the most difficult one to be included in the model. The design of

simulation plans which are compatible with the present density data base and given computing resources is given here.

Within the coarse grid model domain, the fresh river inflows primarily come from the Duwamish and the Puyallup. The Duwamish and the Puyallup have the respective average annual discharges of only 39 and 97 m^3s^{-1} (Ebbesmeyer et al., 1982). The amount of freshwater discharged from these two rivers is trivial when compared to either the total volume or tidal prism of Central Puget Sound. Besides, with our present horizontal resolution of 762 m by 762 m and layer thickness of 60 m or more for Central Puget Sound, calculated nodal density values will not change significantly over the time scale of the study model. It is for this reason and the fact that there are no compatible boundary condition data, density effects in the Central Puget Sound simulations are ignored.

Density effects should become more important as the model is applied to Elliott Bay. It has been observed that density near the surface of Elliott Bay varies significantly between ebb and flood tides due to the fresh water plume from Duwamish River, but much less density variation was seen in the deeper portions of Elliott Bay (Curl et al., 1988).

To include density variation in Elliott Bay simulations in a meaningful way, the model will require the input of salinity boundary conditions (it is assumed that density variation is a function of salinity only) at all the boundaries, and a salinity initial condition at every computational node of the domain. Such data are not available in Elliott Bay. To investigate the influence of density on tidal currents in Elliott Bay with a reasonable amount of computing resource, these data must somehow be derived from best available observations and the simulation runs be carefully designed. If the model starts with an arbitrary set of initial condition and a reasonable form of boundary conditions, the modeler is immediately faced with the "spin-up" problem. The model must run for an unknown number of tidal cycles until all the nodal salinity values are

influenced by the prescribed boundary conditions. Because of the slow temporal and spatial variation of salinity, the spin-up period for a three-dimensional model can be as long as 155 days (Oey and Mellor, 1985). It is estimated that the spin-up period for Elliott Bay simulations will be at least 60 days, i.e. the model will need to be run for 60 consecutive tidal days (with 60 days of boundary conditions) until the calculated salinities (and density) are completely influenced by the boundary conditions.

Most of existing salinity data in Elliott Bay were taken near the water surface (Helseth et al. 1979; Sillcox et al. 1981; and Curl et al. 1988). The fresh water plume in Elliott Bay is generally confined in the upper two to three meters near the shoreline and thins (0.5-1 m) out toward the center of the Bay (Curl et al.,1988). In the winter, the fresh water lens can reach about 5 meters thickness (Sillcox et al., 1982). In order to resolve the fresh water plume better, the thickness for the first and second layers of the fine grid model were adjusted to 5 and 55 m respectively. The initial salinity conditions were interpolated from the data given by Curl et al. (1988) and entered as averaged values in a control volume with surface area of 64516 m^2 (254 m by 254 m) and thickness of 5 to 80 m.

Since the purpose of the simulations is to determine whether density effects are important to the tidal currents in Elliott Bay, it was decided not to run a three-dimensional salt transport model in this simulation. Instead, it was assumed that salinity in Elliott Bay is transported horizontally in each layer and no vertical exchange of salinity between any two layers is allowed. The simulations would start from an initial salinity field synthesized from observation data and would last only for an ebb tide period of 6 hours in which the most significant salinity changes would take place. During the ebb tide, the salinity values at the north and south open boundaries (in the main channel) of the model domain were assumed to be constant and the salinities at East and West Waterways boundaries were

assumed to decrease linearly from 28.3 (at higher high tide) to 25.3 (at higher low tide) parts per thousand.

Three different sets of input initial conditions were created. All three sets have same surface layer horizontal salinity distribution, but different lower layers horizontal salinity gradients. The contour (isohaline) distributions for the first set of data are plotted in Fig.5.5. The contour distributions for the other two sets of data (lower layers only) are shown in Fig.5.6. Although it is known that horizontal salinity gradients are weaker in the deeper layers, not enough actual data are available to construct (by interpolation) a nodal salinity distribution as precise as that in the surface layer. All three sets of initial conditions will be used in the simulation (with the same boundary conditions) for the purpose of comparing and contrasting the effect of lower layer salinity gradients on the current and transport in Elliott Bay.

The layer-averaged salt transport equation (eq. (3.24)) was solved by a two-dimensional Eulerian-Lagrangian transport model (Chu et al., 1988). Because the model is based on a streamwise coordinate system, it requires the input of dispersion coefficients in the directions tangent (Ds) and normal (Dn) to the streamlines (Chu et al., 1988). Three sets of Ds and Dn values, which were 3 and 0.3 m^2s^{-1}, 30 and 3 m^2s^{-1}, and 100, 10 m^2s^{-1} respectively, were used and their results were compared in this study (Cheng et al., 1984). The selection of rm value in eq. (3.16a) is based on sensitive analysis. The model was run by using different rm values of 0.04, 0.4, and 4. The discrepancies between the results of these runs were insignificant. Therefore, the middle rm value of 0.4 which was also suggested by Leendertse and Liu (1975) was used in this model.

5.1.3 Model Simulation Plan

To investigate the effects of tide, wind, river discharge, and density variation on the tidal circulation and transport in the study area, a total of six coarse grid model runs and thirteen fine grid
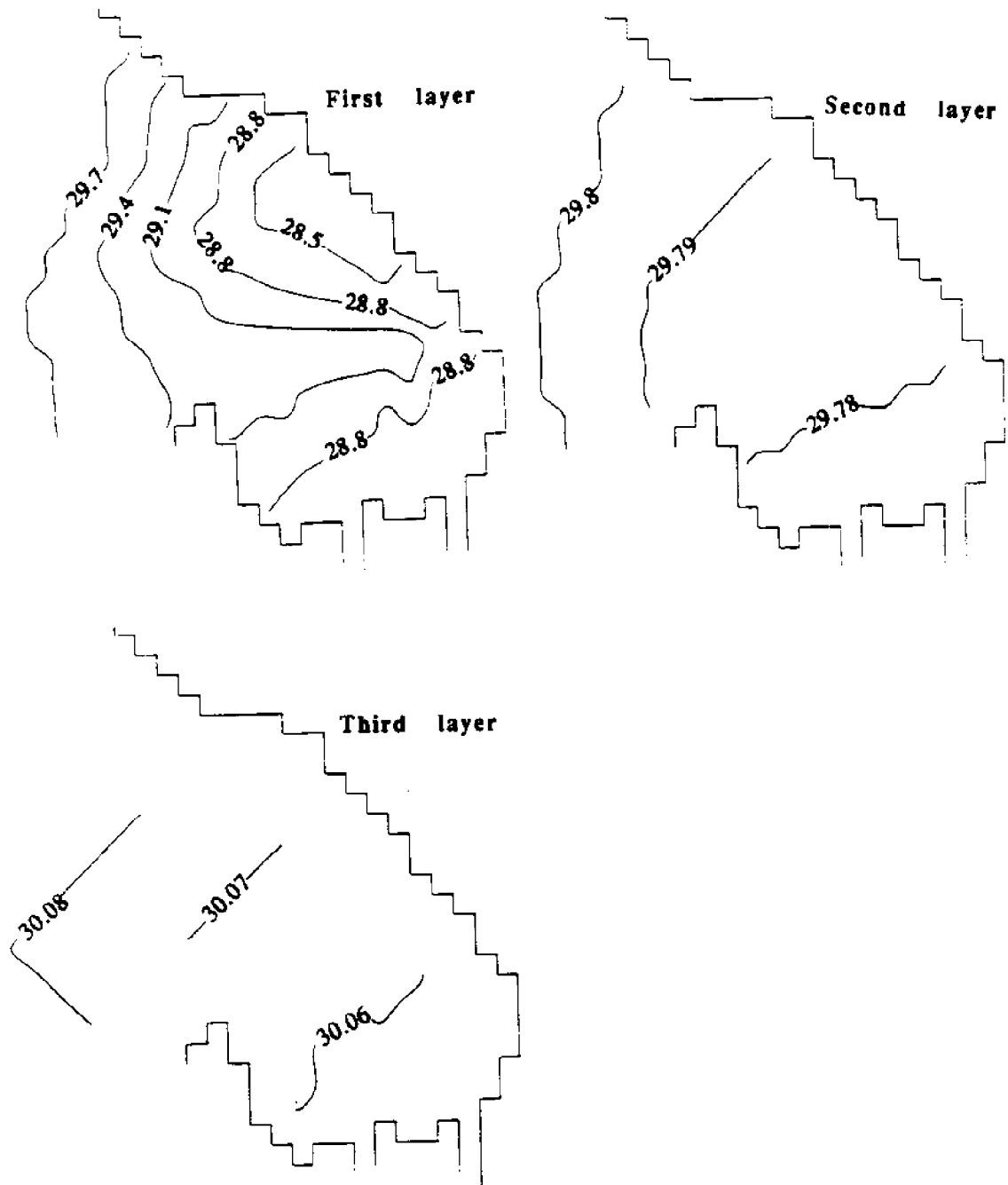
Fig.5.5 First set of input initial salinity distribution for Elliott Bay. Horizontal salinity gradients in the lower layers are small (Note : there are only three layers inside Elliott Bay).
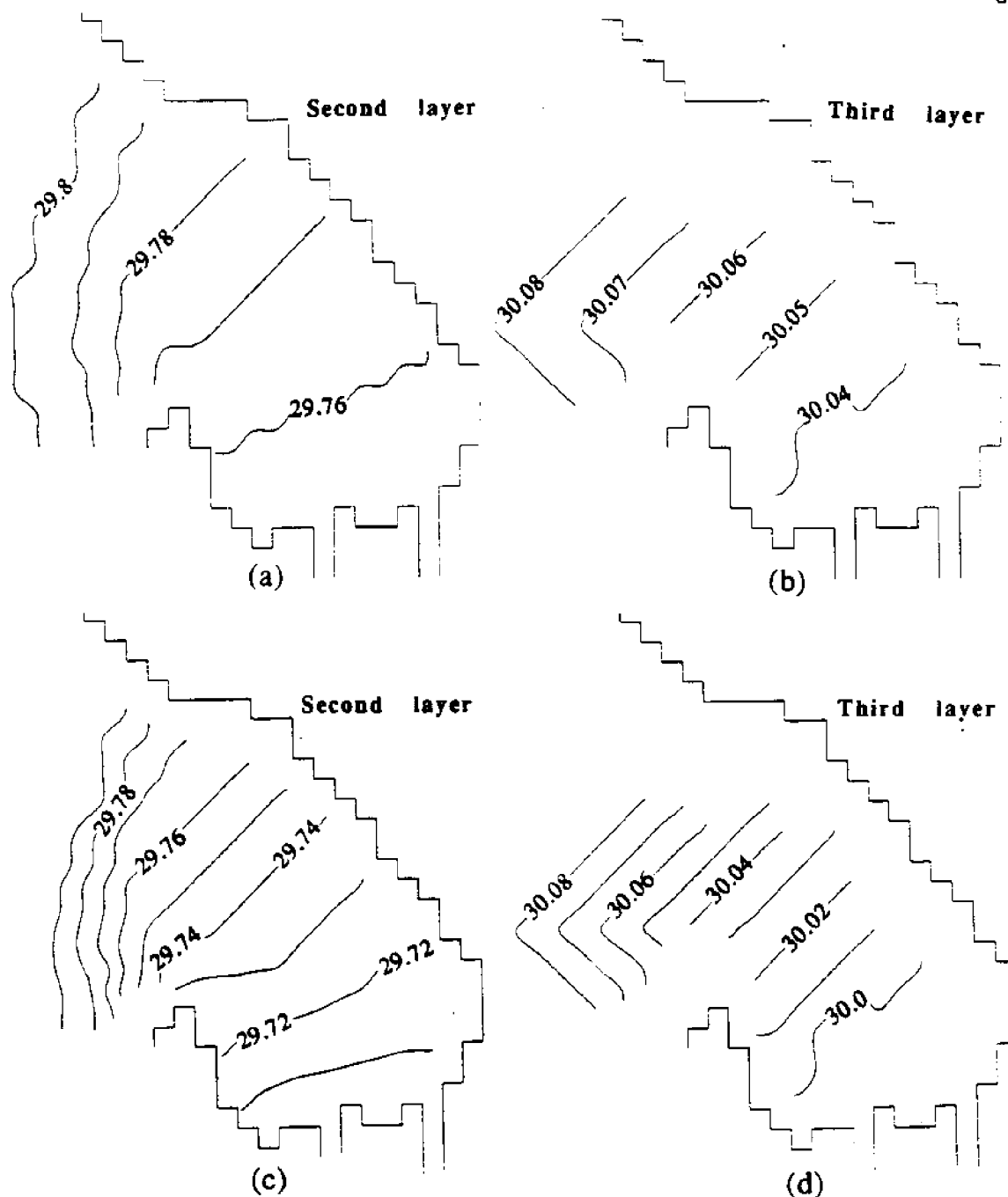
Fig.5.6 Second ((a) and (b)) and third ((c) and (d)) sets of input initial salinity distribution for Elliott Bay. The second set has a mild lower layers horizontal salinity gradients and the third set has a strong lower layers horizontal salinity gradients. The salinity gradient in the first layer for both cases remains the same as the one shown in Fig.5.5.

model runs were designed. These cases are listed and explained in Tables 5.1 to 5.3.

Table 5.1 Coarse Grid Model Simulation Runs

Case	Tide	River Discharge	Wind Field	Density Variation
Case 1	Medium	Low	None	None
Case 2	Medium	High	None	None
Case 3	Medium	High	Southerly	None
Case 4	Medium	Low	Northerly	None
Case 5	Spring tide	Low	None	None
Case 6	Neap tide	Low	None	None

Table 5.2 Fine Grid Model Simulation Runs

Case	Tide	River Discharge	Wind Field	Density Variation
Case 7	Medium	Low	None	None
Case 8	Medium	High	None	None
Case 9	Medium	High	Southerly	None
Case 10	Medium	Low	Northerly	None
Case 11	Spring tide	Low	None	None
Case 12	Neap tide	Low	None	None

Table 5.3 Simulation Runs for Investigating Baroclinic Effect
(All cases are for a 6-hour ebb tide only)

Case	River Discharge	Wind Field	Density Variation
Case 13	High	None	HDG*=0, Ds=30, Dn=3
Case 14	High	None	HDG in the top layer only, Ds=30, Dn=3
Case 15	High	None	HDG in the all layers, (see Fig.5.5) Ds=30, Dn=3
Case 16	High	None	milder HDG in deeper layers (see Fig.5.6), Ds=30, Dn=3
Case 17	High	None	stronger HDG in deeper layers (see Fig.5.6), Ds=30, Dn=3
Case 18	High	None	With HDG in Case 15, but Ds=3, Dn=0.3
Case 19	High	None	With HDG in Case 15, but Ds=100, Dn=10

* : HDG= horizontal density gradient

Cases 1 and 7 in Table 5.1 and 5.2 were the base cases for coarse grid and fine grid model simulation, respectively. Cases 2 and 8 were designed for higher river inflow. Cases 3, 4, 9, and 10 were for the study of wind effect. Cases 5, 6,11 and 12 were for the study of effect of tidal inequality. Cases 13 to 19 in Table 5.3 were for the investigation of baroclinic effect.

All simulations were run on two supercomputers (Cray X/MP-48 and IBM 3090). For the coarse grid cases, each run required about 30 SRU's (system resource units) on the Cray X/MP-48. Because of the smaller time step used, each fine grid model run took about 100 SRU's on the Cray and 650 CPU on the IBM 3090.

5.2 Description and Analysis of Simulation Results

5.2.1 Comparison Between Model Results and Available Observations

The calculated tides from Case 1 (Table 5.1) at 12 stations within Central Puget Sound (see Fig.4.12) and the calculated tide at Seattle from Case 7 were compared with observed data in Fig.5.7. The observed tides were constructed from O_1, K_1, P_1, M_2, N_2, and S_2 tidal constituent data in Lavelle et al. (1988). The overall agreements between the calculated and the observed tides reveal that the tidal results from the model are reasonably accurate. It should be noted that the "observed" tides at 12 stations are almost the same, except for the large phase lag between Seattle (station 3) and Dyes Inlet (station 10). Earlier results of M2 constituent showed that the phase lag between the two stations was about 20 degrees (40 minutes) (see Fig.4.17).

Since tidal currents inside the study domain are strongly influenced by boundary conditions, the comparisons between computed and observed currents should be made when the observed data including those used for boundary conditions were measured over the same time period. Unfortunately, this is not the case in our Puget Sound study. In this research, the tidal elevations during the fourth tidal cycle of our model simulation period (Fig.5.2) are similar to the tidal elevations during which current observations were taken by Sillcox et al. (1981) (Fig.5.8). Therefore, the observed currents by Sillcox et al. (1981) were compared with calculated fourth tidal cycle currents from Case 7.

The hourly averaged tidal currents at two ebbs and two floods (g, h, i, and j in Fig.5.8), which were taken by four current meter moorings in Elliott Bay (Sillcox et al., 1981), are shown in Fig.5.9b. The letters g, h, i, and j in Figs.5.9a-b represent the times of ebb and flood indicated in Fig.5.8. Since the observations were taken at 30-meter depth (Sillcox et al., 1981), they were compared with layer-

Station 1

Water El. (m)

3
2
1
0
-1
-2
-3

80 100 120 140 160

Time (hour)

——— Observed tide

▪ Calculated tide

Station 2

Water El. (m)

3
2
1
0
-1
-2
-3

80 100 120 140 160

Time (hour)

Station 3

Water El. (m)

3
2
1
0
-1
-2
-3

80 100 120 140 160

Time (hour)

Station 4

Water El. (m)

3
2
1
0
-1
-2
-3

80 100 120 140 160

Time (hour)

Station 5

Water El. (m)

3
2
1
0
-1
-2
-3

80 100 120 140 160

Time (hour)

Station 6

Water El. (m)

3
2
1
0
-1
-2
-3

80 100 120 140 160

Time (hour)

Station 7

Water El. (m)

3
2
1
0
-1
-2
-3

80 100 120 140 160
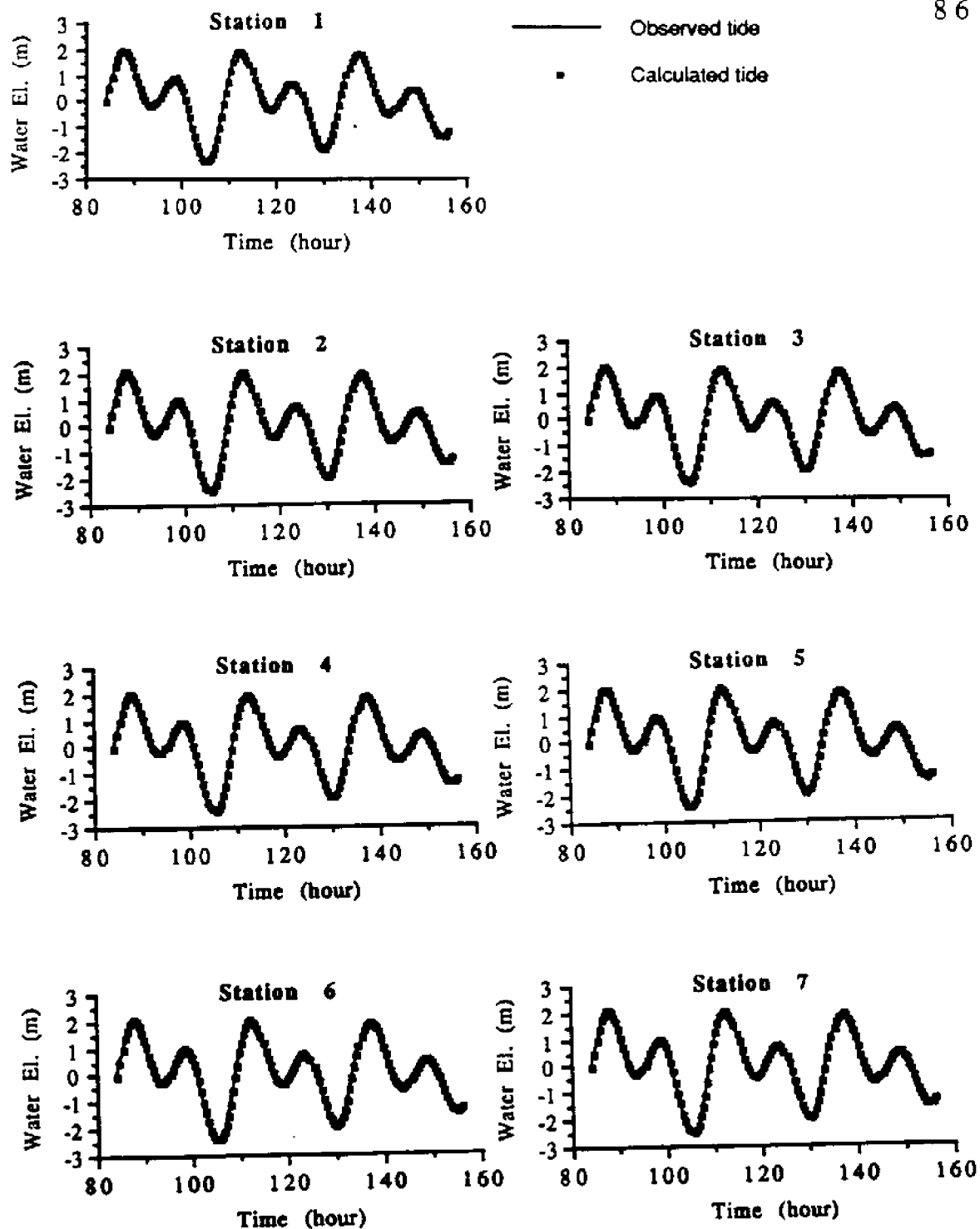
Time (hour)

Fig.5.7 The comparisons between calculated and observed
tide (12 stations for coarse grid model and
Seattle station for fine grid model). Zero water
elevation represents mean sea level.
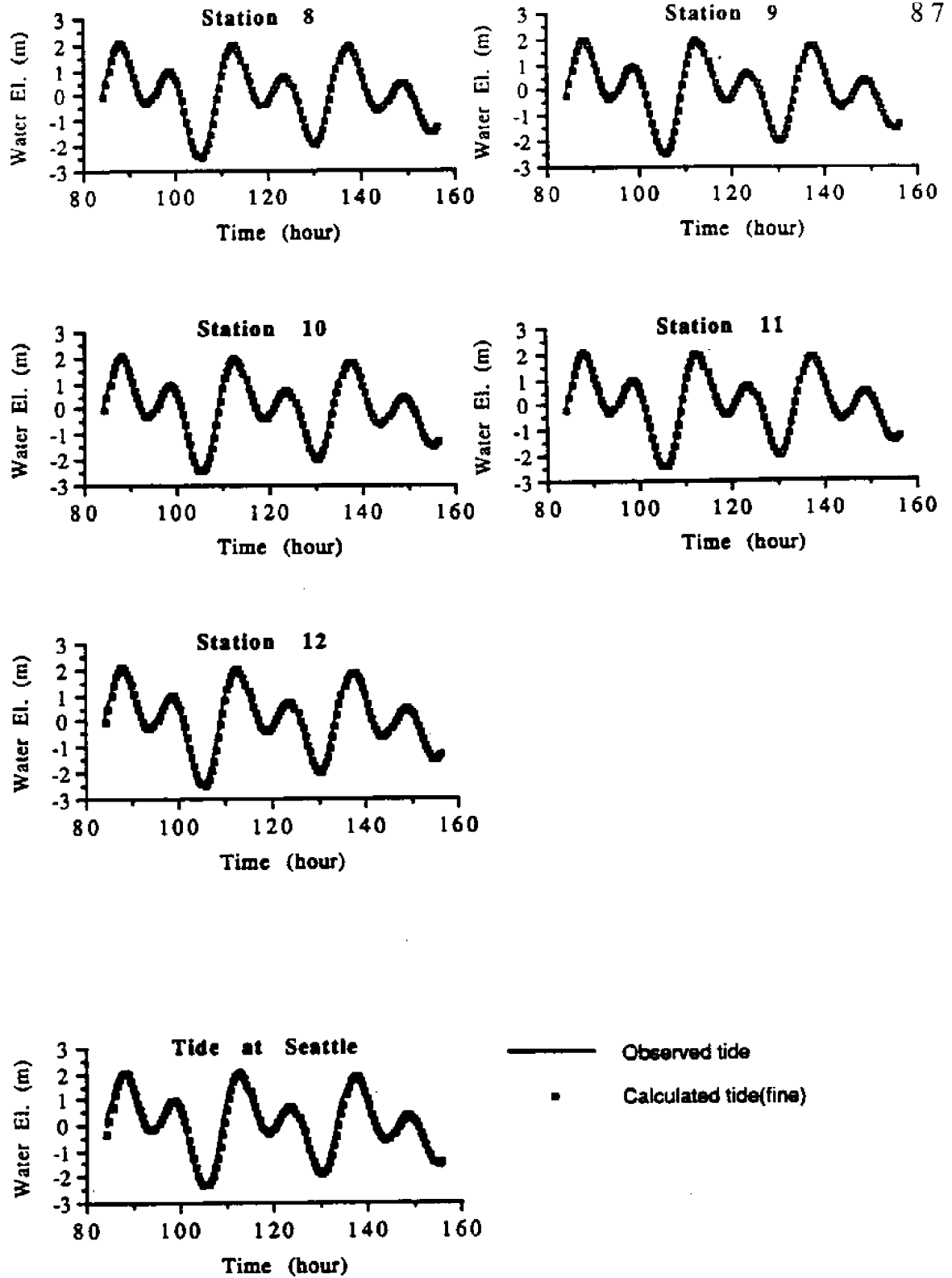
Fig.5.7 (continued)
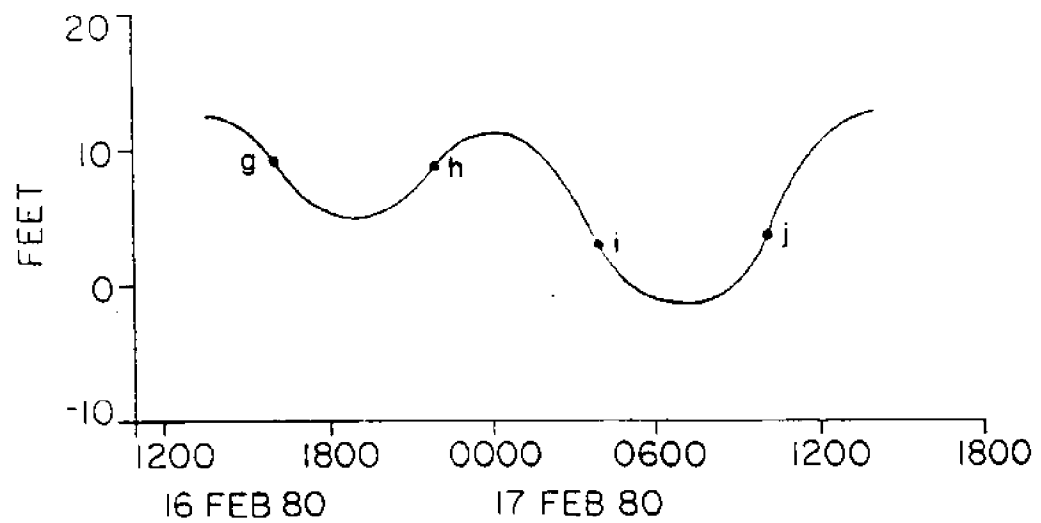
Fig.5.8 Times and heights of tides in Elliott Bay
corresponding to tidal currents in Fig.5.9. Zero
water elevation represents mean lower low water
(From Sillcox et al., 1981)
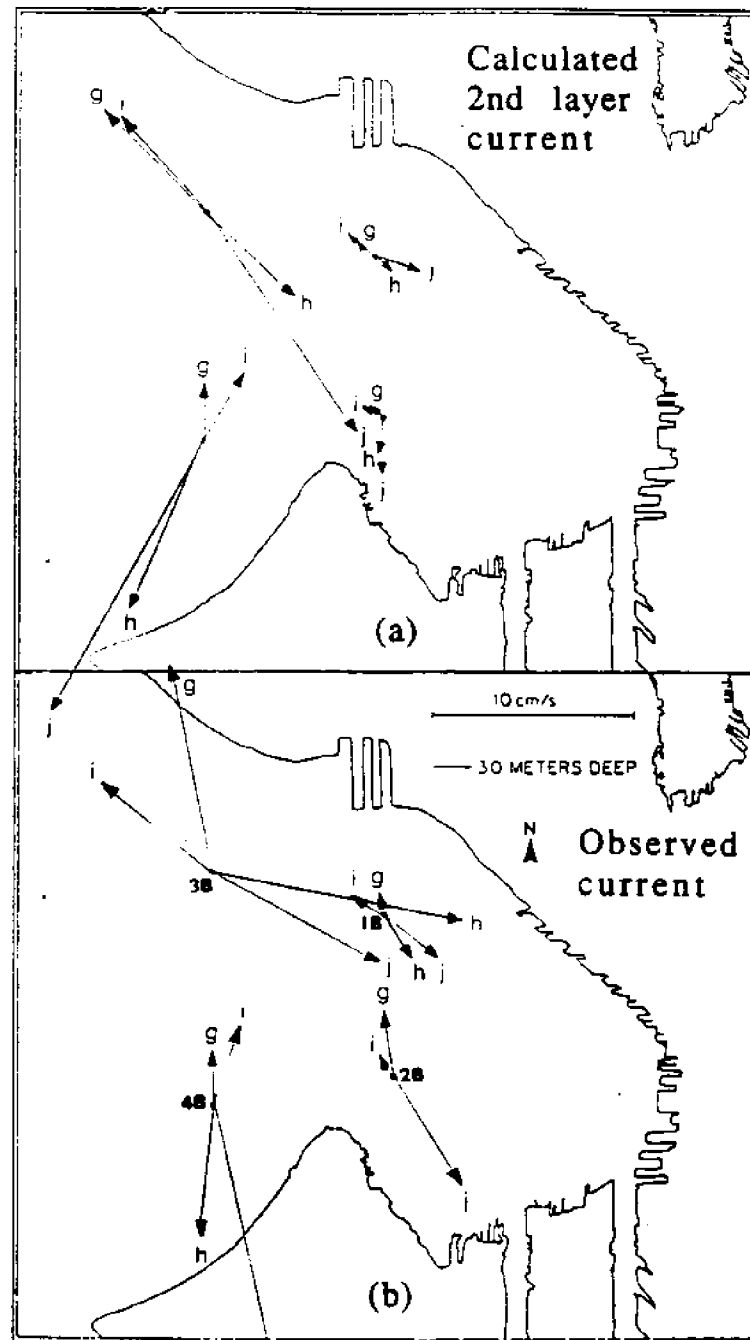
Figs.5.9a-b The comparisons between calculated 2nd layer current
and observed current (at 30 meters depth) at four stations in
Elliott Bay on two ebb and two flood tides shown in Fig.5.8.
(Note : 1B, 2B, 3B, and 4B are the positions of moorings (Sillcox
et al., 1981))

averaged currents in the second layer (between 15 m and 60 m depth) of the model.

The comparisons between Figs.5.9a and 5.9b show that the strengths of calculated tidal currents are consistent with those of the observations except at mooring 2B. The observed currents at mooring 2B exhibit stronger strength than the calculated currents for both ebb and flood tides. The current directions of both the calculated and the observed currents at all stations are highly influenced by the local bathymetry. Generally speaking, the differences between observed and calculated currents are considered acceptable because the comparison was made between currents observed at 30-meter depth and layer-averaged currents in the second layer of the model.

5.2.2 Tidal Currents in Central Puget Sound

In this section, tidal currents, and the effects of wind, river discharge, and tidal inequality on the currents in Central Puget Sound calculated by the developed model are presented.

5.2.2.1 Tide Induced Current and Circulation in Central Puget Sound

The bathymetry of Central Puget Sound (see Figs.4.12 and 4.14) can be separated into two distinct portions by Vashon and Bainbridge Islands. To the west of these two islands the bathymetry is complex and the water is shallow. The area west of Bainbridge Island includes many shallow inlets and channels such as Dyes Inlet, Sinclair Inlet, Port Orchard, and Liberty Bay, and it is called the West Sound Inlets (Burns, 1985). This area is connected to the main channel through Agate and Rich Passages located at the north and the south of Bainbridge Island respectively. To the west of Vashon Island there is a straight north-south waterway, called Colvos Passage, which connects to the Southern Basin of Puget Sound through The Narrows. In contrast, to the east of Bainbridge and Vashon Islands, the bathymetry is simple and the water is much

deeper. The basin encloses a broad and deep north-south channel. Except at places nearshore, most of the area has water depths over 100 meters.

Tidal currents in Central Puget Sound

The simulated tidal currents in both layers for Case 1 in Table 5.1 at eight selected time for the fifth tidal cycle of Fig.5.2 are given in Appendix I. It is difficult to derive basin wide time-related flow patterns from such detailed velocity vector diagrams unless tens and hundreds of them were produced. For the convenience of the reader, general qualitative Central Puget Sound flow patterns derived from the detailed vector diagrams (see Appendix I) are shown in Figs.5.10a-d. The calculated currents in the two model layers have similar flow directions at most of the locations within Central Puget Sound. The lower layer current speeds are always weaker due to the drag at the sea bottom. However, Lavelle et al. (1988) reported that the observed K1 tidal currents are strongest near the bottom. That is probably due to baroclinic effects (personal communication with H. O., Mofjeld, 1991).

During flood tide, the water tends to move southward in the main channel while some water moves westward into the West Sound Inlets through Agate and Rich Passages (Fig.5.10c). During ebb tide, the water in the West Sound Inlets moves eastward and joins the northward outflow in the main channel (Fig.5.10a). Most of the flows are directed nearly parallel to the shorelines. This general characteristics of the water movement derived from the model is rather consistent with the observed surface current in the hydraulic model (McGary and Lincoln, 1977). Since the tidal current at Rich Passage is stronger than that at Agate Passage and the channel cross-section there is larger as well, the direction of the tidal current in Port Orchard is primarily determined by the direction of the current at Rich Passage. Therefore, the flow in Port Orchard goes northward during flood tide and southward during ebb tide.
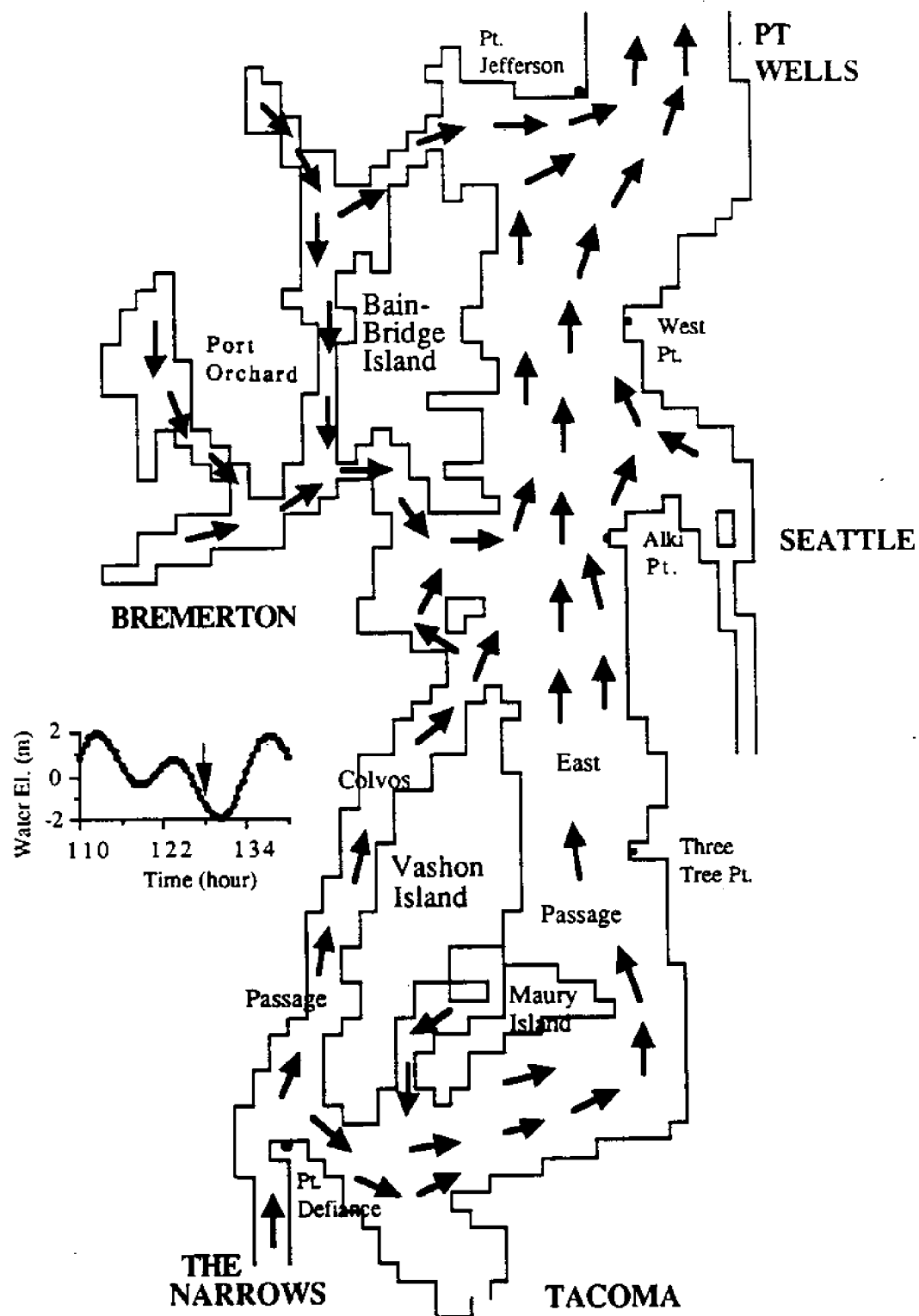
Fig.5.10a General surface layer flow pattern in Central Puget
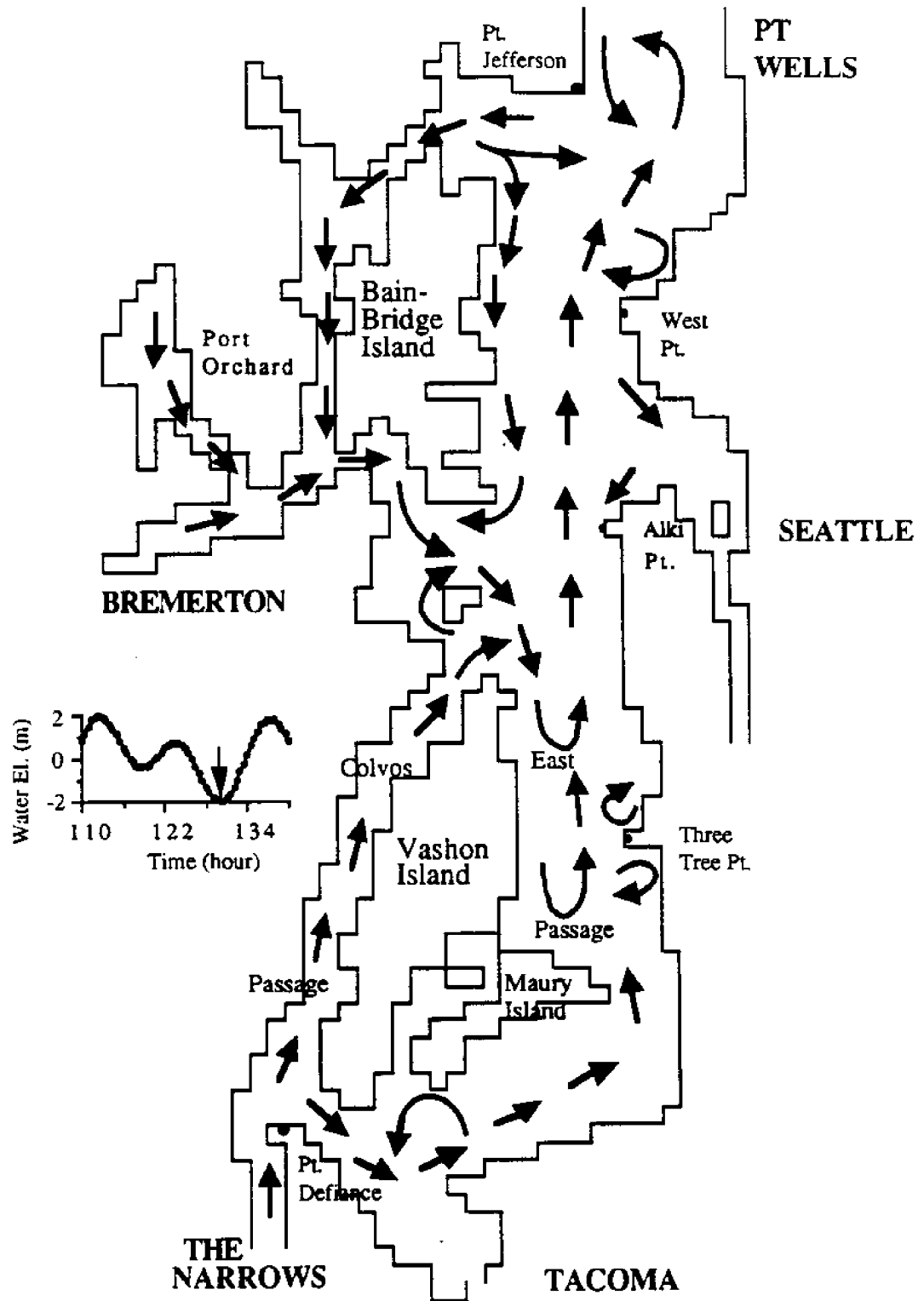   Sound at ebb tide

Fig.5.10b General surface layer flow pattern in Central Puget
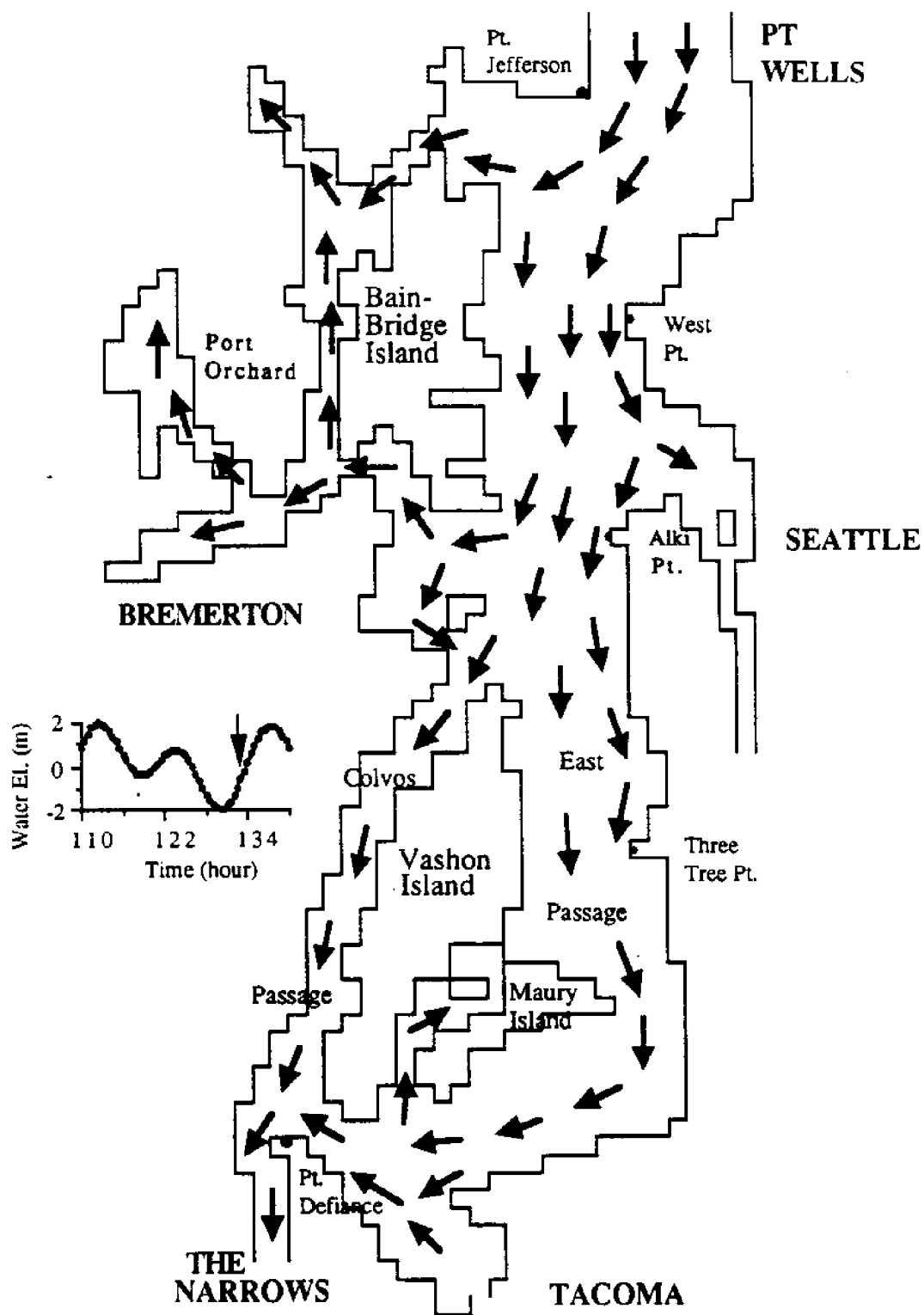Sound at low slack tide

Fig.5.10c General surface layer flow pattern in Central Puget
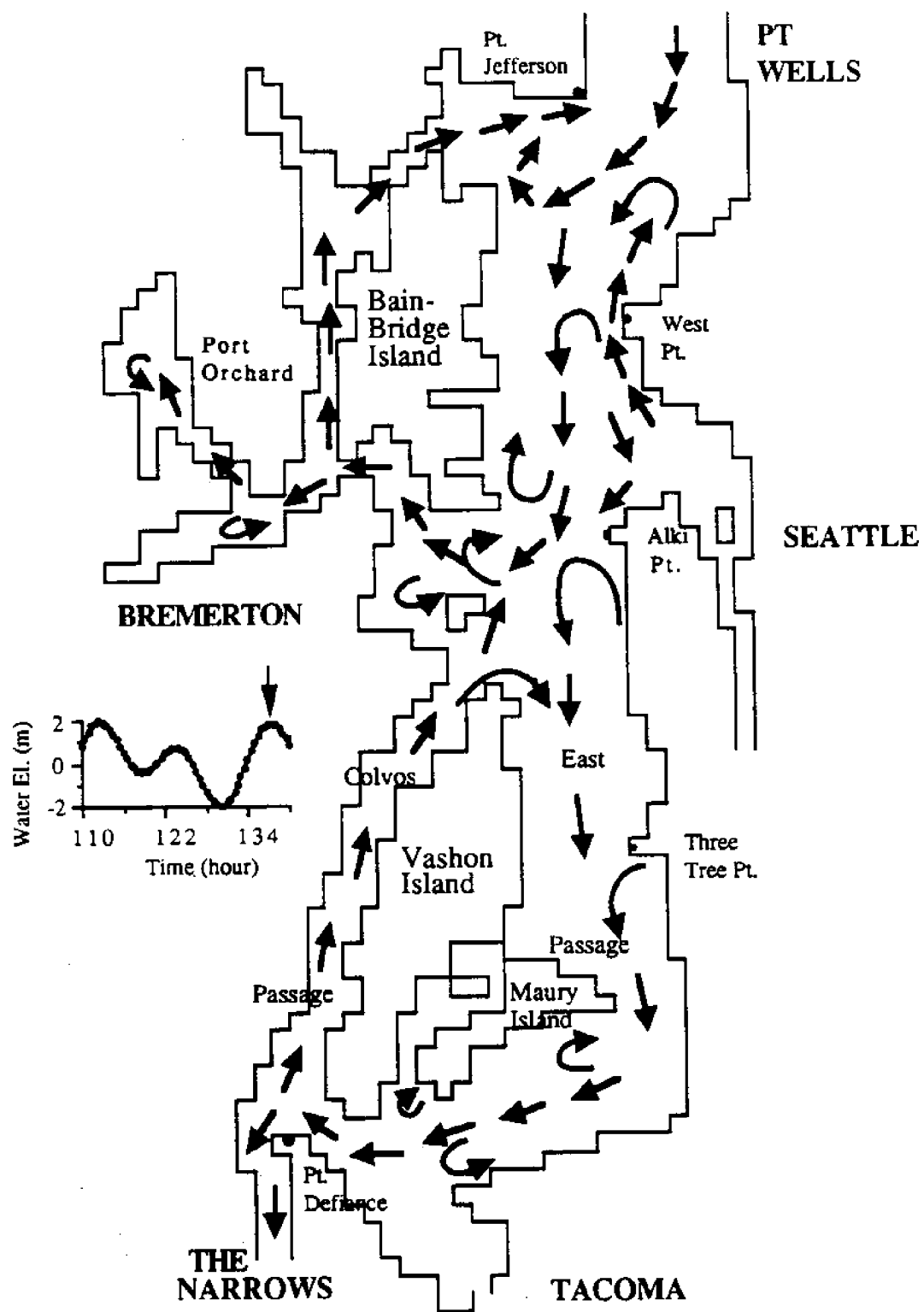Sound at flood tide

Fig.5.10d General surface layer flow pattern in Central Puget
Sound at high slack tide

During low and high slack tides, the tidal currents at most of the locations begin to reverse their directions. In the broad channel, the tidal current reverses by gradually rotating its direction (as shown in Fig.4.23). The rotations depend strongly on the local bathymetry. Because of their smaller momentum, tidal currents in the shallower waters can accelerate and decelerate easier than those in the deeper waters for the same longitudinal (streamwise) pressure gradients. Therefore, the currents in shallower waters reverse their directions sooner than those in deeper waters during slack tides which in turn causes the formation of eddies in the nearshore zones, especially near promontories. These eddies are found in the model output near the coasts of Point Jefferson, West Point, Alki Point, and southern shore of Maury Island (Figs.5.10b and 5.10d). Similar eddies have also been observed at slack water in the hydraulic model of Puget Sound (McGary and Lincoln, 1977; Winter, 1977; Ebbesmeyer, et al., 1977). Mofjeld and Larsen (1984) explained that these eddies were formed behind promontories when the current was sufficiently strong and were detached from the shoreline when the current reverses direction. Due to the coarse resolution (762 meter), the eddies observed behind the larger promontories during strong flood and ebb currents in the hydraulic model (McGary and Lincoln, 1977; Winter, 1977) were not found in the numerical model results.

The maximum current speeds within the fifth simulation tidal cycle (see Fig.5.2) at all grid locations for both layers are shown in Figs.5.11a-b. Under the particular tide investigated, the maximum current speed in the main channel appeared to be around 0.4 m/s. The stronger currents occurred at The Narrows at Tacoma, Rich Passage, Agate Passage, and Port Washington Narrows, or near the shoreline around Point Jefferson and West Point, and over the sill between Vashon and Blake Islands (Figs.5.11a-b). The current speeds at The Narrows and Port Washington Narrows reached 2.6 and 1.9

PT WELLS

Pt.
Jefferson

Agate
Passage

West Pt.

Port Wash. Narrows

Rich
Passage

SEATTLE

BREMERTON

Blake Island

Unit : m/sec

☐ 0.0 < U < 0.1

☐ 0.1 < U < 0.2

▣ 0.2 < U < 0.3

▣ 0.3 < U < 0.4

▨ 0.4 < U < 0.5

▧ 0.5 < U < 0.6

▨ 0.6 < U < 0.8

■ 0.8 < U < 1.0

■ 1.0 < U < 2.6

VASHON
ISLAND

THE
NARROWS

Dalco
Passage

TACOMA
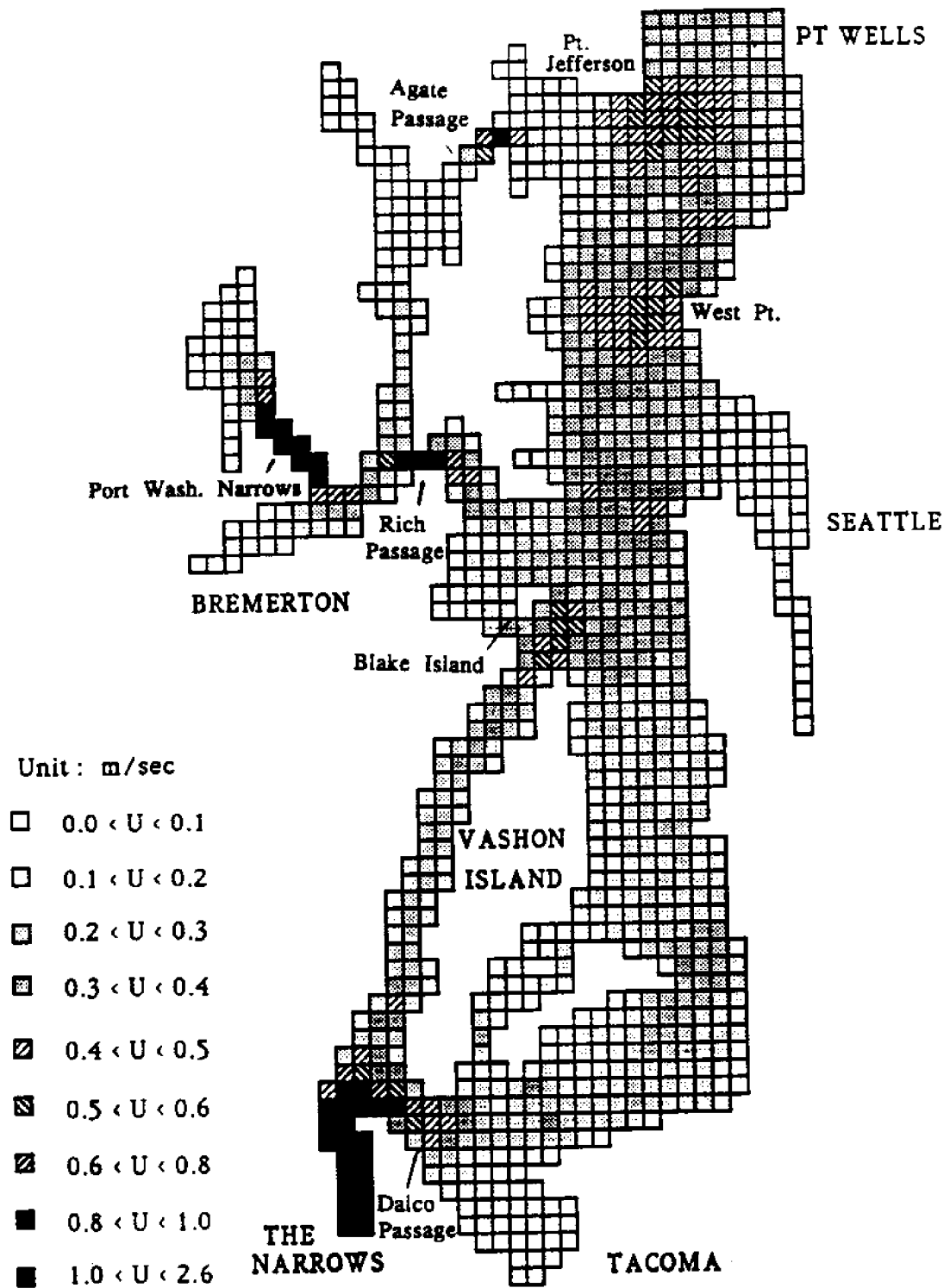
Fig.5.11a First layer maximum current speeds in Central Puget
Sound (for the 5th tidal cycle of Fig.5.2).

PT WELLS

SEATTLE

Unit : m/sec

☐ 0.0 < U < 0.1

☐ 0.1 < U < 0.2

☐ 0.2 < U < 0.3

▦ 0.3 < U < 0.4

▨ 0.4 < U < 0.5

▨ 0.5 < U < 0.6

▨ 0.6 < U < 0.8

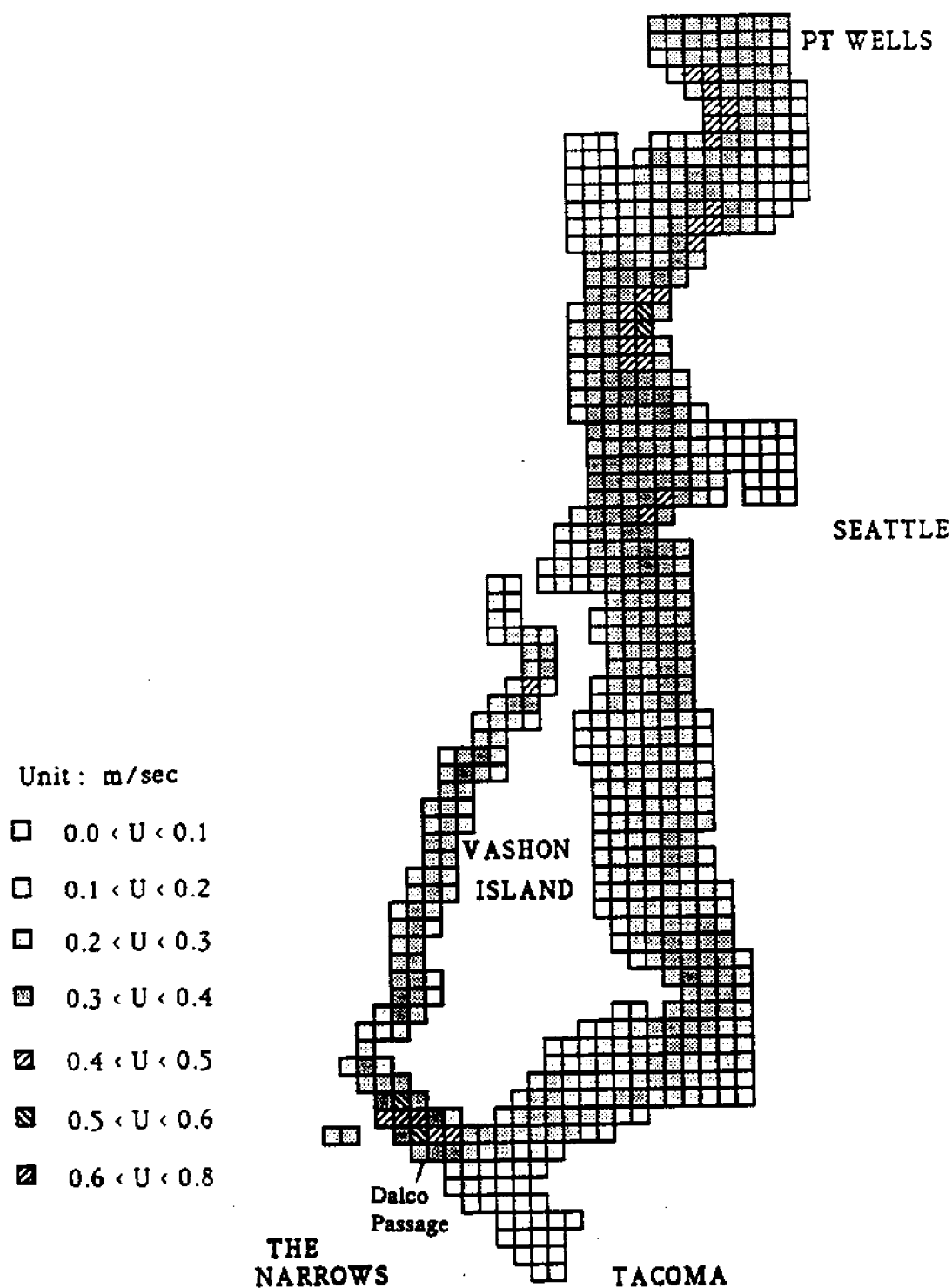VASHON
ISLAND

Dalco
Passage

THE
NARROWS

TACOMA

Fig.5.11b Second layer maximum current speeds in Central Puget
Sound (for the 5th tidal cycle of Fig.5.2).

m/s respectively. The strongest currents in the second model layeroccurred at Dalco Passage, and reached 0.8 m/s for the given tidal condition.

Residual Current in Central Puget Sound

Residual circulation is loosely defined as the velocity field obtained by averaging the velocity at each point in the estuary over a given tidal cycle (Fischer et al., 1979). In this study, the residual circulations in Central Puget Sound were obtained by averaging the velocity at each model grid over a 24.7-hour period. The residual circulations for the fifth simulation tidal cycle (see Fig.5.2) for both layers are plotted in Figs.5.12a-b.

Residual currents are generally weak in most of the areas in Central Puget Sound except at several locations near the promontories. Due to the sharp corners of the promontories, the tidal currents during flood and ebb tides are very unsymmetrical and thus are not cancelled by the tidal averaging process. The stronger residual circulations found near Point Jefferson and Dalco Passage in Fig.5.12a are two such examples. The maximum residual current speed at Dalco Passage reached 0.18 m/s in the first layer and 0.12 m/s in the second layer. Also seen in Figs.5.12a-b are northward residual currents near the coast of West Point, and outside the coast of Alki Point, and several small circulation patterns at junctions in the West Sound Inlets.

In order to investigate the model-generated residual currents around Vashon Island in greater details, the vector diagram outputs were enlarged and plotted in Figs.5.13a-b. Clear northward residual currents in both layers in Colvos Passage can be seen in Figs.5.13a-b. Between Blake and Vashon Islands, these northward residual currents merged with the counterclockwise circulation near Alki Point and turned southward. In East Passage, most of the water traveled southward on the west side, but some weaker northward residual currents can be seen along the eastern shoreline. Despite a

Pt. Jefferson ....
Point Wells

Bain-
bridge
Island

West Pt.

Seattle

Alki
Pt.

Blake Island

0.181 m/s
MAXIMUM VECTOR

Vashon
Island

0.121 m/s
MAXIMUM VECTOR

The
Narrows

Tacoma

Dalco
Passage

(a) 1st layer

(b) 2nd layer
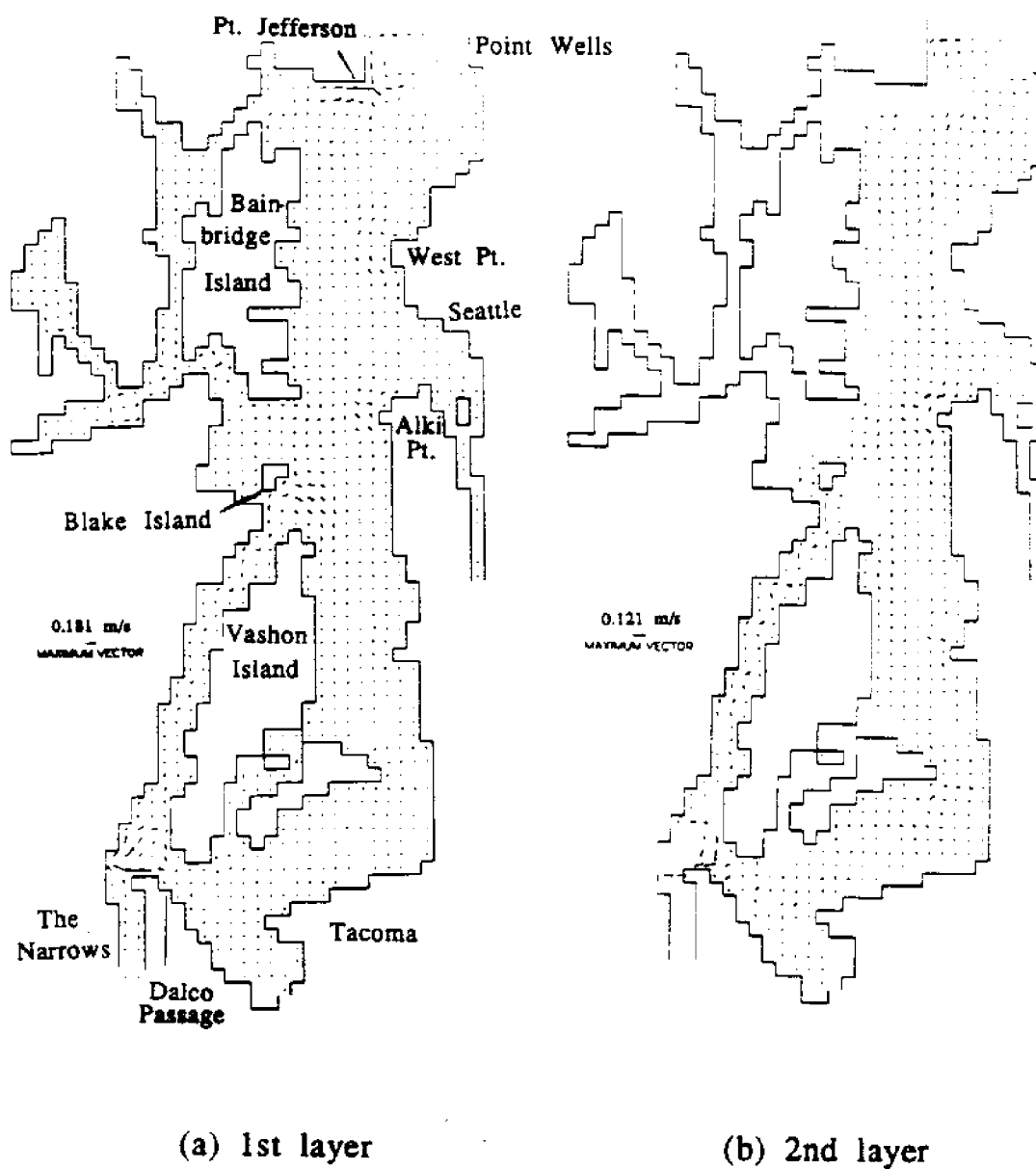
Fig.5.12 Residual circulation in Central Puget Sound (for the 5th tidal cycle of Fig.5.2).

(b) 2nd layer

0.121 m/s
MAXIMUM VECTOR

(a) 1st layer

0.182 m/s
MAXIMUM VECTOR

East Passage

Blake Island

Colvos Passage
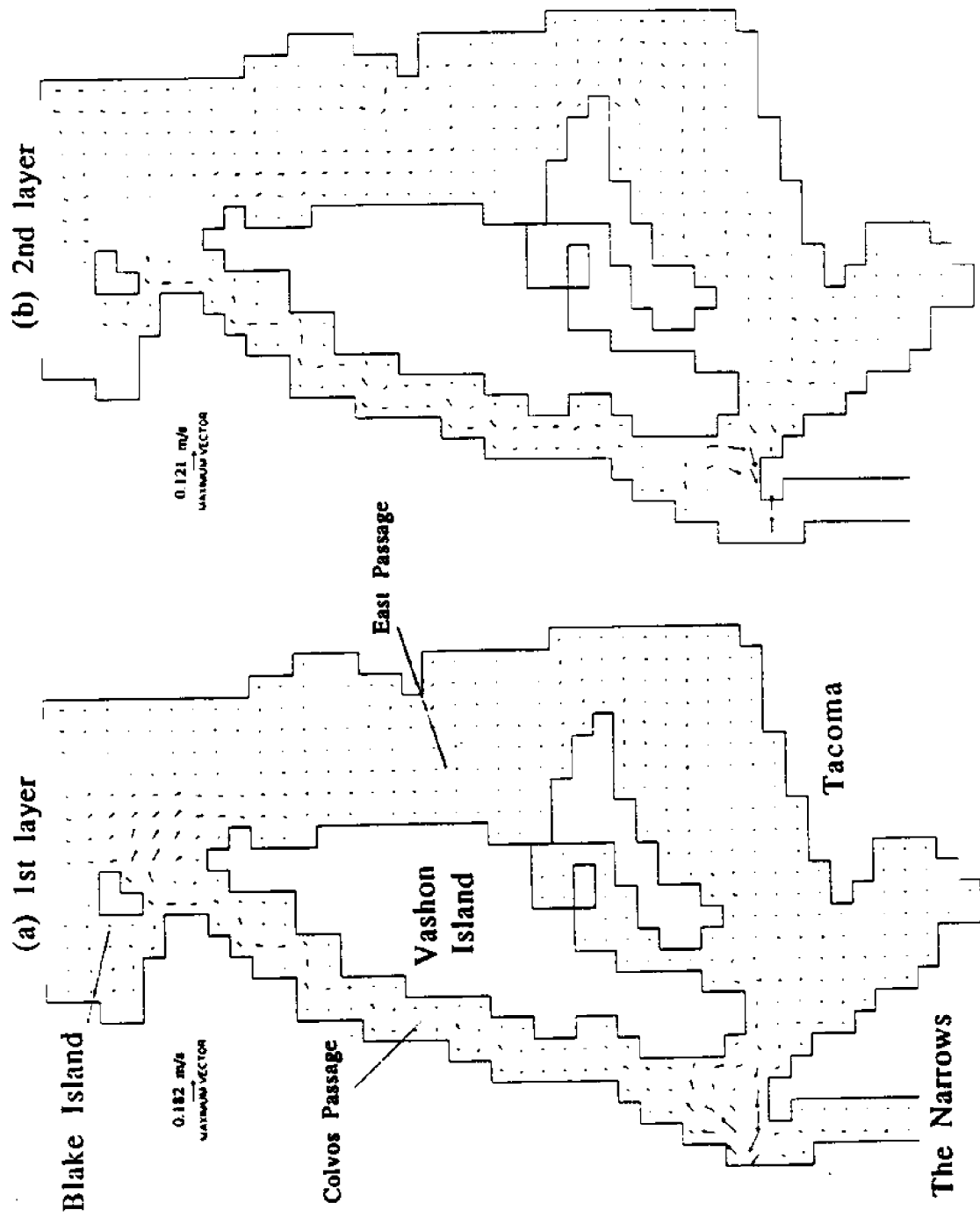
Vashon Island

Tacoma

The Narrows

Fig.5.13 Residual circulation around Vashon Island (for the 5th tidal cycle of Fig.5.2).

weak clockwise circulation, most of the water at the south of Maury Island tended to move westward. On the whole, the occurrence of these current patterns seem to coincide with the well known theory that there exists a clockwise net circulation around Vashon Island (Geyer and Cannon, 1982; Bretschneider, 1985). The existence of the northward residual currents on the east side of the main channel and the presence of the southward residual currents on the west side of the main channel are believed to have been caused by Coriolis force and local bathymetry.

5.2.2.2 Results of Particle Tracking Model Application

To better demonstrate the above observed current patterns, the particle tracking model (Chapter 3) was used to further reveal how a parcel of water moves over time. Particles were released at 9 chosen locations within Central Puget Sound in the simulations. Four of the release sites were located around Vashon Island for the purpose of verifying residual circulation around the Island. The other five release sites were chosen to be near West Point, Duwamish Head, Alki Point, Three Tree Point, and Commencement Bay. At each location, 25 particles were released in a 5 by 5 matrix covering one grid space, allowing 190 meters between each two adjacent particles. The results of the particle tracking model simulation are given below.

Experiment to Confirm Circulation around Vashon Island

To track the water movement around Vashon Island, particles were released at the south end of Colvos Passage and off the coasts of Point Beals, Point Robinson, and Dash Point. All 25 particles were simultaneously released at 10-meter depth and at higher high water (HHW in Fig.5.14) and continuously tracked for 9 consecutive tidal cycles (about 9 days). The positions of the particles at the end of 2nd, 4th, 6th, and 8th tidal cycles (see Fig.5.14) are displayed in Figs.5.15a-d.
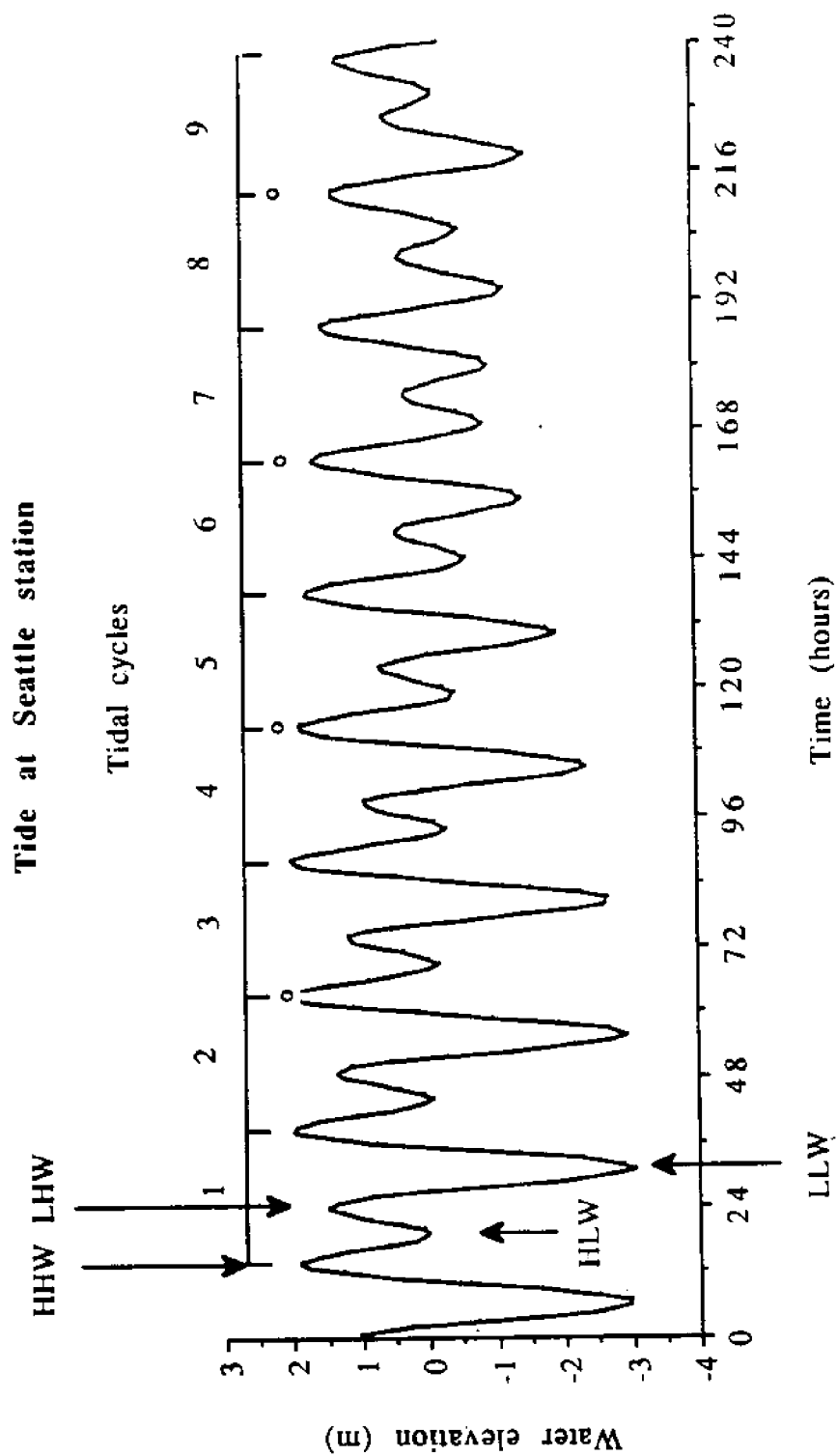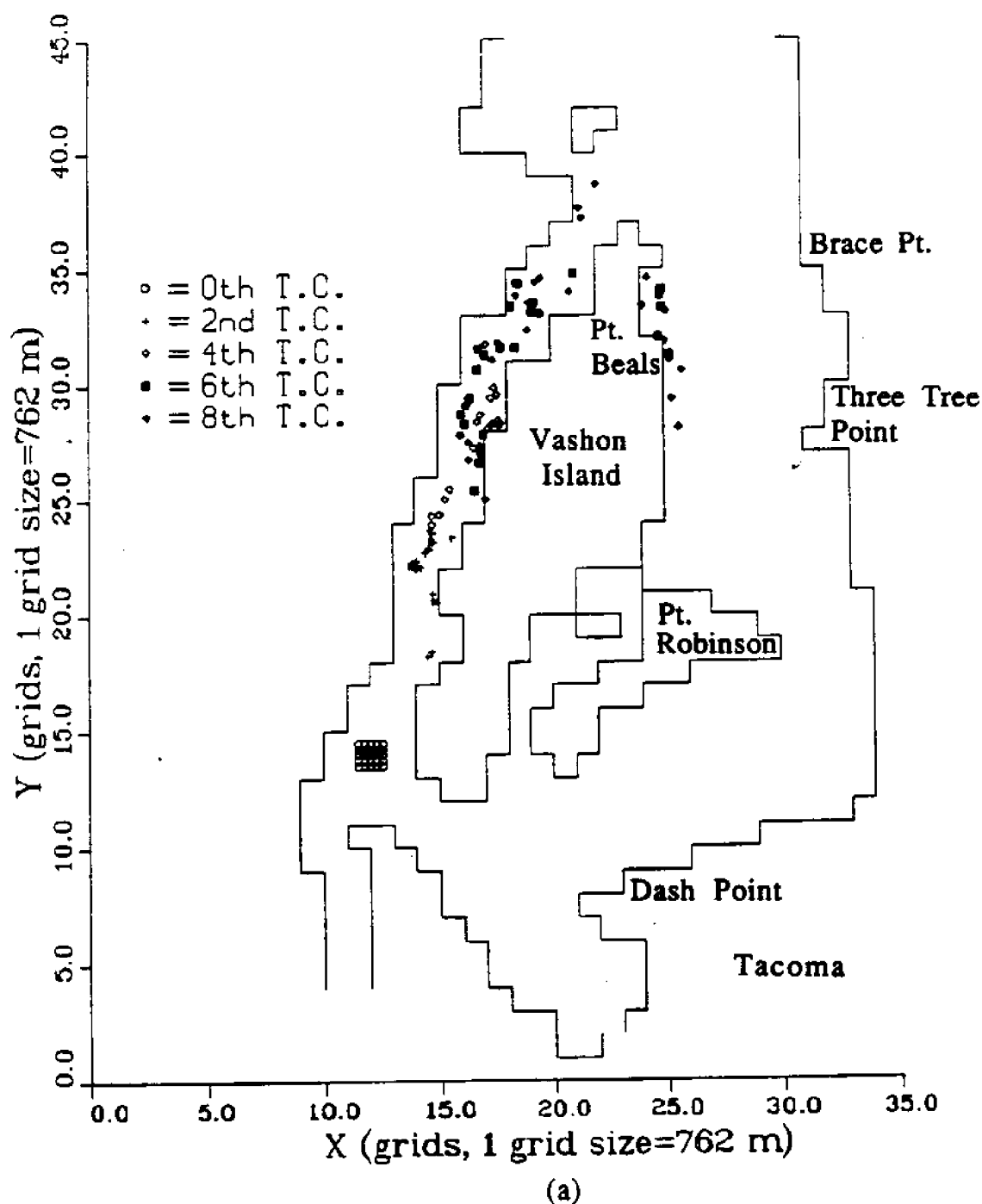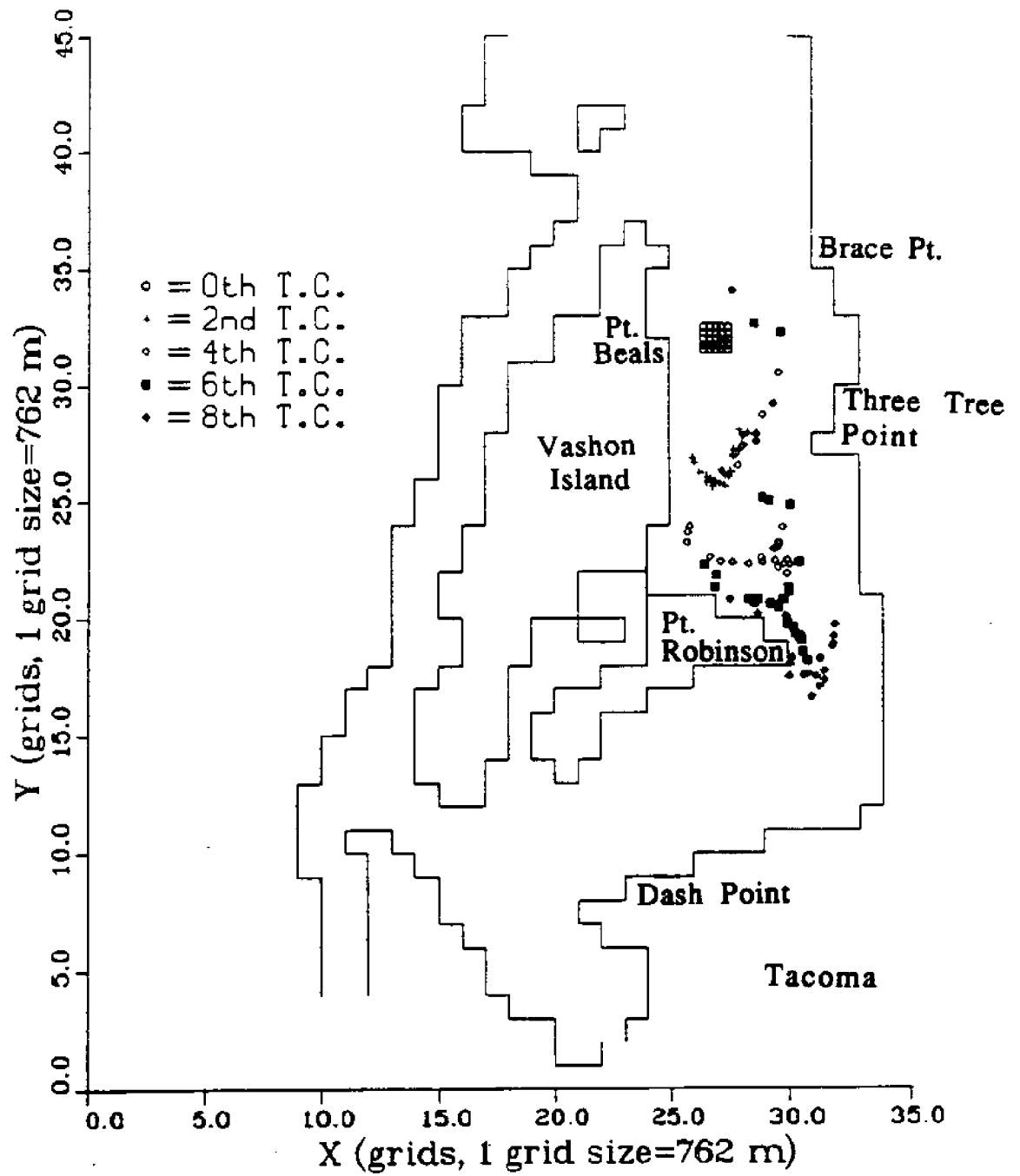
Fig.5.14 Simulation period and releasing time for particle tracking model "Circle" signs represent the end of 2nd, 4th, 6th, and 8th tidal cycles
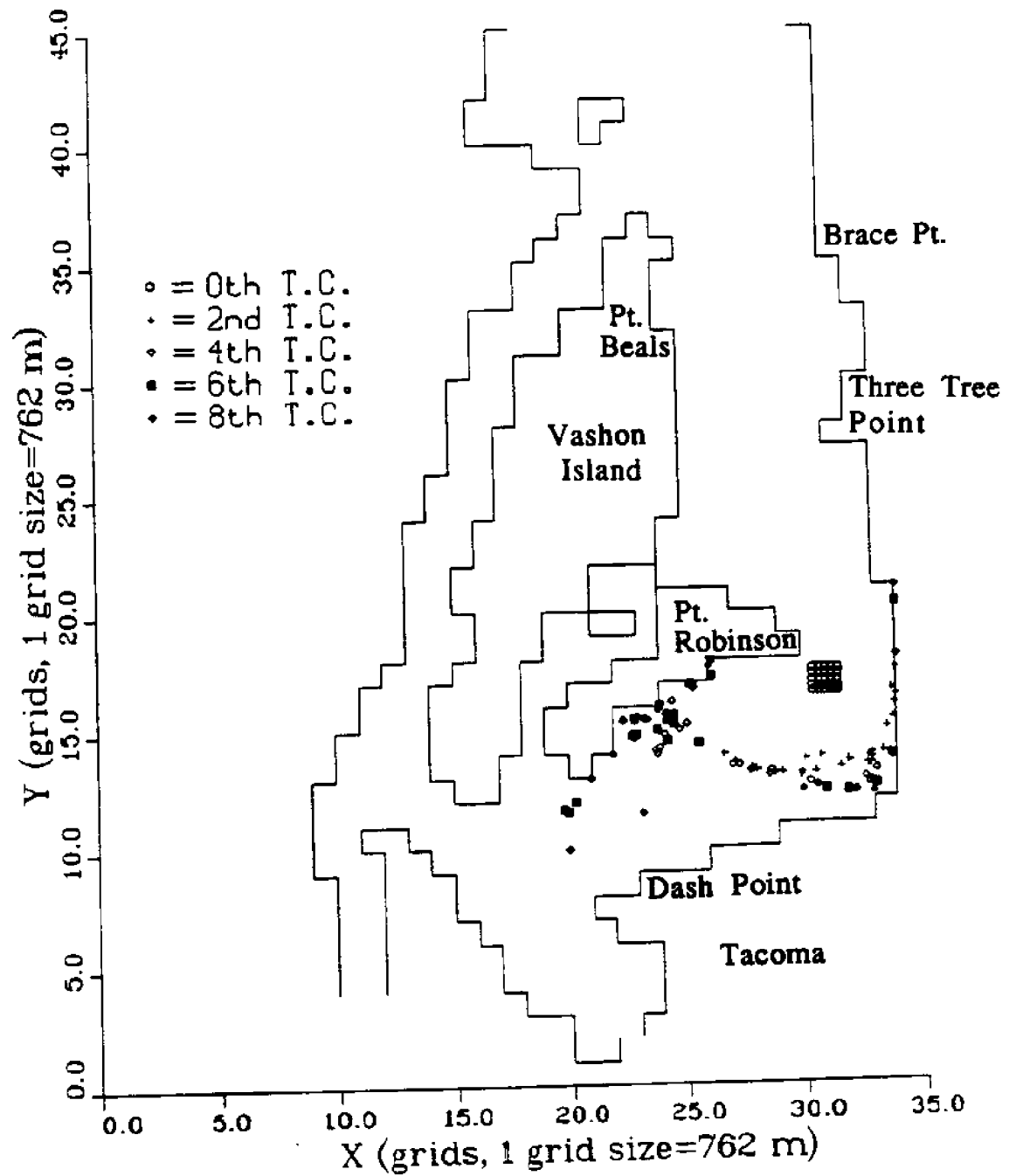
(a)

Figs.5.15a-d Particle tracking around Vashon Island; particles release at south end of Colvos Passage and off the coasts of Point Beals, Point Robinson, and Dash Point.
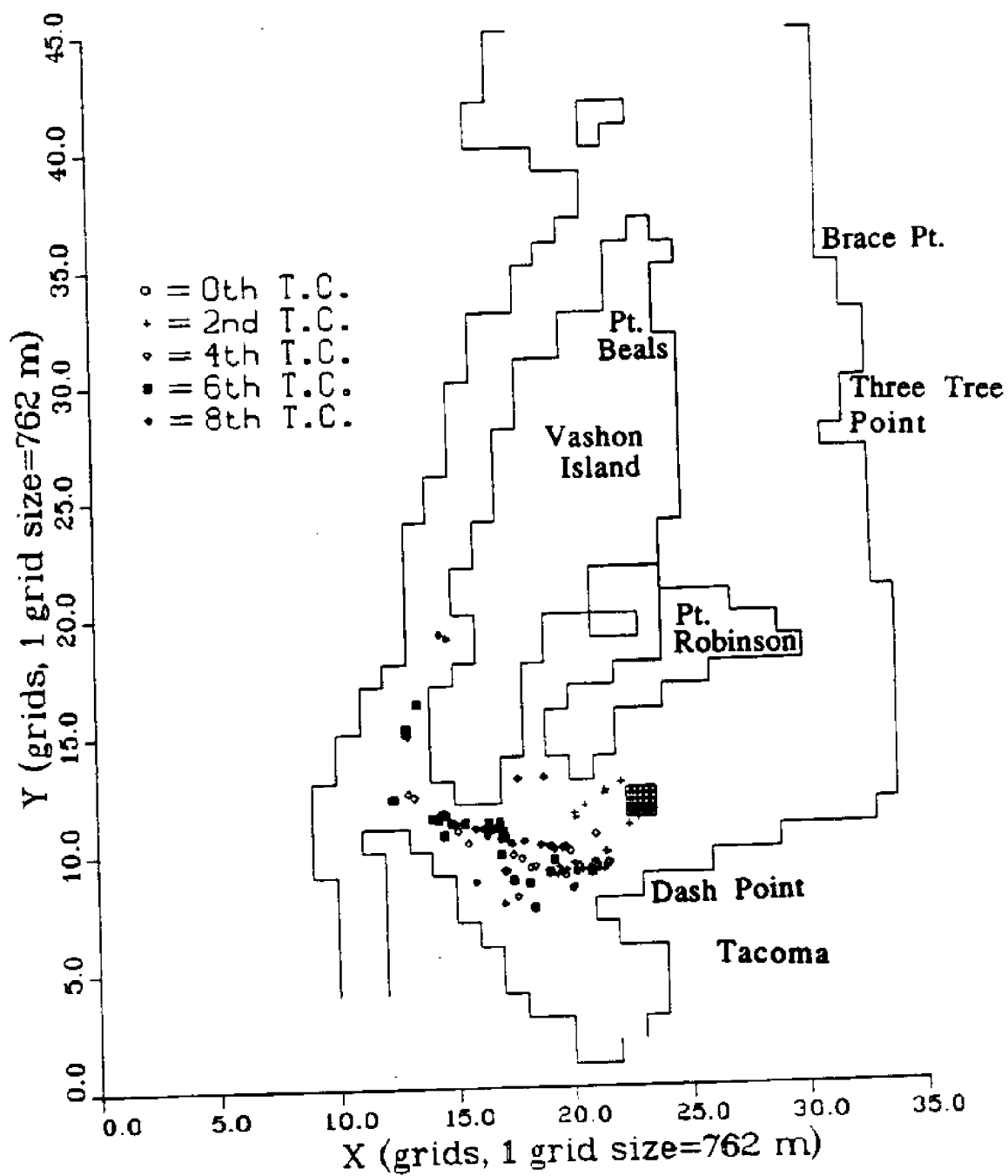
Figs.5.15a-d (continued)

Figs.5.15a-d (continued)

(d)

Figs.5.15a-d (continued)

It can be seen in Fig.5.15a that particles released at the south end of Colvos Passage would clearly move northward. After the fourth tidal cycle, the front of the released particles moved through Colvos Passage and crossed the sill between Vashon and Blake Islands and turned southward. It can be seen in Fig.5.15c that particles released near Point Robinson moved southward during the first two tidal cycles, turned northwest toward the southern end of Maury Island, and then moved westward along the southern coast of Maury Island. The excursion and distribution of released particles in this location were shorter and were more diverse, respectively, because the flow in this region was weaker and more erratic. From Fig.5.15d, it can be seen that the particles released north of Dash Point moved westward through Dalco Passage, and entered Colvos Passage. The particles that went into South Puget Sound through The Narrows were assumed to be "picked up", and never returned back into our model domain. Although no specific particles made it all the way around Vashon Island during the simulation period, the simulation results once again demonstrated the existence of a clockwise residual circulation around Vashon Island.

The trajectories of the particles will depend on the times of their released. Additional experiments in which particles were released at higher low water (HLW), lower high water (LHW), and lower low water (LLW) (see Fig.5.14) were made. The results show that the excursions of particles released at HLW and LHW were shorter than those released at HHW, but the clockwise residual circulation was evident for every case studied.

The tidal currents at Colvos Passage and Dalco Passage are much stronger than those at East Passage. Based on our model results, it is speculated that the released particles may take about one week to pass through both Dalco and Colvos Passages but they need about three weeks to pass through East Passage. The released particles may take as long as one month to circulate around Vashon Island.

Other Particle Tracking Experiments

Other experiments in which particles were released near West Point, Duwamish Head, Alki Point, Brace Point, and Commencement Bay were conducted. All particles were simultaneously released at 10-meter depth and at higher high water (HHW in Fig.5.14) and continuously tracked for 9 consecutive tidal cycles. The locations of these particles at the end of 2nd, 4th, 6th, and 8th tidal cycles (see Fig.5.14) are shown in Figs.5.16-19.

The particles released near West Point did not move too far after 8 tidal cycles (Fig.5.16). Most of the released particles were found in the main channel from the north end of Bainbridge Island to the entrance of Elliott Bay. There were more particles along the shore of Bainbridge Island. There was no sign indicating that these particles might move into Elliott Bay. Using dye as tracer in the hydraulic model, it was found that water around West Point would disperse across the main channel in a similar manner (Winter, 1977).

The trajectories of the particles released north of Duwamish Head and west of Alki Point are given in Figs.5.17-18. The trajectories of the particles released in these two locations looked similar. Except for a few that moved to the north and the west, most of the released particles tended to move southward along the main channel with the farthest reaching Point Beals on Vashon Island in eighth tidal cycle.

The movements of particles released near the coast of Three Tree Point and in Commencement Bay are exhibited in Fig.5.19. The particles released near Three Tree Point all traveled northward along the east shore of East Passage confirming the northerly residual current presented in section 5.2.2.1. The particles released in Commencement Bay slowly moved toward the northwest and into Dalco Passage.
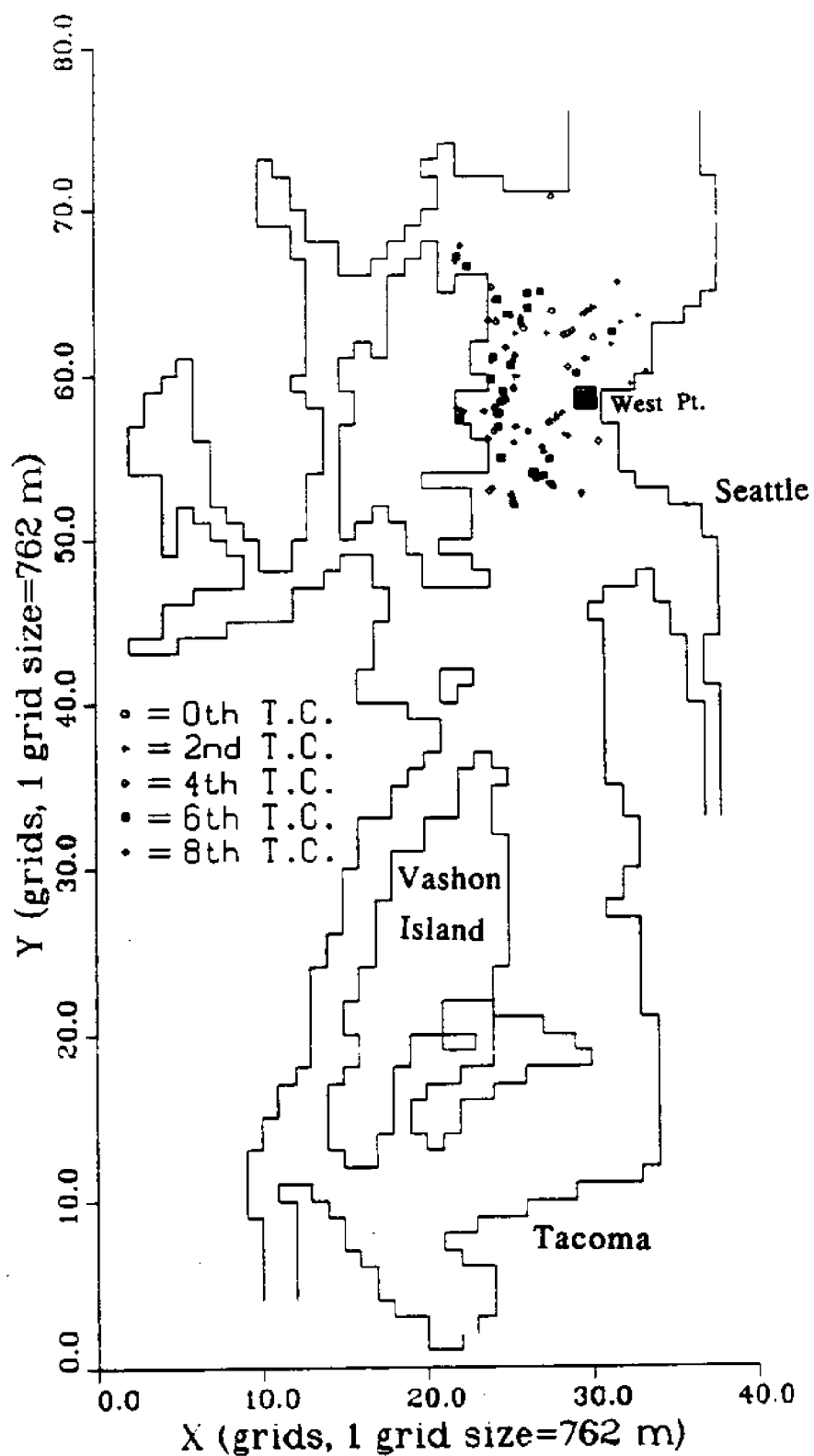
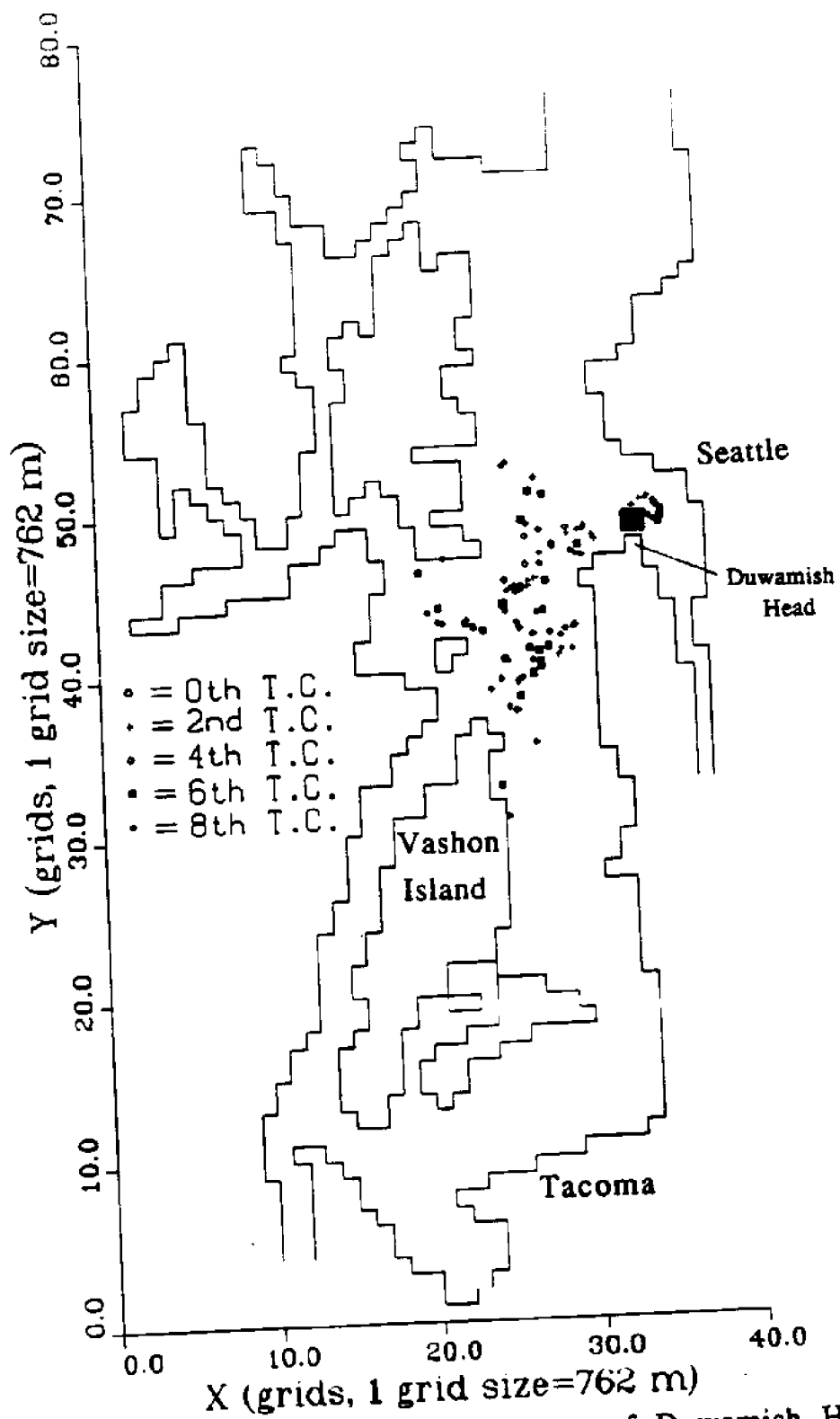Fig.5.16 Particles released near the coast of West Point

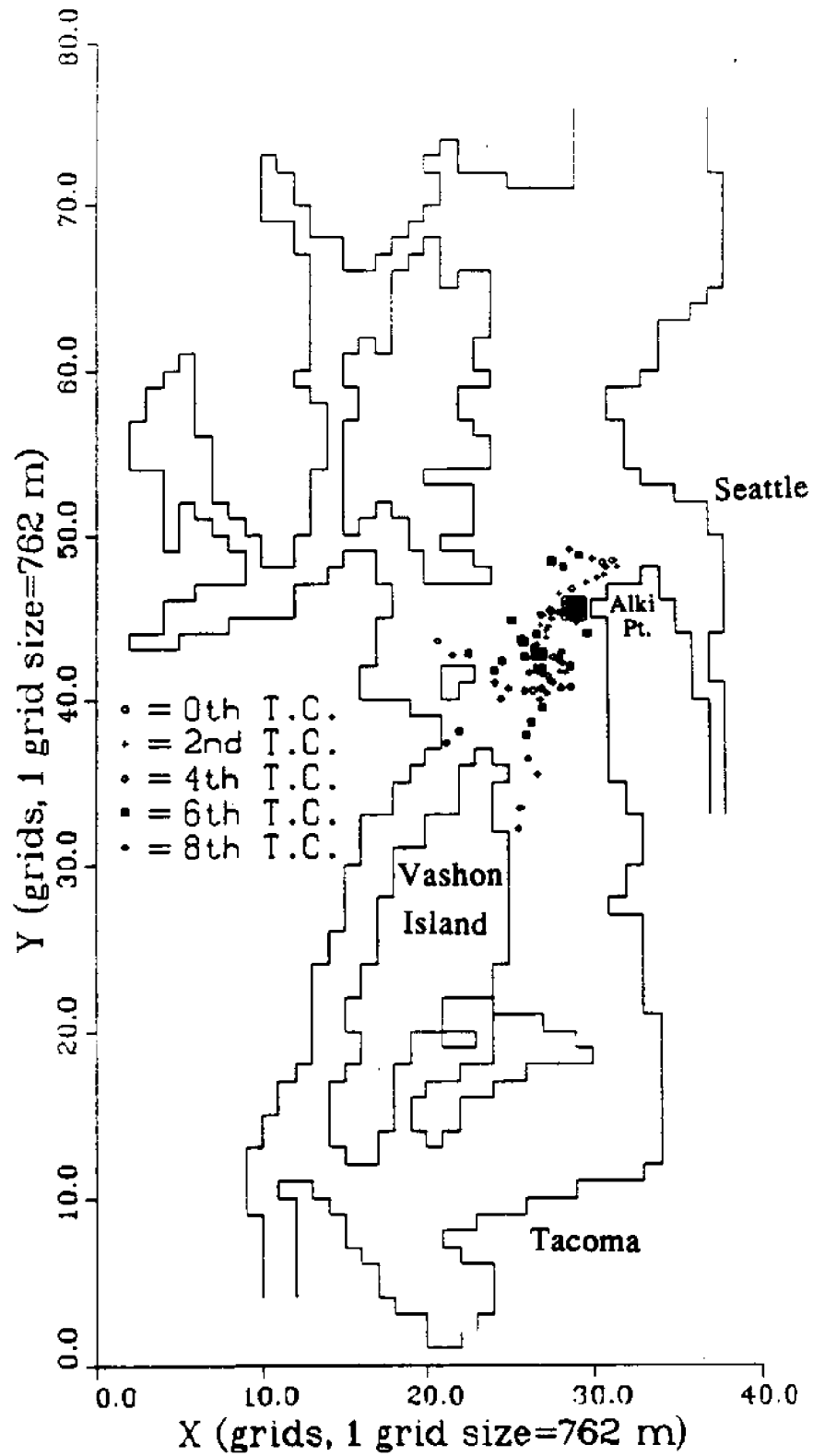Fig.5.17 Particles released near the coast of Duwamish Head

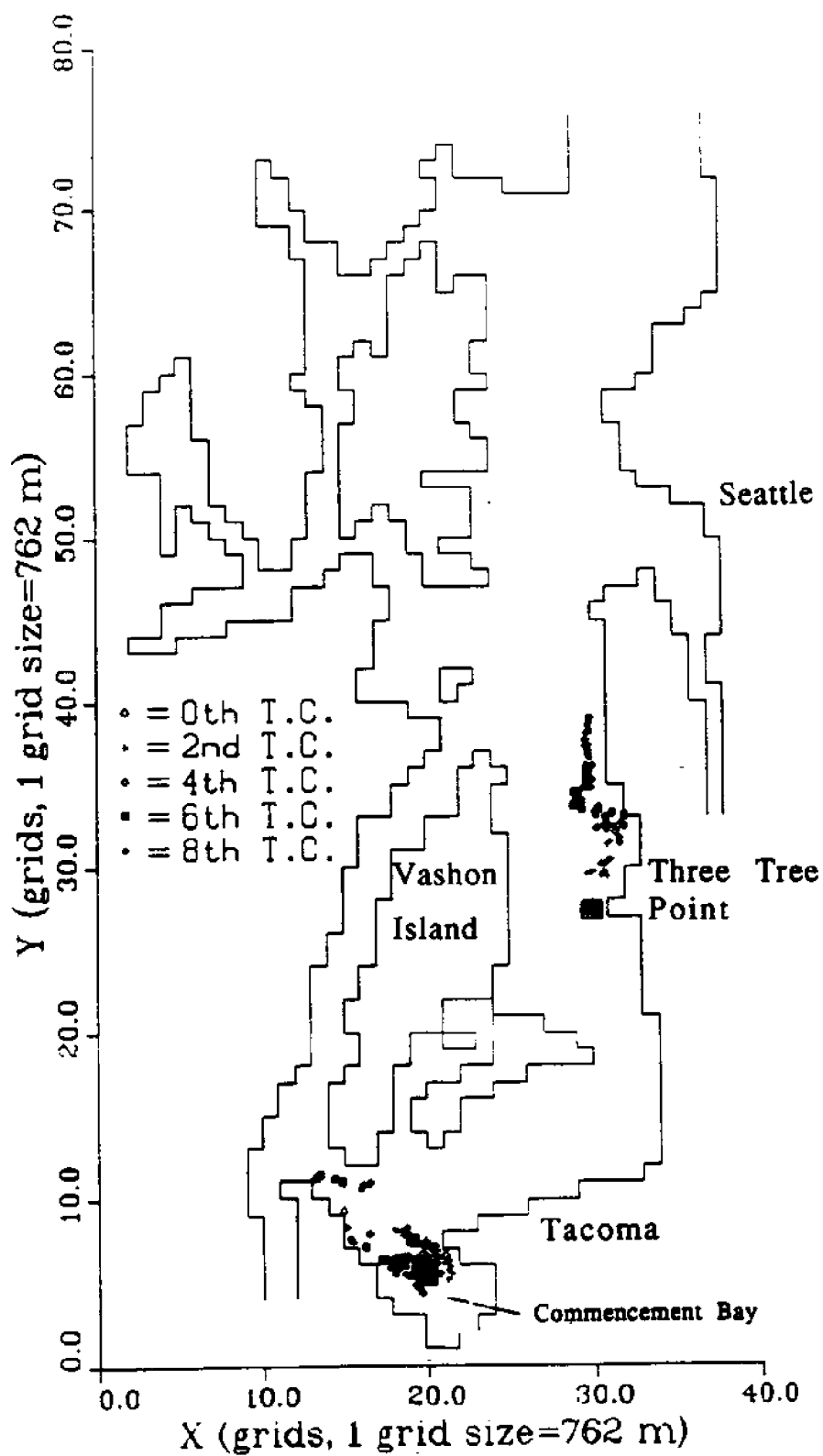Fig.5.18 Particles released near the coast of Alki Point

Fig.5.19 Particles released near the coasts of Three Tree Point and Commencement Bay

It should be remarked that the particle movements here were all driven by tide only. These particle movements are likely to change when the effects of river inflow, wind, and density variation are included.

5.2.2.3 Study of Tidal Currents Modifications of Due to River Discharge, Wind, and Tidal Inequality

The characteristics of tidal currents in Central Puget Sound described in the previous sections were derived from the calculated results of Case 1 in Table 5.1 (basic case). In this section, the effects of river inflow, wind, and tidal inequality on Central Puget Sound tidal hydrodynamics are presented.

Effect of River Discharge

The Puyallup and Duwamish discharges used in Case 2 were 120 m^3s^{-1} (12 times of that in Case 1) and 60 m^3s^{-1} (6 times of that in Case 1) respectively. The effect of increased river discharge on the residual circulation is shown in Figs.5.20a-b. The vector plots in these two figures were obtained by subtracting the residual currents of Case 1 from those of Case 2. The results reveal that the effect of river inflow in most parts of the study area is very small. The effect of river inflow is confined within Elliott Bay and Commencement Bay. The maximum difference in Fig.5.20 is less than 0.005 m/s, which is too small to be observed because of the small scale of the vector plots.

The increase in river inflows in Case 2 has a net volume increase that corresponds to about 2 cm each day within the study domain. Because the boundary conditions used by the model were obtained by ignoring river inflows from the Duwamish and Puyallup, therefore the added river inflows were not allowed to leave the model boundaries and would in turns push more water into West

Point Wells

Bain-
bridge
Island

Seattle

0.005 m/s
MAXIMUM VECTOR

Vashon
Island

0.003 m/s
MAXIMUM VECTOR

Tacoma
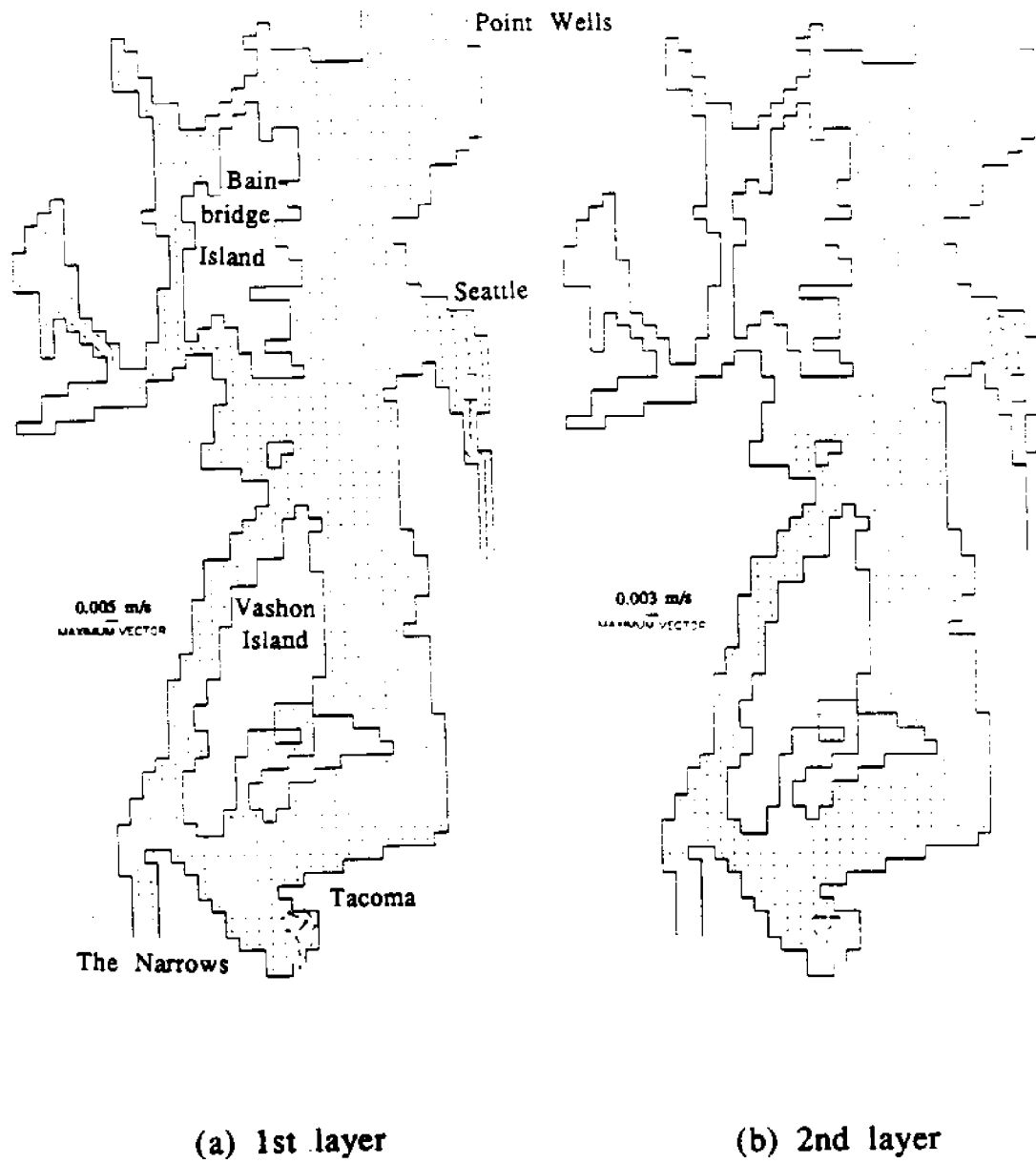
The Narrows

(a) 1st layer   (b) 2nd layer

Fig.5.20 The difference in mean current caused by high and low river inflow.

Sound Inlets. This is a possible explanation for the increase of residual currents in West Sound Inlets (Fig.5.20a).

Effect of Wind

The effect of wind on tidal currents depends on the speed, duration, direction, and fetch length of the wind, and the topography of the land surrounding the basin. In this study, only one southerly wind and one northerly wind (in Fig.5.4) were used in the simulations (Cases 3 and 4 in Table 5.1). The effect of wind on both the tidal and residual tidal currents in the top layer was so small that the differences in vector plots for the cases simulated were indistinguishable. Wind effect is even less significant in the West Sound Inlets. This is due to the small fetch length of the winds in this region. Wind effect in the main channel is more pronounced in or near Port Madison, Elliott Bay, and Commencement Bay.

Because the velocities calculated from the model are layer-averaged, for a given wind condition the calculated wind induced currents in shallower waters will be larger than those in deeper waters. To produce a more accurate wind induced current field, more refined vertical resolution near the water surface should be used.

Effect of Tidal Inequality

The tidal currents described in the previous sections were all driven by tidal transport due to "medium tide" labelled in Fig.5.2. The tidal currents due to spring and neap tides are investigated next.

After comparing the results, it is seen that the calculated flow patterns due to spring, medium, and neap tides are almost identical. The only difference is in the calculated maximum current speed. It is therefore proposed here that tidal currents in Central Puget Sound can be characterized by one general flow pattern. The maximum current speed at any location is affected by the range of the tide driving the flow. Based on this thesis, it was postulated that perhaps an empirical function that relates the tide range at a specific location

(say Seattle) to maximum current speeds everywhere within the study domain could be derived from our model results. The derivation of such relationship would allow the efficient estimation of maximum current speed at any grid location from Tide Table data. The derivation and the results of this "Tidal Current Function" are given below.

5.2.2.4 Derivation of Tidal Current Function

Each diurnal tide in Puget Sound contains two floods and two ebbs. Each flood tide (or ebb tide) is characterized by a tide range (R), a time duration (T_d) which is defined here as the time interval between two adjacent low and high (or high and low) waters, and a maximum current speed (V_{max}). As an initial step, a relationship between the Seattle tide range (R) and the product of the time duration at Seattle (T_d) and the maximum current speed (V_{max}) (which has the physical meaning of tidal excursion, see Mofjeld and Larsen, 1984) at five specific locations was sought. The five locations are near the five current stations (MESA 2,3,5,6 and 7) given in Fig.4.12. The derived results are shown in Fig.5.21. Plots in Fig.5.21 were obtained by running the model for Central Puget Sound for nine consecutive tidal cycles. From Fig.5.21, it is seen that the relationship sought can be adequately described by a family of linear functions with stronger current speeds corresponding to larger tide ranges.

To derive more general functions to relate Seattle tide ranges to maximum current speeds at any node within the model domain, further analysis ensued. Firstly, the relationships between Seattle tide range and maximum current speeds at all the nodes inside the study domain were examined. During flood tide, the relationship between the tide range at Seattle and the product of the time duration at Seattle and the maximum current speed at all the nodes inside the domain was found to be linear. During ebb tide, the relationships were not exactly linear, although most of the r^2 (coefficient of determination in the least square fit) values were still larger than 0.9.
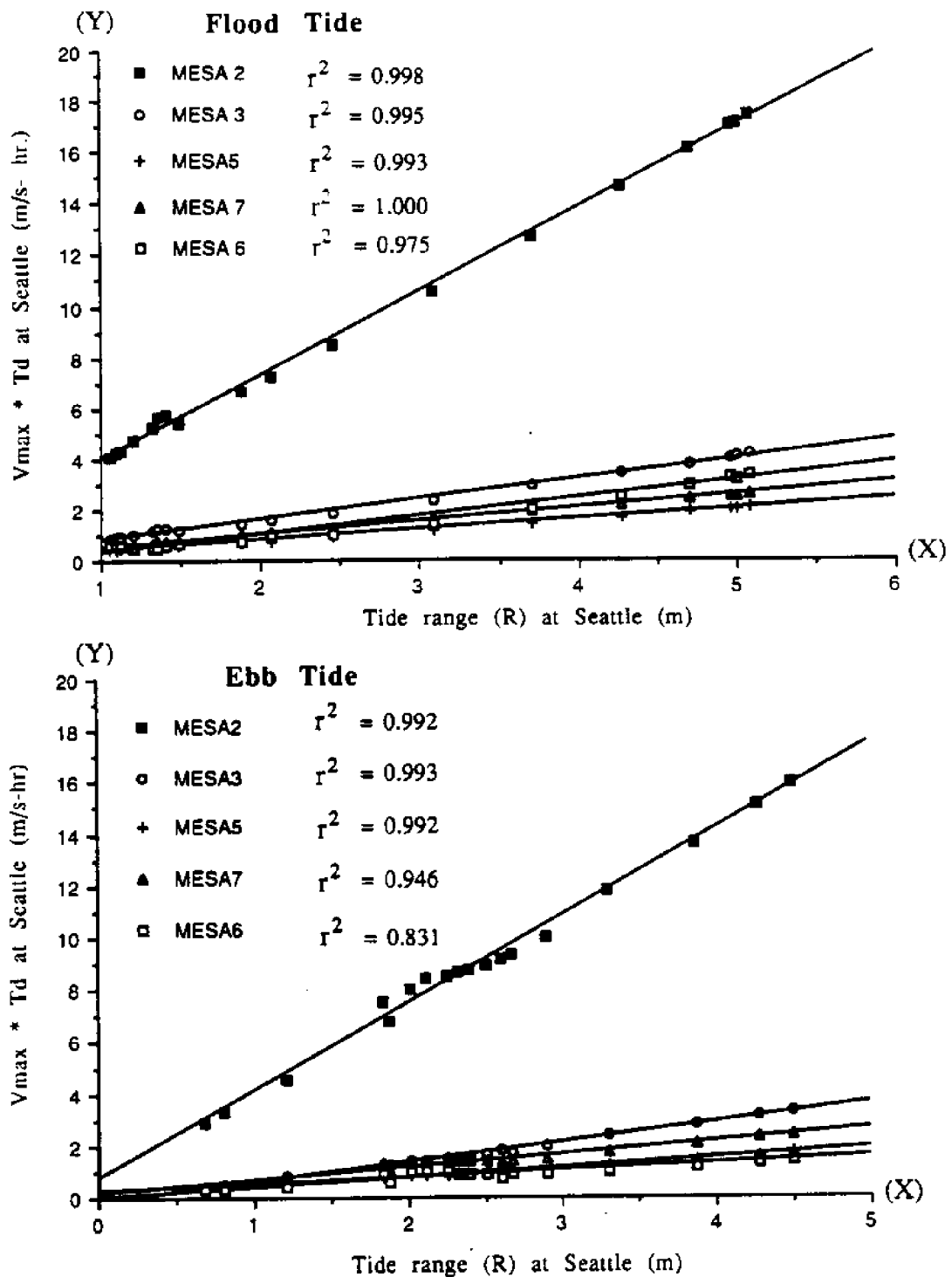
Fig.5.21 The relationships between the Seattle tide ranges and maximum current speeds at five MESA stations for flood and ebb tide (note : r^2 denotes r square)

Since there are a total of 1075 "wet" nodes inside our study domain, 1075 regression lines are required to develop tidal current functions (see Fig.5.21) for the entire Central Puget Sound. To avoid such lengthy computation and to reduce the size of the listing of the results, the study domain was divided into 17 sub-regions according to specific maximum flood (Fig.5.22) and ebb current strengths (Fig.5.23). The derived tidal current functions for all the sub-domains are shown in Fig.5.24 for flood tide and in Fig.5.25 for ebb tide.

Using the Tidal Current Functions

The functions given in Figs.5.24 and 5.25 enable users to approximate maximum current speed during any flood or ebb period in divided regions of Central Puget Sound. To determine the maximum tidal current at a given time within any of the subregions in Figs.5.22 and 5.23, the user can first look up tide range (R), time duration (Td) and tide condition (ebb or flood) at Seattle at the given time of interest from Tide Tables (National Ocean Survey, 1989). Secondly, from the specific tidal current function corresponding to the region of interest (Figs.5.22 and 5.23), the maximum current speed in the region can be determined from the specific tide range and time duration value.

5.2.2.5 Summary of Central Puget Sound Hydrodynamics According to the Model

According to our model results, the water movement in Central Puget Sound is primarily driven by tide. The current directions in the two model layers are similar but the current magnitudes are smaller in the lower layer due to bottom stress.

During flood tide, the water in Central Puget Sound moves southward along the main channel. Part of the water enters the West Sound Inlets through Agate and Rich Passages. During ebb tide, the
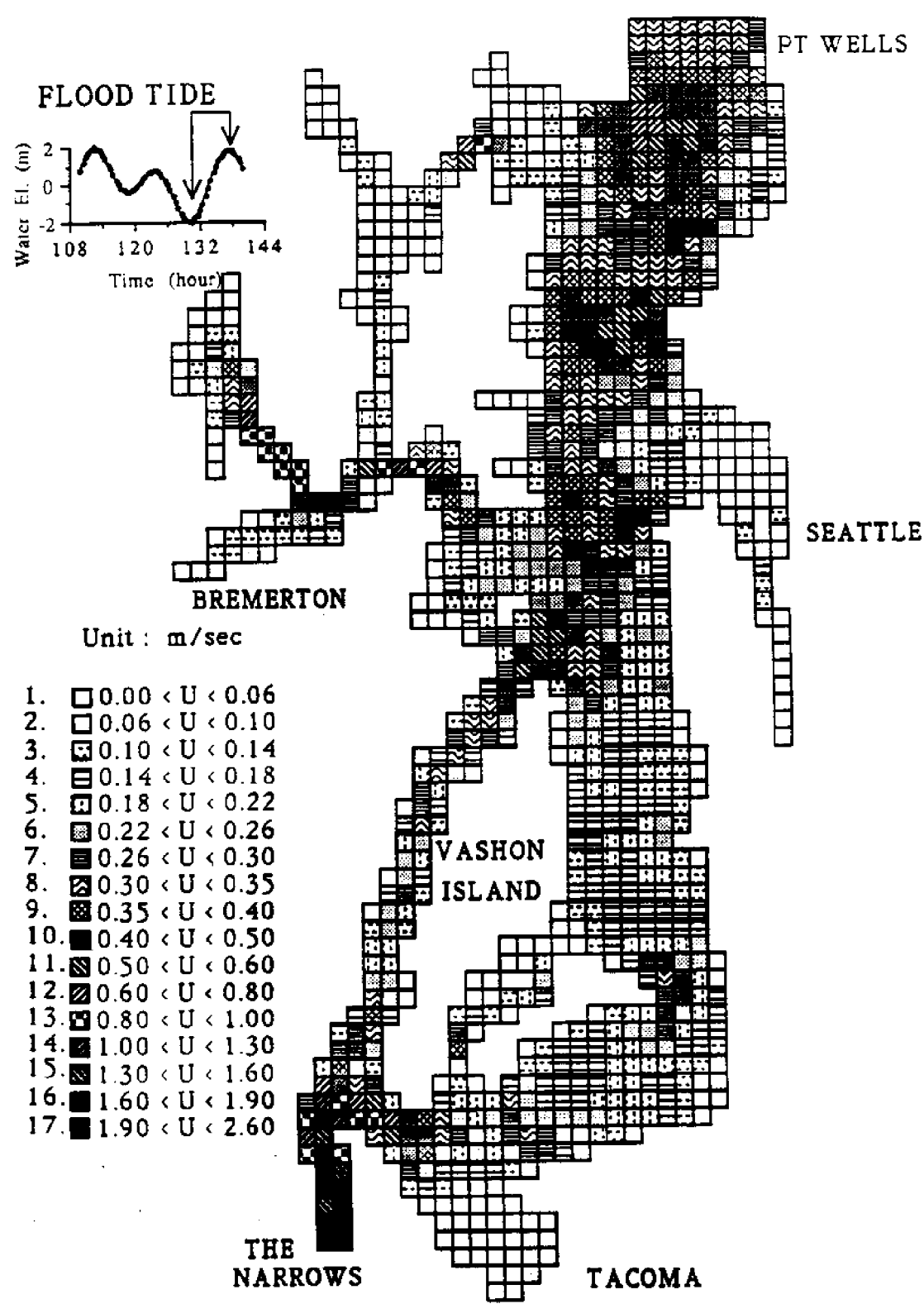
FLOOD TIDE

Water El. (m)

2
0
-2

108 120 132 144

Time (hour)

PT WELLS

SEATTLE

BREMERTON

Unit : m/sec

1. ☐ 0.00 < U < 0.06
2. ☐ 0.06 < U < 0.10
3. ▣ 0.10 < U < 0.14
4. ▤ 0.14 < U < 0.18
5. ▨ 0.18 < U < 0.22
6. ▦ 0.22 < U < 0.26
7. ▬ 0.26 < U < 0.30
8. ▧ 0.30 < U < 0.35
9. ▩ 0.35 < U < 0.40
10. ■ 0.40 < U < 0.50
11. ▩ 0.50 < U < 0.60
12. ▨ 0.60 < U < 0.80
13. ▣ 0.80 < U < 1.00
14. ▦ 1.00 < U < 1.30
15. ▨ 1.30 < U < 1.60
16. ■ 1.60 < U < 1.90
17. ■ 1.90 < U < 2.60

VASHON
ISLAND

THE
NARROWS

TACOMA

Fig.5.22 Subdomains of Central Puget Sound with equal range of maximum current speed for a given flood tide period (upper left).
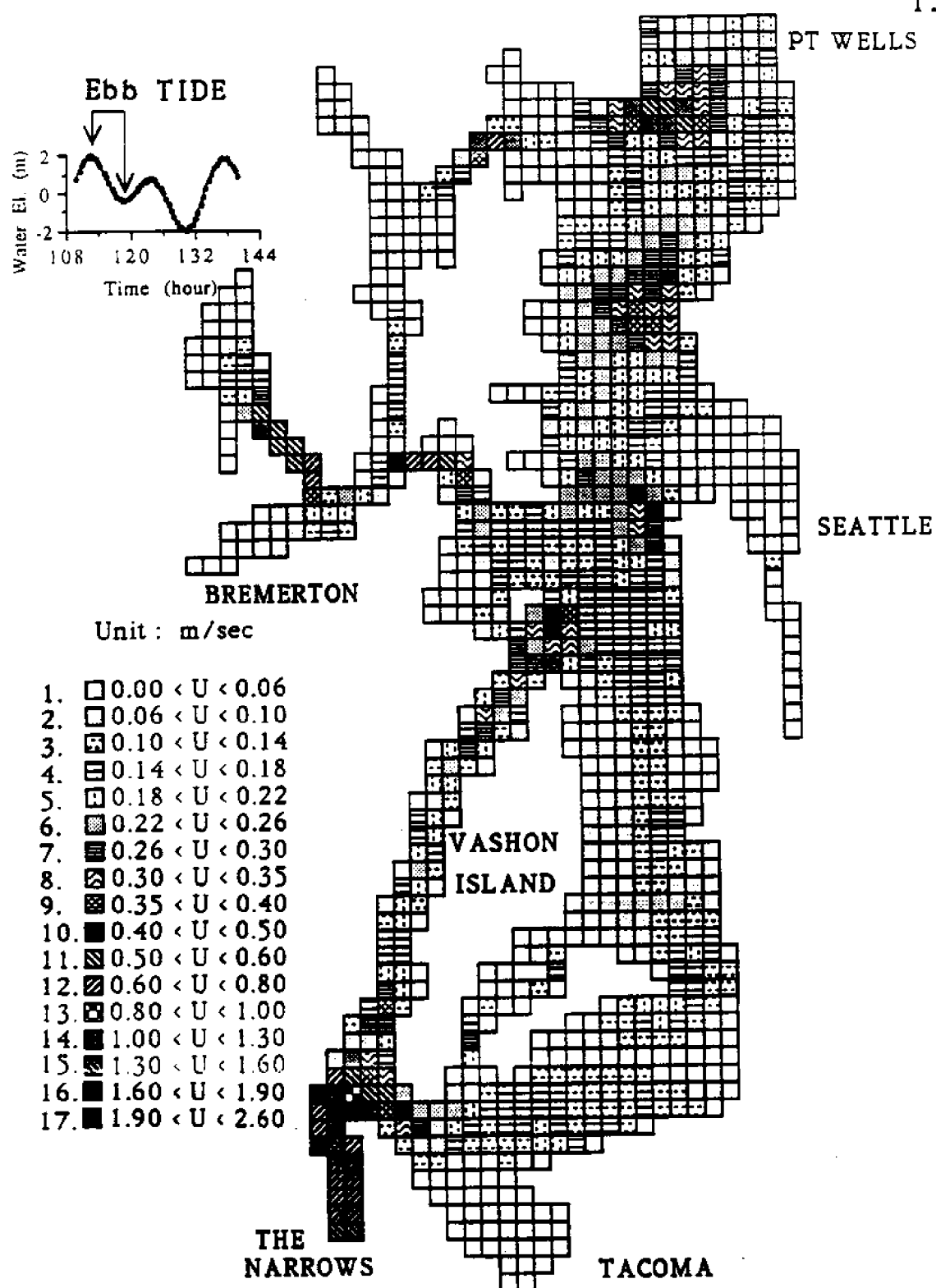
PT WELLS

Ebb TIDE

Water El. (m)

2
0
-2
108   120   132   144
Time (hour)

BREMERTON

Unit : m/sec

SEATTLE

1. ☐ 0.00 < U < 0.06
2. ☐ 0.06 < U < 0.10
3. ☒ 0.10 < U < 0.14
4. ⊟ 0.14 < U < 0.18
5. ☐ 0.18 < U < 0.22
6. ▨ 0.22 < U < 0.26
7. ▤ 0.26 < U < 0.30
8. ▨ 0.30 < U < 0.35
9. ▨ 0.35 < U < 0.40
10. ■ 0.40 < U < 0.50
11. ◨ 0.50 < U < 0.60
12. ▨ 0.60 < U < 0.80
13. ▣ 0.80 < U < 1.00
14. ■ 1.00 < U < 1.30
15. ▨ 1.30 < U < 1.60
16. ■ 1.60 < U < 1.90
17. ■ 1.90 < U < 2.60

VASHON
ISLAND

THE
NARROWS

TACOMA

Fig.5.23 Subdomains of Central Puget Sound with equal range of maximum current speed for a given ebb tide period (upper left).
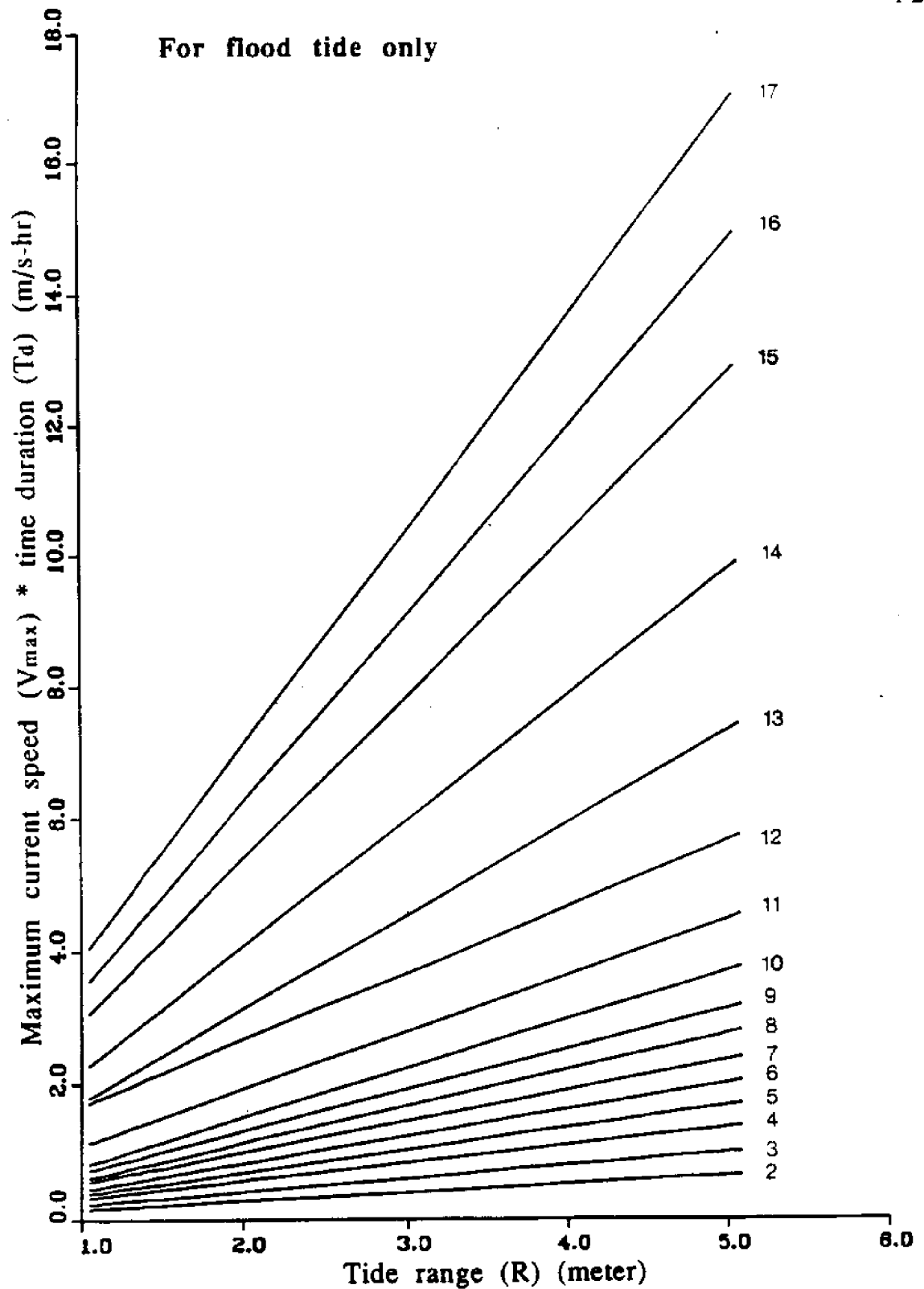
Fig.5.24   Tidal Current Functions for 16 subdomains in Cental Puget Sound (Fig.5.22). The number on the right hand side of each regression line is the subdomain number given in Fig.5.22.
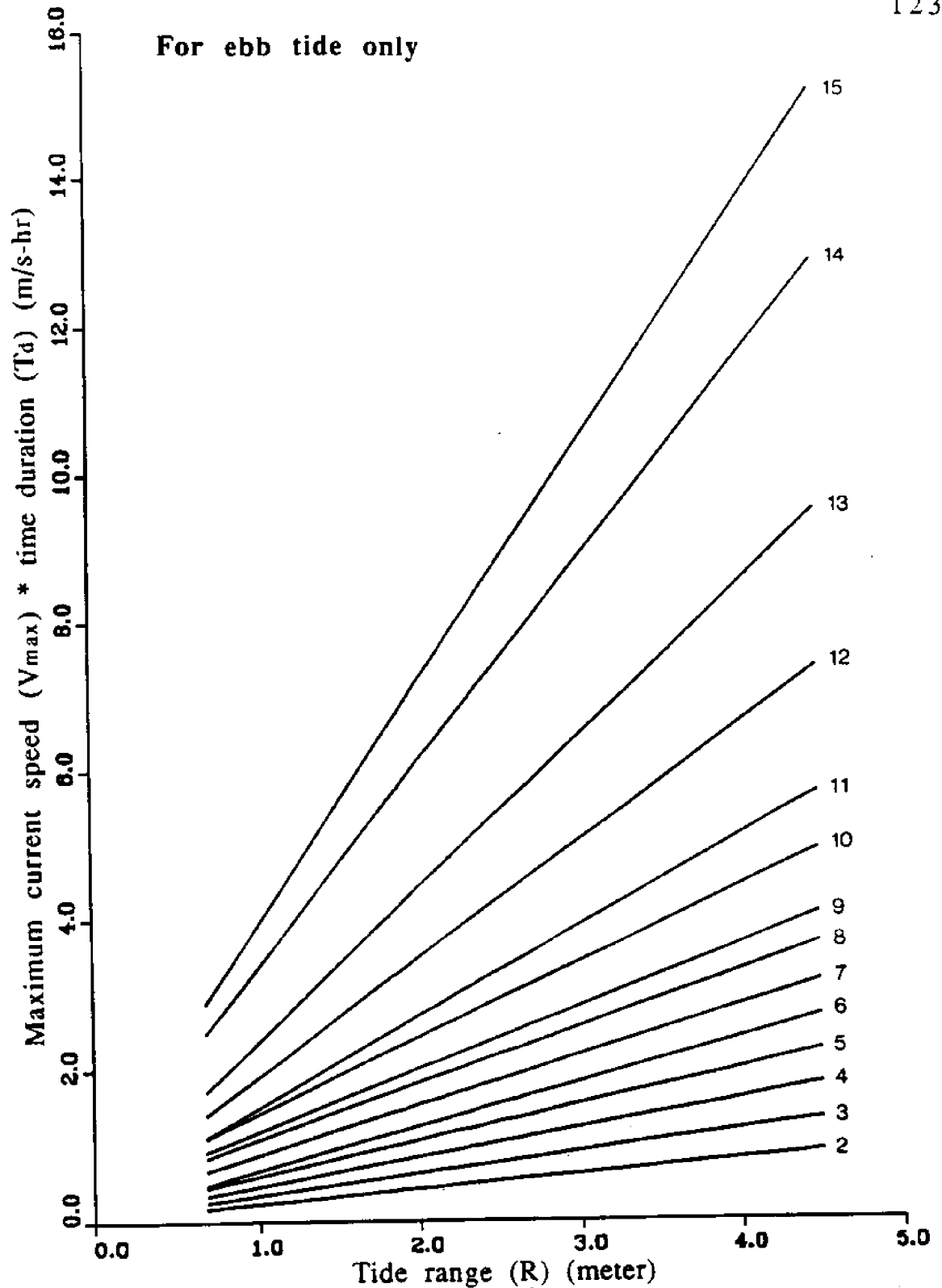
For ebb tide only

Fig.5.25   Tidal Current Functions for 16 subdomains in Cental Puget Sound (Fig.5.23). The number on the right hand side of each regression line is the subdomain number given in Fig.5.23.

water in the West Sound Inlets moves back to main channel and joins the northward ebb current. Since the current speed at Rich Passage is stronger than that at Agate Passage, the water movement in the West Sound Inlets is primarily dominated by the inflow and outflow through Rich Passage. The tidal current in Port Orchard goes northward during flood tide and southward during ebb tide.

During slack tide periods, the currents in most regions of Central Puget Sound are weak. Some significant eddies are formed along the shore of main channel due to phase lag between the currents in the deep and the shallow waters. Current phase lag exists in the West Sound Inlets as well. For example, at the high slack tide after the flood, the flood current at Rich Passage can continue to move westward with its remaining momentum while the current at Agate Passage has already turned its direction eastward.

Stronger currents in Central Puget Sound are always observed in narrow channels or the nearshore zones. The maximum current speed at The Narrows can reach 2.6 m/s, and the maximum current speed in the main channel is only about 0.4 m/s. The currents in side embayments such as Elliott Bay, Commencement Bay, and West Sound Inlets are always weak. The maximum current speeds in these areas are all less than 0.3 m/s.

The calculated residual currents in most regions in Central Puget Sound are weak. The stronger residual currents or circulations always occur off the coasts of promontories, such as those near Point Jefferson, Alki Point, West Point, and Point Defiance. Several weak residual circulations were also found in the West Sound Inlets and at the south coast of Maury Island. The well-known clockwise residual circulation around Vashon Island was observed in the model results.

The particle tracking model revealed that water near West Point could transect the main channel and make it to the east coast of Bainbridge Island over eight tidal cycles. Most of the waters near Duwamish Head and Alki Point tended to move southward along the

main channel. There were no signs of waters from West Point, Alki Point, and Duwamish Head within Elliott Bay over nine tidal cycles. The water in Commencement Bay tended to travel northwestward toward Dalco Passage. Water would take about one week to pass through Colvos Passage and about three weeks to traverse the entire East Passage.

The effect of river discharge was examined using simple constant inflows (summer and winter averaged flows) for both the Duwamish and the Puyallup. It was found that river discharges have no effect on the tidal currents but can cause net volume increase with the given boundary conditions.

Two sets of wind data (summer and winter cases) were used to investigate the wind effect on the tidal currents in Central Puget Sound. The results reveal that the wind effect on the Central Puget Sound tidal currents is insignificant except in nearshore regions and in Elliott and Commencement Bays.

On the whole, the coarse grid resolution (762 m) and two vertical layers used in this research are capable of capturing the key features of the tidal hydrodynamics in the main channel, but the flow features in the embayments along the Sound cannot be clearly characterized. To understand such flows in more details, this study uses the model to "zoom in on" Elliott Bay with a horizontal grid resolution of 254 m and four vertical layers.

5.2.3 Circulation and Transport in Elliott Bay

Tidal flow inside Elliott Bay could be driven by tide, river inflow, wind, density variation, and the Bay's geometric and bathymetric features. Among them, tide is possibly the most dominant forcing mechanism. The tide driven current would follow the coastline and the bathymetry of the Bay and form the fundamental flow pattern. The basic flow pattern could be modified by river discharge, wind, and density variation. The basic flow

pattern in Elliott Bay and the modifications due to river discharge, wind, tidal inequality, and density variation are analyzed and presented in this section.

5.2.3.1 Tide Induced Circulation and Transport in Elliott Bay

Elliott Bay is a deep embayment located on the east shore of Central Puget Sound (see Fig.4.12 and Fig.5.26). The Bay is connected to the main channel of the Sound by a broad opening. The Bay can be considered as having an inner and an outer basin separated by a line connecting Smith Cove to Duwamish Head (Sillcox et al.,1981). The bathymetry of the Bay is dominated by an east-west submarine canyon in the outer basin which extends and diverges into two canyons in the inner basin (Fig.5.26). The canyon at the outer basin is embraced by two steep shelves which parallel the shorelines around Magnolia and Duwamish Head. The region between the two shelves is deep and flat. In the inner basin, the northern submarine canyon runs parallel to the eastern shoreline and the southern submarine canyon is to the east of Duwamish Head. These two submarine canyons are separated by a shallow area north of West Waterway.

Tidal Currents in Elliott Bay

To analyze tidal currents in Elliott Bay, model computed results at 10-minute intervals at each grid in every layer were saved on magnetic tapes. The velocity vectors at eight selected times during the fifth tidal cycle (Fig.5.2) are presented in Appendix II. The general flow patterns derived from such detailed model results at ebb tide, low slack tide, flood tide, and high slack tide are shown in Figs.5.27a-d.

According to the model results, the northward ebb flow in the main channel would bring water out of Elliott Bay along the eastern shore during ebb tide (Fig.5.27a). The speed of the outgoing current near the coast of Magnolia can reach 0.3 m/s. Due to the bathymetric
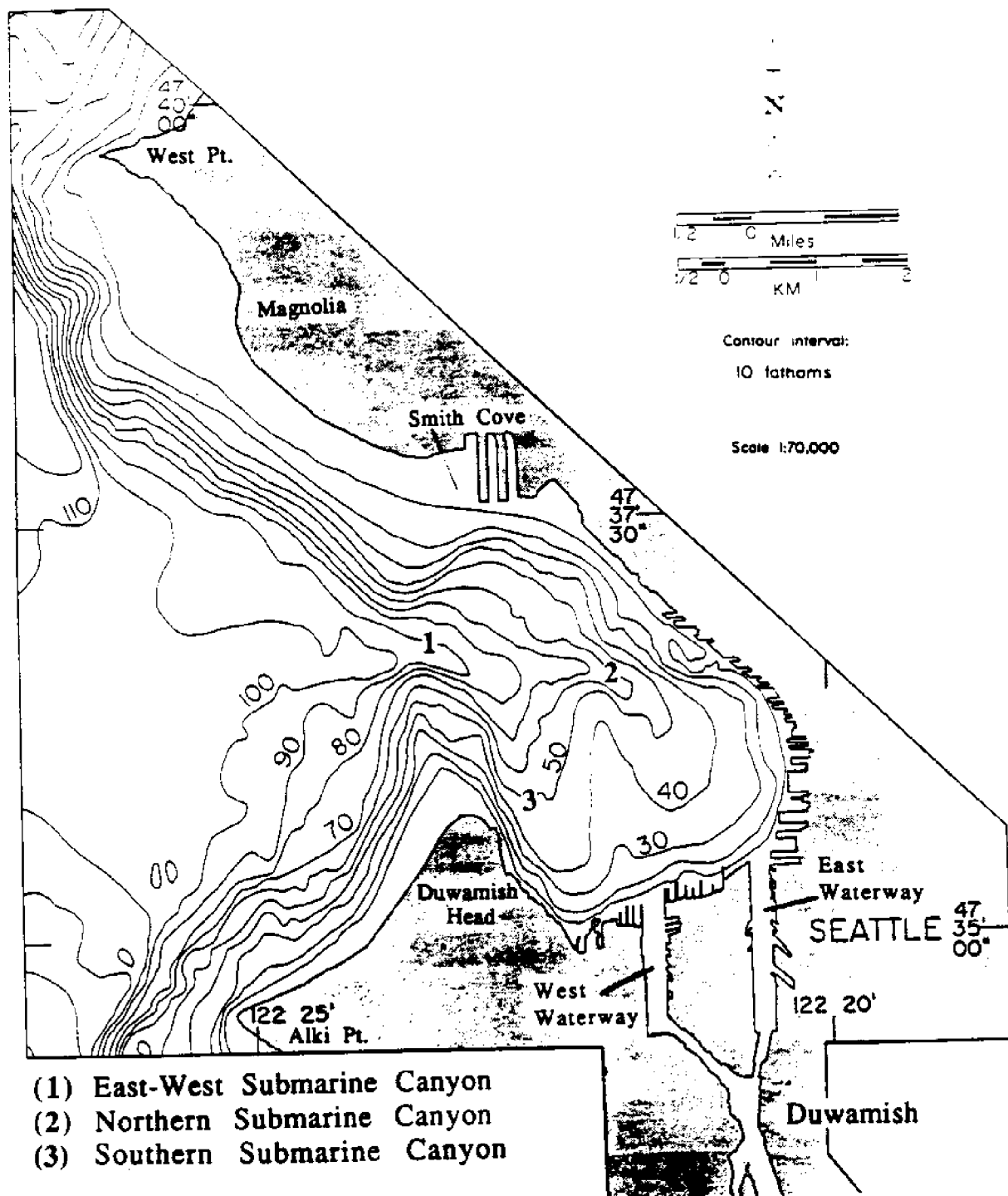
West Pt.

Magnolia

Smith Cove

47
37
30°

Contour interval:
10 fathoms

Scale 1:70,000

10

1

2

100

90

80

50

40

3

70

30

00

East
Waterway

47
35
00°

SEATTLE

Duwamish
Head

West
Waterway

122 25'
Alki Pt.

122 20'

Duwamish

(1) East-West Submarine Canyon
(2) Northern Submarine Canyon
(3) Southern Submarine Canyon

Fig.5.26 The bathymetry of Elliott Bay (modified from Puget Sound
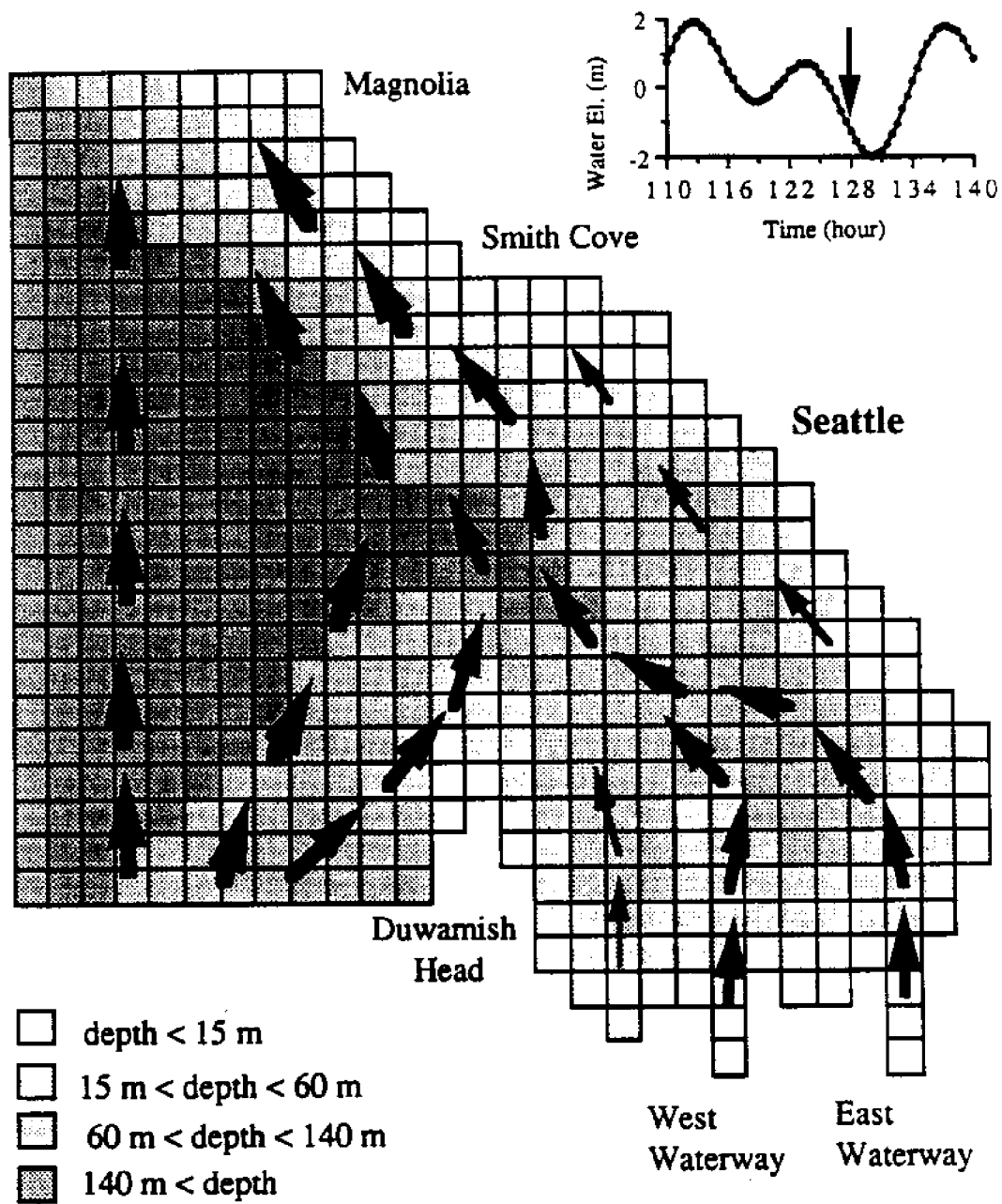Environmental Atlas, compiled by Evans-Hamiton, Inc., 1986).

Fig.5.27a General surface layer flow pattern in Elliott Bay
at ebb tide. Thicker arrows represent stronger currents.
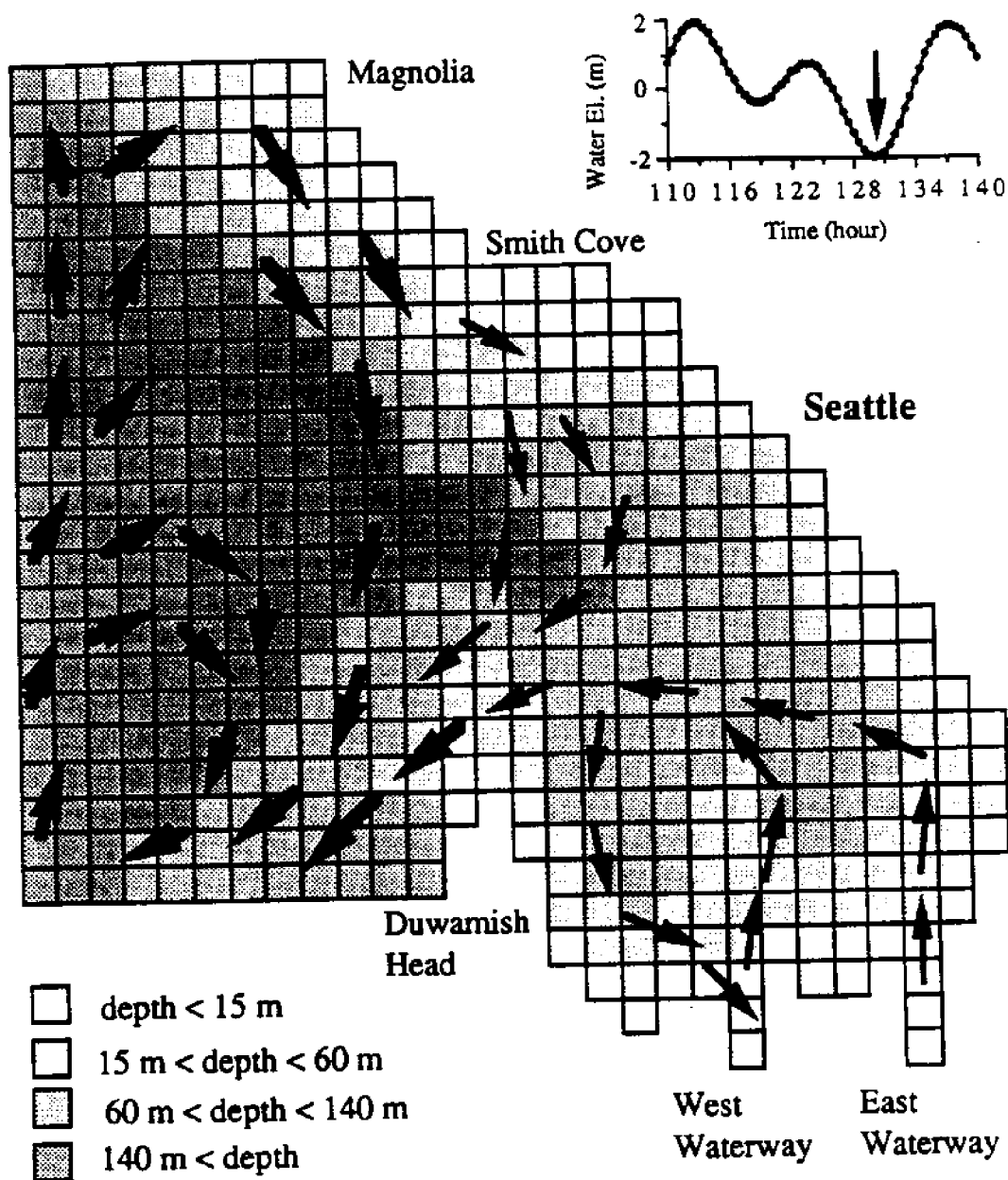
Fig.5.27b General surface layer flow pattern in Elliott Bay at low slack tide. Thicker arrows represent stronger currents.
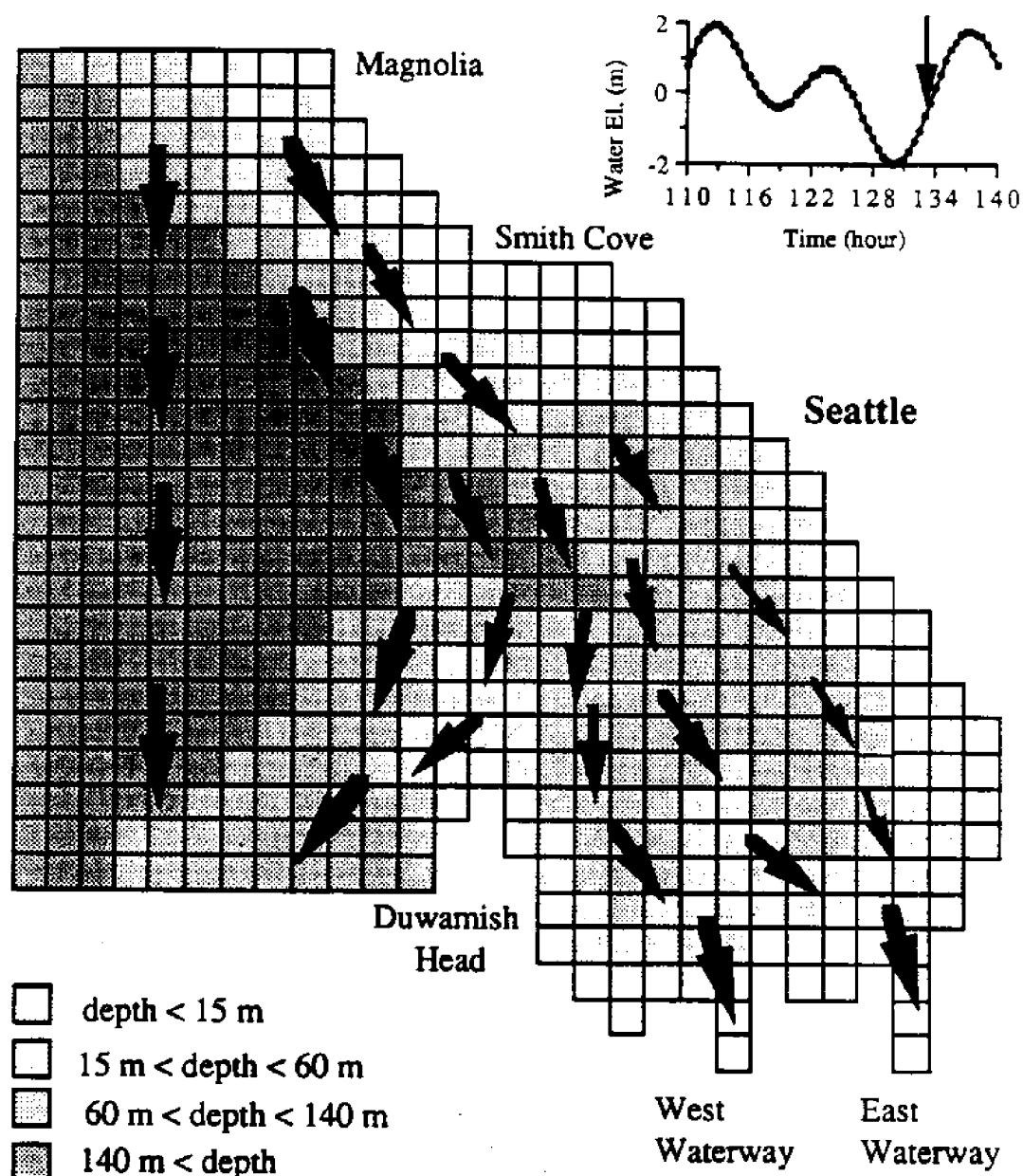
Fig.5.27c General surface layer flow pattern in Elliott Bay at
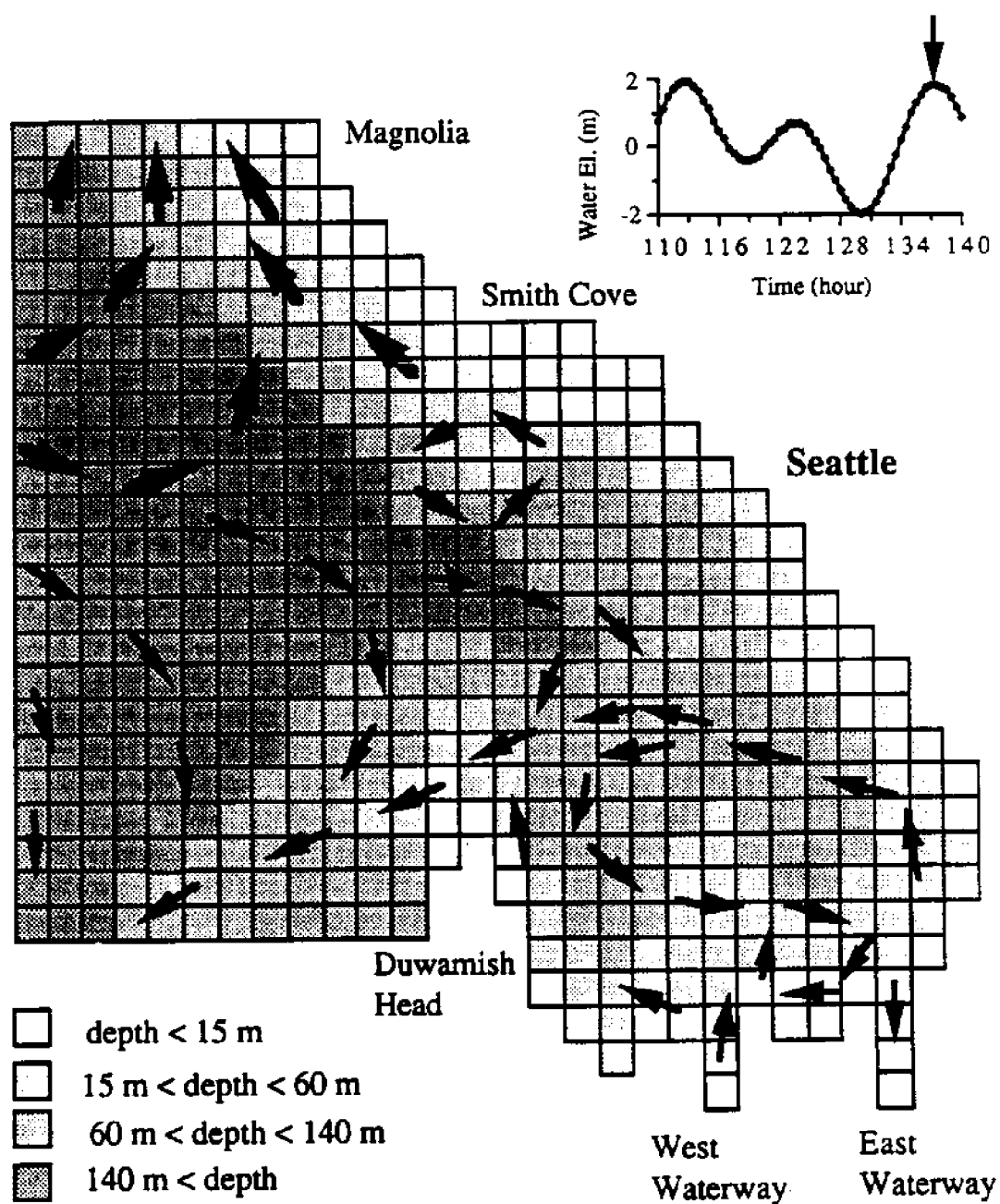flood tide. Thicker arrows represent stronger currents.

Fig.5.27d General surface layer flow pattern in Elliott Bay at high
slack tide. Thicker arrows represent stronger currents.

feature near the coast of Duwamish Head, part of the northward ebb flow in the main channel is diverted into the inner Bay along the coast of Duwamish Head. This weak inward flow is immediately deflected to the north when it encounters the outgoing flow from Elliott Bay. In the inner Elliott Bay, two strong jets from East and West Waterways are present. The jet from East Waterway moves northward first, then turns gradually toward the northwest following the contour of the northern submarine canyon (Fig.5.26). After merging with the jet from West Waterway, the flow travels westward, then is slightly deflected toward the northwest when it encounters the inward current along the coast of Duwamish Head. During ebb tide, most of the waters from both waterways converge toward the northern submarine canyon (Fig.5.26).

The current pattern during low slack tide is shown in Fig.5.27b. During slack tide, the ebb flow in the deeper portions of main channel and the two jets in Elliott Bay continue to move north with their remaining momentum. But in the meantime, flood currents from Magnolia to Duwamish Head have already developed. The occurrence of these flood and ebb flows causes the formation of several gyres in the Bay. In the southern portion of the outer Bay, the degenerated northward ebb flow in the main channel turns northeastward, meets the flood flow from the north, and forms a clockwise gyre northwest of Duwamish Head. In the inner Bay, the northward moving jet from West Waterway is turned westward by the flood current from the north and forms a counterclockwise gyre east of Duwamish Head. These circulation patterns disappear soon when the flood flow grows stronger.

During flood tide, part of the flood current in the main channel enters Elliott Bay near the coast of Magnolia (Fig.5.27c). Some of this inward flow will be deflected southwesterly by the bathymetric feature north of Duwamish Head and leave the Bay. The rest of the inward flow will intrude into Elliott Bay and push the Bay water up the two submarine canyons (Fig.5.26). Contrary to the ebb tide

condition, the flood current in the southern submarine canyon is stronger than that in the northern submarine canyon. The flood water enters East and West Waterways at the peak velocity of 0.3 m/s.

The flow pattern in Elliott Bay at the high slack tide is shown in Fig.5.27d. This figure reveals that during high slack tide the magnitudes of the southerly flood flow in the main channel (outside the Bay entrance) and the southwesterly flood flow along the coast of Duwamish Head have weakened, but the directions remain unchanged. At the same time, ebb flow has already been developed along the coast of Magnolia. Because of this ebb flow, the flood flow in the northern portion of outer Elliott Bay reverses its direction in counterclockwise direction. Unlike the tidal currents observed during low slack tide, the current speeds in the southern portion of outer Elliott Bay are very weak during high slack tide. The remaining flood flow along the coast of Duwamish Head and newly developed ebb flow along the coast of Magnolia are pulling water out of inner Elliott Bay past Duwamish Head and Smith Cove respectively. When the outward flow through Smith Cove meets the remaining flood flow just north of the east-west submarine canyon, a counterclockwise gyre in the northern portion of inner Elliott Bay is formed. Another weak counterclockwise gyre is found in southern inner Bay. This circulation is formed mainly by a westerly outgoing flow in the middle of the Bay and a southerly flow along the southern submarine canyon.

In general, the current speeds in the inner Elliott Bay are weaker than those in the outer Elliott Bay. The strongest currents in the outer Bay occur near the main channel and along the coast of Magnolia. The maximum surface layer current speed in the outer Bay can reach 0.4 m/sec. The surface layer current speeds at most locations inside inner Bay are smaller than 0.05 m/sec. Surface current speeds outside the two waterways and around Smith Cove can reach 0.3 m/s.

The tidal currents in the deeper layers are generally weaker than the surface currents. In the outer Elliott Bay, the directions of the tidal currents are almost independent of the bathymetry. But in the inner Elliott Bay, tidal currents in the deeper layers closely follow the bathymetry of the Bay. The stronger ebb (northward) flow in the northern submarine canyon and the stronger flood (southward) flow in the southern submarine canyon tend to bring the bottom waters in the northern submarine canyon toward the southern submarine canyon and then upwell to the upper layers.

Residual Circulation in Elliott Bay

The residual current fields in Elliott Bay were obtained by averaging the velocity at each grid over a 24.7-hour tidal period (the fifth tidal cycle in Fig.5.2). Vector plots of the residual currents in all layers are shown in Figs.5.28a-d.

The model results reveal that residual currents in the outer Elliott Bay are dominated by clockwise circulation outside the coast of Duwamish Head. During flood tide, a strong flood current moves southwesterly along the coast of Duwamish Head. But during ebb tide, due to the sharp corners around Alki Point, the northerly ebb current from the main channel can only bring a small amount of water in the northeast direction along the coast of Duwamish Head. This imbalance of flood and ebb currents is believed to be the cause of the clockwise residual circulation along the northwestern shore of Duwamish Head at all depths. Results from an hydraulic model study (Winter, 1977) also showed that a tide-induced clockwise gyre was present in the outer Elliott Bay and resulted in more water flowing out the bay past Duwamish Head than past Smith Cove.
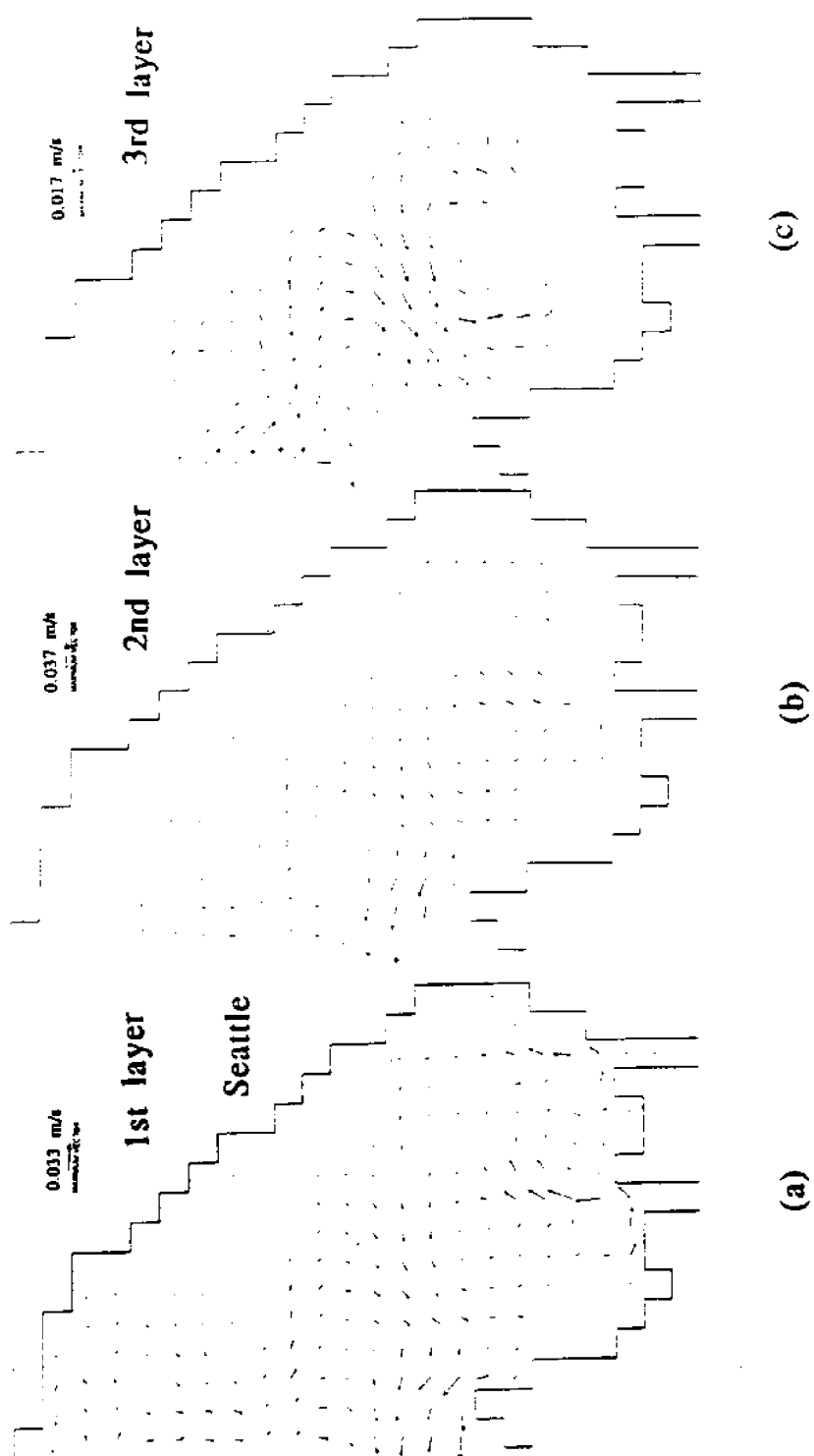
The residual currents in the inner Elliott Bay are strongly affected by the residual currents in the outer Bay. Enlarged vector plots of residual currents in the inner Bay are shown in Figs.5.29a-c. These figures show that residual flow enters the inner Bay through the east-west submarine canyon and leaves primarily along the coast

0.074 m/s
MAXIMUM VECTOR

1st layer

Seattle

(a)

0.074 m/s
MAXIMUM VECTOR

2nd layer

(b)
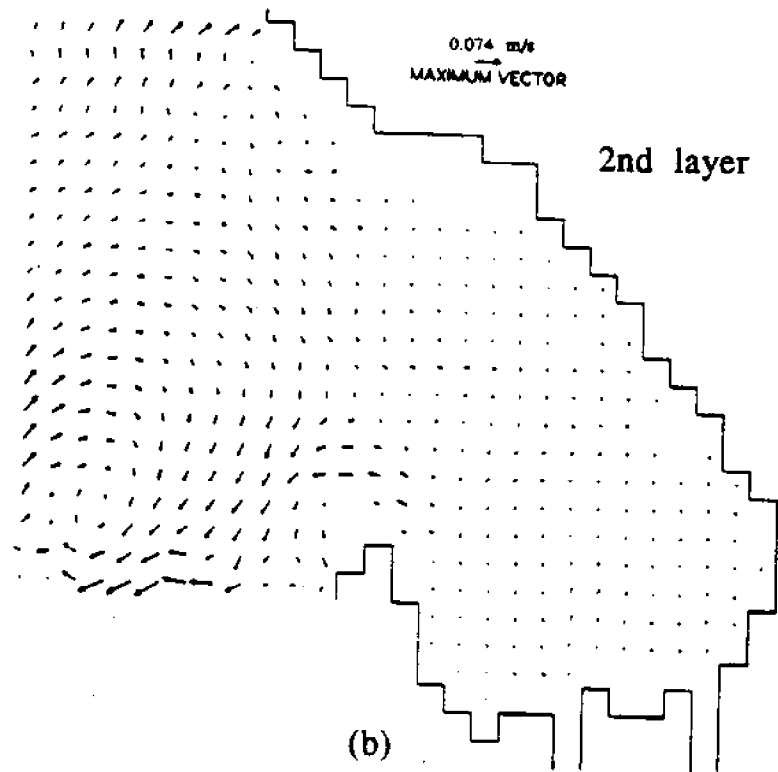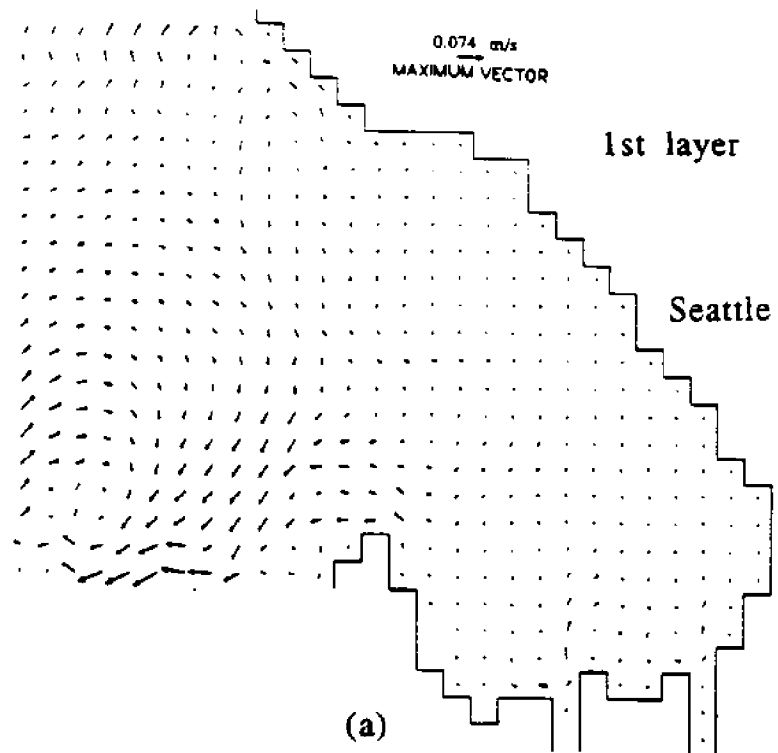
Figs.5.28a-d Residual currents in Elliott Bay.

0.087 m/s
MAXIMUM VECTOR

3rd layer

(c)

0.077 m/s
MAXIMUM VECTOR

4th layer

(d)
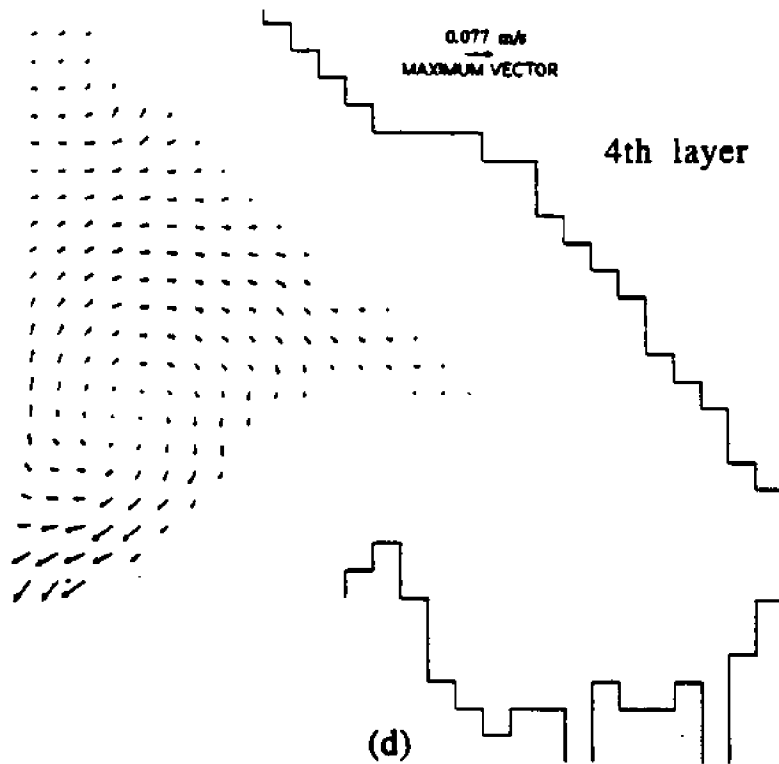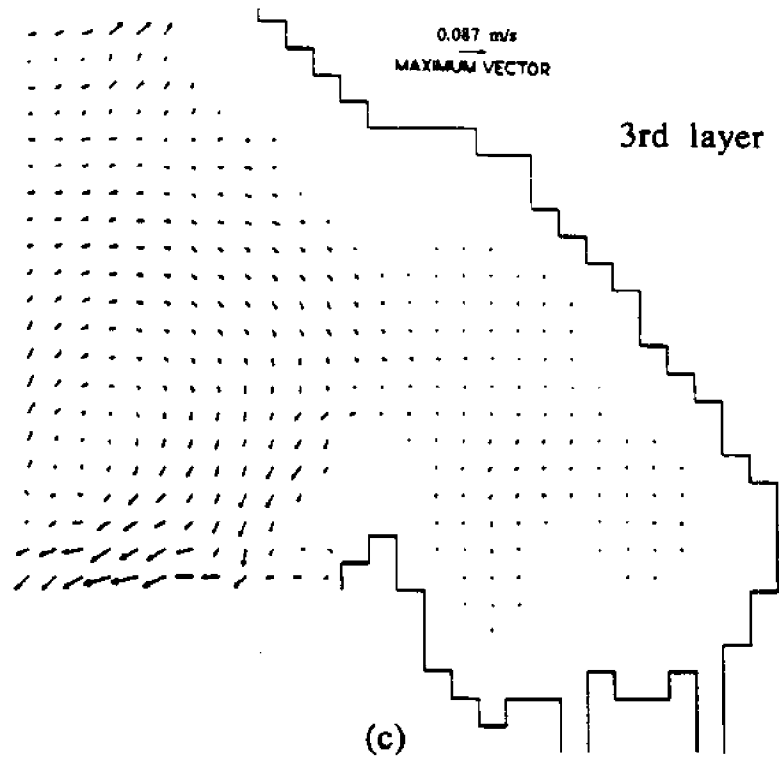
Figs.5.28a-d (continued)

Figs.5.29a-c Residual currents in inner Elliott Bay. (There are only three layers in the inner Bay)

1st layer

Seattle

0.013 m/s

2nd layer

0.037 m/s

3rd layer

0.017 m/s

(a)

(b)

(c)

of Duwamish Head. The residual flow along the east shore of the Bay is very weak (less than 0.01 m/s). A counterclockwise residual circulation exists in southern inner Bay. This circulation is due mainly to the imbalance between strong ebb (northerly) flow in the northern submarine canyon during ebb tide and the strong flood (southerly) flow in the southern submarine canyon during flood tide described in the previous section. Because of this circulation, the water from East and West Waterways (which is only represented in the surface layer of the model) is more likely to leave the Bay near Duwamish Head.

The maximum calculated residual current speed in the outer Bay is 0.07 m/s which is observed near the coast of Duwamish Head. Inside the inner Bay, the maximum residual current speeds occur at the mouths of East and West Waterways and around the coast of Duwamish Head. Their magnitudes are all less than 0.04 m/s. These residual current speeds will vary under different tidal and other forcing conditions.

Except the above described tide-induced residual circulations, results from the hydraulic model also revealed a standard estuarine gravitational convection pattern with saltier water intruding at depth and brackish water flowing out near the surface of Elliott Bay (Winter, 1977).

Although the vector plots shown thus far have provided clear information on how the Bay waters responded to tidal forcing, such instant "snap shots" of the flow cannot answer some important questions regarding the transport of pollutants in the waters, such as, 1) how do the waters enter the Bay during flood tide and how do they move out of the Bay during ebb tide ? 2) how long do they stay in Elliott Bay ? and 3) where do the discharged wastes from known point sources go ? At least some of the answers to these questions can be found by using the developed particle tracking model (PTM). The simulation results are given next.

5.2.3.2 Application of Particle Tracking Model in Elliott Bay

One of the major difficulties in applying the particle tracking model (PTM) in a relatively small embayment is the handling of the open boundary condition. When a particle travels across the open boundary to the outside of the domain, its fate is hard to predict. It may be carried back into the domain or it may leave the domain permanently. In the present study, it is assumed that when the particles move across any open boundary they will be "picked up" and therefore disappear from the domain permanently. Since the scale of vertical movement of the particles is much smaller than that of the horizontal movement of the particles, particle tracking model results will be presented mainly on a horizontal plane.

In the first Elliott Bay application, 300 particles were simultaneously released at evenly spaced locations in the surface layer (0.001 meter depth) of the entire inner basin and part of the outer basin as shown in Fig.5.30. The particles were placed at the center of each surface layer grid. The distance between any two adjacent particles was 254 meters.

In order to understand how the water inside the Bay responds to ebb and flood tides, the PTM was run four times, with the particles released at higher high water (HHW), higher low water (HLW), lower high water (LHW), and lower low water (LLW), respectively. The final locations of the particles after one ebb or flood tide from each run are shown in Figs.5.31a-d. On the tide curve of each figure, the arrow and star signs indicate respectively the releasing time and the final time (6.16 hours after releasing) at which the positions of the particles are shown. The particles located in the same initial column (along a line of x = constant) in inner Elliott Bay (see Fig.5.30) are connected by a line so that the movements of these released particles can be clearly distinguished.

The figures show that during ebb tides all released particles tended to move outward but only the particles released near the
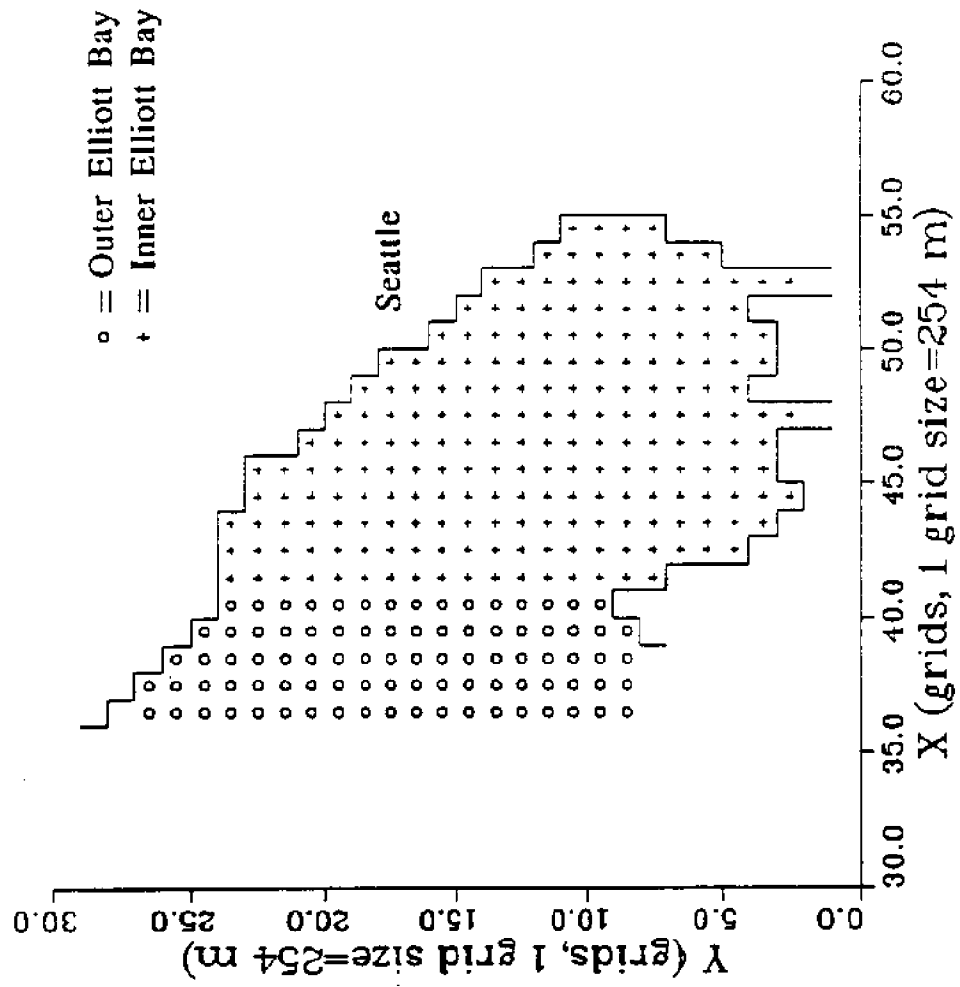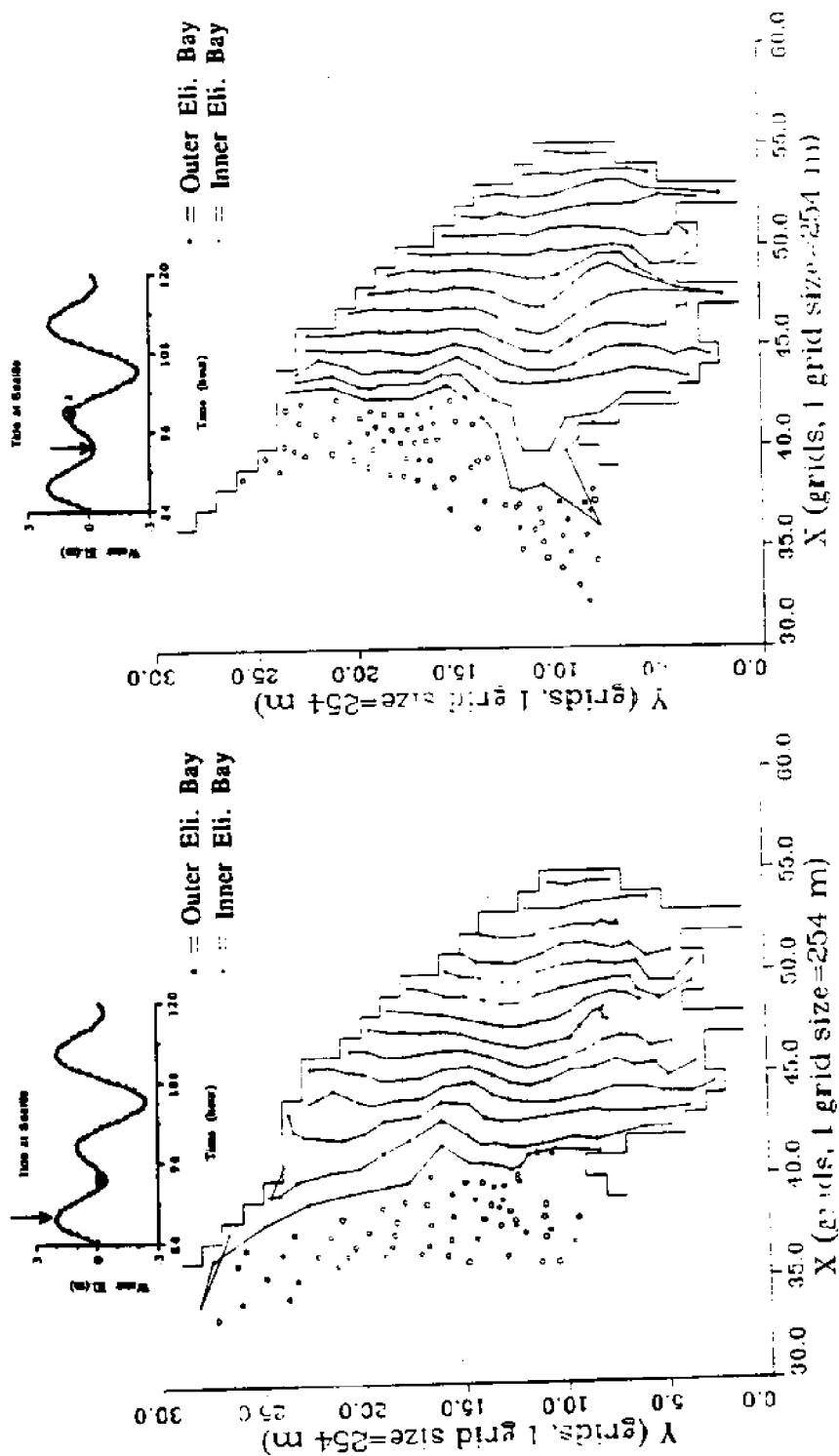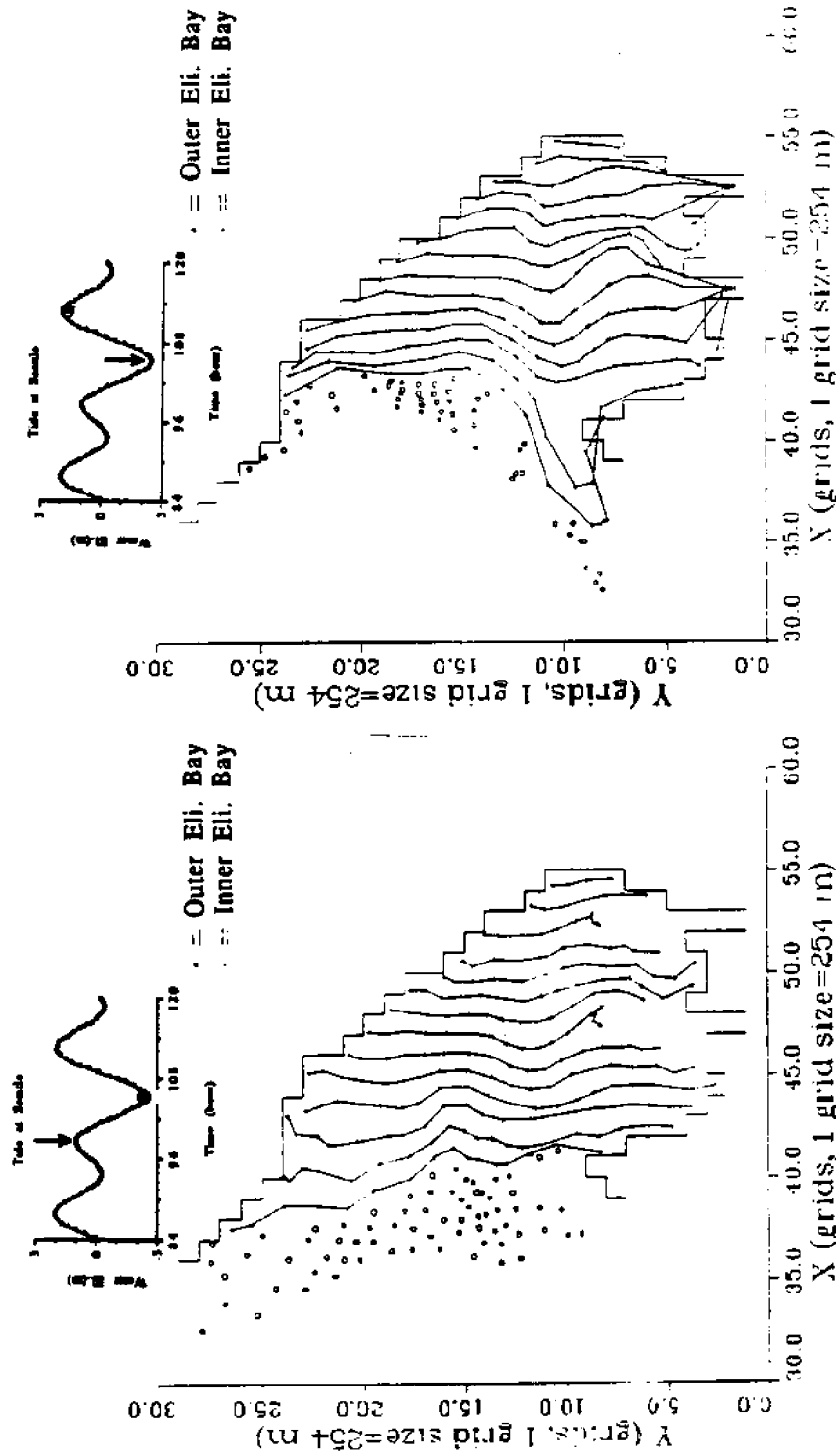
Fig.5.30 The initial locations of released particles in Elliott Bay

Figs.5.31a-d The locations of released particles after one flood or ebb tide. Arrow and star signs represent the releasing time and present time.

(a) After small ebb tide

(b) After small flood tide

(d) After large flood tide

(c) After large ebb tide

Figs.5.31a-d (continued)

coast of Magnolia and outside of the East and West Waterways had significant displacements (Figs.5.31a,c). The released particles at the coast of Magnolia could move out of the Bay in one ebb tide. Most of the particles released around Duwamish Head simply moved northward. In general, the particles released in the outer Bay could not enter inner Bay during the given ebb tide.

During flood tides, most of the released particles were pushed inward, except for those released around Duwamish Head which moved westward and eventually were dragged out of the Bay by the strong longshore flood current along the northwestern shore of Duwamish Head (Figs.5.31b,d). It is interesting to note that more particles left the inner Bay on flood tide than on ebb tide.

The trajectories of particle movement for different tidal conditions are shown in Figs.5.32 and 5.33. To avoid congestion of the lines, only 53 trajectories are included in each figure. Although the trajectories of the particles released at different tide stages are not the same, they do reveal similar water movement patterns.

Those particles released at higher high water in the above case (Fig.5.32) were tracked for 8 additional tidal cycles as a mean to estimate the residence time of the water in the inner basin. The results are shown in Fig.5.34a. Particles released in the grids on the left-hand (west) side of the thick line in Fig.5.34a all moved out of the inner Bay within the indicated tidal cycles. Most of these particles went out of the Bay during the first three tidal cycles, and more particles moved out of the Bay from the coast of Duwamish Head than from the coast of Magnolia. Apparently no particle released in the outer Bay made it into the inner Bay. Most of the particles released in the grids on the right-hand (east) side of the thick line still remained inside the inner basin after 8 tidal cycles. The projection of all remaining particles in inner Elliott Bay onto a vertical (x-z) plane connecting Duwamish Head and Seattle waterfront are shown in Fig.5.34b. Due to the weak vertical velocities
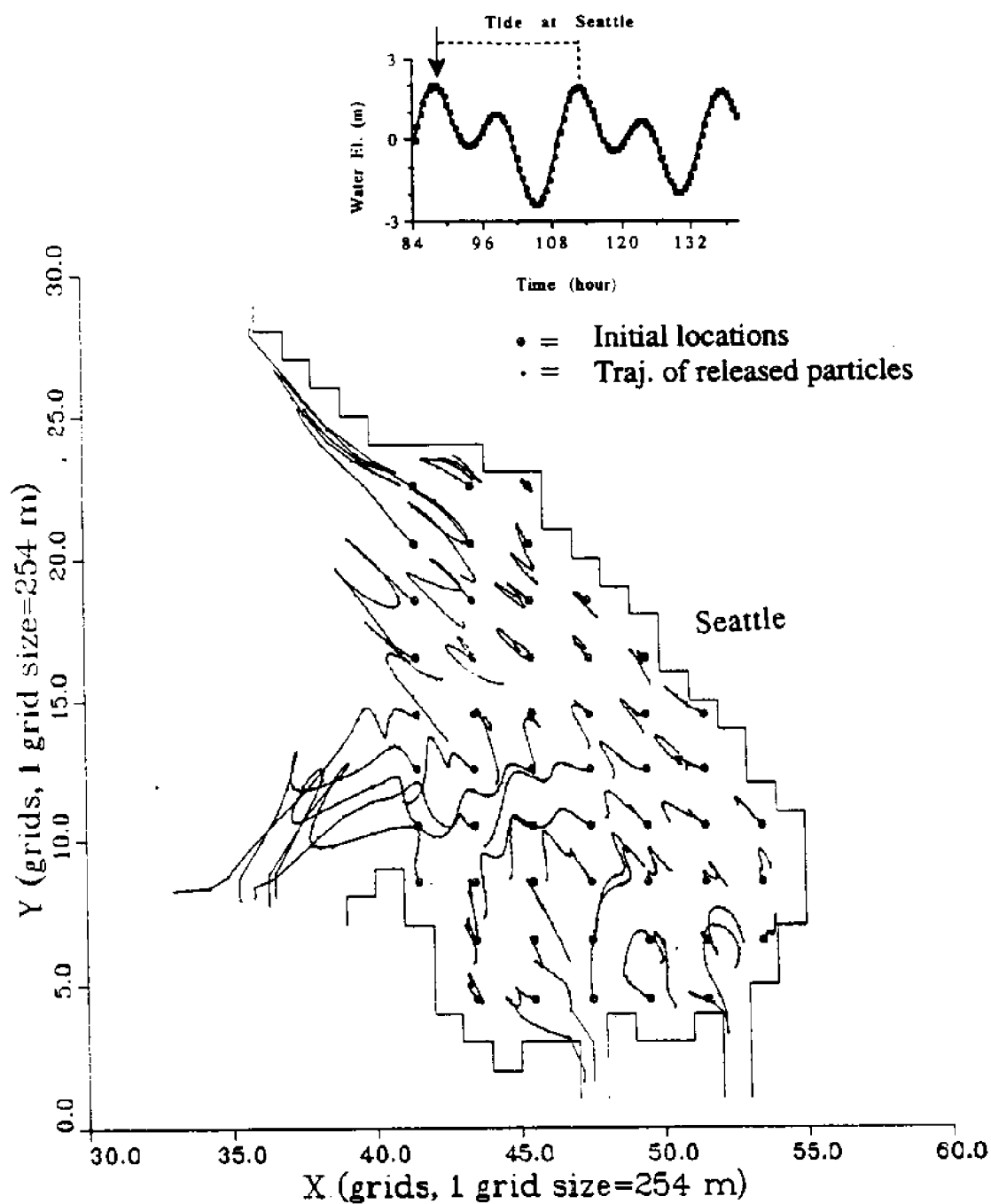
Fig.5.32 The trajectories of particles (released at higher high tide) during one tidal cycle
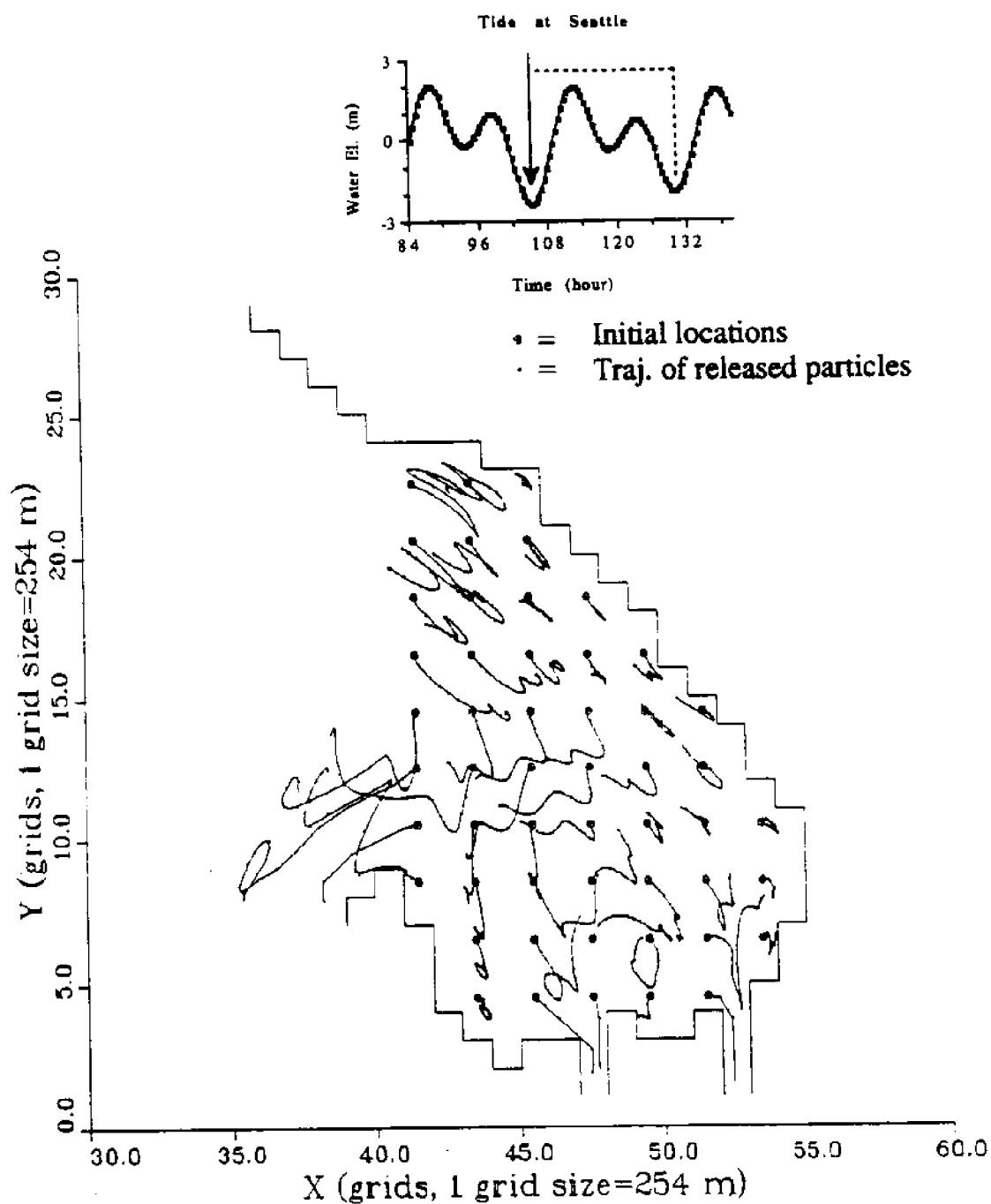
Fig.5.33 The trajectories of particles (released at lower low tide) during one tidal cycle
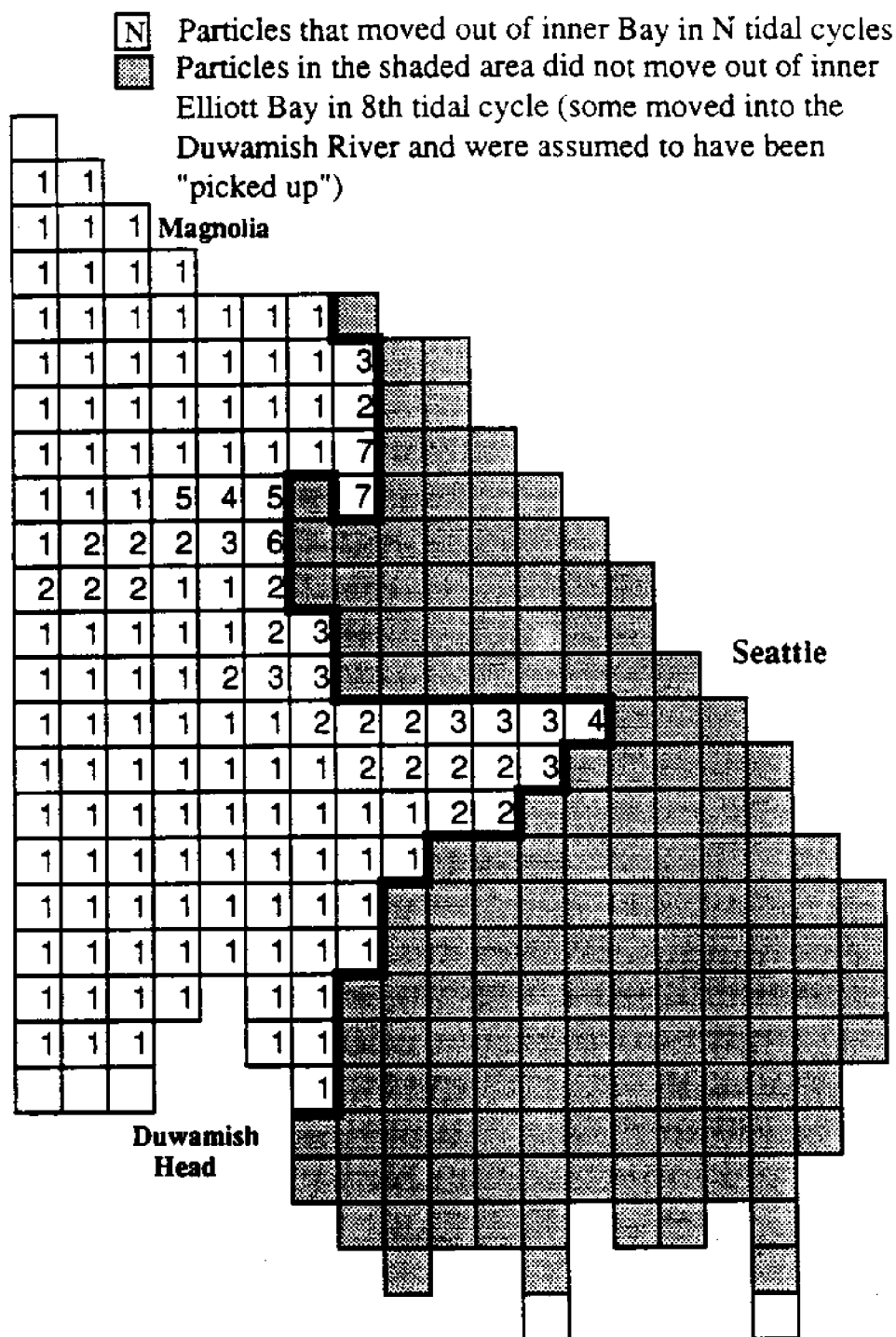
Ⓝ Particles that moved out of inner Bay in N tidal cycles
▓ Particles in the shaded area did not move out of inner
Elliott Bay in 8th tidal cycle (some moved into the
Duwamish River and were assumed to have been
"picked up")

Magnolia

Seattle

Duwamish
Head

Fig.5.34a The locations of released particles at the end of 8th tidal cycle
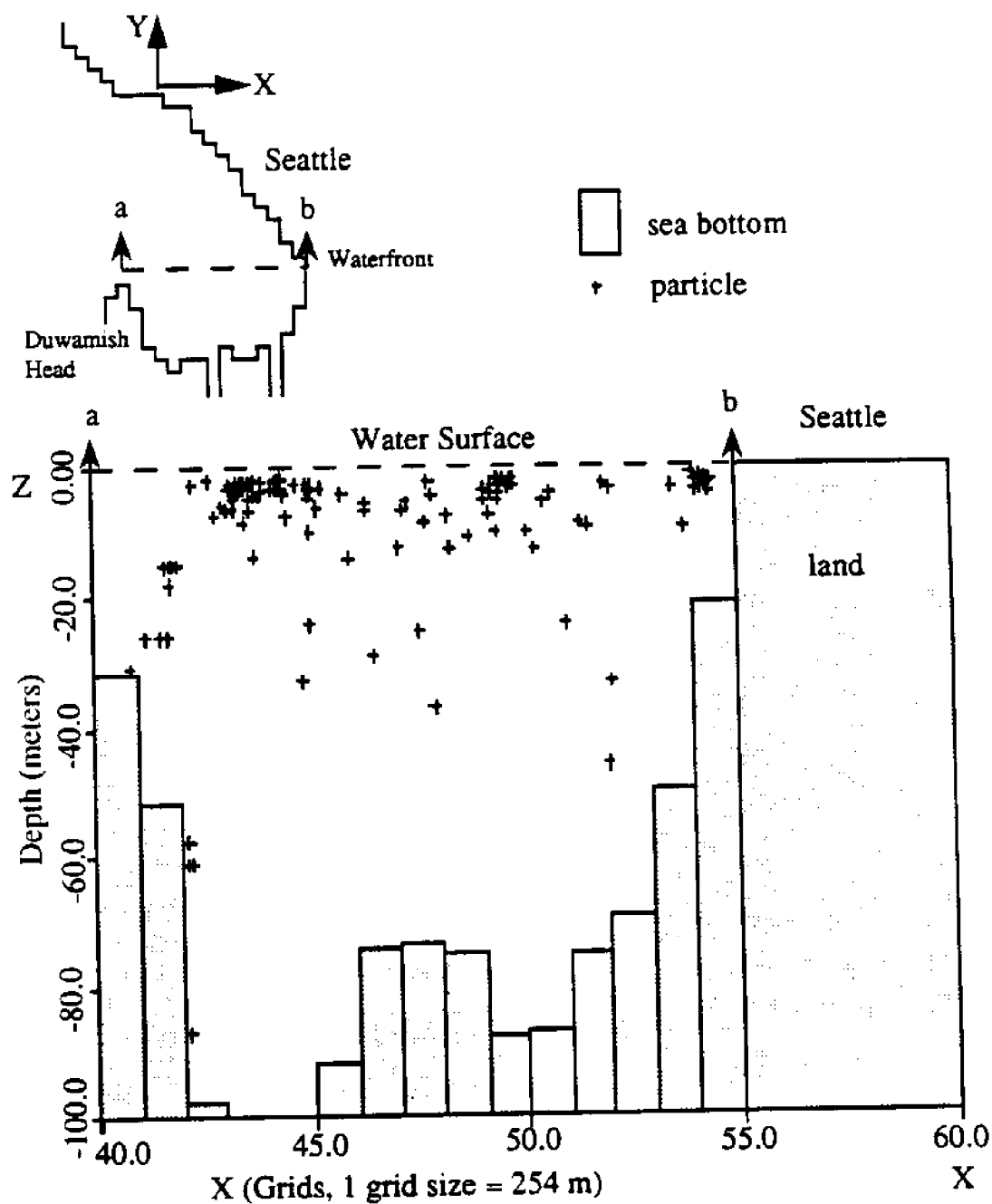
Fig.5.34b The locations of released particles at the end of
8th tidal cycle (on the vertical (X-Z) plane shown
in the upper figure).

in Elliott Bay, most of the released particles still remained in the upper 40 meters of the Bay at the end of 8th tidal cycle.

In order to more clearly examine how particles move in the inner Bay during the 8 tidal cycles, the trajectories of 12 selected particles are shown in Fig.5.35. The 12 numbers in Fig.5.35 are the initial locations of the 12 particles. The trajectories 4, 7, and 8 show the paths of particles moving out of the Bay from Magnolia (trajectory 4) and Duwamish Head (trajectories 7 and 8). The trajectories 5 and 6 show the traces of water movement in northern Elliott Bay. The trajectories of particles 1, 2, 9, 10, 11, and 12 show that the water movement in southern inner Bay is dominated by a counterclockwise circulation.

Since the Denny Way combined sewer overflow (CSO), West Waterway, and East Waterway are three well known pollutant sources in Elliott Bay, it is important to know how the pollutants discharged from these sources might be transported inside Elliott Bay. To examine that, 25 particles were released at each of these locations in surface layer (0.001 meter depth) at higher high water (HHW in Fig.5.14) and tracked for 9 tidal cycles. The initial locations of these released particles are shown in Fig.5.36a. The final locations of these released particles at the end of each tidal cycle are shown in Figs.5.36b-j.

According to Figs.5.36b-j., the particles released at the Denny Way CSO tended to move toward the coast of Duwamish Head within 9 tidal cycles and, according to the above results, they are expected to leave Elliott Bay soon after they arrive near Duwamish Head. Most of the particles released at East and West Waterways remained well inside the inner Bay after 9 tidal cycles.
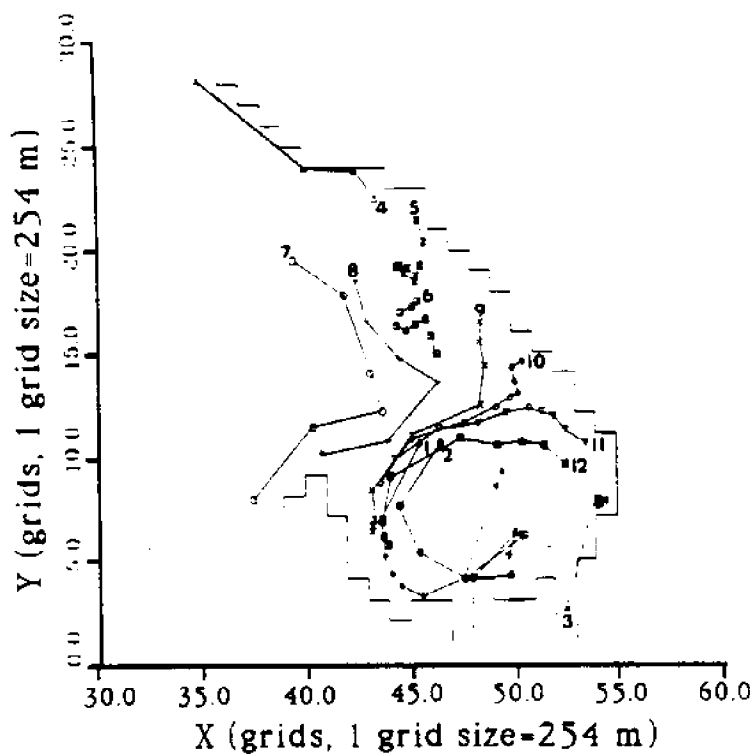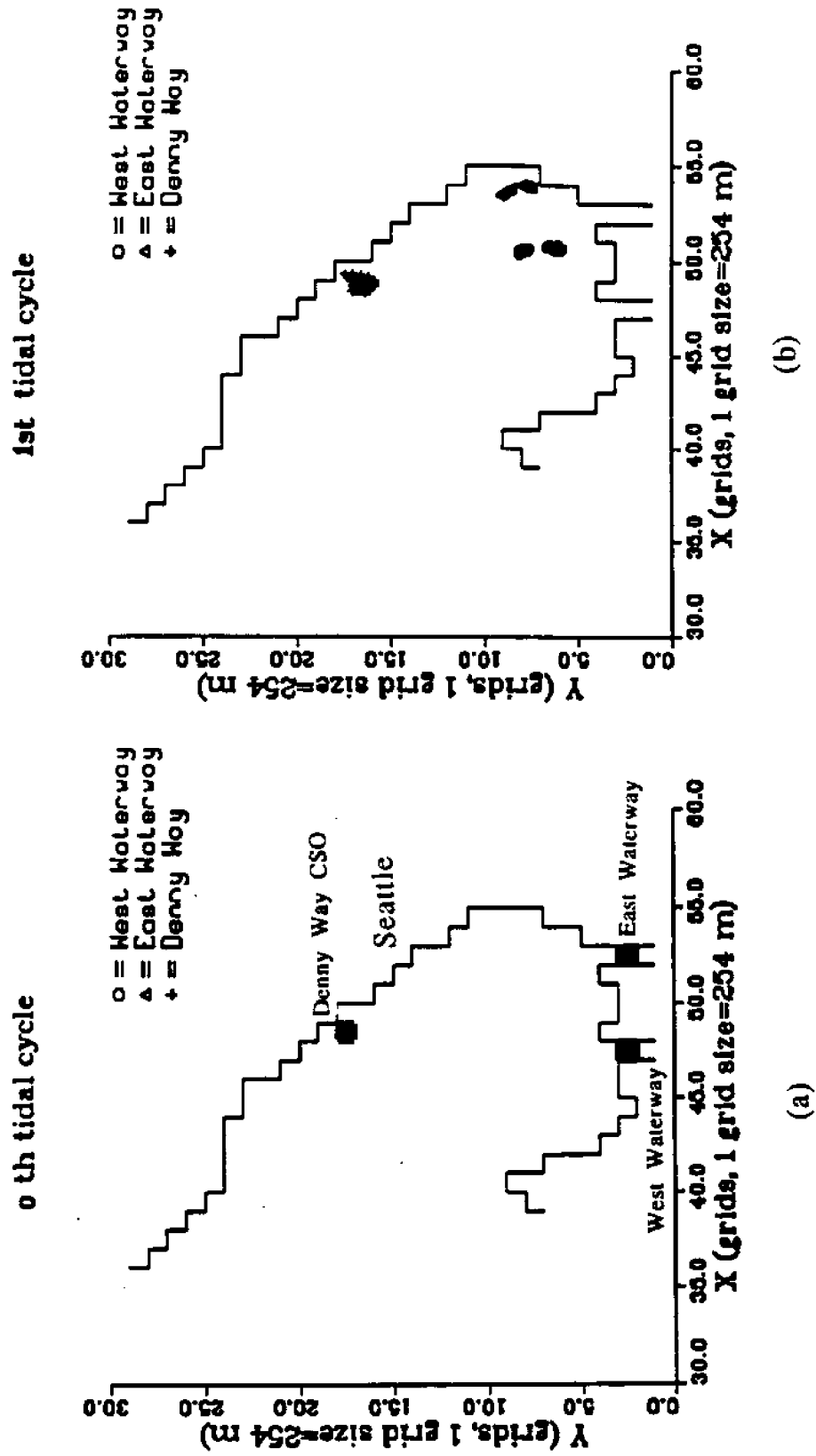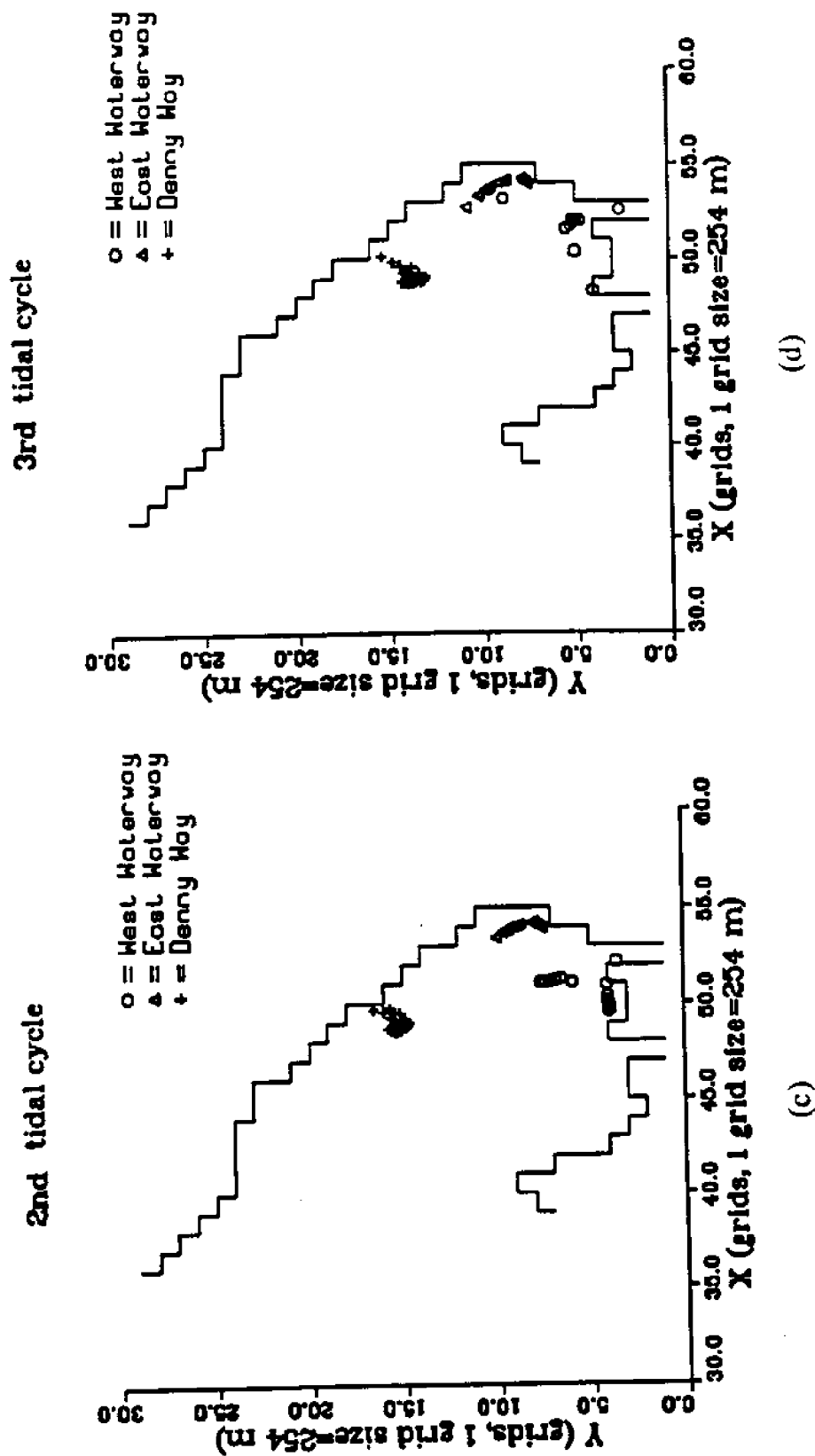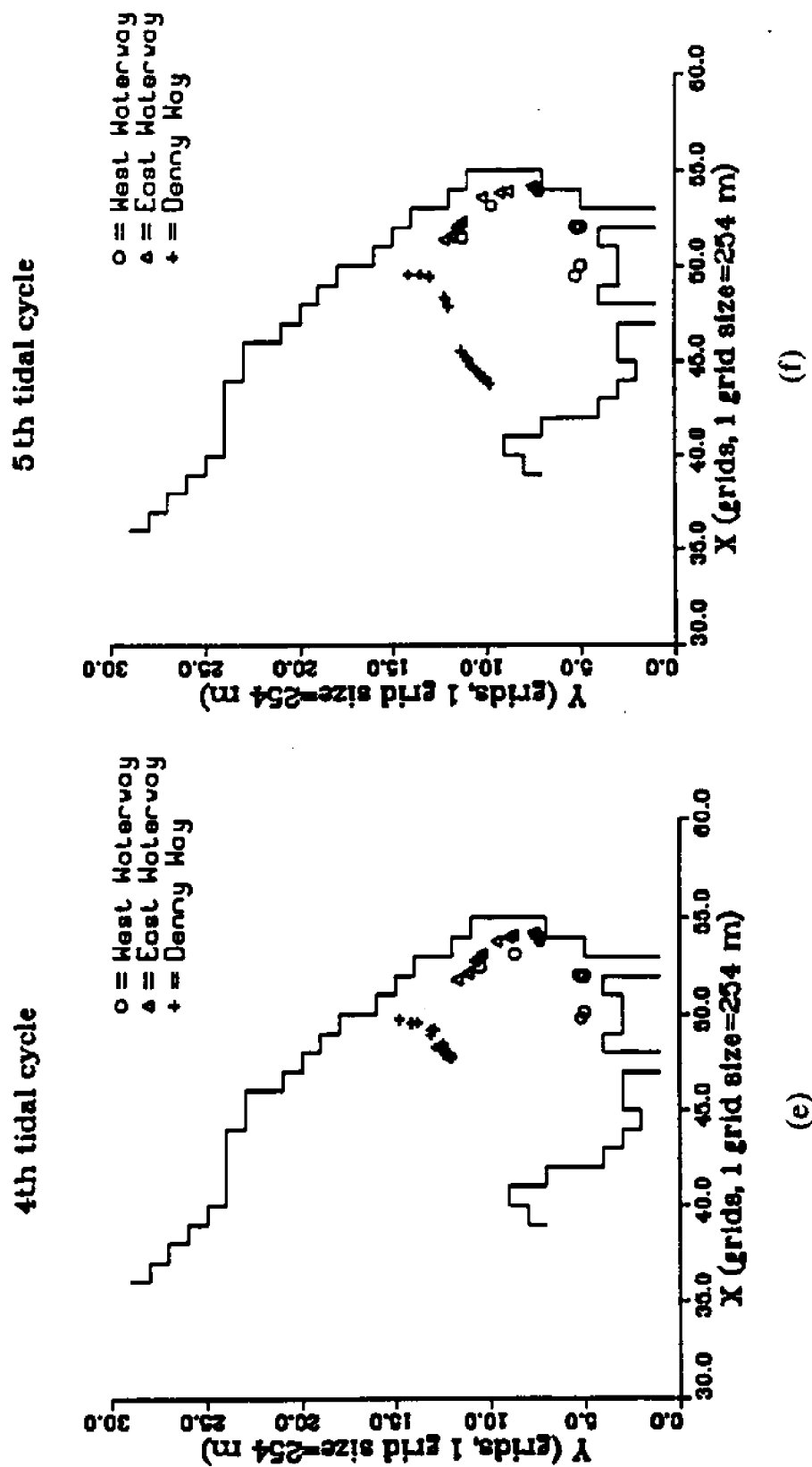
Fig.5.35 The trajectories of 12 released particles in Elliott
Bay. The symbols with a number nearby are the
initial locations of the particles. The symbols in each
line represent the locations of particles at the end
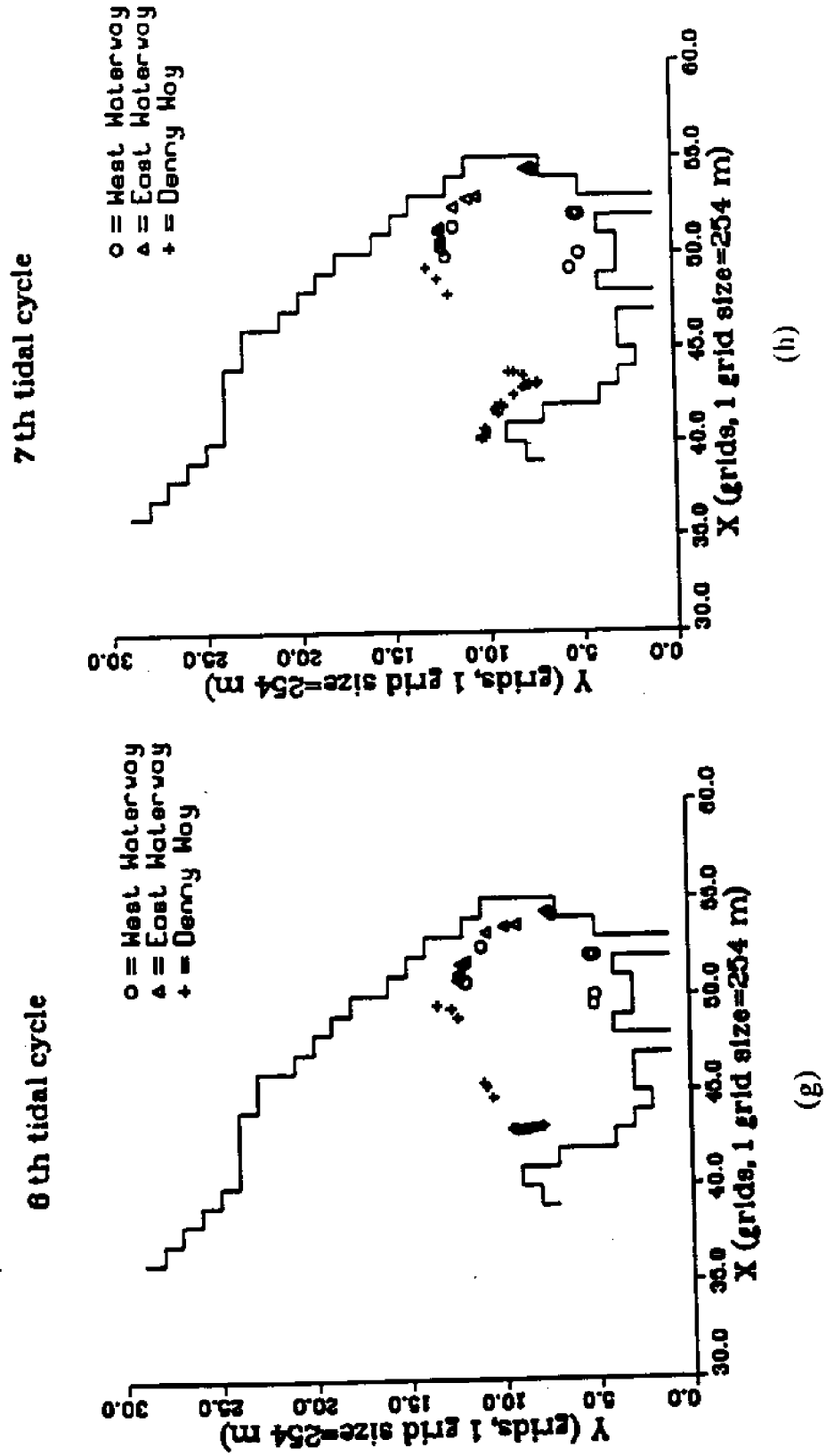of each tidal cycle.

o th tidal cycle

o = West Waterway
Δ = East Waterway
+ = Denny Way

Denny Way CSO

Seattle

East Waterway

West Waterway

Y (grids, 1 grid size=254 m)

X (grids, 1 grid size=254 m)

(a)

1st tidal cycle

o = West Waterway
Δ = East Waterway
+ = Denny Way

Y (grids, 1 grid size=254 m)

X (grids, 1 grid size=254 m)

(b)

Figs.5.36a-j The locations of released particles at the end of each tidal cycle

3rd tidal cycle

o = West Waterway
▲ = East Waterway
+ = Denny Way

Y (grids, 1 grid size=254 m)

X (grids, 1 grid size=254 m)

(d)

2nd tidal cycle

o = West Waterway
▲ = East Waterway
+ = Denny Way

Y (grids, 1 grid size=254 m)

X (grids, 1 grid size=254 m)

(c)

Figs.5.36a-j (continued)

5 th tidal cycle

o = West Waterway
▲ = East Waterway
+ = Denny Way

X (grids, 1 grid size=254 m)

Y (grids, 1 grid size=254 m)

(f)

4th tidal cycle

o = West Waterway
▲ = East Waterway
+ = Denny Way

X (grids, 1 grid size=254 m)

Y (grids, 1 grid size=254 m)

(e)

Figs.5.36a-j (continued)

7th tidal cycle

o = West Waterway
△ = East Waterway
+ = Denny Way

X (grids, 1 grid size=254 m)

Y (grids, 1 grid size=254 m)

(h)

6th tidal cycle

o = West Waterway
△ = East Waterway
+ = Denny Way

X (grids, 1 grid size=254 m)

Y (grids, 1 grid size=254 m)

(g)

Figs.5.36a-j (continued)
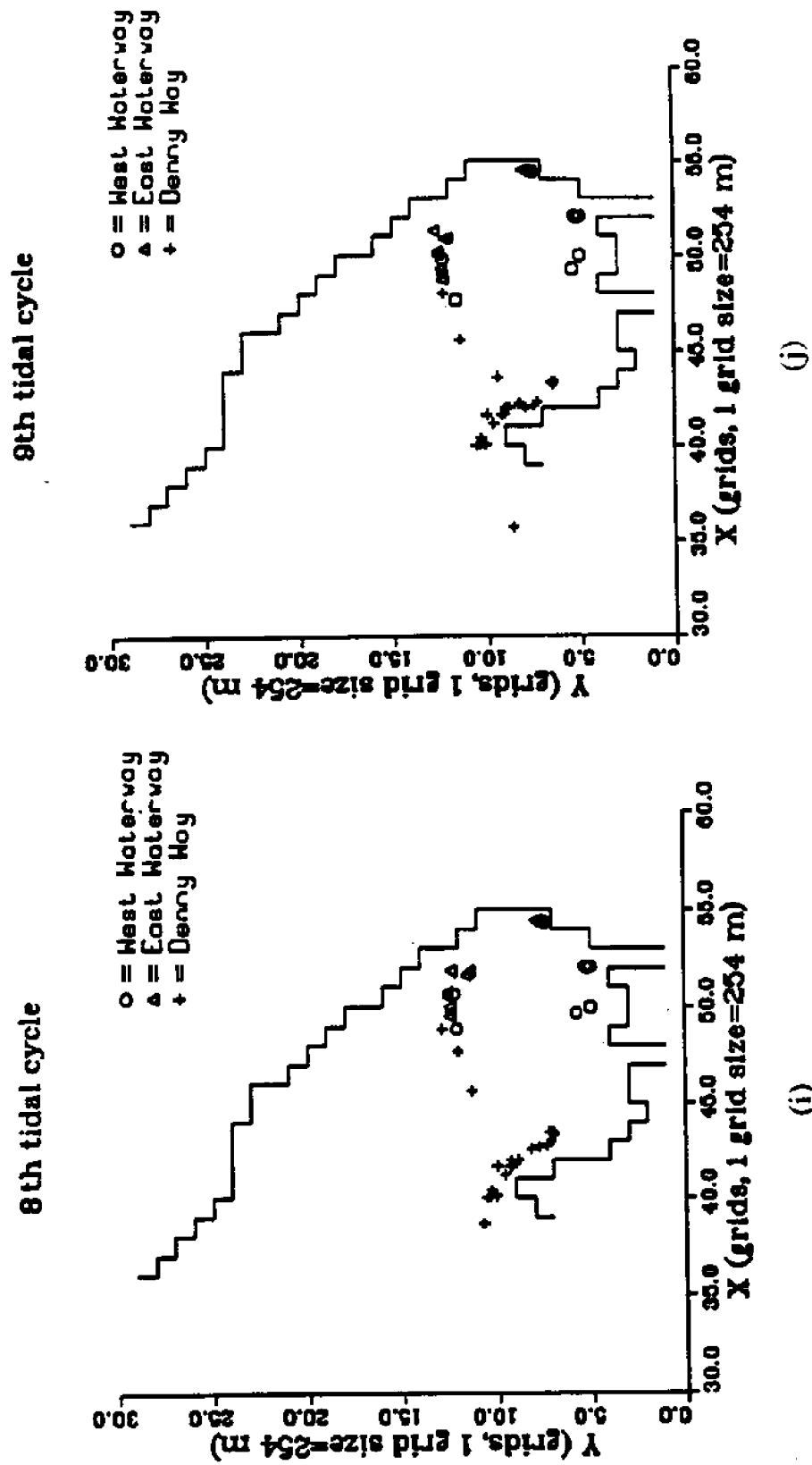
Figs.5.36a-j (continued)

5.2.3.3 Effects of River Discharge, Wind, Tidal Inequality, and Density

The above derived current characteristics in Elliott Bay are driven by tide only. The characteristics of these currents will change when the effects of river discharge, wind, density, or different tidal conditions are considered. In order to more clearly see the effects of river discharge, wind, tidal inequality, and density on tidal currents, tens and perhaps hundreds of velocity vector diagrams for various times in the simulation period would be needed. To avoid the production of such a large number of vector diagrams, this study will focus on the net effects of these forcing mechanisms by examining the tidally averaged (or mean) current field in this section.

Effect of River Discharge

To investigate the effect of river inflow on the tidal transport and circulation in Elliott Bay, the discharge from Duwamish River was increased from 10 (summer condition) to 60 m^3s^{-1} (winter condition).

The effect of river discharge on mean tidal currents (or residual currents) in the top two layers is illustrated in Figs.5.37a-b. The mean current vectors in Figs.5.37a-b were obtained by subtracting the mean currents of Case 7 from the mean currents of Case 8 (high river discharge). These differences show that river inflow has only a minor net contribution to the northward flow along the east coast of the Bay. The effect is confined within the southern portion of the inner Bay.

Effect of Wind

Two sequences of observed wind data presented earlier (Fig.5.4) are used in the simulations (Cases 9 and 10 in Table 5.1). Both wind sequences last for three days with maximum and mean

0.0070 m/s
MAXIMUM VECTOR

1st layer

Seattle

(a)

0.0070 m/s
MAXIMUM VECTOR

2nd layer

(b)
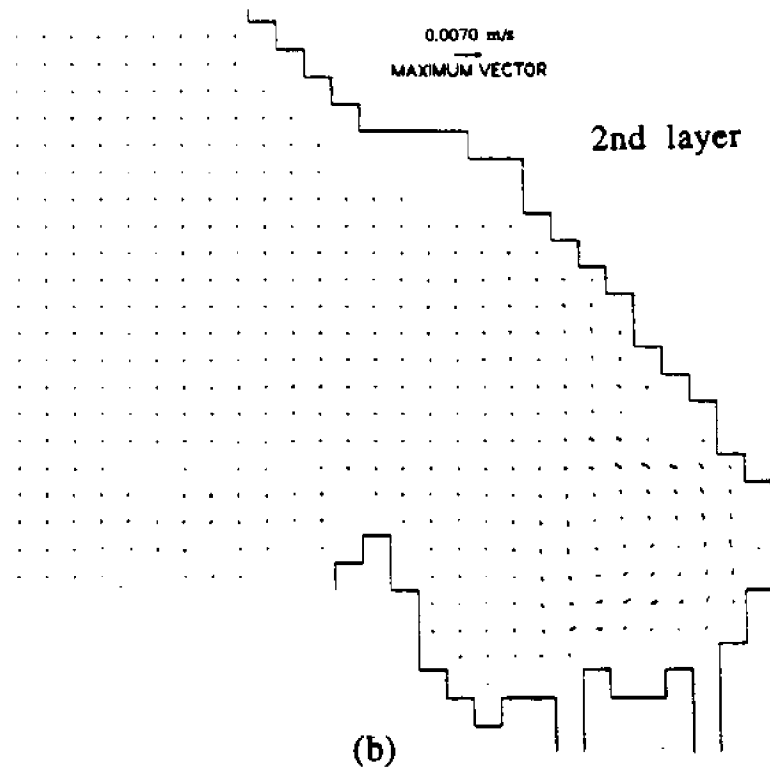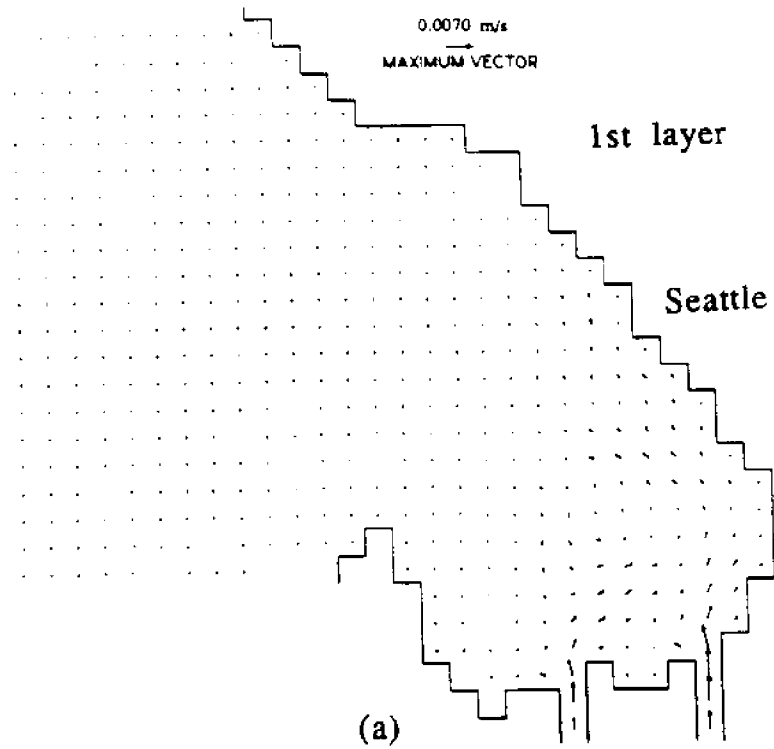
Figs.5.37a-b The difference of mean currents between the cases of high river inflow (Case 8) and low river inflow (Case 7).
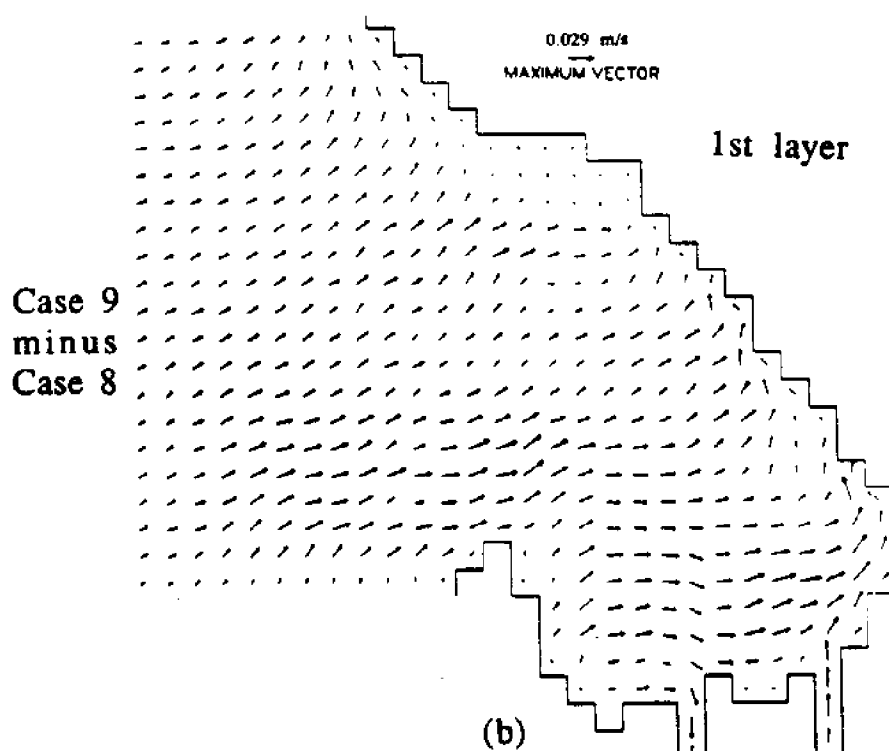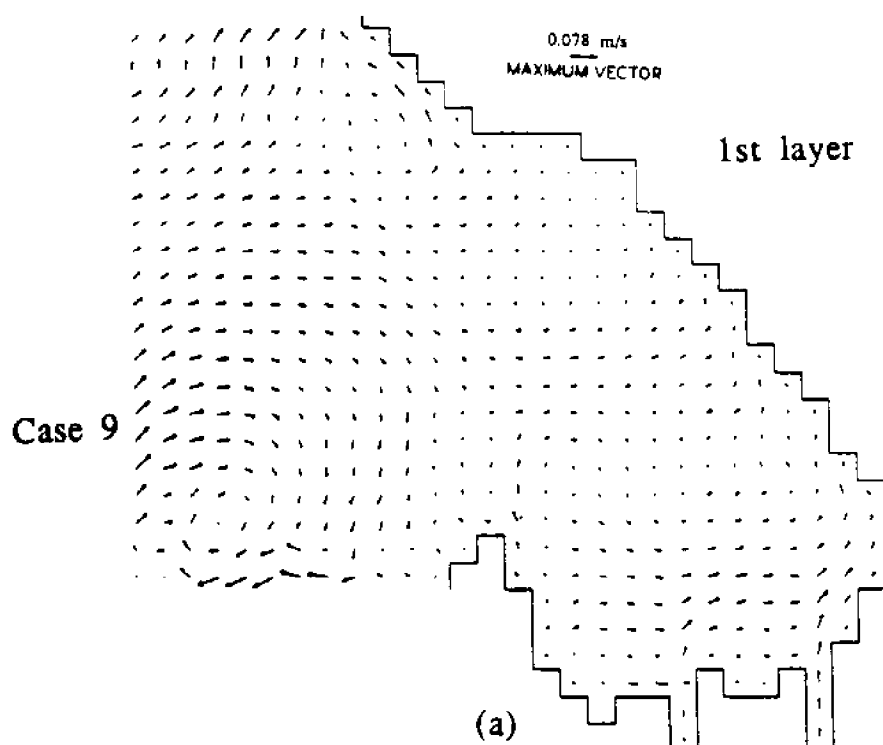
speeds of 9 and 4 m/sec respectively for the southerly wind, and 7 and 2.3 m/sec respectively for the northerly wind (Fig.5.4).

The mean flow patterns in all four layers due to the southerly wind are given in Figs.5.38a,c,e,g. To illustrate more clearly how the winds affect the tidal currents in Elliott Bay, the vector plots which represent the differences between the mean currents due to the southerly wind (Case 9) and those without wind (Case 8) are shown in Figs.5.38b,d,f,g.

Under the influence of the southerly wind, the clockwise residual circulation outside the northwest coast of Duwamish Head still dominated the mean currents in the outer Bay (Figs.5.38a,c,e,g), but more surface water in the main channel is carried into Elliott Bay (Figs.5.38a,b). The outgoing flow along the shore of Duwamish Head is weakened significantly. In the inner Bay, the southerly wind deflects the directions of surface layer tidal currents and causes the occurrence of onshore currents. When these surface onshore currents reach the east shore of the Bay, portions of these onshore currents sink to the bottom and form a westward offshore flow in the deeper layers (Figs.5.38d,f). Except for these westerly offshore currents near the east shore of the Bay, the wind induced effect in the deeper layer flow system (Figs.5.38d,f,h) is pretty weak.

The mean flow patterns due to northerly wind and the vector plots representing the differences between the mean currents with and without the northerly wind at all four layers are shown in Figs.5.39a-h. The effect of the northerly wind (Figs.5.39a,c,e,g) is in general smaller than that of the southerly wind. In the outer Bay, the flow pattern is still dominated by the same clockwise residual circulation at all depths (Figs.5.39a,c,e,g). Due to the northerly wind, the outgoing flow along the shore of Duwamish Head is enhanced (Figs.5.39a,b).
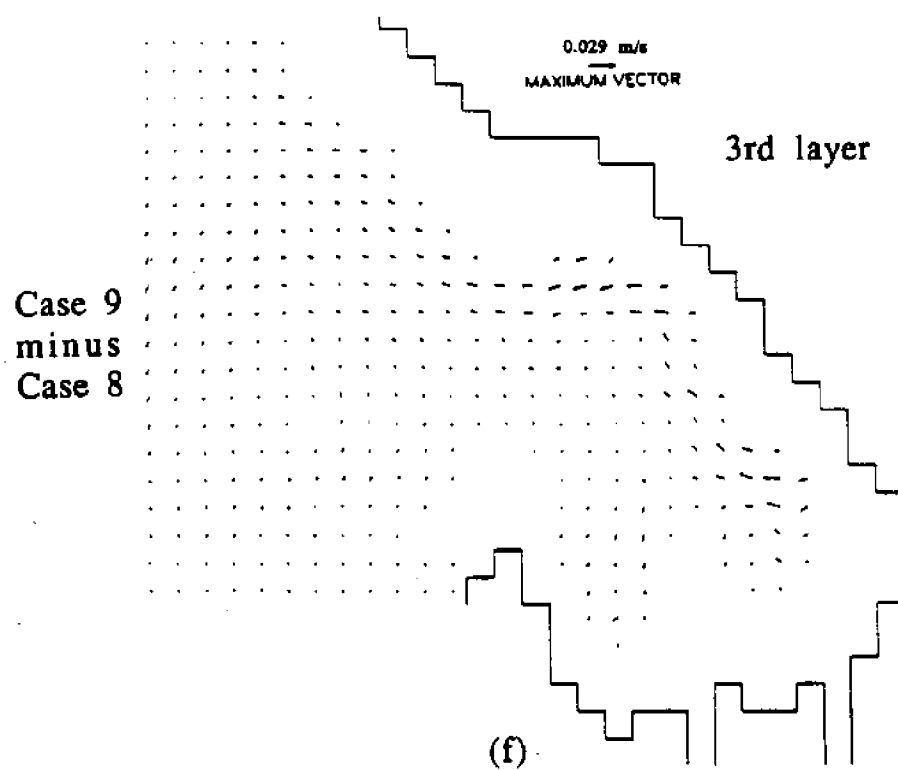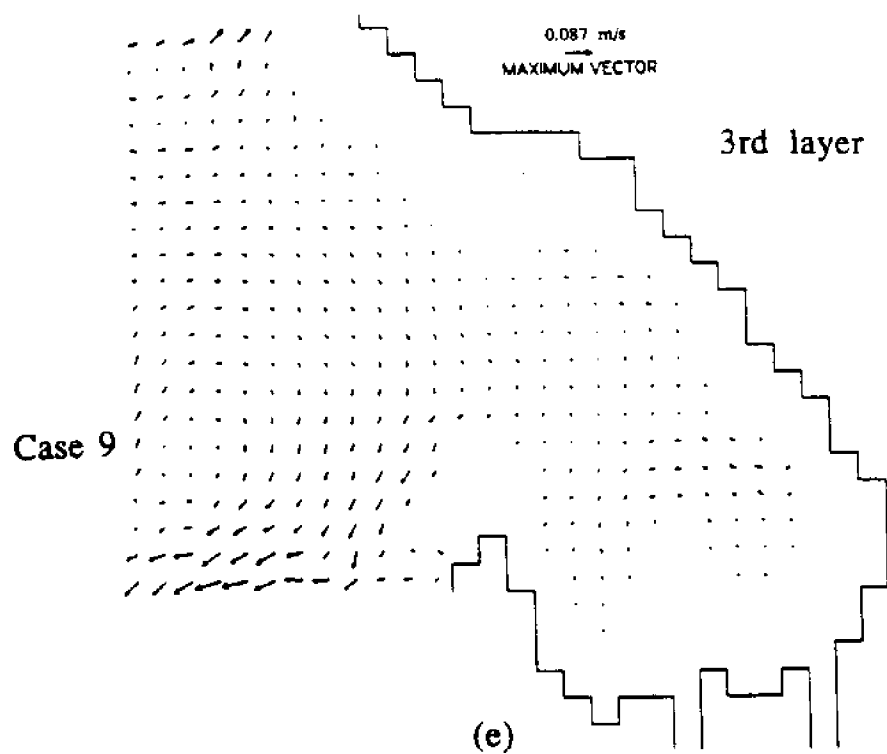
The northerly wind does have one marked effect on the tidal currents along Seattle waterfront. The north wind tends to force the

0.078 m/s
MAXIMUM VECTOR

1st layer

Case 9

(a)

0.029 m/s
MAXIMUM VECTOR
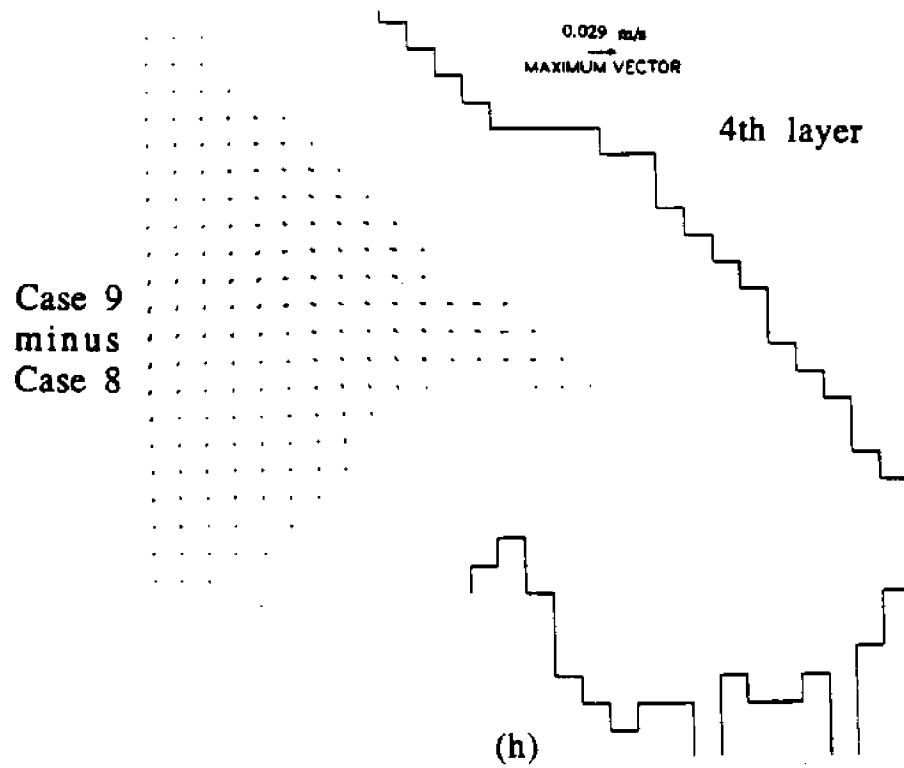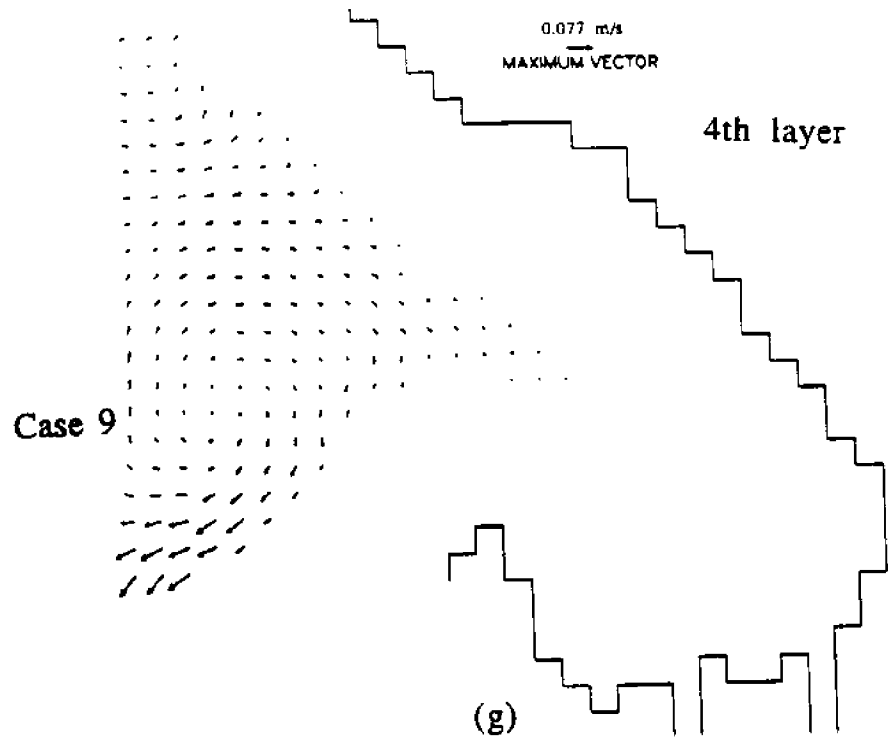
1st layer

Case 9
minus
Case 8

(b)

Figs.5.38a-h The mean currents of southerly wind case (a,c,e,g) and
the difference of mean currents between the cases of
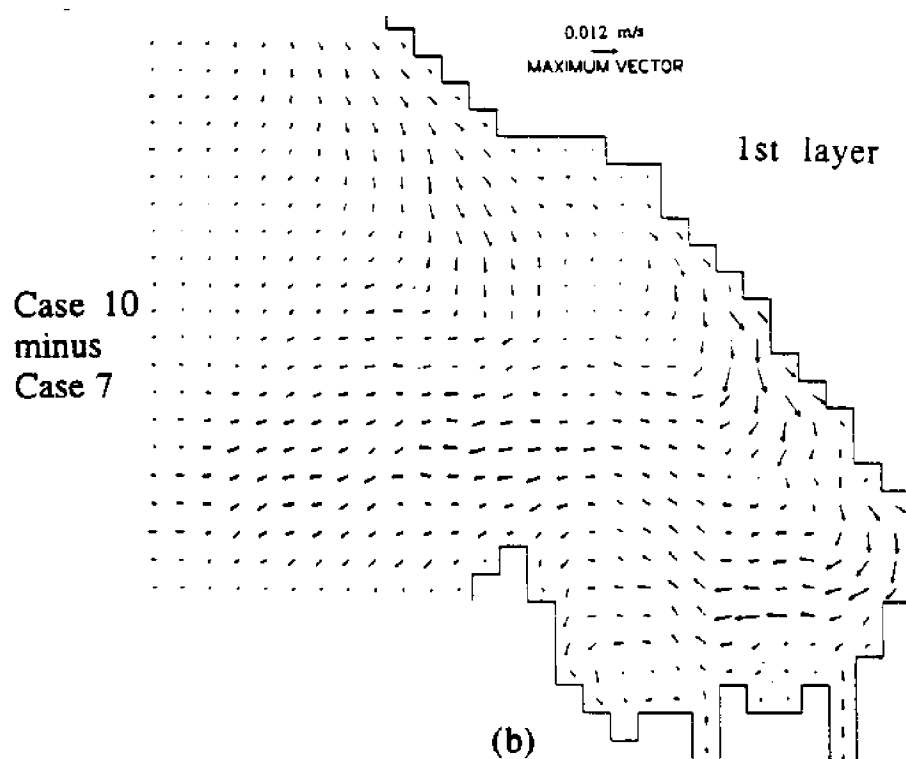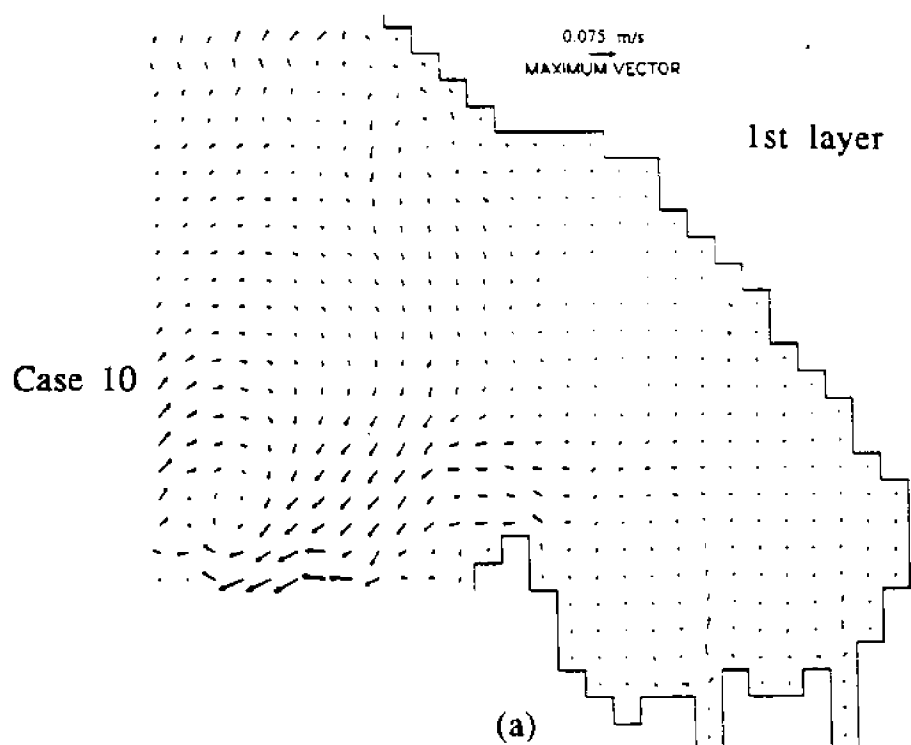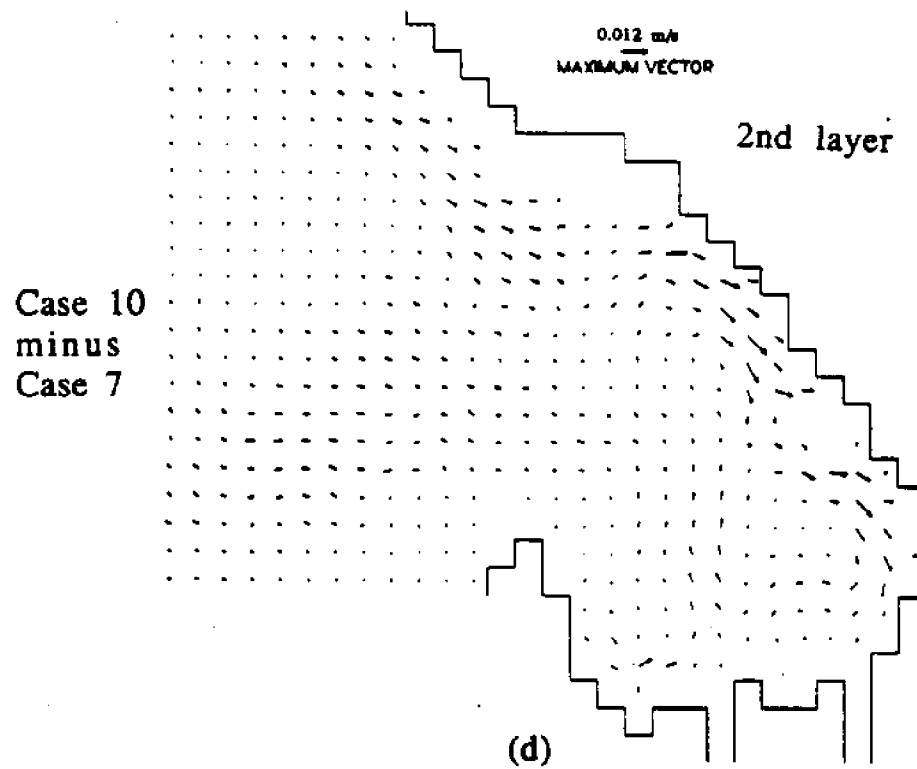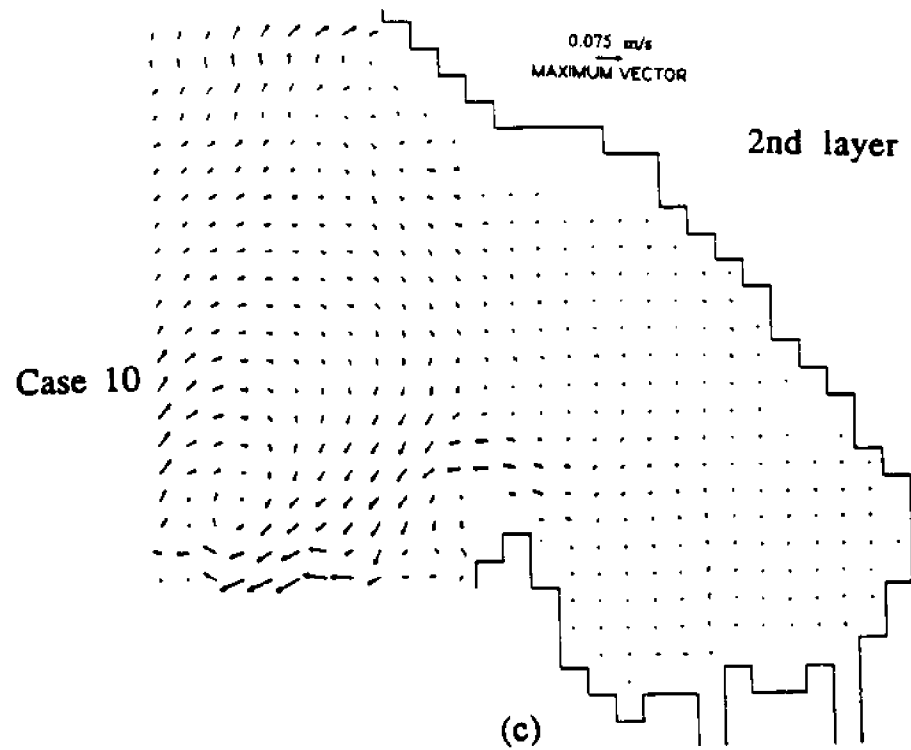southerly wind (Case 9) and calm wind (Case 8).

0.072 m/s
MAXIMUM VECTOR

2nd layer

Case 9

(c)

0.029 m/s
MAXIMUM VECTOR

2nd layer

Case 9
minus
Case 8

(d)

Figs.5.38a-h (continued)

0.087 m/s
MAXIMUM VECTOR

3rd layer

Case 9

(e)

0.029 m/s
MAXIMUM VECTOR

3rd layer

Case 9
minus
Case 8

(f)

Figs.5.38a-h (continued)

0.077 m/s
MAXIMUM VECTOR

4th layer

Case 9

(g)

0.029 m/s
MAXIMUM VECTOR

4th layer

Case 9
minus
Case 8

(h)

Figs.5.38a-h (continued)

0.075 m/s
MAXIMUM VECTOR

1st layer

Case 10

(a)

0.012 m/s
MAXIMUM VECTOR

1st layer

Case 10
minus
Case 7
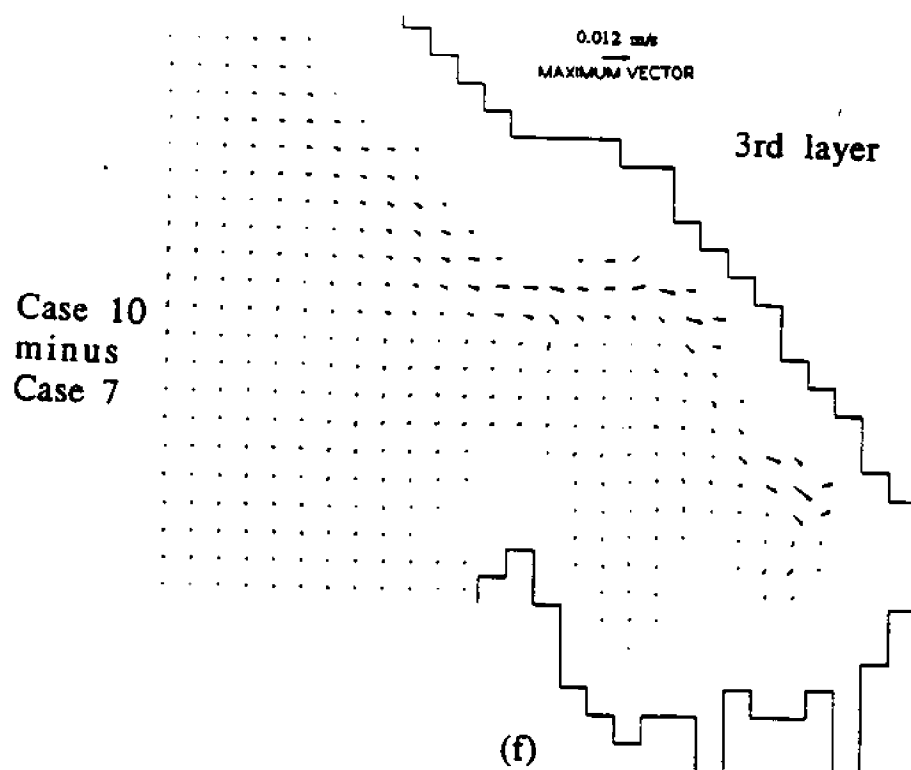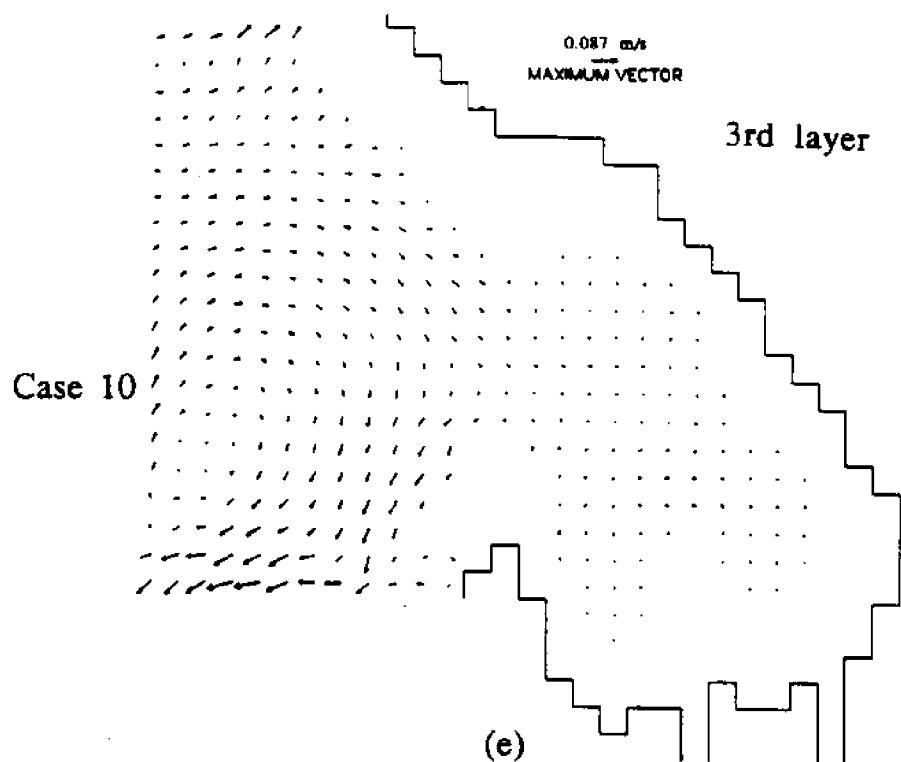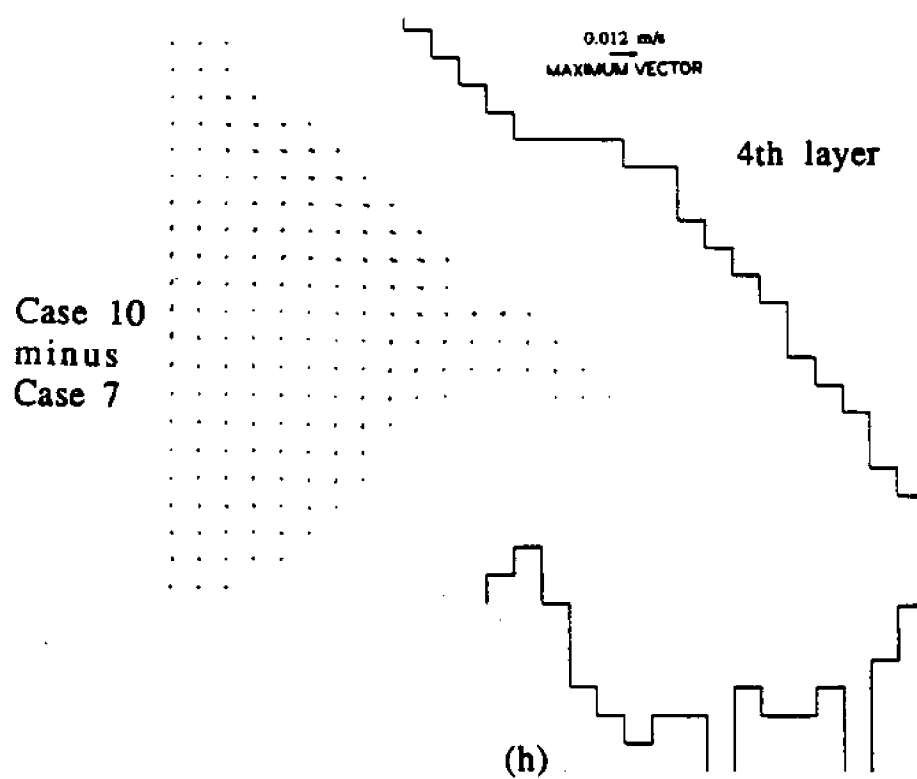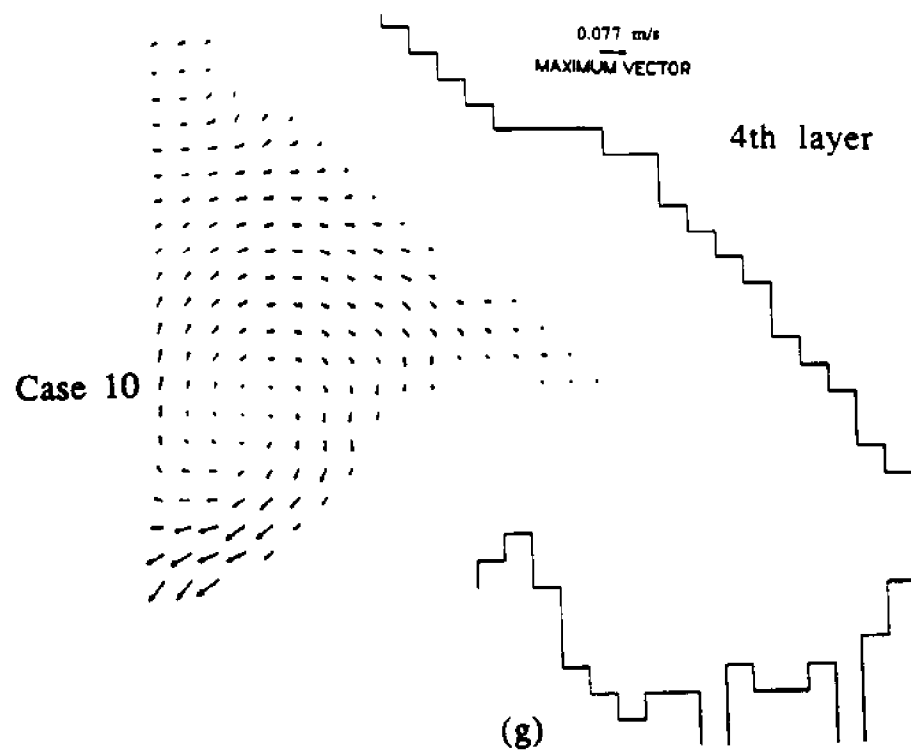
(b)
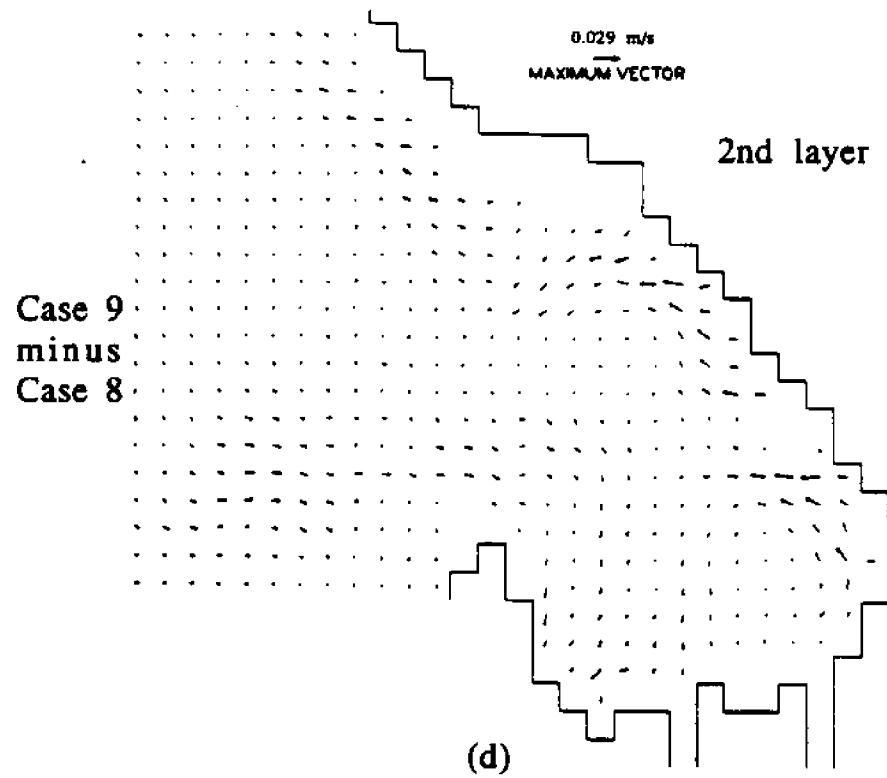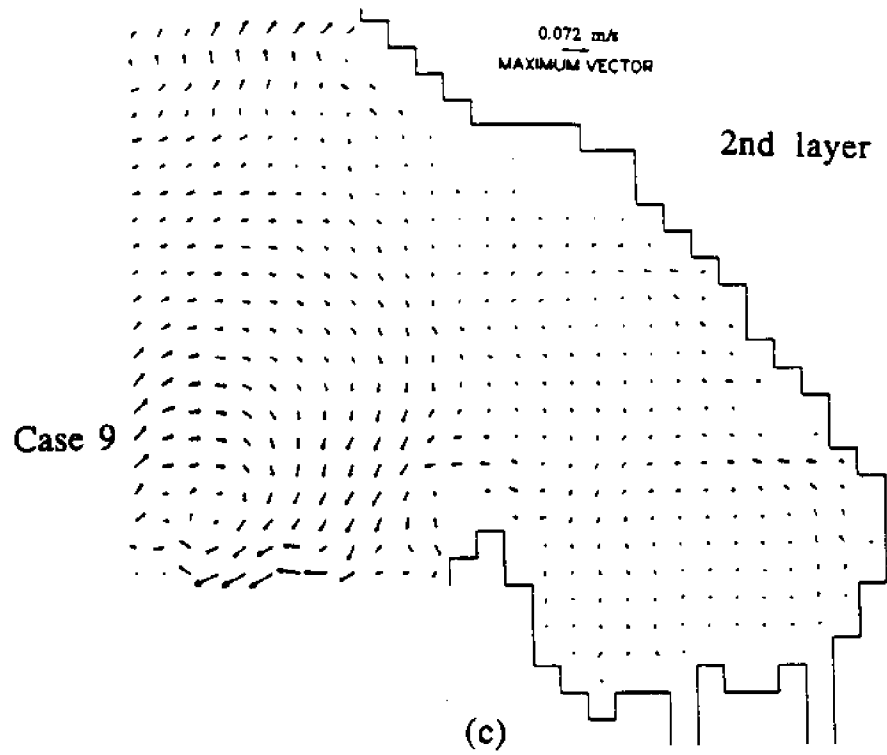
Figs.5.39a-h The mean currents of northerly wind case (a,c,e,g) and
the difference of mean currents between the cases of
northerly wind (Case 10) and calm wind (Case 7).

0.075 m/s
MAXIMUM VECTOR

2nd layer

Case 10

(c)

0.012 m/s
MAXIMUM VECTOR

2nd layer

Case 10
minus
Case 7

(d)

Figs.5.39a-h (continued)

0.087 m/s
MAXIMUM VECTOR

3rd layer

Case 10

(e)

0.012 m/s
MAXIMUM VECTOR

3rd layer

Case 10
minus
Case 7

(f)

Figs.5.39a-h (continued)

0.077 m/s
MAXIMUM VECTOR

4th layer

Case 10

(g)

0.012 m/s
MAXIMUM VECTOR

4th layer

Case 10
minus
Case 7

(h)

Figs.5.39a-h (continued)

tidal currents in the surface layer to move southward and thus causes the occurrence of surface offshore currents along the east shore of the Bay (Fig.5.39b). The occurrence of these offshore currents in turn induces both onshore and longshore currents in the lower layers (Figs.5.39d,f).

While it is interesting to see the simulated results due to wind, all the above presented wind effect in Elliott Bay can be strongly influenced by local land form topography (such as bluffs along the northeast side of Duwamish Head) and high rise buildings surrounding the Bay.

Effect of Tidal Inequality

The tidal currents described above were all driven by a "medium tide" shown in Fig.5.2. Additional simulations were carried out to investigate the effect of changing tidal conditions on the tidal currents. The analysis is again based on the differences between the mean flow patterns of the cases simulated.

The differences between the mean currents due to the spring tide (Case 11) and those due to the medium tide (Case 7) are shown in Fig.5.40a. It can be seen in Fig.5.40a that spring tide enhances the eastward currents along the east-west submarine canyon and brings more water into the inner Bay. But in the meantime, spring tide also enlarges the outward flows along the shores of Duwamish Head and Magnolia and takes more water out of the Bay.

The differences between the mean currents due to the neap tide (Case 12) and those due to the medium tide (Case 7) are shown in Fig.5.40b. This figure shows that during the neap tide less water enters the Bay from the east-west submarine canyon and less water leaves the Bay from the shores of Duwamish Head and Magnolia. The maximum mean current speeds in Elliott Bay due to the spring tide, the medium tide, and the neap tide are 0.11, 0.09, and 0.06 m/s, respectively.
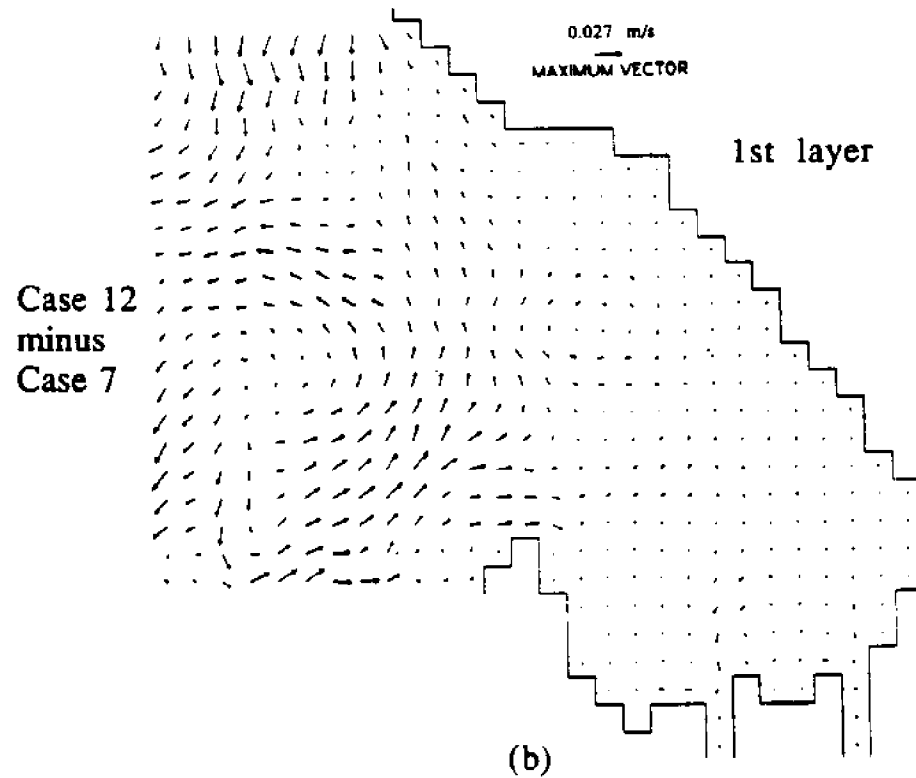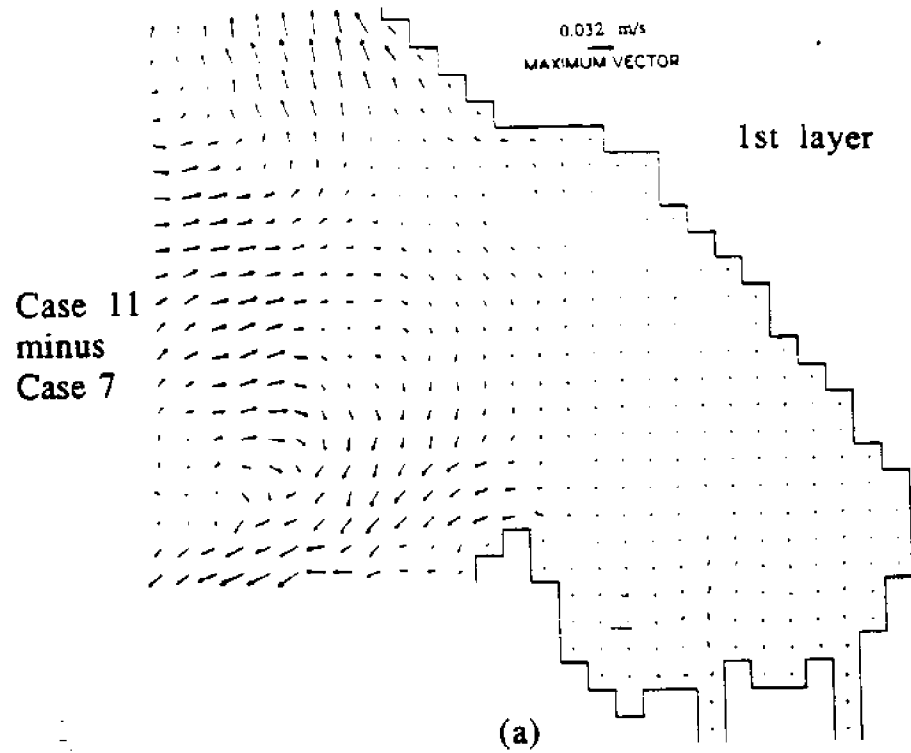
Figs.5.40a-b The difference of surface layer mean currents between the cases of spring tide (Case 11) and medium tide (Case 7) and between the cases of neap tide (Case 12) and medium tide (Case 7)

Discharges between Inner and Outer Bay

The mean discharge across a vertical plane separating the inner and outer Bays (Fig.5.41) is calculated here. This plane in Fig.5.41 contains four vertical layers; each layer, from top to bottom, includes 15, 12, 6, and 2 grids respectively. The discharge through each grid is obtained by multiplying the horizontal grid dimension (254 m) by the layer depth and the velocity component in the direction normal to the plane. Mean discharges can then be attained by averaging the discharges over one tidal cycle. The tidally averaged discharges from Cases 7, 8, 9, 10, 11, and 12 (see Table 5.2) are shown in Figs.5.42a-c. The numbers on the ordinates of these figures correspond to the locations shown in Fig.5.41. On the abscissas, positive values represent water moving into the inner basin and negative values represent water moving out of the inner basin.

In the calm wind case (Case 7), more than 90 percent of the inward flow (1030 m^3s^{-1}) enters the inner Bay along the east-west submarine canyon and about 85 percent of the outgoing flow (950 m^3s^{-1}) leaves the inner Bay along the coast of Duwamish Head. The discharges near Smith Cove are always weak. The mean discharge difference between low river inflow case (Case 7) and high river inflow case (Case 8) are insignificant (Figs.5.42a,b). The total mean inward and outward discharges across the dividing plane are approximately 1090 and 1120 m^3s^{-1} for the Case 7 and 1055 and 1115 m^3s^{-1} for Case 8.

In the case with the south wind (Fig.5.42a), more water enters the inner Bay from the surface layer and the outgoing flow along the shore of Duwamish Head decreases significantly. In addition, a large amount of bottom water (about 580 m^3s^{-1}) leaves the inner Bay along the northern edge of the east-west submarine canyon. Under the north wind influence (Fig.5.42b), more water in the deeper layers moves into the inner Bay through the northern edge of the east-west submarine canyon. The outward discharge through the shore of Duwamish Head also increases (to about 1150 m^3s^{-1}). The total mean

Dividing line

4 layers

3 layers

2 layers

1 layer

Smith Cove

15
14
13
12
11
10
9
8
7
6
5
4
3
2
1

Seattle

east-west
submarine
canyon
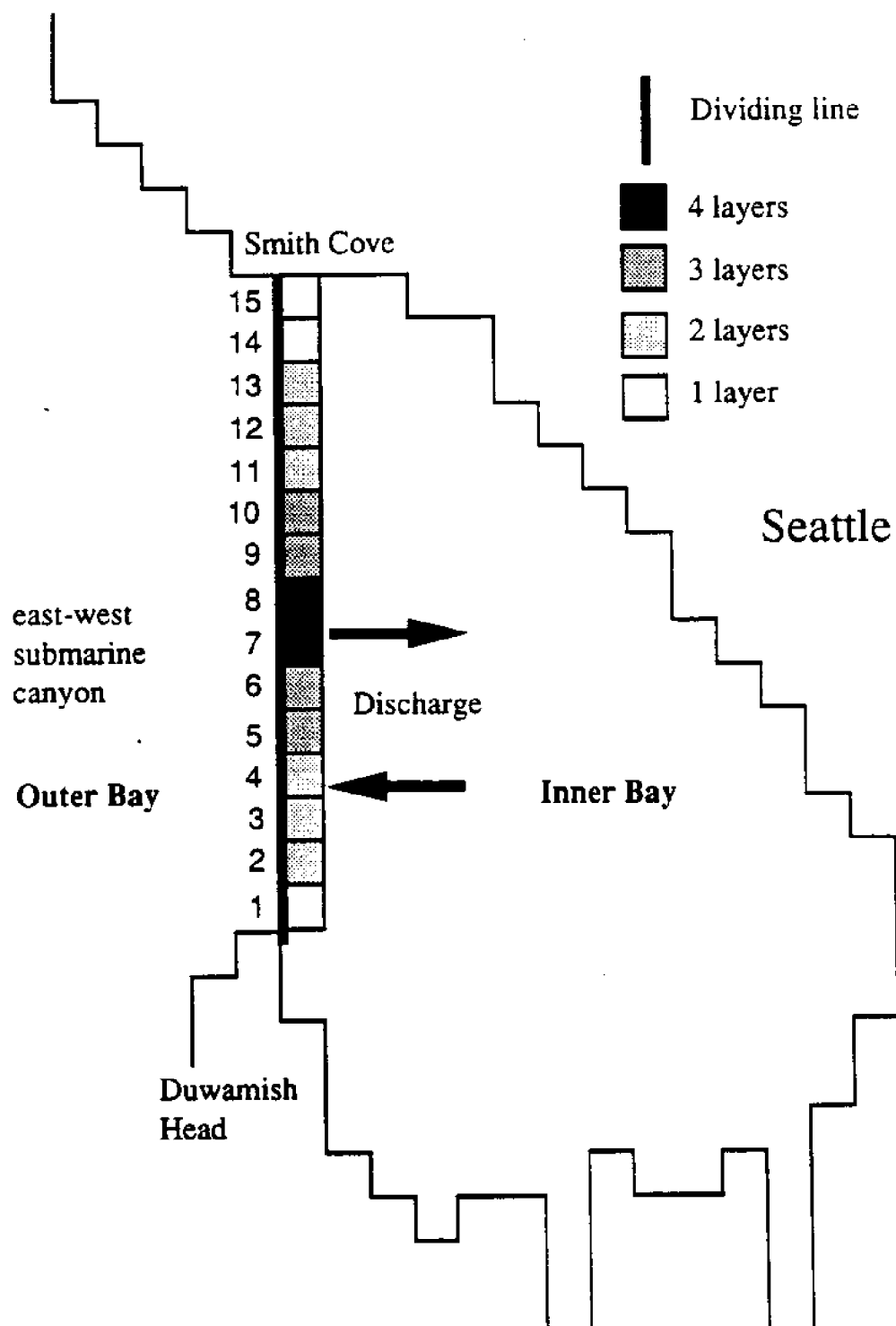
Discharge

Outer Bay

Inner Bay

Duwamish
Head

Fig.5.41 The model layers at the line between Smith Cove and
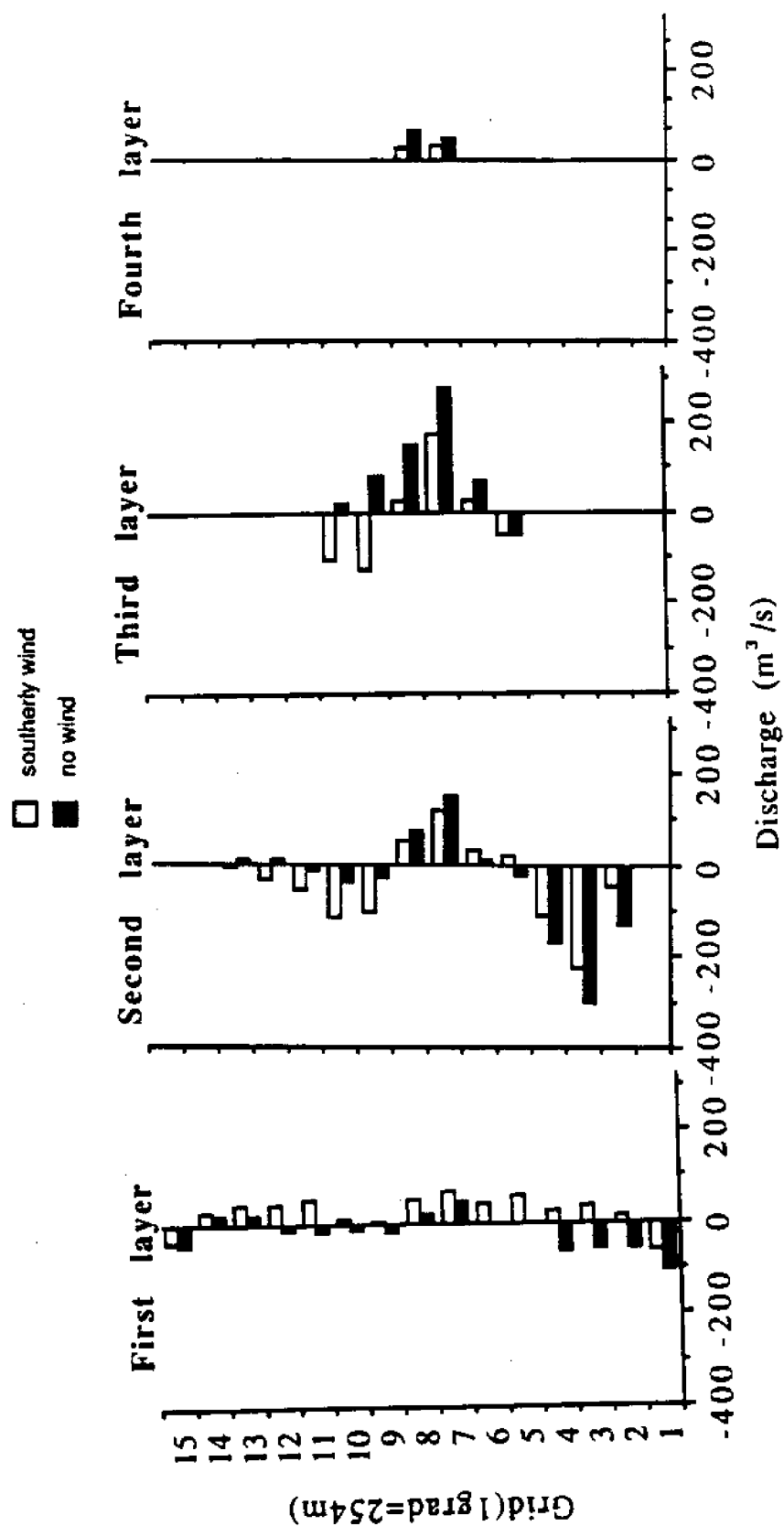Duwamish Head

Fig.5.42a The comparison of tidally-averaged discharges between calm wind case (Case 8) and southern wind case (Case 9)
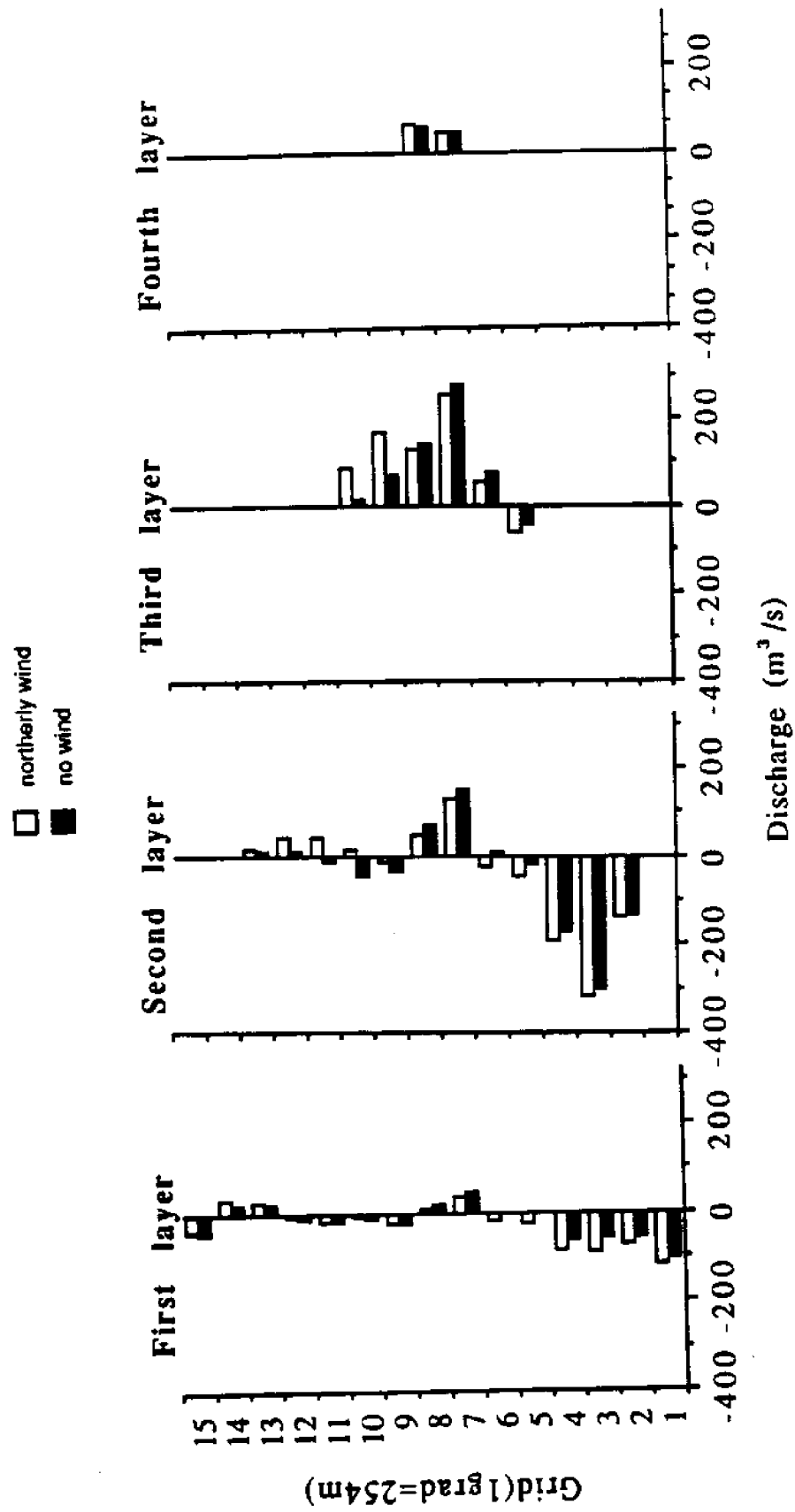
Fig.5.42b The comparison of tidally-averaged discharges between calm wind case (Case 7) and northern wind case (Case 10)
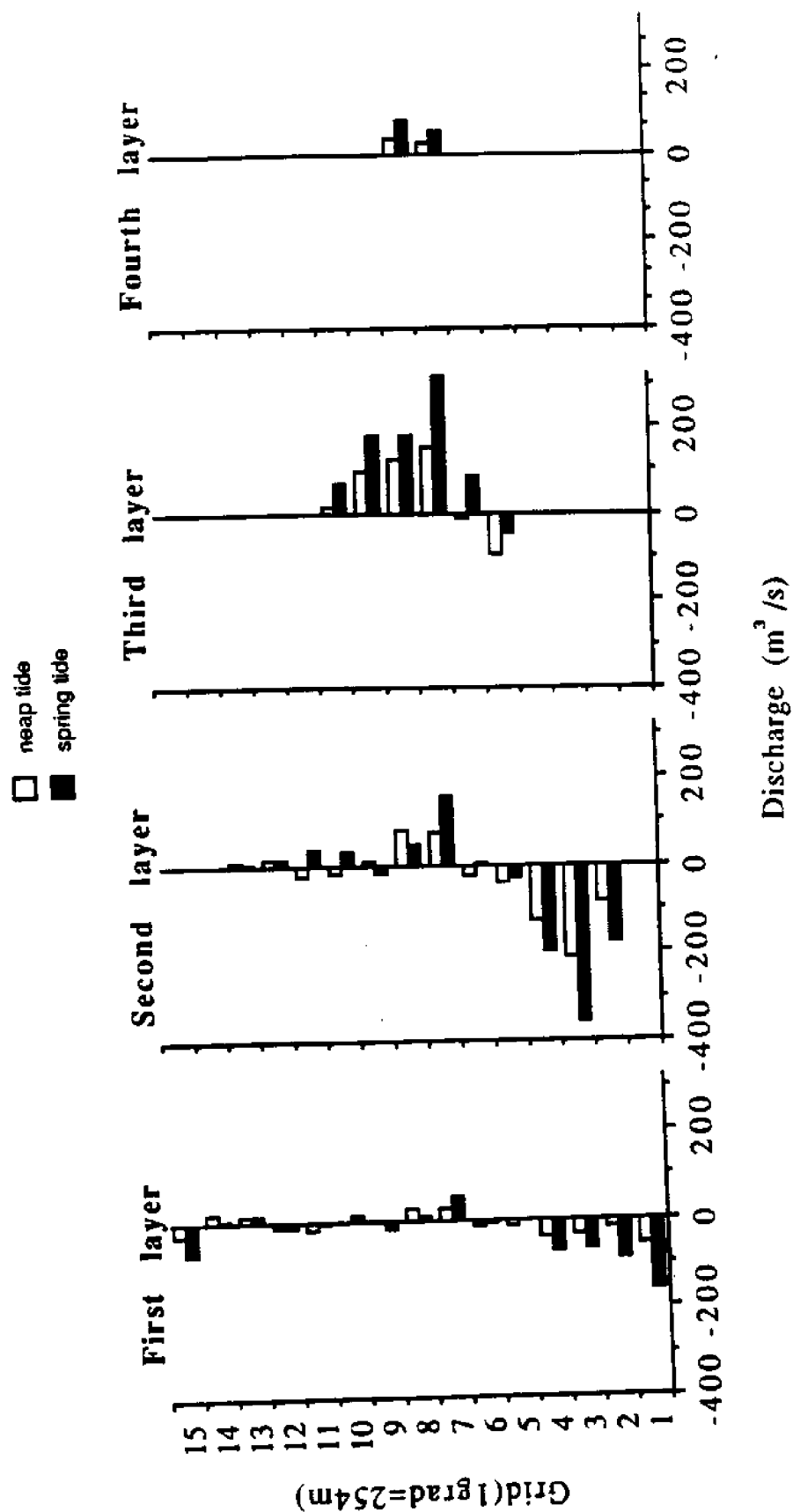
Fig.5.42c The comparison of tidally-averaged discharges between spring tide case (Case 11) and neap tide case (Case 12)

inward and outward discharges are approximated 1035 and 1070 m^3s^{-1} for the southerly wind case and 1220 and 1245 m^3s^{-1} for the northerly wind case.

The results in Fig.5.42c show clearly that a spring tide can bring more water into the inner Bay along the east-west submarine canyon and take more water out of the inner Bay from the shores of Duwamish Head and Smith Cove. The total mean inflow (into the Bay) and outflow across the separating plane are approximately 1370 and 1300 m^3s^{-1} respectively for the spring tide, and 750 and 840 m^3s^{-1} respectively for the neap tide.

For a mass conservation check, the differences between the total mean inward and outward discharges in all the above cases reflect the effects of Duwamish River inflow and the net water volume changes in the inner Elliott Bay. Using the no wind case (Case 7) as an example, the Duwamish River inflow (approximately 20 m^3/s) and net discharge across the vertical plane (approximately -30 m^3/s) will require the water elevation in inner Elliott Bay to drop about 6 cm after one tidal cycle. This value is pretty close to the water surface elevation change (about 10 cm) calculated by the model.

Baroclinic Effect on Tidal Currents in Elliott Bay

Seven numerical experiments were planned for the investigation of the effect of horizontal density gradient on tidal circulation and transport in Elliott Bay. The cases investigated in the experiments are listed in Table 5.3. Each case was run for one ebb tide period i.e., 88th hour to 94th hour of the tide shown in Fig.5.2. To avoid the production of a massive volume of current vector diagrams, the effect was analyzed based on averaged current fields. The averaged current fields were obtained by averaging the calculated currents over the simulation period (one ebb tide).

The averaged current fields due to the influence of baroclinic effect are presented in Figs.5.43a-d. These current vectors were obtained by subtracting the averaged currents of Case 15 (Table 5.3) from those of Case 13 (no density variation case see Table 5.3). These results illustrate that baroclinic effects bring more denser water from the main channel into Elliott Bay along the submarine canyons (Figs.5.43c-d) and force more outward flow in the upper layers, especially around Duwamish Head and Smith Cove (Figs.5.43a-b).

To confirm that the outward flow in the surface layers was caused by the density driven inward flow at the bottom, another experiment was conducted that used the same conditions of Case 15 but without any horizontal density gradient in the deeper layers (Case 14 in Table 5.3). The vector plots obtained by subtracting the averaged currents of Case 14 from those of Case 13 are presented in Figs.5.44a-d. By comparing the differences between Figs.5.43a-d and Figs.5.44a-d, it can be seen that the surface averaged currents in Figs.5.43a-b were significantly reduced when the horizontal density gradients at deeper layers were removed (Figs.5.44a-b). In the meantime, the bottom inward flow observed in Figs.5.43c-d disappeared in Figs.5.44c-d. This experiment verifies that the density driven outward flow in the surface layer was indeed produced by the intrusion of salt waters in the deeper layers!

The averaged discharges from Cases 13, 14, and 15 through the selected cross section inside Elliott Bay (see Fig.5.41) are shown in Fig.5.45. This figure again reveals that the presence of a density gradient tended to move more water into the Bay from the bottom (about 500 m^3s^{-1} for Case 13 and 800 m^3s^{-1} for Case 15) and out of the Bay from the surface (about 2700 m^3s^{-1} for Case 13 and 3000 m^3s^{-1} for Case 15). Although the horizontal density gradient near the surface is much steeper than that in the deeper waters, the horizontal density gradient in deeper waters actually has a more significant effect on the tidal currents than density gradient near the surface during ebb tide.

(a) First layer — Seattle — 0.02 m/s

(b) Second layer — 0.02 m/s

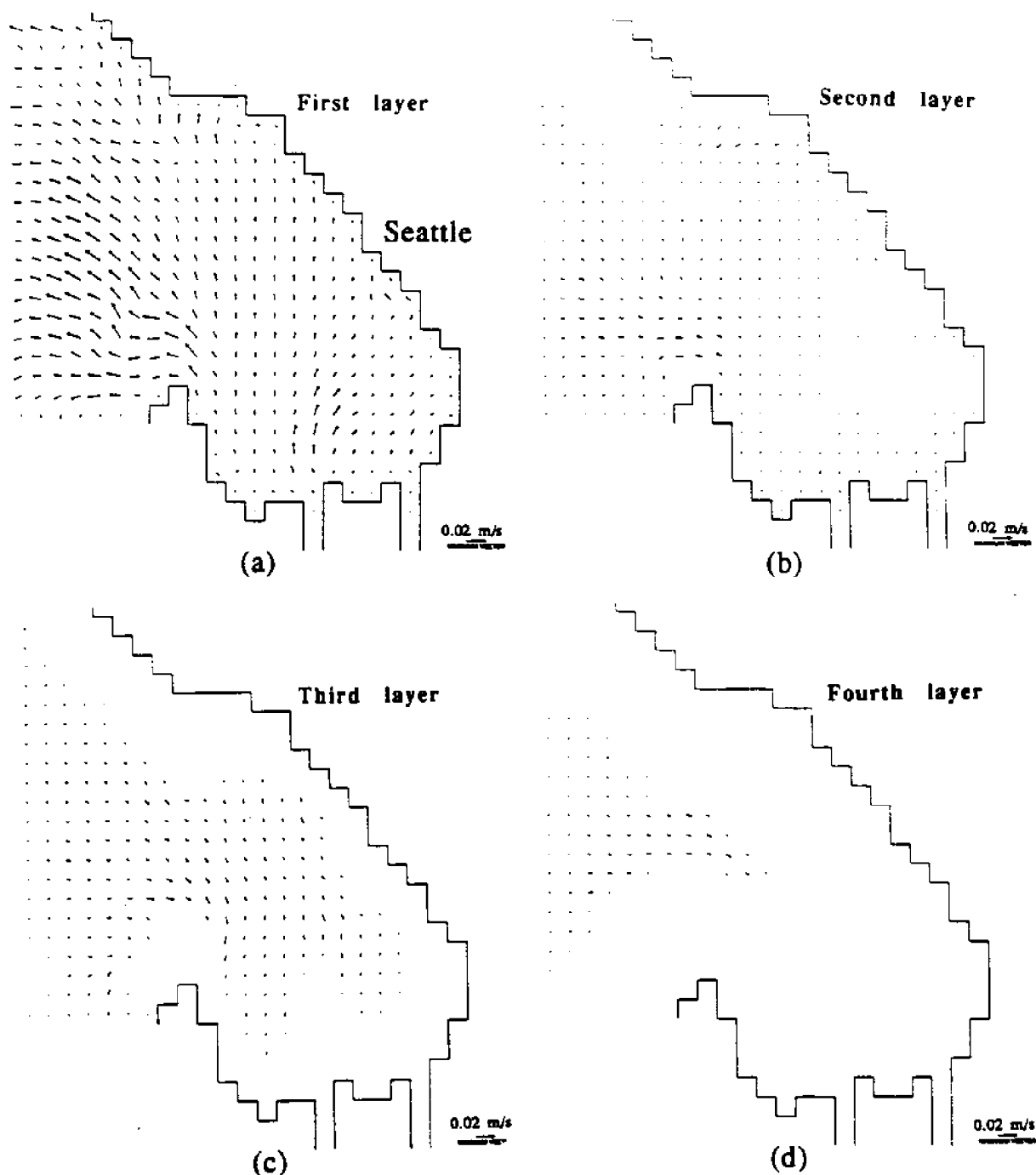(c) Third layer — 0.02 m/s

(d) Fourth layer — 0.02 m/s

Fig.5.43 Averaged current induced by baroclinic effects during the simulation period (one ebb tide). Vectors shown are the differences between the averaged current fields of Case 15 (with the horizontal salinity gradients at all layers) and Case 13 (no salinity gradient case)
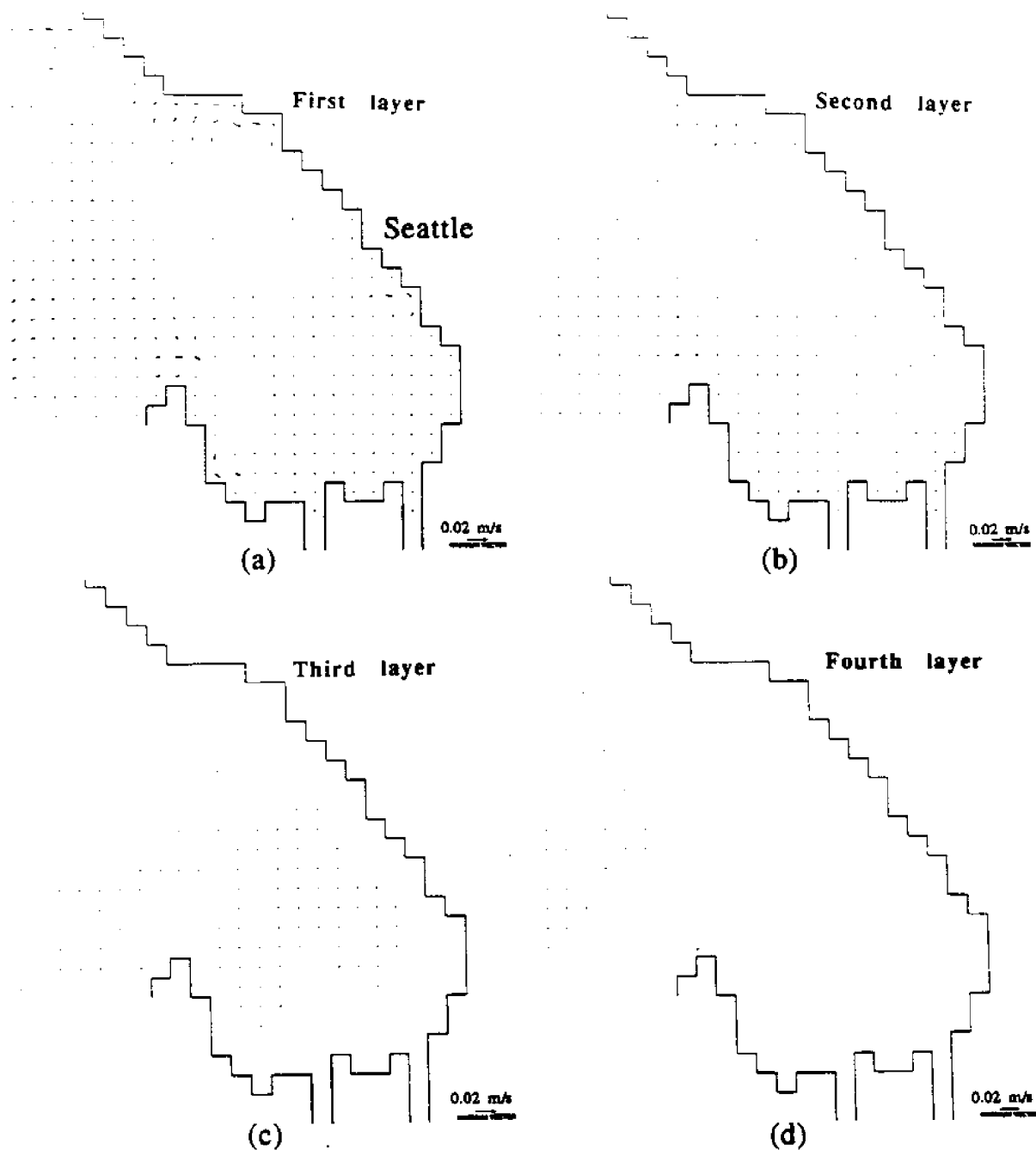
First layer

Seattle

0.02 m/s

(a)

Second layer

0.02 m/s

(b)

Third layer

0.02 m/s

(c)

Fourth layer

0.02 m/s

(d)

Fig.5.44 Averaged current induced by baroclinic effects during the simulation period (one ebb tide). Vectors shown are the differences between the averaged current fields of Case 14 (with the horizontal salinity gradient at the first layer only) and Case 13 (no salinity gradient case)
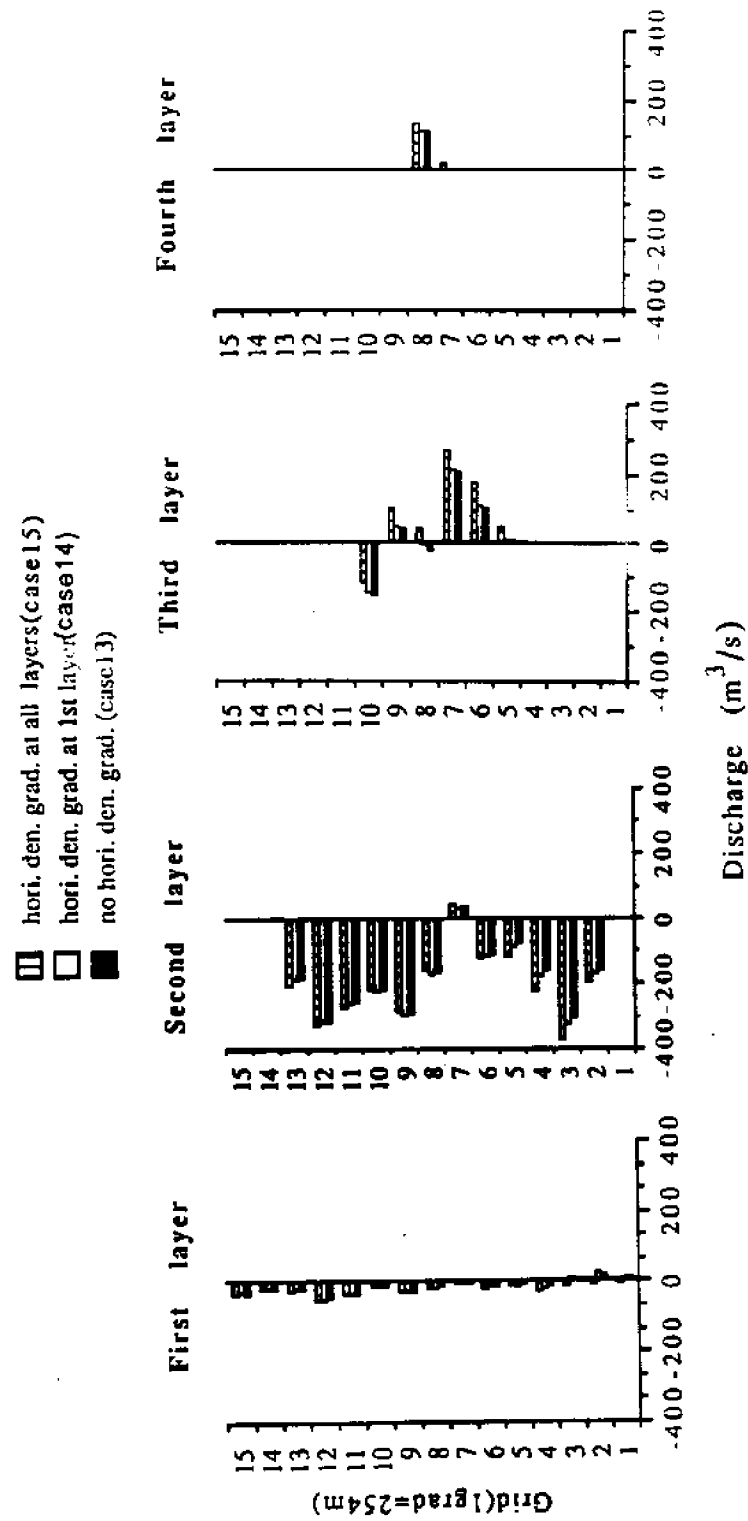
Fig.5.45 The discharge comparison between Cases 13, 14, and 15 at cross section from Duwamish Head to Smith Cove.

To evaluate the sensitivity of the model to horizontal salinity gradients, two more experiments using initial horizontal salinity gradients in the deeper waters which are approximately two and four times higher than that in Case 15 were run. These steeper salinity gradients were chosen to represent the salinity field under high river inflow condition. The discharges of all three cases (Cases 15, 16, and 17) in the same cross section shown earlier (Fig.5.41) were given in Fig.5.46. As expected, the increase of pressure gradient due to the larger density gradient drove more water into the Bay from the deeper portion of the Bay (about 800 m^3s^{-1} for Case 15, 1100 m^3s^{-1} for Case 16, and 1500 m^3s^{-1} for Case 17), and in the meanwhile, pushed more water out of the Bay from the upper portion along the coasts of Duwamish Head and Smith Cove (about 3000 m^3s^{-1} for Case 15, 3200 m^3s^{-1} for Case 16, and 3700 m^3s^{-1} for Case 17).

Additional simulations were made to investigate the sensitivity of the model results to input dispersion coefficients (Cases 18 and 19 in Table 5.3). The calculated discharges for Cases 15, 18, and 19 in the cross section given by Fig.5.41 are shown in Fig.5.47. The discrepancies in the results are small.

5.2.3.4 Summary of Elliott Bay Hydrodynamics According to the Model

The water movement in Elliott Bay is primarily driven by tidal currents in Puget Sound and its own configuration and bathymetry. River inflow, wind, and density variation have relatively minor effect.

The tidal currents inside Elliott Bay are dominated by the northward ebb flow (leaving the Bay) and southward flood flow (entering the Bay) in the main channel and the discharges from the East and West Waterways. During slack tides, several gyres are found
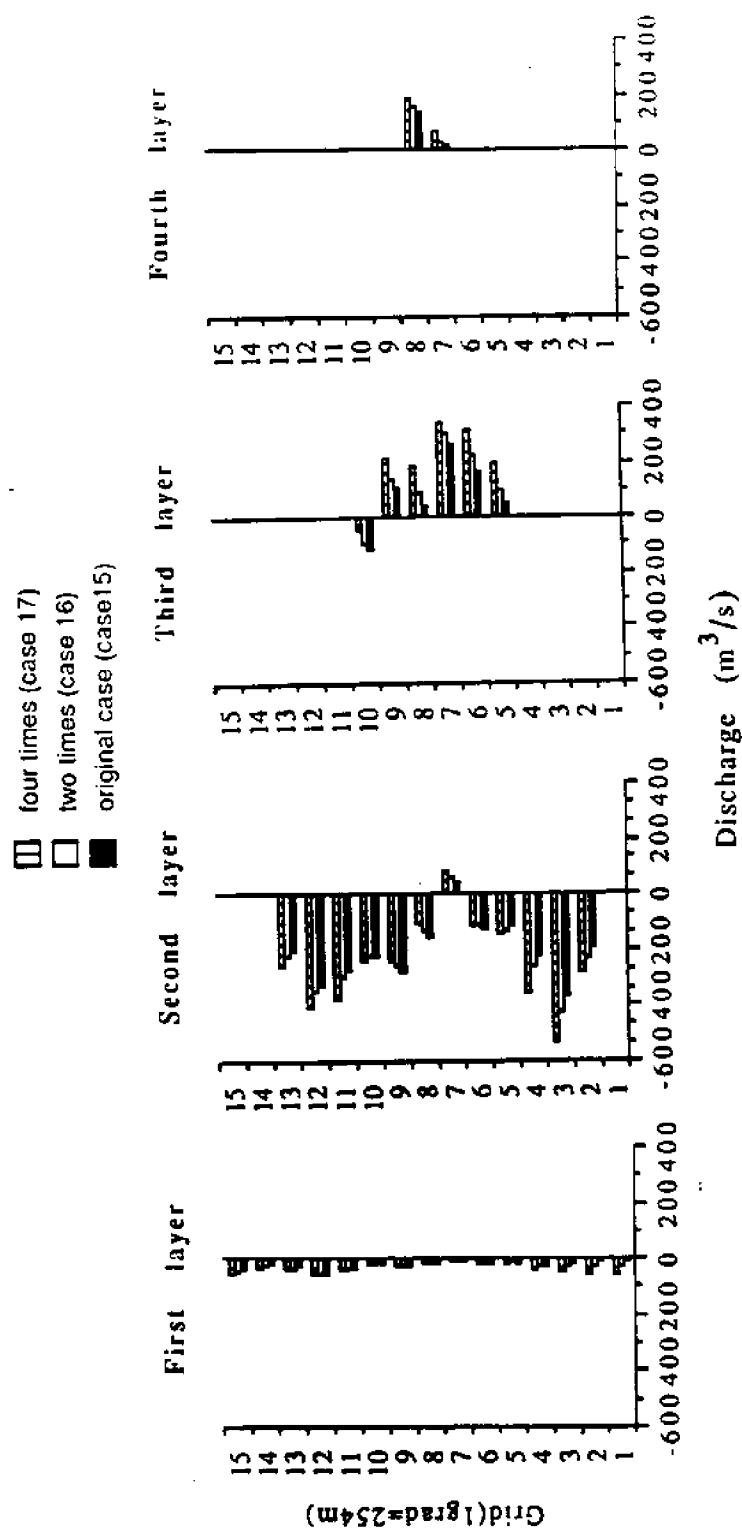
Fig.5.46 The discharge comparison between Cases 15, 16, and 17 at cross section from Duwamish Head to Smith Cove.
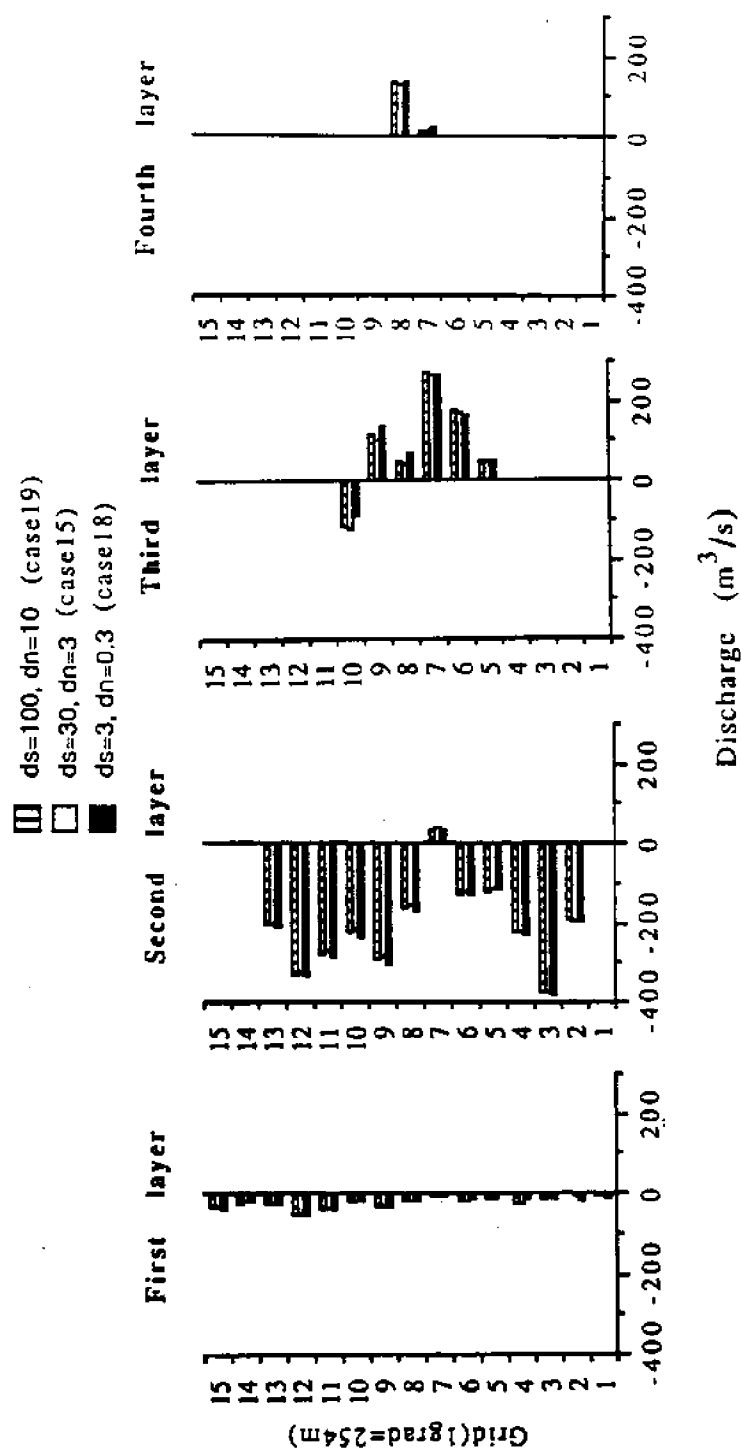
Fig. 5.47 The discharge comparison between Cases 15, 18, and 19 at cross section from Duwamish Head to Smith Cove.

in Elliott Bay due to the phase lag between the tidal currents at different locations. More than 90 percent of the inward discharge enters inner Elliott Bay along the east-west submarine canyon and about 85 percent of the outward discharge leaves inner Elliott Bay from the shore of Duwamish Head. The tidal currents in the deeper layers are generally weaker than the surface currents, but their directions are similar except for modifications due to bathymetric changes. In the inner Elliott Bay, the tidal currents in the deeper layers mainly move along the two submarine canyons.

In general, the calcuated tidal current speeds in the inner Bay are weaker than those in the outer Bay. The maximum surface layer current speeds in the outer Bay can reach 0.4 m/sec. The surface layer current speeds in most places inside the inner Bay are smaller than 0.05 m/sec except near the two waterways and Smith Cove. In these places, the surface layer current speeds can reach 0.3 m/s.

The residual flows in Elliott Bay are mainly caused by its bathymetry and are dominated by a strong clockwise gyre outside the northwest coast of Duwamish Head and a counterclockwise gyre in southern inner Bay.

The calculated flow patterns due to the spring tide, the medium tide, and the neap tide were almost identical. But the mean discharges (both the inward and the outward parts) between inner and outer Bay due to the spring tide are approximately 70 percent more than those due to the neap tide. The tidal currents can be slightly modified by wind and density variation. The effect of river inflow on the tidal currents beyond the inner Bay is insignificant.

Southerly winds would bring more surface water from the main channel into the Bay, and would reduce the amount of water leaving the Bay from the coast of Duwamish Head. In the inner Bay, southerly winds tend to drive surface water to the east shore of the Bay. Part of this on-shore flow would sink to the bottom and generate off-shore currents in the deeper layers. The remaining on-

shore flow would turn into longshore flow along the Seattle waterfront and eventually exit the Bay. Under a typical northerly wind condition, more bottom water would enter the inner Bay through the northern edge of the east-west submarine canyon and more water would leave the Bay along the coast of Duwamish Head. Northerly wind would also generate off shore surface current away from the northern and eastern shoreline of the Bay.

Seven simulation scenarios were used to examine the baroclinic effect. Results of these simulations showed that the baroclinic effect on the computed tidal current field is minor. More pronounced multi-layer current structure can be observed only when the baroclinic effect is included along with a strong wind sequence and a higher river inflow. The horizontal density gradient in deeper waters has more significant effect on the tidal currents than the density gradient near the surface. The density gradient in deeper waters tends to bring more bottom (saltier) water into the Bay and force more outward flow in the upper layers.

The water movement inside Elliott Bay was also studied with the aid of a particle tracking model. The particles released along the eastern shore of the Bay simply moved sluggishly back and forth along the shoreline. The particles released far from the coast had larger net displacements. The model results suggest that outgoing water from the Bay leaves the Bay mainly along the coast of Duwamish Head. Most of the waters that do not make it out of the Bay were trapped in southern inner Bay. No water originated from the outer Bay could enter and stay inside the inner Bay. In general, more surface water could leave inner Elliott Bay under the northerly wind than under the southerly wind.

Water around Denny Way CSO tends to move toward the coast of Duwamish Head and quickly exits the Bay. Waters that came from the East and the West Waterways are likely to stay in the southern inner Bay due to the presence of counterclockwise residual circulation in this area.

CHAPTER SIX

CONCLUSIONS AND RECOMMENDATIONS

6.1 Conclusions

The objective of this research was to characterize and understand the detailed hydrodynamics in Central Puget Sound through the use of a three-dimensional numerical model. A specific model was built for this purpose. The three-dimensional hydrodynamic model developed was first validated by comparing the calculated model results with laboratory and field data. Model results matched very well with both sets of data. After the validation, the model was used along with a particle tracking model and a single layer salinity transport model to investigate tidal flow features in Central Puget Sound and Elliott Bay.

It is concluded that the 762 m horizontal resolution and the two-layered vertical resolution used in Central Puget Sound simulations and the 254 m horizontal resolution and the four-layered vertical resolution used in Elliott Bay simulations were sufficient to capture key features of tidal hydrodynamics and transport phenomena in the study area. No other numerical study in the past has produced comparable results in Puget Sound.

Major conclusions from the study are given below. Detailed findings produced by the model are given in Chapter 5.

Flows in Central Puget Sound and Elliott Bay are both predominately tide driven. During the flood tide, the majority of the water in Central Puget Sound moves southward along the main channel. Part of the water enters the West Sound Inlets, primarily through Rich Passage. During the ebb tide, the water in the West Sound Inlets moves back to the main channel and joins the northward ebb current. The water movement in the West Sound Inlets is dominated by the flow through Rich Passage. At slack tides,

significant eddies can be observed near Point Jefferson, West Point, Alki Point and southern shore of Maury Island. The stronger residual circulations in Central Puget Sound are found near Point Jefferson and Dalco Passage.

The stronger tidal currents in Central Puget Sound are always observed in narrow channels (matching a maximum speed of 2.6 m/s at The Narrows for a "medium" tide condition) or in nearshore zones. The maximum current speeds in the main channel are about 0.4 m/s. The tidal currents in side embayments and West Sound Inlets are always weak; their maximum current speeds are all less than 0.3 m/s.

The water movement in outer Elliott Bay is driven primarily by tidal currents in the main channel. More than 90 percent of the inward discharge enters inner Elliott Bay through an east-west submarine canyon and about 85 percent of the outward discharge leaves inner Elliott Bay along the shore of Duwamish Head. The tidal currents in the deeper layers mainly move along the submarine canyons. The stronger ebb flow in the northern submarine canyon and the stronger flood flow in the southern submarine canyon tend to bring the bottom waters in the northern submarine canyon toward the southern submarine canyon and force them to upwell to the upper layers. The residual circulation in Elliott Bay is dominated by a clockwise gyre near the shore of Duwamish Head and a counterclockwise gyre in the southern portion of inner Elliott Bay.

River inflows from the Duwamish and the Puyallup have very little effect on the tidal currents in Central Puget Sound, and Duwamish River inflows have little effect on most of Elliott Bay.

The chosen wind conditions had insignificant effect on the computed currents in Central Puget Sound, due partially to the thick surface layer used in the model. Wind effects are important in Elliott Bay. A typical southerly wind can drive the surface water to the east shore of the Bay and generate northward longshore currents and

bottom off-shore currents at that shore. A typical northerly wind can drive more water out of the Bay along the shore of Duwamish Head and generate off shore surface currents away from the northern and eastern shoreline of the Bay.

Due to the lack of appropriate boundary conditions, density effects were not considered in Central Puget Sound simulations. Using data synthesized from field observations, density effects were considered in Elliott Bay simulations through the use of a four-layer transport model over ebb portion of one tidal cycle. The baroclinic effect on the tidal current field is minor, and it is primarily caused by the horizontal density gradient in deeper waters.

Water borne pollutants released near the shore of West Point can spread across the main channel to Bainbridge Island. Pollutants released around the coasts of Duwamish Head and Alki Point are more likely to travel southward along the main channel; very small percentage of them enter and stay inside Elliott Bay. Pollutants released from Commencement Bay are more likely to travel northwesterly toward Dalco Passage.

Water leaves Elliott Bay mainly from the shore of Duwamish Head. When only tidal forcing is considered, pollutants discharged near the Denny Way CSO will most likely travel across the Bay to the coast of Duwamish Head and eventually out to the Sound. Pollutants from the mouths of the East and West Waterways will be trapped in southern inner Elliott Bay by a counterclockwise circulation cell for a longer period. These transport patterns are subject to change when the effects of river inflow, wind, tidal inequality, and density variation are considered. Stronger river discharges, southerly winds, and intrusion of denser bottom waters can push the surface waters from the East and the West Waterways northward along the eastern shore of the Bay and out of the Bay from the northern shore. Northerly winds and spring tides can trap the waters from the East and West Waterways longer in inner Elliott Bay, but they can

accelerate the water around the Denny Way CSO toward the coast of Duwamish Head.

6.2 Recommendations for Future Study

Because the current in the main channel is relatively homogeneous in the vertical direction, two-dimensional depth-averaged models or a three-dimensional model with two layers will be sufficient to characterize general flow features in Central Puget Sound. In the small side embayments, a three-dimensional model is required to resolve the possible multi-layer flow structure caused by local bathymetry, strong river inflows, wind, or density variation.

To more accurately study the current field in Elliott Bay, the river inflow, wind, and salinity data at the open boundaries of the model have to be taken simultaneously for a period no shorter than three months in the summer and winter seasons.

The particle tracking model developed only transports weightless particles. In order to simulate the transport of pollutants in more realistic manner, the model must be modified to include dispersion, reaction, and settling (or resuspension) effects.

The three-dimensional hydrodynamic model can be applied to study tidal hydrodynamics in any sub-basin or embayment within the Sound where appropriate boundary conditions exist. When faster (much faster than the Cray X/MP used in this study) computers become available in the future, smaller horizontal and vertical resolutions (100 m or less horizontally, 5 m vertically) should be used.

Numerical modeling is one of the approaches to the study of complex flow dynamics in estuaries. There are three major remaining problems in numerical modeling of estuarine system. First, computer limitations have severely restricted our abilities to accurately characterize the bathymetries and geometries of the estuaries and have caused discrepancies in our models. Second, the performance of

estuarine numerical modeling depends very much on the quality and quantity of field data. Much more field observation are needed as initial and boundary conditions and as verification data for our models. The computational power has been steadily increasing (although still far from being adequate), but field data collection efforts for numerical modeling purpose are still rare. Finally, our models need to be equipped with more advanced graphics softwares to efficiently display and interpret the output.

REFERENCES

Abbott, M. B., J. Larsen, and J. Tao, "Modelling circulations in depth-integrated flows, I, The accumulation of the evidence", J. of Hydraulic Research, 23, 309-322, 1985.

Awaji, T., N. Imastao, and H. Kunishi, "Tidal exchange through a strait: A numerical experiment using a simple model basin", J. of Physical Oceanography, 10, 1499-1508, 1980.

Awaji, T., "Water mixing in a tidal current and the effect of turbulence on tidal exchange through a strait", J. of Physical Oceanography, 12, 501-514, 1982.

Backhaus, J., "First results of a three dimensional model on the dynamics in the German Bight", in Marine Forecasting, ed. by J. C. J. Nihoul, Elsevier, 333-349, 1979.

Bloss, S., R. Lehfeldt, and J. C. Patterson, "Modeling turbulent transport in stratified estuary", J. of Hydraulic Engineering, ASCE, 114(9), 1115-1133, 1988.

Blumberg, A. F., "Numerical tidal model of Chesapeake Bay", J. of the Hydraulics Division, ASCE, 103(1), 1-10, 1977.

Blumberg, A. F., and G. L. Mellor, "Diagnostic and prognostic numerical circulation studies of the South Atlantic Bight", J. of Geophysical Research, 88(C4), 4579-4592, 1983.

Boulot, F., "Modeling of heated water discharges on the French Coast of the English Channel", in Transport Models for Inland and Coastal Waters, ed. by H. B. Fischer, Academic Press, New York, N.Y., 362-407, 1981.

Brandes, R. J., and F. D. Masch, "A slowly-varying conservative transport model for shallow estuaries", Tech. Rep. HYD 12-7103, Univ. of Texas, Austin, 1971.

Bretschneider, D. E., G. A. Cannon, J. R. Holbrook, and J. D. Pashinski, "Variability of subtidal current structure in a fjord estuary : Puget Sound, Washington", J. of Geophysical Research, 90(C6), 11,949 - 11,958, 1985.

Burns, R., The Shape and Form of Puget Sound, University of Washington Press, Seattle, WA, 100 pp., 1985.

Cheng, R. T., and C. Tung, "Wind-driven lake circulation by the finite element method", Proc. of the 13th Conf. Great Lakes Res., Ann Arbor, Michigan, 891-903, 1970.

Cheng, R. T., "Modeling of hydraulic systems by finite-element methods", in Advances in Hydroscience, 11, ed. by V. T. Chow, Academic Press, New York, N.Y., 208-279, 1978.

Cheng, R. T., and V. Casulli, "On Lagrangian residual currents with applications in South San Francisco Bay, California", Water Resources Research, 18(6), 1652-1662, 1982.

Cheng, R. T., V. Casulli, and S. N. Milford, "Eulerian Lagrangian solution of the convective-dispersion equation in natural coordinates", Water Resources Research, 27(7), 944-952, 1984.

Choi, B. H., "Tidal computations for the Yellow Sea", Proc. of the 20th International Conference on Coastal Engineering, 67-81, ASCE, New York, 1986.

Chu, W-S., and W. W-G. Yeh, "Two-dimensional tidally averaged estuarine model", J. of the Hydraulics Division, ASCE, 106(4), 501-518, 1980.

Chu, W-S., and W. W-G Yeh, "Calibration of a two-dimensional hydrodynamics model", Coastal Engineering, 9, 293-307, 1985.

Chu, W-S., and S. Gardner, "A two-dimensional particle tracking estuarine transport model", Water Resources Bulletin, 22(2), 944-952, 1986.

Chu, W-S., B. L. Barker, and A. M. Akbar, "Modeling tidal transport in Arabian Gulf", J. of Waterway, Port, Coastal and Ocean Engineering, ASCE, 114(4), 455-471, 1988.

Chu, W-S., J-Y. Liou, and K. D. Flenniken, "Numerical modeling of tide and current in Central Puget Sound: Comparison of a three-dimensional and a depth-averaged model", Water Resources Research, 25(4), 721-734, 1989.

Cokelet, E. D., R. J. Stewart, and C. C. Ebbesmeyer, "The exchange of water in fjords: A simple model of two layer advective reaches separated by mixing zones", Proc. of 19th Int'l Conf. on Coastal Engr., ASCE, New York, 3124-3133, 1984.

Cokelet, E. D., and R. J. Stewart, "The exchange of water in Fjords: The efflux/reflux theory of advective reaches separated by mixing zones", J. of Geophysical Research, 90(C4), 7287-7306, 1985.

Collias, E. E., N. McGary, and C. A. Barnes, Atlas of Physical and Chemical Properties of Puget Sound and Its Approaches, University of Washington Press, Seattle, Washington, 235 pp., 1974.

Curl, H. C., E. T. Baker, T. S. Bates, G. A. Cannon, R. A. Feely, T. L. Geiselman, M. F. Lamb, P. P. Murphy, D. J. Pashinski, A. J. Paulson, and D. A. Tennant, "Contaminant transport from Elliott and Commencement Bays", NOAA Technical Memorandum ERL PMEL-78, PMEL/NOAA, Seattle, Washington,1988.

Dahlquist, G., A. Björck, and N. Anderson, Numerical Methods, Prentice Hall, Inglewood Cliff, NJ, 1974.

Downing, J., M. Eble, A. Petillo, and P. Roberts, "Alki wastewater treatment plant outfall improvements predesign study", Tech. Memo No. 8.2 circulation and effluent transport, Municipality of Metropolitan Seattle, Washington, 1985.

Dronkers, J. J., Tidal Computations in Rivers and Coastal Waters, North-Holland Pub., Amsterdam, 1964.

Ebbesmeyer, C. C., J. M. Helseth, C. A. Barnes, J. H. Lincoln, and W. P. Bendiner, "On nearshore trapping of pollutants by tidal eddies downstream from points in Puget Sound, Washington", 134-145, Proceedings of The Use, Study and Management of Puget Sound, University of Washington, WSG-W077-1, 1977.

Ebbesmeyer, C. C., C. A. Coomes, J. M. Cox, and J. M. Helseth, Historical Oceanographic Data in East Passage and Approaches, Report for Municipality of Metropolitan Seattle, 1982.

Evans-Hamiton, Inc., Puget Sound Environmental Atlas, 1986.

Falconer, R. A., "Residual currents in Port Talbot Harbor : a mathematical model study", Proceeding Inst. Civil Engineering, Part 2, 79, Mar., 33-53, 1985.

Falconer, R. A., and L. Mardapitta-Hadjipandeli, "Application of a nested numerical model to idealized rectangular harbors", Coastal Engineering, 176-192, 1986.

Fischer, H. B., E. J. List, R. Koh, J. Imberger, and N. H. Brooks, Mixing in Island and Coastal Waters, Academic Press, New York, N. Y., 1979.

Geyer, W. R., and G. A. Cannon, "Sill processes related to deep water renewal in a fjord", J. of Geophysical Research, 87(101), 7985-7996, 1982.

Hansen, W., Hydrodynamical methods applied to oceanographic problems, Mitt. Inst. Meereskd., Univ. of Hamburg, Hamburg, 1962.

Heaps, N. S., "A two-dimensional numerical sea model", Philos. Trans. R. Soc., London, Ser. A 265, 93-137, 1969.

Heaps, N. S., "Three-dimensional numerical model of the Irish Sea", Geophys. J. R. Astron. Soc., 35, 99-120, 1973.

Helseth, J. M., L. Hinchy, J. Cox, C. C. Ebbesmeyer, and D. Browning, "Observations from Washington State ferry Walla-Walla of near surface temperature and salinity across Puget Sound's main basin", report to MESA Puget Sound Project Office, NOAA, Evans-Hamiton, Inc., 1979.

Hess, K. W., "A three-dimensional numerical model of the estuary circulation and salinity in Narragansett Bay", Estuarine and Coastal Marine Science, 4, 325-338, 1976.

Hinwood, J. B., and I. G. Wallis, "Classification of models of tidal waters", J. of the Hydraulics Division, ASCE, 101(11), 1315-1331, 1975.

Horton, B., "Modeling the Effect of Wind on Surface Layer Transport in Elliott Bay, Washington", MSCE Thesis, Department of Civil Engineering, University of Washington , Seattle, WA., 1989.

Jamart, B. M., and D. F. Winter, "A new approach to the computation of tidal motions in estuaries", in Hydrodynamics of Estuaries and Fjords, ed. by J. C. J. Nihoul, Elsevier, 1978.

Jamart, B. M., "Report on the preliminary modeling of tides in East Passage", unpublished report to Municipality of Metropolitan Seattle, Washington, 1983.

Jozsa, J., "2-D particle model for predicting depth-integrated pollutant and surface oil slick transport in rivers", Hydraulic and Environmental Modeling of Coastal, Estuarine, and River Waters, ed. by R. A. Falconer, et al., Gower Publishing Co., Brookfield, Vermont, 332-340, 1989.

Kamphuis, J. W., "Mathematical tidal study of St. Lawrence River", J. of the Hydraulics Division, ASCE, 96(3), 643-664, 1970.

Killworth, P. D., "A note on smoothing techniques for leapfrog time integration scheme", unpublished manuscript, Hooke Institute for Atmospheric Research, University of Oxford, Oxford, England, 1984.

Kurihara, Y., "On the use of implicit and interactive methods for the time integration of the wave equation", Monthly Weather Review, 93(1), 33-46, 1965.

Laevastu, T., "Multilayer hydrodynamical-numerical models", Proceeding Symp. Modeling Tech., ASCE, 1010, 1975.

Lavelle, J. W., "A laterally averaged model of Admiralty Inlet and the main basin of Puget Sound", paper presented in the Workshop on Modeling Physical Oceanography of Puget Sound, Seattle, Washington, 1987.

Lavelle, J. W., H. O. Mofjeld, E. Lempriere-Doggett, G. A. Cannon, D. J. Pashinski, E. D. Cokelet, L. Lytle, and S. Gill, "A multiply-connected channel model of tides and tidal currents in Puget Sound, Washington and a comparison with updated observations", NOAA Technical Memorandum ERL PMEL-84, PMEL/NOAA, Seattle, WA., 1988.

Leendertse, J. J., "A water quality simulation model for well mixed estuaries and coastal seas; Vol. I principles of computation", Report No. RM-6230-RC, Rand Corp., Santa Monica, California, 1970.

Leendertse, J. J., R. C. Alexander, and S-K. Liu, "A three-dimensional model for estuaries and coastal seas: Vol. I, Principles of computation", Report No. R-1417-OWRR, Rand Corp., Santa Monica, California, 1973.

Leendertse, J. J., and S-K. Liu., "A three-dimensional model for estuaries and coastal seas: Vol. II, Aspects of computation", Report No. R-1764-OWRT, Rand Corp., Santa Monica, California, 1975.

Leendertse, J. J., and S-K. Liu., "A three-dimensional model for estuaries and coastal seas: Vol. IV, Turbulent energy computation", Report No. R-2178-OWRT, Rand Corp., Santa Monica, California, 1977.

Leendertse, J. J., A. Langerak, and M. A. M. de Ras, "Two-dimensional tidal models for the delta works", in Transport Models for Inland and Coastal Waters, ed. by H. B. Fischer, Academic Press, New York, N. Y., 1981.

Leendertse, J. J., "A new approach to three-dimensional free-surface flow modeling", Report No. R-3712-NETH/RC, Rand Corp., Santa Monica, California, 1989.

Leimkuhler, W., J. Conner, J. Wang, G. Christodoulou, and S. Sundgren, "Two-dimensional finite element dispersion model", Symposium on Modeling Techniques, ASCE, 1467-1468, 1975.

Liu, S-K., and J. J. Leendertse, "Multiple dimensional numerical modeling of estuaries and coastal seas", in Advances in Hydroscience, 11, ed. by V. T. Chow, Academic Press, New York, N.Y., 95-164, 1978.

Liu, S-K., and J. J. Leendertse, "Modeling the Alaskan continental shelf waters", Report No. R-3567-NOAA/RC, Rand Corp., Santa Monica, California, 1987.

Longuet-Higgins, M. S., "On the transport of mass by time-varying ocean current", Deep-Sea Research, 16, 431-447, 1969.

Mcgary, N., and J. H. Lincoln, Tidal Prints, University of Washington Press, Seattle, 51 pp, 1977.

Maier-Reimer, E. and J., Sündermann, "On tracer methods in computational hydrodynamics", in Engineering Applications of Computational Hydraulics, Vol.1, ed. by M. B. Abbott and J. A. Cunge, Pitman, 198-217, 1982.

Messinger, J., and A. Arakawa, Numerical Methods Used in Atmospheric Models, GARP Publication No. 17, World Meteorological Organization, Geneva, Switzerland, 1976.

Mofjeld, H. O., and L. H. Larsen, "Tides and tidal currents of the inland waters of western Washington", NOAA Technical Memorandum ERL PMEL-56, PMEL/NOAA, Seattle, Washington, 1984.

Mofjeld, H. O., J. W. Lavelle, R. A. Walters, and W-S. Chu, "Abstracts of workshop on modeling physical oceanography of Puget Sound", Department of Civil Engineering, University of Washington, Seattle, Washington, 33 pp., 1987.

Nakata, K., "The three-dimensional numerical model of Puget Sound", paper presented in the Workshop on Modeling Physical Oceanography of Puget Sound, Seattle, Washington, 1987.

National Ocean Survey (annual after 1971) Tide Tables, West Coast of North and South America including the Hawaiian Islands. United States Department of Commerce.

Nece, R. E., "Some considerations for an enlarged physical model of Puget Sound", paper presented in the Workshop on Modeling Physical Oceanography of Puget Sound, Seattle, Washington, 1987.

Nece, R. E., and R. A. Falconer, "Modeling of tide induced depth averaged velocity distributions in a square harbor", in Hydraulic and Environmental Modeling of Coastal, Estuarine and River Waters, ed. by R. A. Falconer, et al., Gower Publishing Co., Brookfield, Vermont, 56-66, 1989.

Nece, R. E., "Tidal current measurements in a laboratory harbor", unpublished manuscript, 1989.

Nihoul, J. C. J., and F. C. Ronday, "Three-dimensional marine models for impact studies", Proc. of 18th Int'l Conf. on Coastal Engr., ASCE, New York, 745-764, 1982.

Oey, L. Y., and G. L. Mellor, "A three-dimensional simulation of the Hudson-Raritan Estuary. Part I: Description of the model and model simulations", J. of Physical Oceanography, 15, 1676-1692, 1985.

Owen, A., "A three-dimensional model of the Bristol Channel", J. of Physical Oceanography, 10, 1290-1302, 1980.

Perrels, P. A. J., and M. Karelse, "A two-dimensional laterally averaged model for salt intrusion in estuaries", in Transport Models for Inland and Coastal Waters, ed. by H. B. Fischer, Academic Press, New York, N. Y., 483-524, 1981.

Pinder, G. F., and W. G. Gray, Finite Element Simulation in Surface and Subsurface Hydrology, Academic Press, New York, 1977.

Puget Sound Water Quality Authority, 1989 Puget Sound Water Quality Management Plan, PSWQA, Seattle, Washington, 1989.

Raithby, G. D., R. V. Elliott, and B. R. Hutchinson, "Prediction of three-dimensional thermal discharge flows", J. of Hydraulic Engineering, ASCE, 114(7), 720-737, 1988.

Reid, R. O., and B. R. Bodine, "Numerical model for storm surges in Galveston Bay", J. Waterways Harbors Div., ASCE, 94(WW1), 33-59, 1968.

Richtmyer, R. D., and K. W. Morton, Difference Methods for Initial Value Problems, 2nd ed. Interscience, New York, 206 pp., 1967.

Roache, P., Computational Fluid Dynamics, Rev. ed., Hermosa Publisher, Alburquerque, NM, 1976.

Rogers, E.H., "A pollution study of Puget Sound using an hydraulic model", MSCE Thesis, Department of Civil Engineering, University of Washington , Seattle, WA., 1955.

Sarraf, S., R. Kahawita, and N. Eljabi, "3-D general movable mesh in water circulation modeling", J. of Computing in Civil Engineering, 2(2), 170-187, 1988.

Schmalz, Jr., P. A., "A numerical investigation of astronomic tidal circulation in Puget Sound", Misc. Paper CERC-86-9, U. S. Army Corps of Engineers, Vicksburg, Mississippi, 1986.

Sheng, Y. P., "Mathematical modeling of three-dimensional coastal currents and sediment dispersion : Model development and application", Technical Report CERC-83-2, Office of the Chief of Engineers, U. S. Army, Washington, D. C., Sept., 1983.

Sillcox, R. L., R. W. Geyer, and G. A. Cannon, "Physical transport processes and circulation in Elliott Bay", NOAA Technical Memorandum OMPA-8, PMEL/NOAA, Seattle, WA., 1981.

Simons, T. J., "Verification of numerical models of Lake Ontario : Part I. Circulation in spring and early summer", J. of Physical Oceanography, 4, 507, 1974.

Simons, T. J., "Part II. Stratified circulation and temperature changes", J. of Physical Oceanography, 5, 98-110, 1975.

Smith, L. H., and R. T. Cheng, "Tidal stream flow solved by Galerkin technique", Proceeding of the 15th Int'l Conf. on Coastal Engineering, ASCE, 3385-3376, 1976.

Smith, L. H., and R. T. Cheng, "Tidal and tidally averaged circulation characteristics of Suisun Bay", California, Water Resources Research, 23(1), 143-155, 1987.

Spaulding, M. L., and C. H. Beauchamp, "Modeling tidal circulation in coastal seas", J. of Hydraulic Engineering, ASCE, 109(1), 116-132, 1983.

Sündermann, J., "A three-dimensional model of a homogeneous estuary", Proceeding of the 14th Int'l Conference Coastal Engineering, ASCE., 2337-2390, 1974.

Taylor, C., and J. Davis, "Tidal and long wave propagation--A finite element approach", Comput. Fluids, 2(3), 125-148, 1975.

Tee, K. T., "The structure of three-dimensional tide-generating currents, Part I : Oscillating currents", J. of Physical Oceanography, 9, 930-944, 1979.

Tee, K. T., "A three-dimensional model for tidal and residual currents in bays", in Transport Models for Inland and Coastal Waters, ed. by H. B. Fischer, Academic Press, 284-309, 1981.

Verboom, G. K., H. J. de Vriend, G. J. Akkerman, R. A. H. Thabet, and J. C. Winterwerp, "Nested models : applications to practical problems", Presented at the 5th International Conference on Finite Elements in Water Resources, Burlington, VT, 1984.

Wang, H. H., P. Halpern, J. Jr. Douglas, and T. Dupont, "Numerical solutions of the one-dimensional primitive equations using Galerkin approximations with localized basis functions", Monthly Weather Review, 100(10), 738-746, 1972.

Wang, J. D., and J. J. Connor, "Mathematical modeling of near coastal circulation", Technical Report 200, Department of Civil Engineering, Mass. Inst. Technol., Cambridge, MA., 1975.

Water Resources Engineers, Inc., "Ecological modeling of Puget Sound and adjacent waters", Report to the U.S. Environmental Protection Agency, Walnut Creek, California, 119 pp., 1975.

Winter, D. F., "Studies of circulation and primary production in deep inlet environments", EPA, Ecological Research Series Report EPA 600/3-77-049, EPA, Corvallis, Or., 99 pp., 1977.

Wu, J., "Wind-stress coefficients over sea surface near neutral conditions : A revisit", J. of Physical Oceanography, 10, 727-740, 1980.

APPENDIX I

TIDAL CURRENTS IN CENTRAL PUGET SOUND

The tidal currents in Central Puget Sound at two vertical model layers and eight tide stages are presented in Figs.A.1a-h. The first model layer has a variable thickness of 60 meters or less. The second model layer resolved the deeper portion of Central Puget Sound with a variable thickness that follows the Sound's bottom bathymetry. The eight stages correspond to two high waters, two low waters and four mid tides during the fifth tidal cycle shown in Fig.5.2.

Tide at Seattle

1st layer

h=60 m

2nd layer

(a)
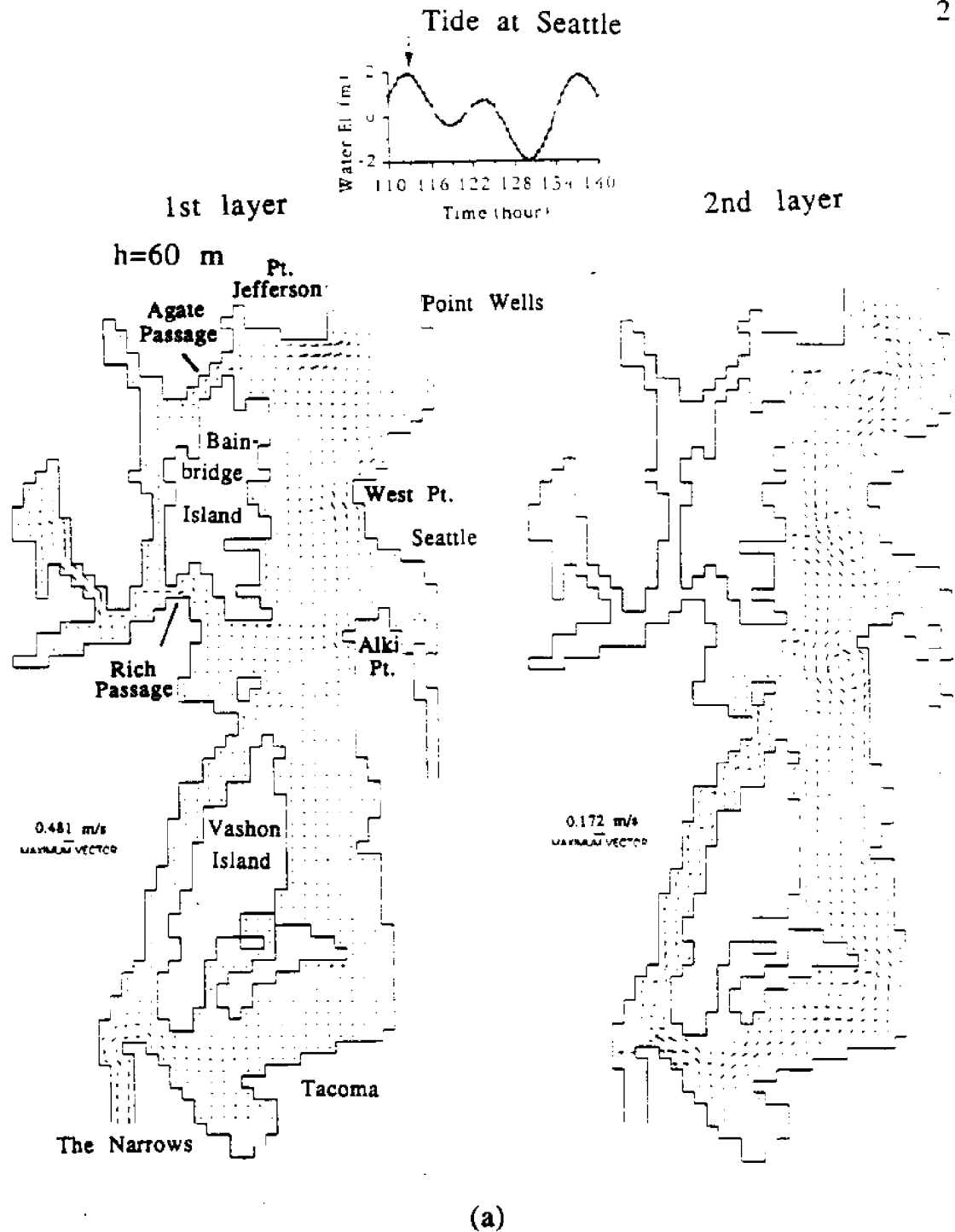
Figs.A.1a-h The tidal currents at 8 tide stages in Central Puget Sound.
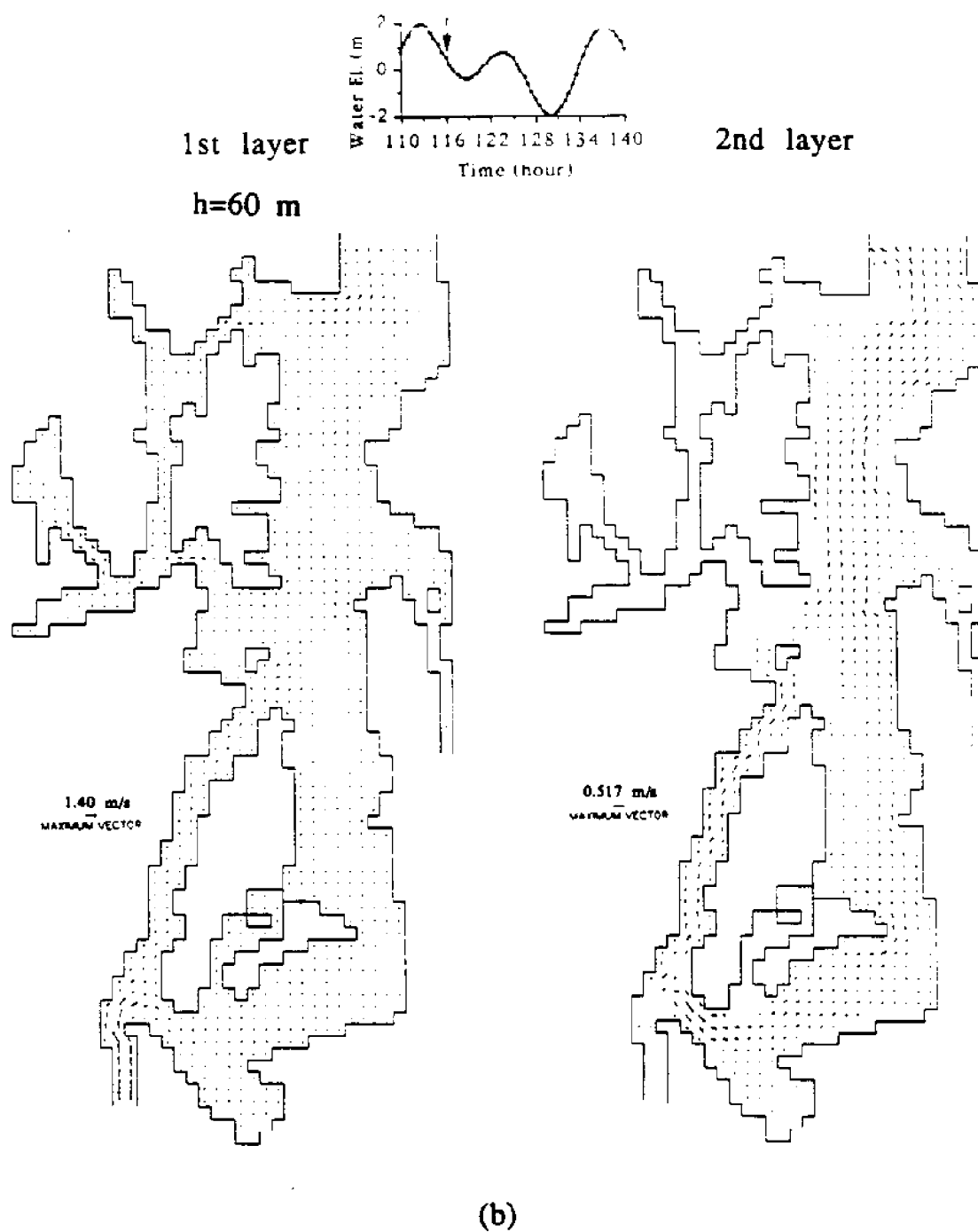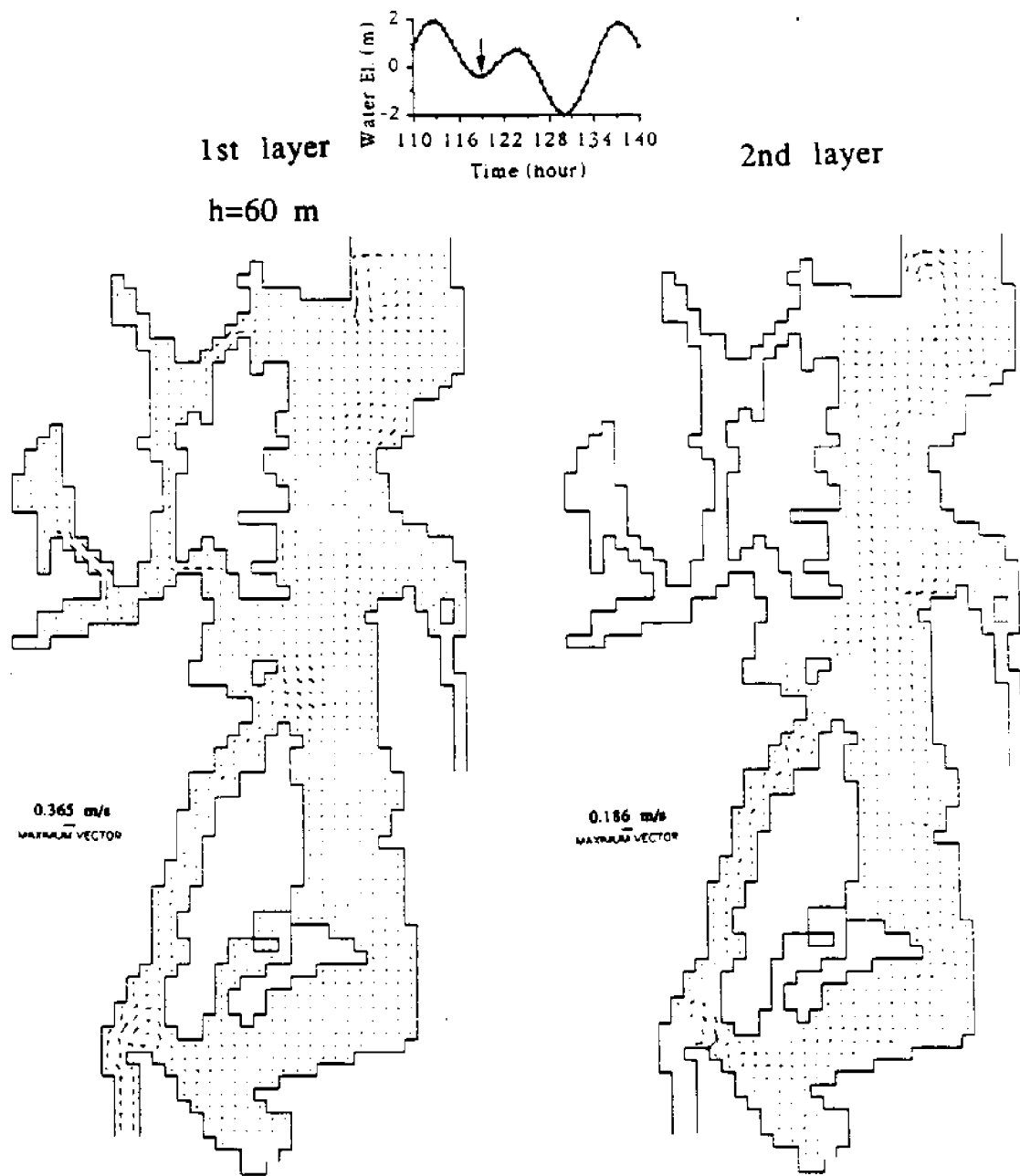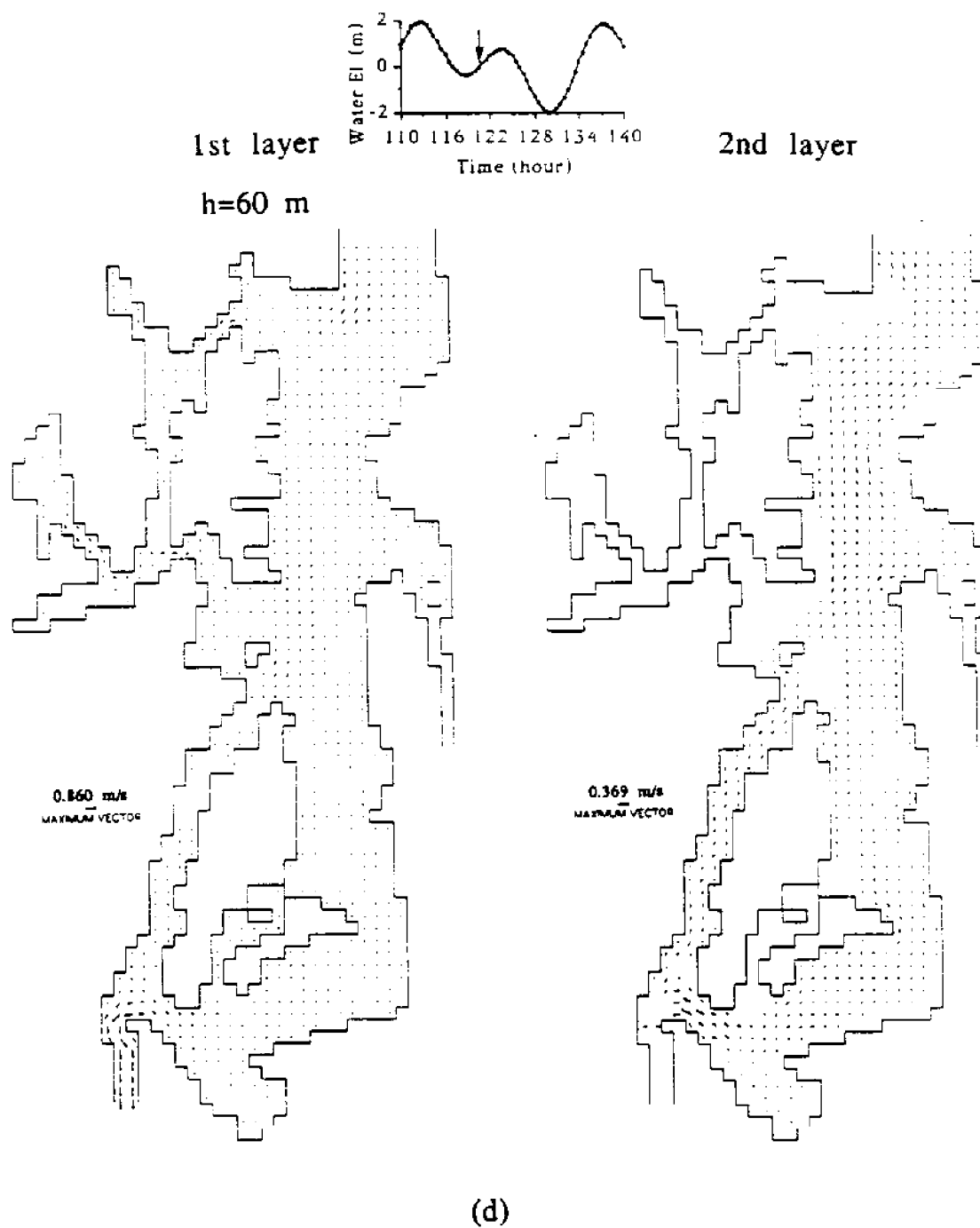
1st layer

h=60 m

2nd layer

1.40 m/s
MAXIMUM VECTOR

0.517 m/s
MAXIMUM VECTOR

(b)

Figs.A.1a-h (continued)

1st layer

2nd layer

h=60 m

(c)

Figs.A.1a-h (continued)

1st layer

h=60 m

2nd layer

Water El (m)

110 116 122 128 134 140
Time (hour)

0.860 m/s
MAXIMUM VECTOR

0.369 m/s
MAXIMUM VECTOR

(d)

Figs.A.1a-h (continued)

1st layer

Water El (m)

2nd layer

h=60 m

0.694 m/s
MAXIMUM VECTOR

0.138 m/s
MAXIMUM VECTOR

(e)

Figs.A.1a-h (continued)

1st layer

2nd layer

h=60 m

1.35 m/s
MAXIMUM VECTOR

0.499 m/s
MAXIMUM VECTOR

(f)

Figs.A.1a-h (continued)

1st layer 2nd layer

h=60 m

(g)

Figs.A.1a-h (continued)

1st layer   2nd layer

h=60 m

1.73 m/s
MAXIMUM VECTOR

0.684 m/s
MAXIMUM VECTOR
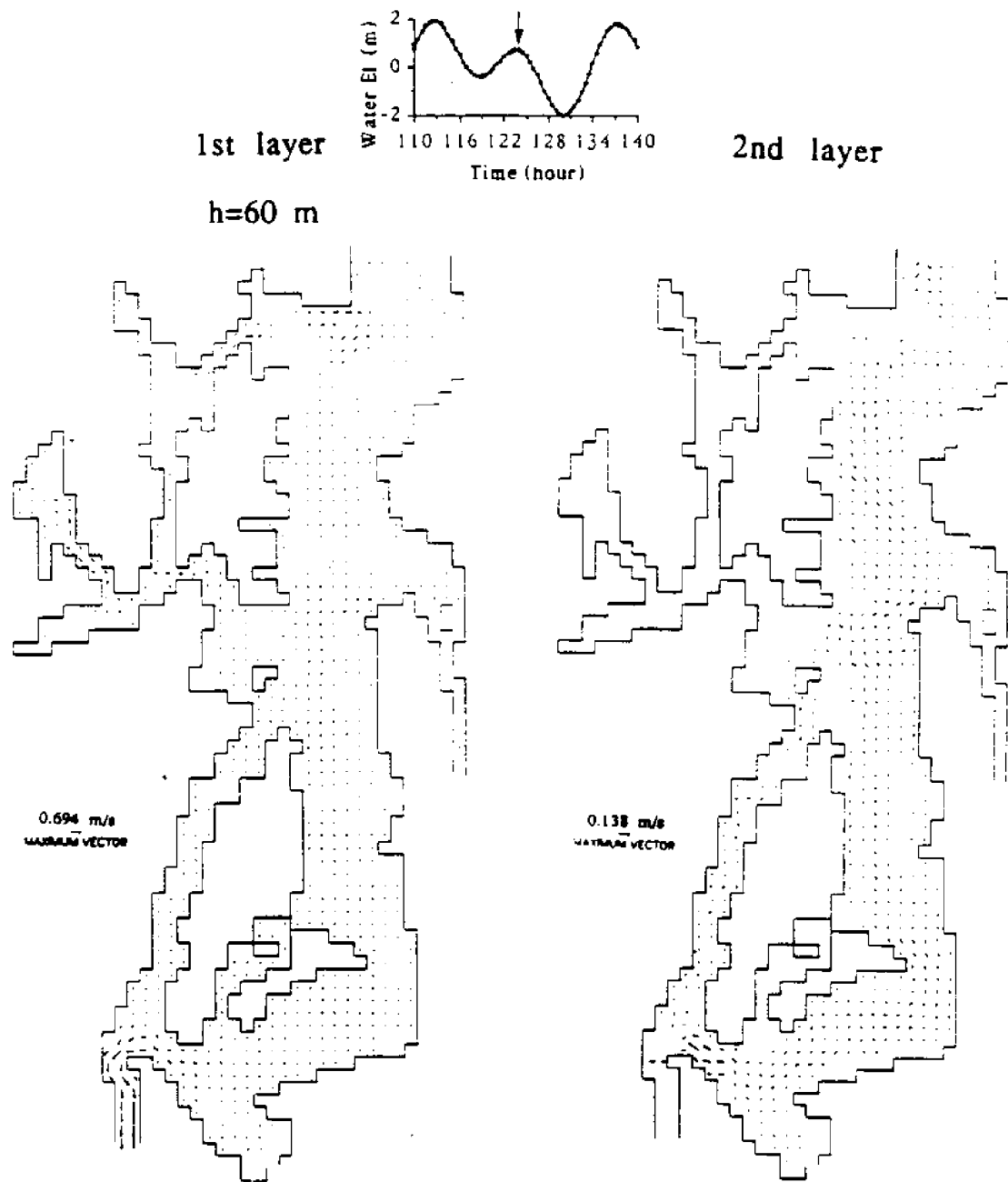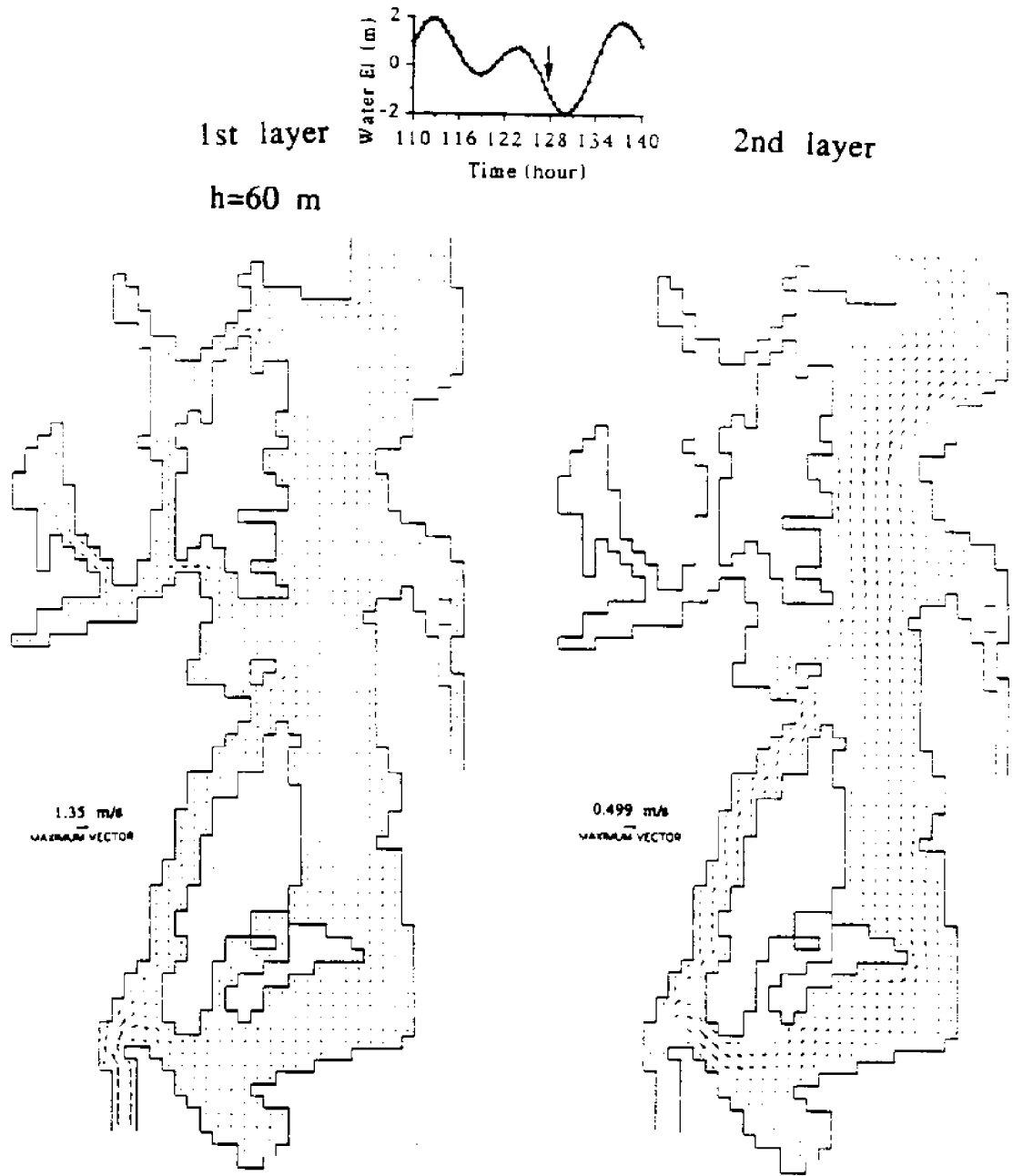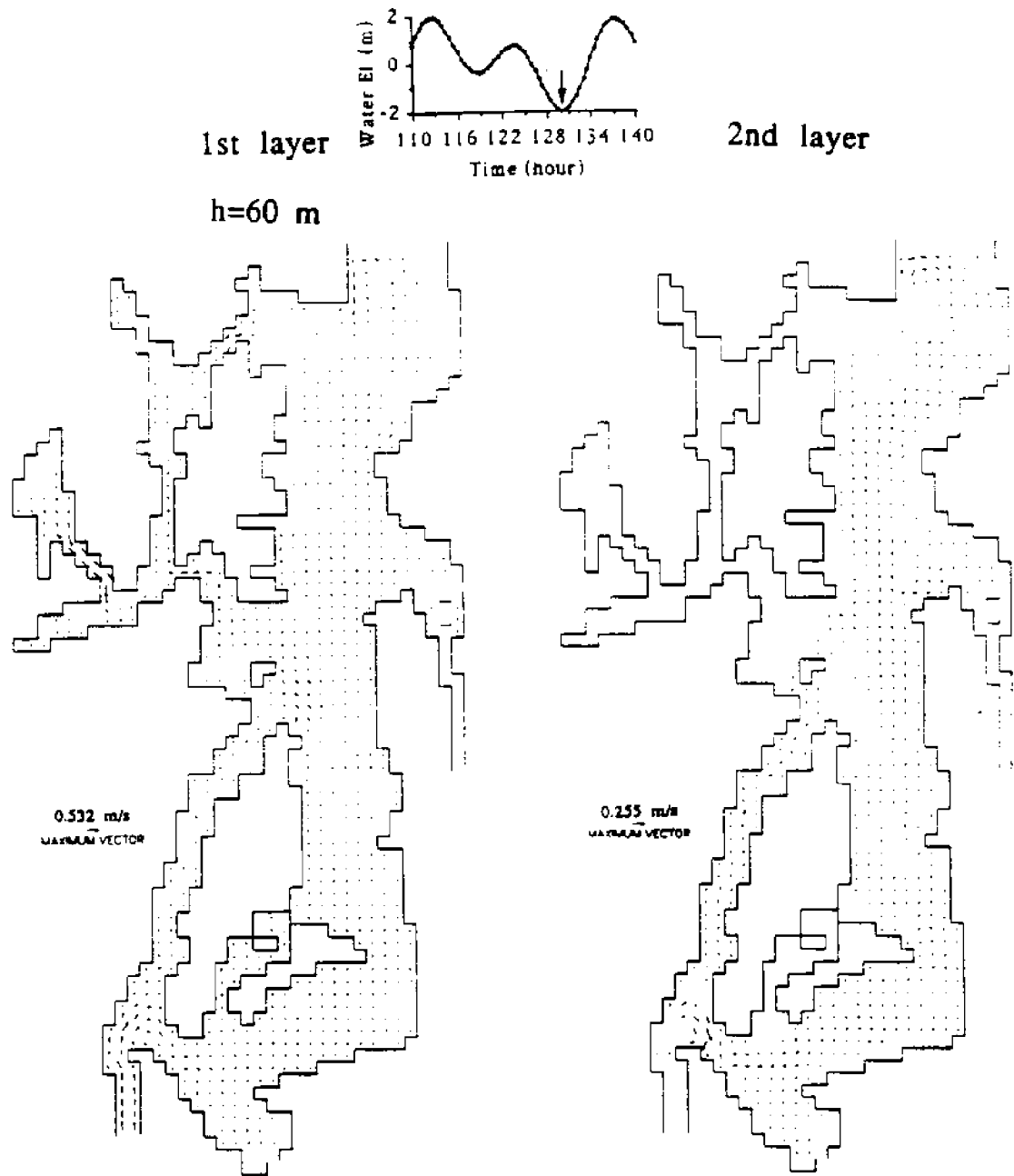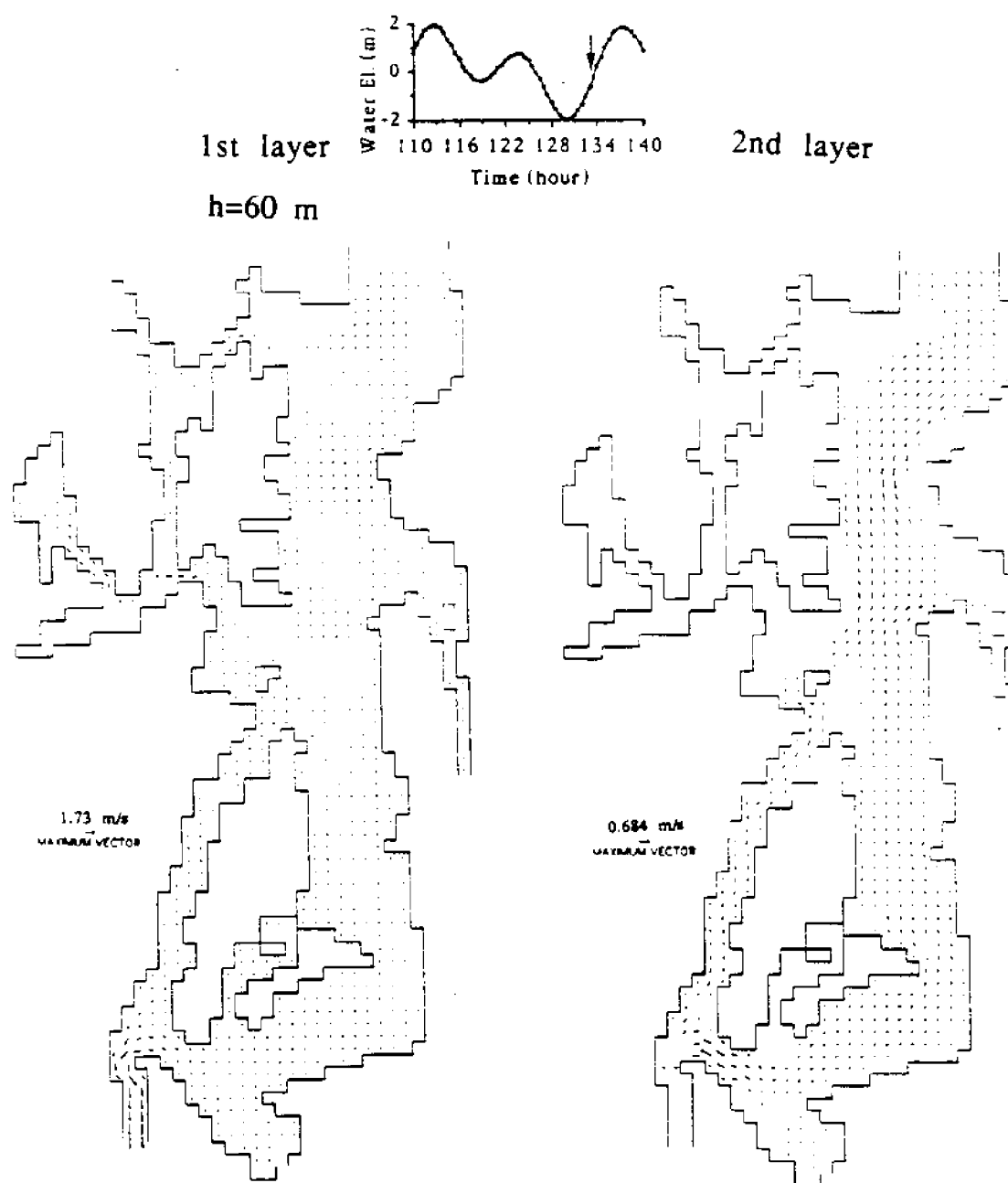
(h)

Figs.A.1a-h (continued)

APPENDIX II

TIDAL CURRENTS IN Elliott Bay

The tidal currents in Elliott Bay at four vertical model layers and eight tide stages are presented in Figs.A.2a-h. The first, second, and third model layers have a variable thickness of 15 meters or less, 45 meters or less, and 80 meters or less, respectively. The fourth model layer resolved the deeper portion of Elliott Bay with a variable thickness that follows the Bay's bottom bathymetry. The eight stages correspond to two high waters, two low waters and four mid tides during the fifth tidal cycle shown in Fig.5.2.

1st layer

Tide at Seatle

Magnolia

Seattle

enlarged

Duwamish
Head

0.274 m/s
MAXIMUM VECTOR

0.157 m/s

(a)
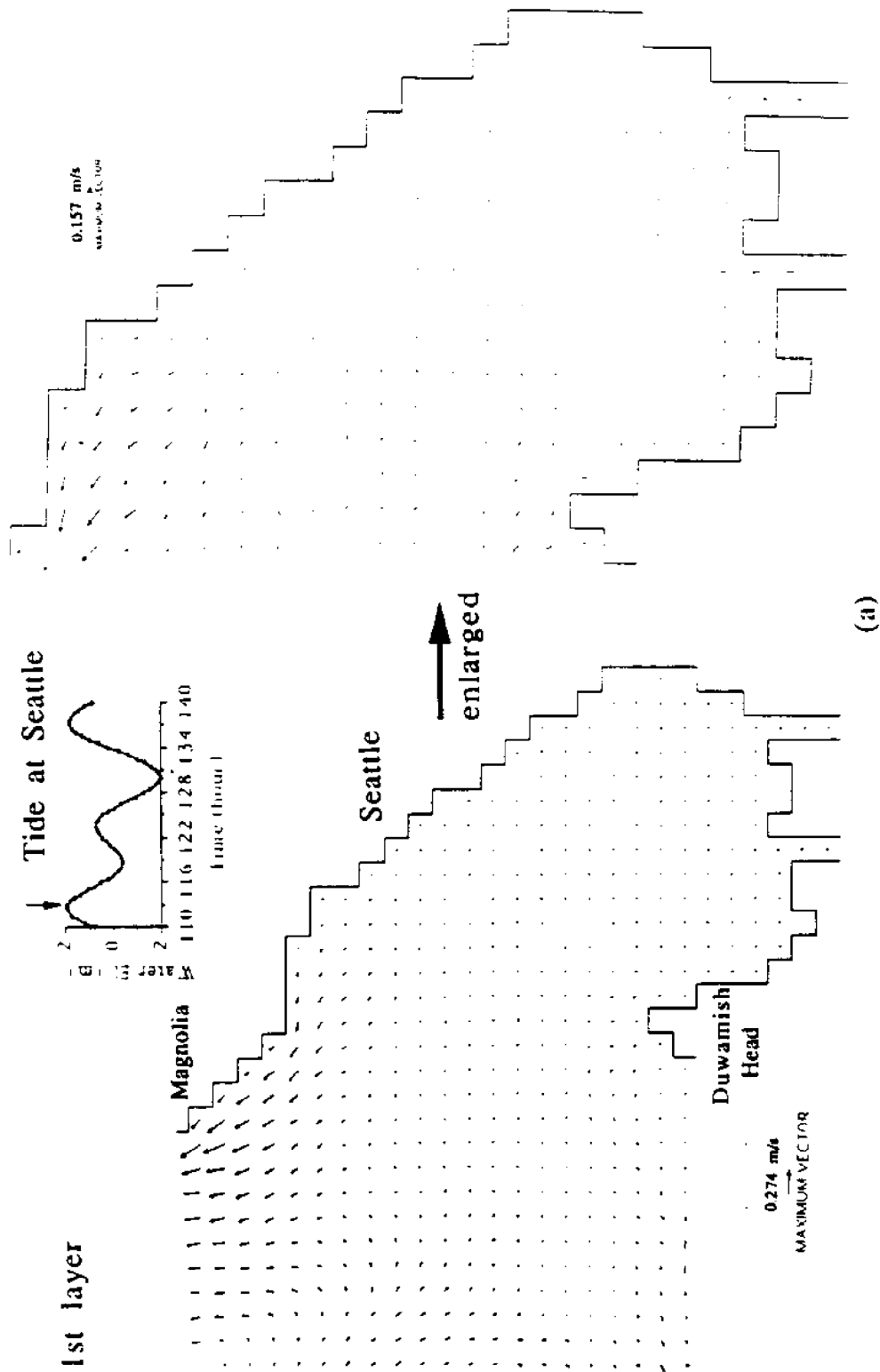
Figs.A.2a-h The tidal currents at 8 tide stages in Elliott Bay.

2nd layer

0.046 m/s
MAXIMUM VECTOR

enlarged

0.228 m/s
MAXIMUM VECTOR

Figs. A.2a-h (continued)

3rd layer

enlarged

0.035 m/s
MAXIMUM VECTOR

0.147 m/s
MAXIMUM VECTOR

Figs.A.2a-h (continued)

4th layer

0.106 m/s
MAXIMUM VECTOR

Figs.A.2a-h (continued)

1st layer

Magnolia

Seattle

enlarged

Duwamish Head

0.336 m/s
MAXIMUM VECTOR

0.195 m/s
MAXIMUM VECTOR

Figs.A.2a-h (continued)

(b)

2nd layer

enlarged

0.064 m/s
MAXIMUM VECTOR

0.289 m/s
MAXIMUM VECTOR

Figs.A.2a-h (continued)

3rd layer

enlarged

0.033 m/s
MAXIMUM VECTOR

0.220 m/s
MAXIMUM VECTOR

Figs.A.2a-h (continued)

4th layer

0.195 m/s
MAXIMUM VECTOR

Figs.A.2a-h (continued)

Figs.A.2a-h (continued)

(c)

2nd layer

enlarged

0.042 m/s
MAXIMUM VECTOR

0.138 m/s
MAXIMUM VECTOR

Figs.A.2a-h (continued)

3rd layer

enlarged

0.034 m/s
MAXIMUM VECTOR
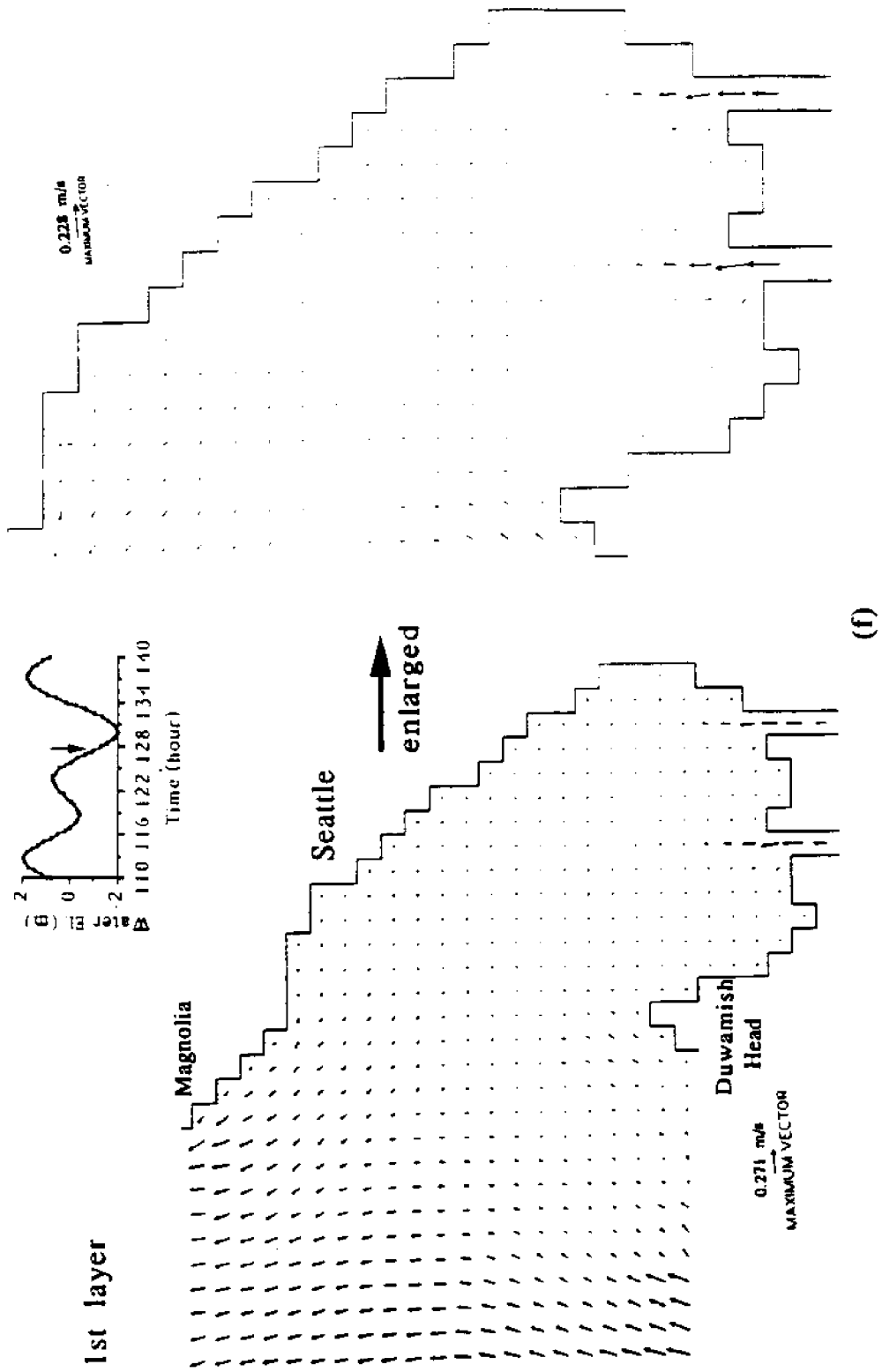
0.139 m/s
MAXIMUM VECTOR

Figs.A.2a-h (continued)

4th layer

0.109 m/s

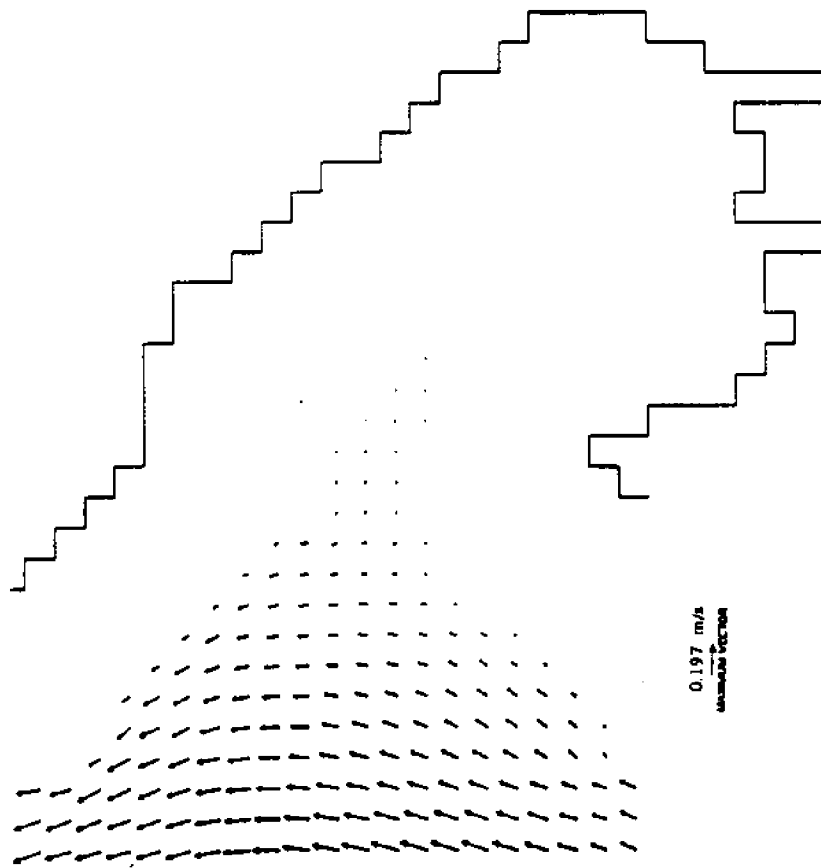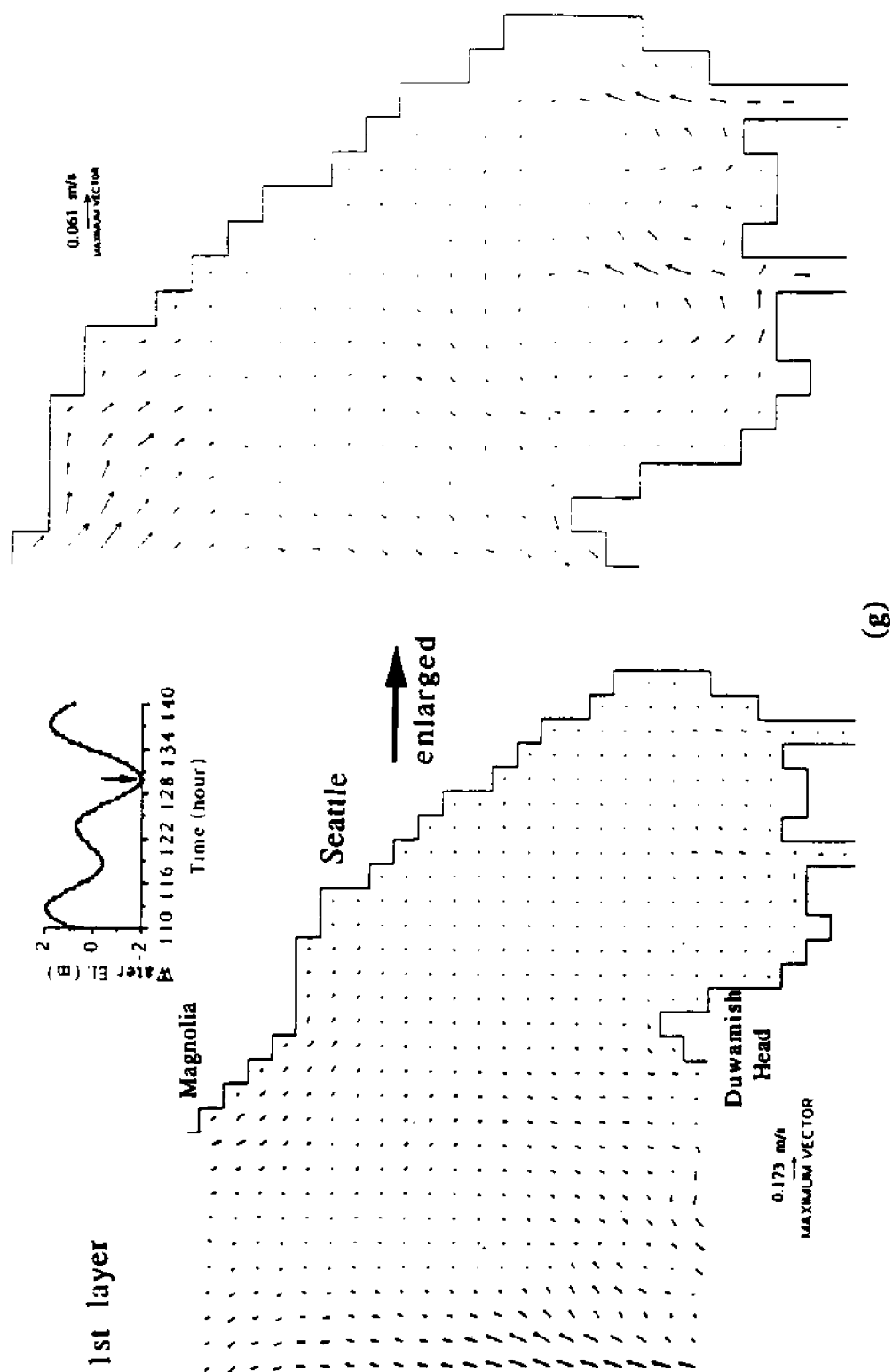Figs.A.2a-h (continued)

Figs. A.2a-h (continued)

(d)

2nd layer

0.066 m/s
MAXIMUM VECTOR

0.193 m/s
MAXIMUM VECTOR

enlarged

Figs.A.2a-h (continued)

3rd layer

0.049 m/s
MAXIMUM VECTOR

enlarged

0.201 m/s
MAXIMUM VECTOR

Figs.A.2a-h (continued)

4th layer

0.201 m/s
MAXIMUM VECTOR

Figs.A.2a-h (continued)

1st layer

Magnolia

Seattle

enlarged

Duwamish
Head

0.050 m/s
MAXIMUM VECTOR

0.107 m/s
MAXIMUM VECTOR

Water El. (m)

2
0
2

110 116 122 128 134 140
Time (hour)

Figs.A.2a-h (continued)

(e)

2nd layer

enlarged

0.040 m/s
MAXIMUM VECTOR

0.108 m/s
MAXIMUM VECTOR

Figs.A.2a-h (continued)

3rd layer

enlarged

0.016 m/s
MAXIMUM VECTOR

0.083 m/s
MAXIMUM VECTOR

Figs.A.2a-h (continued)

4th layer

0.080 m/s
MAXIMUM VECTOR

Figs.A.2a-h (continued)

1st layer

Magnolia

Seattle

enlarged

Duwamish Head

0.271 m/s
MAXIMUM VECTOR

0.228 m/s
MAXIMUM VECTOR

Figs.A.2a-h (continued)

(f)

2nd layer

enlarged

0.057 m/s
MAXIMUM VECTOR

0.253 m/s
MAXIMUM VECTOR

Figs.A.2a-h (continued)

3rd layer

enlarged

Figs.A.2a-h (continued)

4th layer

0.197 m/s

Figs.A.2a-h (continued)

1st layer

Magnolia

Seattle

enlarged

Duwamish Head

0.173 m/s
MAXIMUM VECTOR

0.061 m/s
MAXIMUM VECTOR

Water El. (m)

Time (hour)

110 116 122 128 134 140

Figs.A.2a-h (continued)

(g)

2nd layer

enlarged

Figs.A.2a-h (continued)

3rd layer

enlarged

0.038 m/s
MAXIMUM VECTOR

0.132 m/s
MAXIMUM VECTOR

Figs.A.2a-h (continued)

4th layer

0.108 m/s

MAXIMUM VECTOR

Figs.A.2a-h (continued)

Figs.A.2a-h (continued)

2nd layer

enlarged

0.094 m/s
MAXIMUM VECTOR

0.319 m/s
MAXIMUM VECTOR

Figs. A.2a-h (continued)

3rd layer

enlarged

0.071 m/s
MAXIMUM VECTOR

0.362 m/s
MAXIMUM VECTOR

Figs.A.2a-h (continued)

4th layer

0.359 m/s
MAXIMUM VECTOR

Figs.A.2a-h (continued)

VITA

Name:	Jiing-Yih Liou
Date of Birth:	June 28, 1959
Place of Birth:	Taipei, Taiwan, Republic of China

EDUCATION

Bachelor of Science in Hydraulic Engineering:	Cheng-Chung University, Republic of China, 1981
Master of Science in Oceanography:	Taiwan University, Republic of China, 1983